National Library of Canada
Acquisitions and Bibliographic Services Branch
395 Wellington Street
Ottawa, Ontario
K1A 0N4

Bibliothèque nationale du Canada
Direction des acquisitions et des services bibliographiques
395, rue Wellington
Ottawa (Ontario)
K1A 0N4

Your file Votre référence

Our file Notre référence

## NOTICE

The quality of this microform is heavily dependent upon the quality of the original thesis submitted for microfilming. Every effort has been made to ensure the highest quality of reproduction possible.

If pages are missing, contact the university which granted the degree.

Some pages may have indistinct print especially if the original pages were typed with a poor typewriter ribbon or if the university sent us an inferior photocopy.



## AVIS

La qualité de cette microforme dépend grandement de la qualité de la thèse soumise au microfilmage. Nous avons tout fait pour assurer une qualité supérieure de reproduction.

S'il manque des pages, veuillez communiquer avec l'université qui a conféré le grade.

La qualité d'impression de certaines pages peut laisser à désirer, surtout si les pages originales ont été dactylographiées à l'aide d'un ruban usé ou si l'université nous a fait parvenir une photocopie de qualité inférieure.



Canada

# Web Buckling in Thin Webbed Castellated Beams

by

**Walid Jacques Zaarour**

**May 1995**

**Department of Civil Engineering**

**and Applied Mechanics**

**McGill University**

**Montreal, Canada**

A thesis submitted to the Faculty of Graduate Studies and Research in partial fulfillment of the requirements for the degree of Master of Engineering.

ISBN 0-612-07992-9

# ABSTRACT

An experimental test program was conducted at McGill University which incorporated 14 castellated steel beams provided by Chaparral Steel. The notable feature of these beams is their thin webs. The modes of failure and their corresponding loads were predicted based on a number of previous studies. A nonlinear finite element analysis was carried out in order to provide a new assessment tool. The program used was NASTRAN. The geometries of the castellated steel beams were predicted to be susceptible to web post buckling.

The applied load which causes the formation of the mechanism failure (Redwood 1978), and the load which causes a horizontal yield failure, (Blodgett 1963), were calculated and compared to the predicted buckling load to anticipate the mode of failure. The web post buckling loads were predicted based on an analysis by Blodgett (1963), Aglan and Redwood (1974) and on the finite element analysis. The above analyses were repeated for five of the seven beams tested by Bazile and Texier (1968) and which failed by web post buckling.

The beams tested were susceptible to web post buckling, as predicted. The web post buckling analysis suggested by Blodgett (1963) resulted in large variations from the experimental failure load. The analysis suggested by Aglan and Redwood (1974) yielded conservative results. The finite element buckling analysis showed a good correspondence with the experimental buckling load and may be a good tool to conduct a more complete parametric study.

# RÉSUMÉ

Un programme d'essais expérimentaux fut effectué à l'université McGill sur 14 poutres ajourées en acier fournies par Chaparral Steel. La caractéristique principale de ces poutres est la minceur de l'âme. La mode de rupture de ces poutres et les charges correspondantes ont fait l'object de plusieurs études antérieures. Dans la cadre de la présente thèse, le programme d'éléments finis non-linéaire NASTRAN fut utilisé afin de modéliser le comportement de ces poutres. Les résultats démontrent la susceptibilité de ce type de poutres au flambage de l'âme.

Les charges de flambage sont estimées suivant les analyses proposées par Blodgett (1963), Aglan et Redwood (1974), et par les analyses d'élément finis. Les charges de flambage obtenues sont comparées à celles correspondant à la formation d'un mécanisme de rupture (Redwood 1978), et à une rupture horizontale par écoulement (Blodgett 1963). Ces analyses furent effectuées pour cinq des sept poutres testées par Bazile et Texier (1968) ayant sont rupturées par flambage de l'âme.

Les analyses ont confirmé la susceptibilité de ces poutres au flambage de l'âme. Les charges obtenues suivant la méthode de Blodgett (1963) différent de façon significative des données expérimentales. Par contre, les charges obtenues suivant la procédure de Aglan and Redwood (1974) sont sécuritaires. En conclusion, l'analyse par éléments finis du flambage est en accord avec les résultats expérimentaux et semble être une technique fiable afin de poursuivre un programme d'analyse paramétrique plus complet.

## ACKNOWLEDGMENTS

I would like to take this opportunity to express my sincere thanks to my supervisor Professor R. G. Redwood for his knowledge and guidance throughout the course of the project.

In addition, I would like to express my gratitude to Chaparral Steel for supplying the test specimens, Hatch Associates Consultants, Inc. for sharing their knowledge and the group Canam Manac for fabricating the specimens.

I am also grateful for the assistance given by Mr. M. Przykorski and the rest of the laboratory staff.

Finally, I would like to express my appreciation to Monique for her help, understanding and support, Fouad for being a true friend and all my fellow students for making my stay at McGill an enjoyable one.

# Table of Contents


page

Abstract ..... i

Résumé ..... ii

Acknowledgments ..... iii

Table of Contents ..... iv

List of Figures ..... viii

List of Tables ..... xi

Notations ..... xiii

**1 Introduction** ..... 1

1.1 Introduction ..... 1

1.1.1 Fabrication ..... 2

1.1.2 Dimensions and Properties ..... 3

1.2 Literature Review ..... 4

1.2.1 Introduction ..... 4

1.2.2 Overall Lateral Torsional Buckling ..... 4

1.2.3 Web Failures ..... 4

1.2.4 Plastification of Upper and Lower Tee-Section ..... 5

1.2.5 Parallelogram Action ..... 6

1.2.6 Points of Support and Concentrated Loads ..... 6

1.3 Program of Research ..... 6

1.3.1 Objective ..... 6

1.3.2 Outline of Thesis ..... 7

**2 Analysis** ..... 13

2.1 Elastic Stress Distribution ..... 13

2.1.1 Bending Moment ..... 13

2.1.2 Shear ..... 14

2.2 Shear at Welded Joint ..... 16

2.3 Formation of Mechanism (plastic analysis) ..... 17

2.4 Buckling Analysis ..... 19

2.4.1 Aglan and Redwood ..... 19
2.4.2 Blodgett ..... 21

**3 Finite Element Analysis** ..... 28
3.1 Introduction ..... 28
3.2 Analytical Options ..... 28
3.3 Modeling of Beams ..... 30
3.3.1 Load Application ..... 31
3.3.2 Boundary Conditions ..... 32
3.3.3 Mesh and Element Type ..... 32
3.3.4 Load Convergence ..... 33
3.4 Application of MSC/NASTRAN ..... 33
3.4.1 Input File ..... 33
3.4.2 Cold Start ..... 34
3.4.3 Restart ..... 34

**4 Test Set-up and Test Specimen** ..... 42
4.1 Test Specimen and Section Properties ..... 42
4.2 Measurements ..... 43
4.3 Test Set-up ..... 43
4.3.1 Vertical End Supports ..... 43
4.3.2 Load Application ..... 44
4.3.3 Lateral Supports ..... 44
4.3.4 Bearing Stiffeners ..... 45
4.4 Instrumentation ..... 46
4.4.1 Strain Gauges ..... 46
4.4.2 Vertical Deflections ..... 46
4.4.3 Jig for Web Deformations ..... 47
4.5 Testing Procedure ..... 47

**5 Test Results and Observations** ..... 54
5.1 General ..... 54
5.2 Tee-Section Buckling ..... 56
5.3 Overall Lateral Torsional Buckling ..... 56
5.4 Web-Post Buckling ..... 57

**6 Results and Discussion** ..... **99**
6.1 Prediction of the Mode of Failure ..... **99**
6.2 Failure by the Formation of the Mechanism ..... **100**
6.3 Comparison of Buckling Loads ..... **101**
6.3.1 Blodgett ..... **101**
6.3.2 Aglan and Redwood ..... **101**
6.3.3 Finite Element Analysis (NASTRAN) ..... **102**
6.4 Overall Comparison ..... **102**
6.5 Influence of Parameters on Section Behavior ..... **102**
6.6 Influence of Initial Imperfections ..... **104**
6.7 Lateral Supports ..... **105**
6.8 Analysis of Beams Tested by Bazile & Texier (1968) **105**

**7 Summary and Conclusion** ..... **120**
7.1 Summary ..... **120**
7.2 Conclusion ..... **121**

**References** ..... **124**

**A Finite Element Analysis (NASTRAN)** ..... **128**
A.1 Nonlinear Static Analysis Strategies ..... **128**
A.1.1 Advancing Schemes ..... **129**
A.1.2 Stiffness Update ..... **130**
A.1.3 Displacement Prediction ..... **132**
A.1.4 Element State Update ..... **132**
A.1.5 Convergence Criteria ..... **133**
A.2 Restart ..... **133**
A.3 Buckling ..... **134**
A.3.1 Instability ..... **134**
A.3.2 Linear vs. Nonlinear Buckling ..... **134**
A.3.3 Concept and User Interface ..... **135**
A.4 Nonlinear Elements ..... **137**
A.4.1 Types of Nonlinear Elements ..... **137**
A.4.2 Nonlinear Shell and Plate Elements ..... **137**

B Spreadsheet Samples ..... 152

C Shape Properties ..... 161

# List of Figures


| | | page |
|---|---|---|
| Fig. 1.1 | Cut and Weld Pattern (Specimen 12-4) ..... | 8 |
| Fig. 1.2 | Typical Section ..... | 8 |
| Fig. 1.3 | Web Post Buckling (Ward 1990) ..... | 9 |
| Fig. 1.4 | Typical Web Post Modeling ..... | 10 |
| Fig. 1.5 | Shear & Moment Diagram ..... | 11 |
| Fig. 1.6 | Yield of Upper & Lower Tee ..... | 11 |
| Fig. 1.7 | Plastic Hinges ..... | 12 |
| Fig. 1.8 | Shear & Moment Diag. for Test Specimen ..... | 12 |
| Fig. 2.1 | Elevation View ..... | 24 |
| Fig. 2.2 | Longitudinal Forces ..... | 24 |
| Fig. 2.3 | Transverse Forces ..... | 24 |
| Fig. 2.4 | Individual & Combined Stresses ..... | 24 |
| Fig. 2.5 | Diagram for Shear Force ..... | 25 |
| Fig. 2.6 | Design Aids (Aglan and Redwood 1974) ..... | 25 |
| Fig. 2.7 | Section With Intermediate Plate ..... | 26 |
| Fig. 2.8 | Buckling (Blodgett 1963) ..... | 26 |
| Fig. 2.9 | Buckling Stresses (Blodgett 1963) ..... | 27 |
| Fig. 3.1 | Model Used for Finite Element Analysis ..... | 36 |
| Fig. 3.2 | Typical Mesh ..... | 37 |
| Fig. 3.3 | Typical Mesh (1) ..... | 38 |
| Fig. 3.4 | Typical Mesh (2) ..... | 38 |
| Fig. 3.5 | Typical Mesh (3) ..... | 39 |
| Fig. 3.6 | Typical Mesh (4) ..... | 39 |
| Fig. 3.7 | Typical Mesh (5) ..... | 40 |
| Fig. 3.8 | Load vs. Relative Flange Deflection (8-3) ..... | 41 |
| Fig. 3.9 | Load vs. Relative Flange Deflection (12-2) ..... | 41 |
| Fig. 4.1 | Load and Support Point Details ..... | 51 |
| Fig. 4.2 | Location of Lateral Supports ..... | 51 |
| Fig. 4.3 | Lateral Support ..... | 52 |
| Fig. 4.4 | Location of LVDT & Strain Gauges ..... | 53 |
| Fig. 4.5 | Displacement Measuring Jig ..... | 53 |
| Fig. 5.1 | Location of LVDTs on Web Post ..... | 60 |

| | | | |
|---|---|---|---|
| Figs. 5.2-5.7 | Plotting of Test Results (8-1a) | ..... | 61-62 |
| Figs. 5.8-5.13 | Plotting of Test Results (8-2a) | ..... | 63-64 |
| Figs. 5.14-5.18 | Plotting of Test Results (8-3a) | ..... | 65-66 |
| Figs. 5.19-5.23 | Plotting of Test Results (8-4a) | ..... | 67-68 |
| Figs. 5.24-5.35 | Plotting of Test Results (8-3) | ..... | 69-71 |
| Figs. 5.36-5.47 | Plotting of Test Results (8-4) | ..... | 72-74 |
| Figs. 5.48-5.59 | Plotting of Test Results (10-1) | ..... | 75-77 |
| Figs. 5.60-5.71 | Plotting of Test Results (10-2) | ..... | 78-80 |
| Figs. 5.72-5.83 | Plotting of Test Results (10-3) | ..... | 81-83 |
| Figs. 5.84-5.95 | Plotting of Test Results (10-4) | ..... | 84-86 |
| Figs. 5.96-5.107 | Plotting of Test Results (12-1) | ..... | 87-89 |
| Figs. 5.108-5.119 | Plotting of Test Results (12-2) | ..... | 90-92 |
| Figs. 5.120-5.131 | Plotting of Test Results (12-3) | ..... | 93-95 |
| Figs. 5.132-5.143 | Plotting of Test Results (12-4) | ..... | 96-98 |
| Fig. 6.1 | Prediction of the Failure Mode | ..... | 113 |
| Fig. 6.2 | Comparison of the Mechanism Failure Load | ..... | 113 |
| Fig. 6.3a | Comparison of Buckling Loads (8- ) | ..... | 114 |
| Fig. 6.3b | Comparison of Buckling Loads (10- ) | ..... | 114 |
| Fig. 6.3c | Comparison of Buckling Loads (12- ) | ..... | 114 |
| Fig. 6.4 | Earlier Interpretation of Experimental Results | ..... | 115 |
| Fig. 6.5 | Load vs. Web Strains (8-1a) | ..... | 116 |
| Fig. 6.6 | Load vs. Web Strains (8-2a) | ..... | 116 |
| Fig. 6.7 | Load vs. Web Strains (8-3) | ..... | 116 |
| Fig. 6.8 | Load vs. Web Strains (8-4) | ..... | 116 |
| Fig. 6.9 | Load vs. Web Strains (10-1) | ..... | 117 |
| Fig. 6.10 | Load vs. Web Strains (10-2) | ..... | 117 |
| Fig. 6.11 | Load vs. Web Strains (10-3) | ..... | 117 |
| Fig. 6.12 | Load vs. Web Strains (10-4) | ..... | 117 |
| Fig. 6.13 | Load vs. Web Strains (12-1) | ..... | 118 |
| Fig. 6.14 | Load vs. Web Strains (12-2) | ..... | 118 |
| Fig. 6.15 | Load vs. Web Strains (12-3) | ..... | 118 |
| Fig. 6.16 | Load vs. Web Strains (12-4) | ..... | 118 |
| Fig. 6.17 | Typical Web Post Section | ..... | 119 |
| Fig. 6.18 | Loading at 8 Point (Bazile & Texier 1968) | ..... | 119 |
| Fig. A.1 | Nonlinear Analysis Concept | ..... | 143 |
| Fig. A.2 | Crisfield vs. Load Increment | ..... | 144 |

| | | |
|---|---|---|
| Fig. A.3 | Crisfield Method in Unstable Region | 144 |
| Fig. A.4 | Riks Method | 145 |
| Fig. A.5 | Modified Riks Method | 145 |
| Fig. A.6 | Newton Raphson Method | 146 |
| Fig. A.7 | Snap Through | 147 |
| Fig. A.8 | Bifurcation Buckling | 147 |
| Fig. A.9 | Buckling Concept | 148 |
| Fig. A.10 | Finite Element Model | 149 |
| Fig. A.11 | Finite Element Model (Buckled Shape) | 150 |
| Fig. A. 12 | Failed Test Specimen ( - ) | 151 |
| Fig. A. 13 | Failed Test Specimen ( - ) | 151 |
| Fig. B.1 | Sample Interaction Diagram (12-4) | 159 |

# List of Tables


| | | page |
|---|---|---|
| Table 3.1 | Convergence of Critical Load With Mesh Refinement ..... | 35 |
| Table 4.1 | Summary of Coupon Testing ..... | 49 |
| Table 4.2 | Sweep, Camber & Web Offset ..... | 50 |
| Table 5.1 | Mode of Failure, Maximum Test Load & Vertical Deflection ..... | 58 |
| Table 5.2 | Estimation of Experimental Failure Loads ..... | 59 |
| Table 6.1 | Predicted Yield Failure Loads ..... | 107 |
| Table 6.2 | Prediction of The Failure Mode ..... | 107 |
| Table 6.3 | Failure by the Formation of a Mechanism ..... | 108 |
| Table 6.4 | Comparison of $P_B$ vs. $P_{test}$ ..... | 108 |
| Table 6.5 | Comparison of $P_{AR}$ vs. $P_{test}$ ..... | 109 |
| Table 6.6 | Comparison of $P_{FEM}$ vs. $P_{test}$ ..... | 109 |
| Table 6.7 | Table of Analytical Results ..... | 110 |
| Table 6.3 | Summary of Results ..... | 111 |
| Table 6.9 | Predicted Yield Failure (Bazile and Texier 1968) ..... | 112 |
| Table 6.10 | Summary of results (Bazile and Texier 1968) ..... | 112 |
| Table 6.11 | Comparison of Results (Bazile and Texier 1968) ..... | 112 |
| Table A.1 | Listing of Cold Start ..... | 139 |
| Table A.2 | Listing of Restart ..... | 142 |
| Table B.1 | Sample Input & Output ..... | 153 |
| Table B.2 | Calculation of First Yield (Blodgett 1963) ..... | 154 |
| Table B.3 | Data for Interaction Diagram (Redwood 1978) ..... | 155 |
| Table B.4 | Buckling Analysis (Blodgett 1963) ..... | 156 |
| Table B.5 | Failure Due to Horizontal Shear (Blodgett 1963) ..... | 156 |
| Table B.6 | Buckling Analysis (Aglan & Redwood 1974) ..... | 157 |
| Table B.7 | Calculation For Location of Lateral Supports ..... | 158 |
| Table C.1a | Nominal Dimensions of Test Specimens (8-1 to 8-4) ..... | 161 |
| Table C.1b | Nominal Dimensions of Test Specimens (10-1 to 10-4) ..... | 161 |
| Table C.1c | Nominal Dimensions of Test Specimens (12-1 to 12-4) ..... | 161 |
| Table C.1d | Nominal Dimensions (Bazile and Texier 1968) ..... | 162 |
| Table C.2a | Nominal & Measured Dimensions (8-1a to 8-4a) ..... | 162 |
| Table C.2b | Nominal & Measured Dimensions (8-3 to 8-4) ..... | 162 |
| Table C.2c | Nominal & Measured Dimensions (10-1 to 10-4) ..... | 163 |

Table C.2d Nominal & Measured Dimensions (12-1 to 12-4) ..... 163
Table C.3 Nominal Dimensions (Chaparral Steel, Shape Properties) ..... 164

## NOTATIONS

$A_f$ - area of flange

$A_t$ - area of tee-section

$A_w$ - area of web

b - width of one sloping edge of the hole

$b_f$ - width of flange

$C_w$ - warping constant

d - depth of original beam section

$d_g$ - total depth of castellated beam section

$d_t$ - depth of tee-section

E - modulus of elasticity

e - width of the opening at the top

F - normal force

$F_b$ - allowable compressive bending stress

$F_y$ - yield stress

G - shear modulus

h - height of one sloping edge of the hole

$h_o$ - height of opening

$h_p$ - height of plate

I - moment of inertia

J - St. Venant torsional constant

L - length of beam

M - moment

$M_{o\,cr}$ - critical moment

$M_p$ - plastic moment

$M_u$ - ultimate moment

$M_y$ - yield moment

N - normal resultant force at tee-section

P - applied load

$P_m$ - load causing a mechanism failure (Redwood 1978)

$P_{1^{st}}$ - load causing first yield

$P_{AR}$ - load causing buckling of web post (Aglan and Redwood 1974)

$P_B$ - load causing buckling of web post (Blodgett 1963)

$P_{cr}$ - critical load

$P_{FEM}$ - load causing buckling of web post (finite element analysis)

$P_{hy}$ - load causing a horizontal yield failure (Blodgett 1963)

$P_{test}$ - test load failure

$P_y$ - smaller of $P_m$ and $P_{hy}$

$r_t$ - radius of gyration

S - distance from center-line to center-line of adjacent holes

s.g. - strain gauge

$t_f$ - thickness of the flange

$t_w$ - thickness of the web

V - shear

$V_h$ - horizontal shear

$V_{o\,cr}$ - critical shear

$V_p$ - plastic shear

$y_b$ - distance from inner edge (at the cut) to centroid of tee-section

$y_t$ - distance from top of flange to centroid of tee-section

$\phi$ - angle of cut

$\tau$ - shear stress

$\sigma_m$ - normal stress caused by bending

$\sigma_{ult}$ - ultimate stress

# Chapter 1

## Introduction

### 1.1 Introduction

The idea of splitting and expanding beams to increase their section modulus was first used about 1910, by H. E. Horton of the Chicago Bridge and Iron Works (Altfillisch *et al.* 1957). It has been used in both building and ship construction. The usage increased in building construction as floor joists, roof girders, arched roof girders and many industrial, commercial and bridge structures. The United Steel Structural Company of England fabricated expanded beams as early as 1937 (Toprac and Cooke 1959). The Texas State Highway Department used castellated beams in building a 100 ft (30.5 m) simple span beam bridge in 1951. They were also used in bridge construction in New Zealand. In 1952, a pilot investigation on expanded beams was carried out at The University of Texas. However, their primary use was in Europe, following World War II, when labor was cheap and material very expensive; so, the fabrication costs were not too high because of cheap labor and economy of material was achieved.

Castellated beams have not been used extensively in recent years due to the excessive fabrication costs involved; however, as fabrication methods become more automated, by the use of single or multi-flame oxygen cutting equipment with a controlled path of the burner, they have a better chance of competing economically with other alternatives.

Some recent applications for castellated beams have been in roof purlins, girders in rigid frames, and in composite construction (Temple *et al.* 1993). One of their prime uses is in composite construction in long span floors, where floor depths are kept to a minimum by passing the major service ducts through the openings. They are also used effectively for lightly serviced buildings or for aesthetic reasons where the structure is exposed. They are efficient as secondary long span members subject to uniform loading (Ward 1990).

### 1.1.1 Fabrication

Castellated beams are fabricated using rolled-steel shapes. The web of the beam is cut, usually using single or multi-flame oxygen cutting, in a saw tooth pattern along its center line. The path of the burner may be controlled by one of the three methods (Knowles 1985).

a) a template
b) a mandrel
c) a magic eye following a scale drawing

The split halves of the beam, when cut, bend outwards due to the effect of residual stresses that remain in the beam from the rolling process (Hope and Sheikh 1969; Knowles 1985). Hydraulic or manually operated rams are used in order to return the beam to its original straight alignment. It is held such that the two halves are positioned with the teeth, formed by cutting, aligned and touching . These are tack welded to hold in position. The resulting holes are of hexagonal or octagonal shape, the latter achieved by inserting rectangular plates between the two parts. The beam is

then removed from the press and each of the teeth is butt welded along its full length. The weld may be carried

out from one side only or alternatively first from one side, then the other side. The method depends on the thickness of the web and the equipment used. End plates and intermediate infill plates, if required, are welded in position. The waste at the ends of the beam is then cut off, (Fig. 1.1).

### 1.1.2 Dimensions and Properties

The saw tooth pattern of cutting the web will result in specific geometric properties (Blodgett 1963). Those characteristics will greatly influence the behavior and mode of failure of the beam and the relevant dimensions are defined as follows (Fig. 1.2):

$$\tan\phi = \frac{h}{b}$$
$$d_g = d + h + h_p \quad \textit{where } d = \textit{original depth of beam}$$
$$d_t = \frac{d-h}{2}$$
$$S = 2(b+e) \qquad \text{.....[1.1]}$$

The distance "e" may be increased to provide the required opening for the duct work and the required weld length between the openings. It should be noted that as "e"

increases, the bending stress within the tee-section due to the secondary moment, caused by the applied shear, increases (Hosain and Speirs 1971; Mandel *et al.* 1971). Therefore there exists an optimum range for "e".

## 1.2 Literature Review

### 1.2.1 Introduction

A number of different modes of failure are possible depending on the beam type and the geometry which results from the cutting pattern. The principal modes of failure are as follows:

- Overall lateral torsional buckling
- Web
  - Shear
  - Buckling
- Plastic hinges in upper and lower tee-sections (overall bending failure)
- Parallelogram mechanism
- Local Failure (Locations of concentrated force)

### 1.2.2 Overall Lateral Torsional Buckling

If no adequate lateral support is provided for a castellated beam, it is possible that failure by overall lateral torsional buckling (LTB) will occur. Compared to solid web sections, castellated beams are more susceptible to lateral torsional buckling. They have a deep and slender profile and a reduced torsional stiffness (Ward 1990; Pattanayak and Chesson 1974).

### 1.2.3 Web Failures

The web may fail by yield in shear or by lateral torsional buckling.

shown that the highest shear stress will generally occur at a weld (Knowles 1985). If local and lateral buckling are prevented, with relatively narrow welded joint, there is a possibility of failure by rupture of the welded joint. This failure is usually brittle (Hosain and Speirs 1971). The horizontal shear is developed in the web post due to change in the longitudinal tee-section axial forces which result from the moment; these are considered as acting at the center of gravity of the tee-section.

The web post may also fail in lateral torsional buckling (Fig. 1.3) in regions of high shear force with certain web geometries (Aglan and Redwood 1974). The specific angle of cut, the ratio of the height of intermediate plate to total height of hole, the ratio of hole height to minimum width of the web post and the ratio of minimum web post width to web thickness are parameters affecting this mode of failure. The web post is assumed to be acted upon by two equal and opposite end moments and shearing forces (Fig. 1.4).

An experimental study on seven castellated steel beams was performed in France, (Bazile and Texier 1968). Five of the seven beams which were tested failed by web post buckling . These beams will be analyzed and discussed in greater detail in chapter 6.

### 1.2.4 Plastification of Upper and Lower Tee-Section

This failure occurs in regions of high bending moment (Figs. 1.5 and 1.6). Halleux (1967) tested simply-supported beams and subjected them to two equal loads applied at the third-span points. The central zone is subjected to bending moment of maximum and constant magnitude. Due to the bending moment, normal forces develop at the center of gravity of the upper and lower tee section (at their minimum section). These areas develop complete plastic behavior and failure occurs.

### 1.2.5 Parallelogram Action

Parallelogram action occurs in regions of high shear force (Fig. 1.7). It is due to the formation of plastic hinges at the four corners of a hole which result in a deformation pattern similar to a parallelogram, (Halleux 1967; Knowles 1985). For this failure mode to occur, it is assumed that all adjacent parts of the beam, web post and flange, remain rigid. The plastic hinges are the result of complete plastification of the upper and lower tee-sections at the four reentrant corners of a panel. The total stress on the tee-section is a combination of direct stress due to the normal forces resulting from the primary bending moment at that section and secondary flexural stresses due to the vertical shear carried by the tee-section, (Hosain and Speirs 1971; Altfillisch *et al.* 1957), (Fig. 1.2). In analyses conducted by Redwood (1968, 1978) interaction diagrams are developed which represent the ratios of $M/M_p$* and $V/V_p$ at which the mechanism is formed.

### 1.2.6 Local Failure (Points of Support and Concentrated Loads)

At points of support and concentrated loads, the effect of bearing and buckling should be considered (Ward 1990). Openings at those points should be infilled and stiffeners provided (Fig. 1.1).

## 1.3 Program of Research

### 1.3.1 Objective

The objective of this research is to try and predict the geometries of castellated beams that are susceptible to web post buckling. In the past web post buckling was not

* Subscript "p", indicates plastic value

The failure may be due to horizontal shear in a post, vertical shear at the hole (sum of the shear capacities of the upper and lower tees ) or at a weld (Ward 1990). It is

considered as a primary design criterion, because of typical geometries used. However, for specific geometries, similar to the ones being studied, combined with thinner webs which are now available, buckling may become a principal mode of failure. Chaparral Steel, in Midlothian Texas, is interested in establishing markets for castellated beams produced from their proprietary Bantam Beam shapes. A list of the available shapes is provided in Appendix C. Web post buckling may be a governing criterion for the strength of those shapes because of their thin webs. The castellated beams used in this research project are made from Chaparral Bantam Beam shapes. The beams were provided by Chaparral Steel based on the proposed shapes from Hatch Associates Consultants, Inc. They were fabricated by Le Group Canam-Manac and tested at McGill University. It should be noted that the web thickness is up to 25% thinner than the lightest of the castellated beam shapes used in the U.K. (Temple *et al.* 1993).

### 1.3.2 Outline of Thesis

A number of different analyses for the probable modes of failure are discussed in Chapter 2. The loads at which buckling is predicted is evaluated by using a number of different approaches, previously suggested in the literature, and also by non-linear finite element analyses in Chapter 3. Beams which are predicted to be most sensitive to the web-post buckling mode of failure were tested in the Jamieson Structures Laboratory at McGill University. Chapter 4 describes the test set up and the instrumentation used to gather data during the experiment.

The test results are presented in Chapter 5. Chapter 6 is a comparison of the experimental results, from the specimens tested at McGill University and the specimens tested by Bazile and Texier (1968), with the predicted failure loads from the different analyses and a discussion of the results. Finally, a summary of the study and a conclusion are presented in Chapter 7.

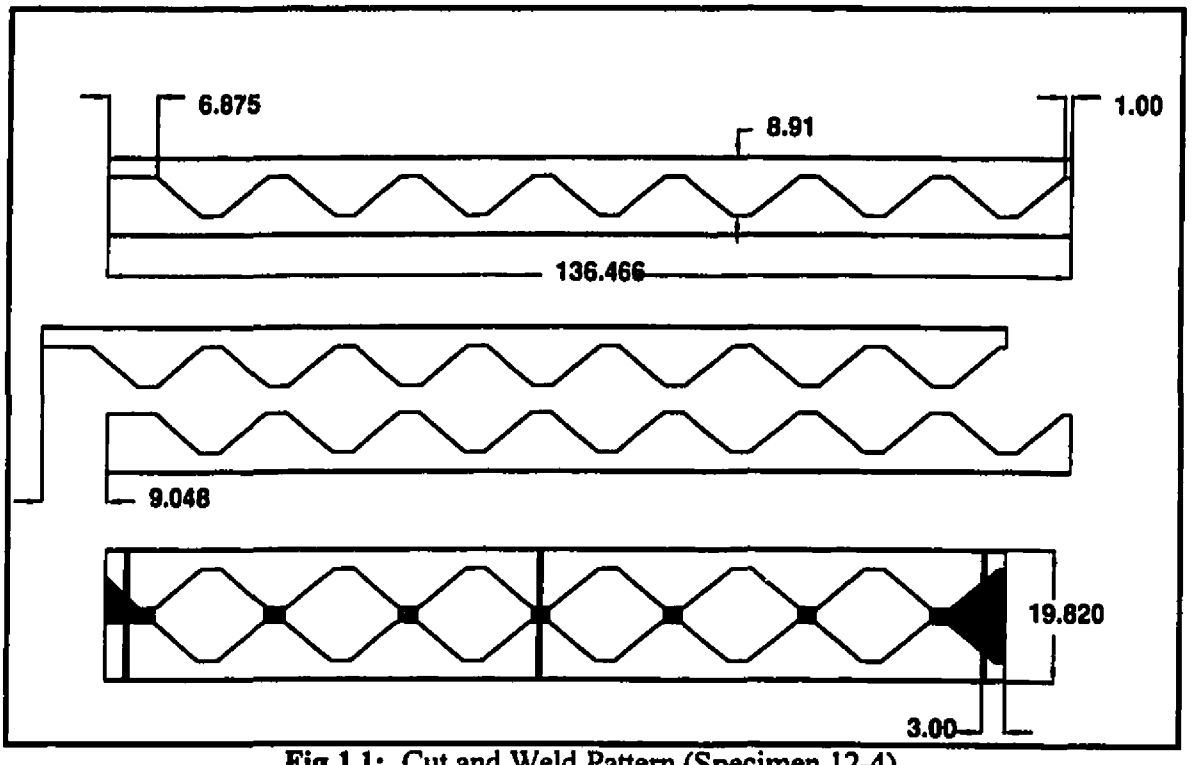


Fig.1.1: Cut and Weld Pattern (Specimen 12-4)

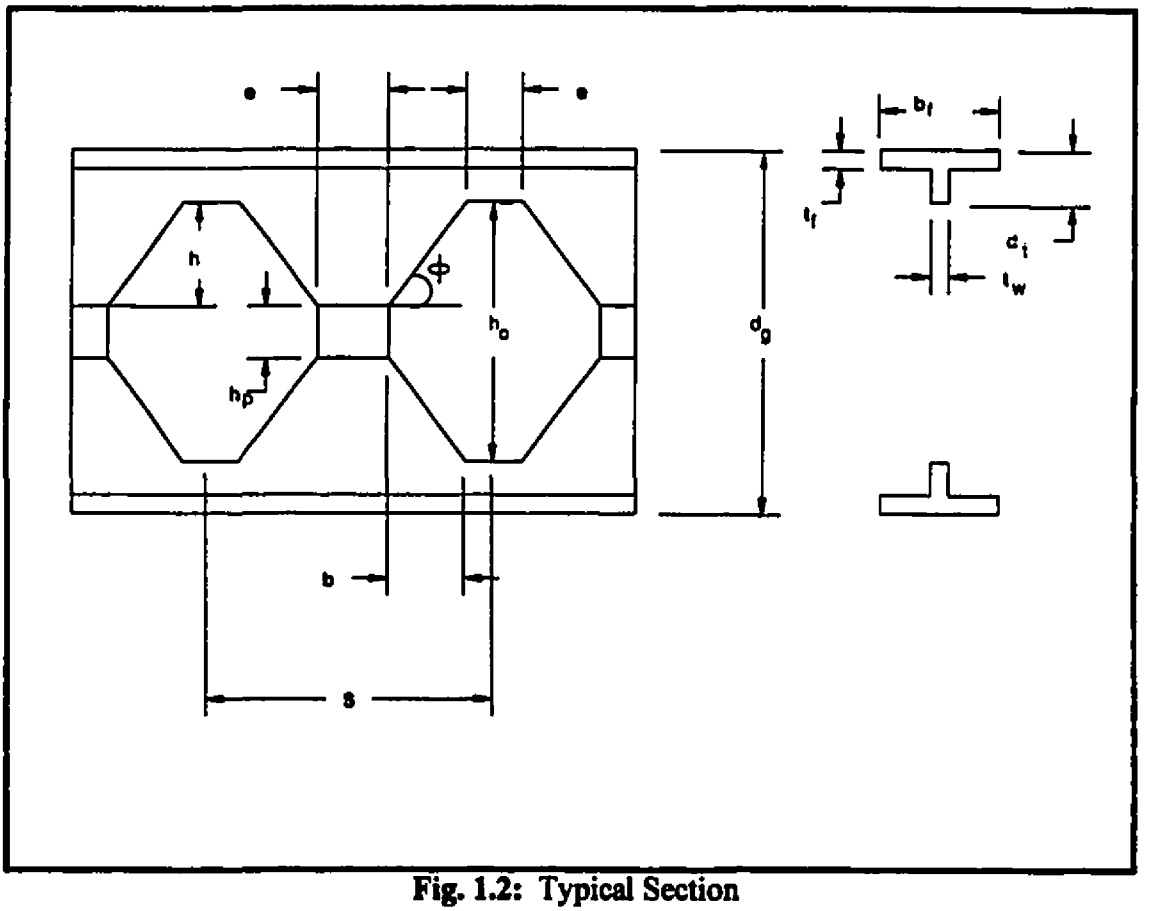


Fig. 1.2: Typical Section

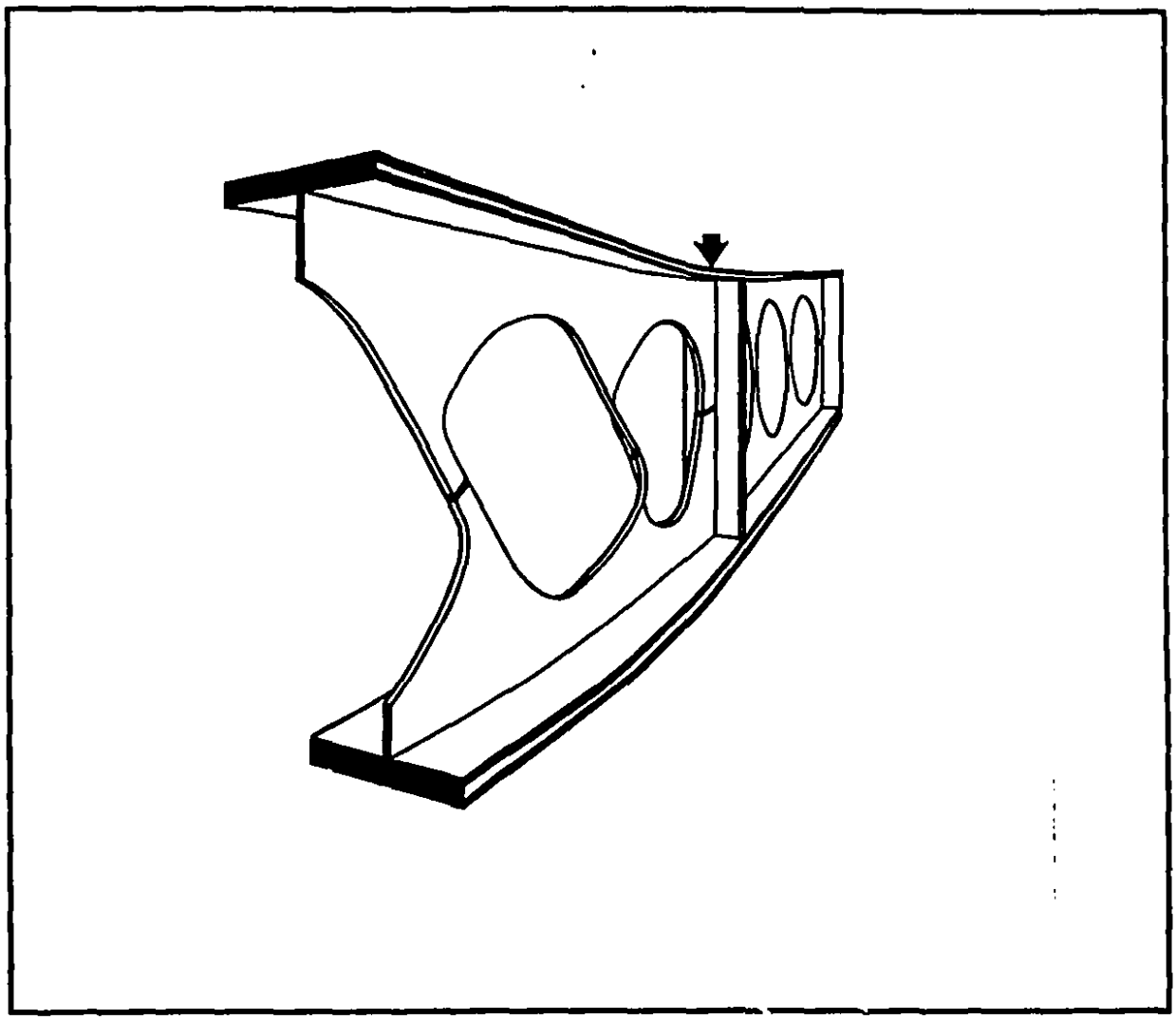

**Fig. 1.3:** Web Post Buckling (Ward 1990)

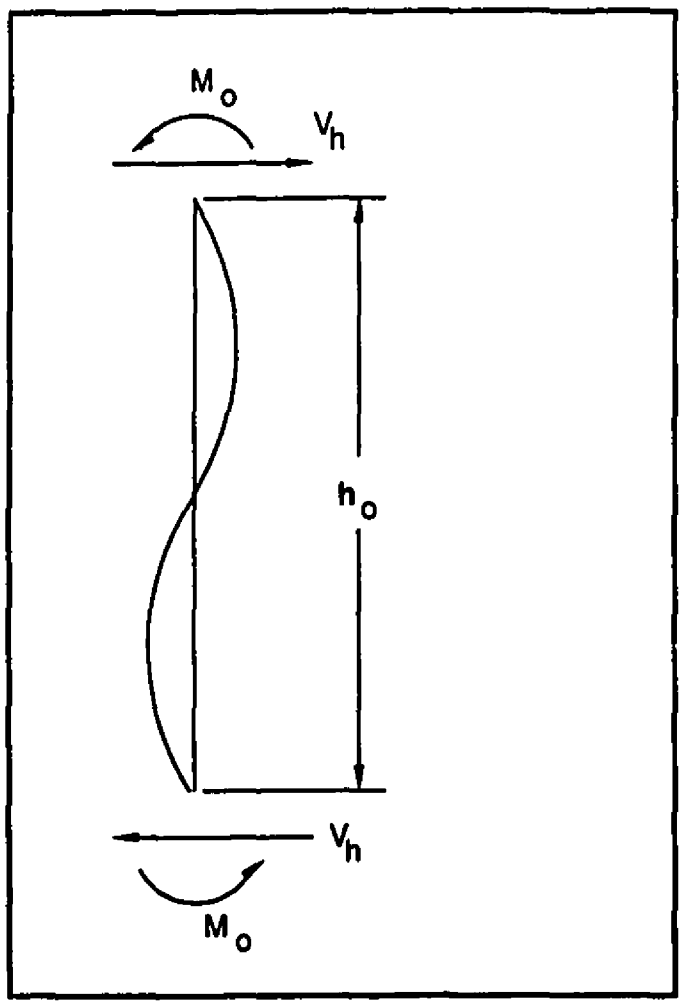


**Fig. 1.4:** Typical Web Post Modelling (Aglan and Redwood 1974)

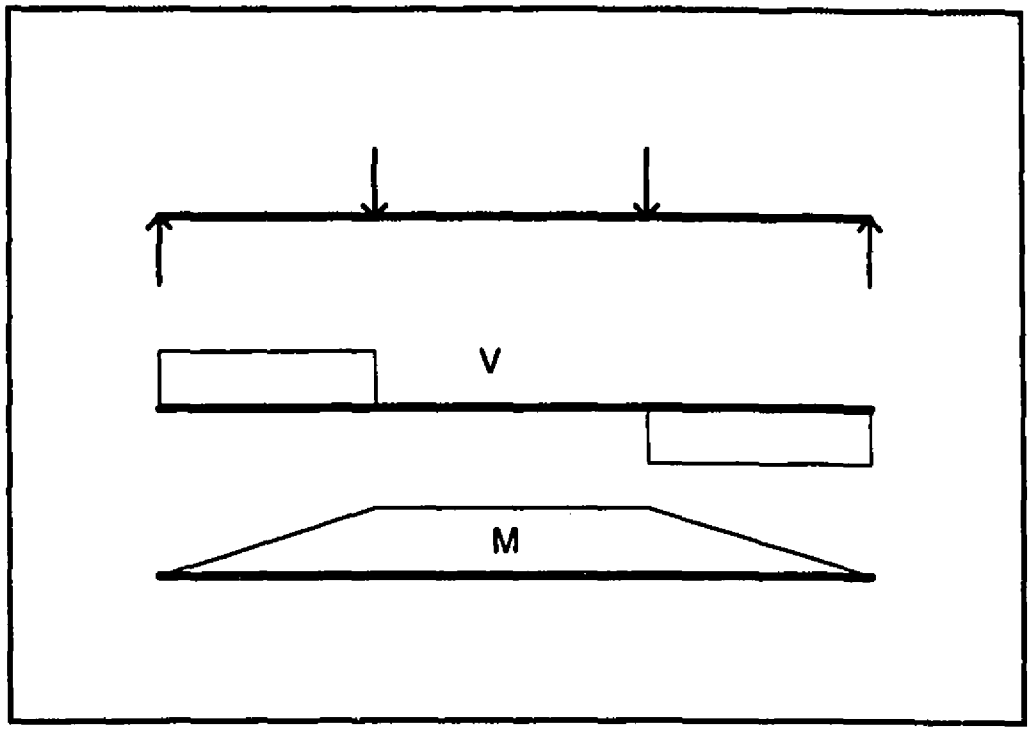


**Fig. 1.5:** Shear and Moment Diagram

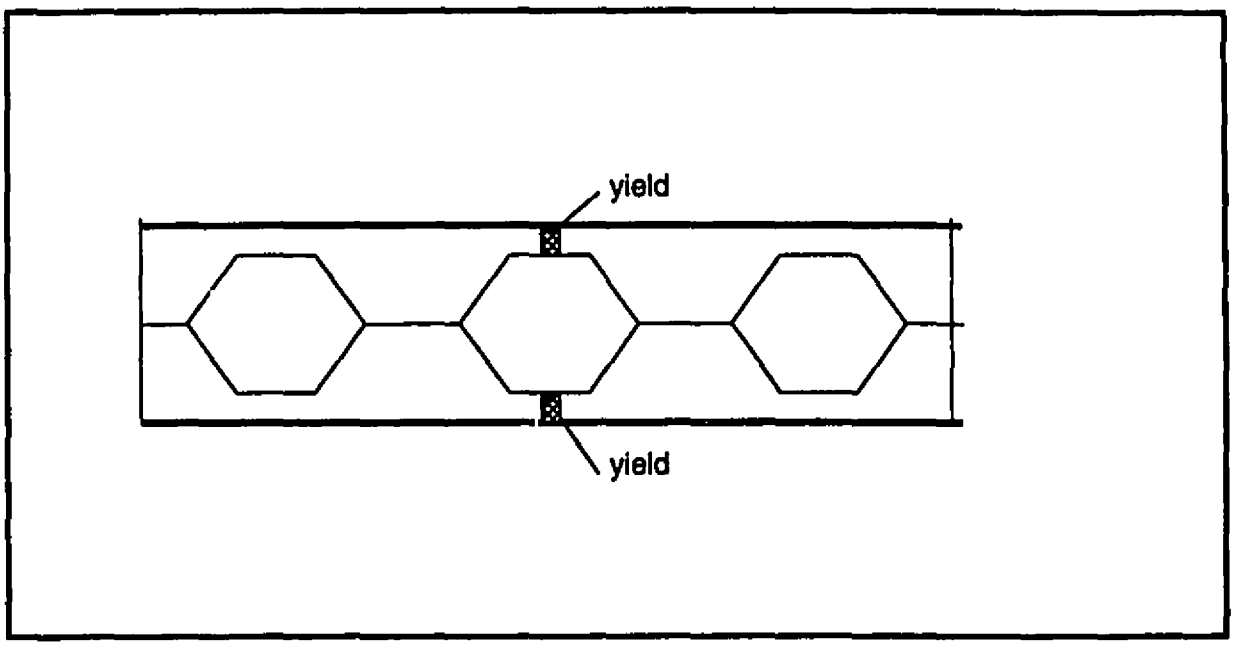


**Fig. 1.6:** Yield of Upper and Lower Tee

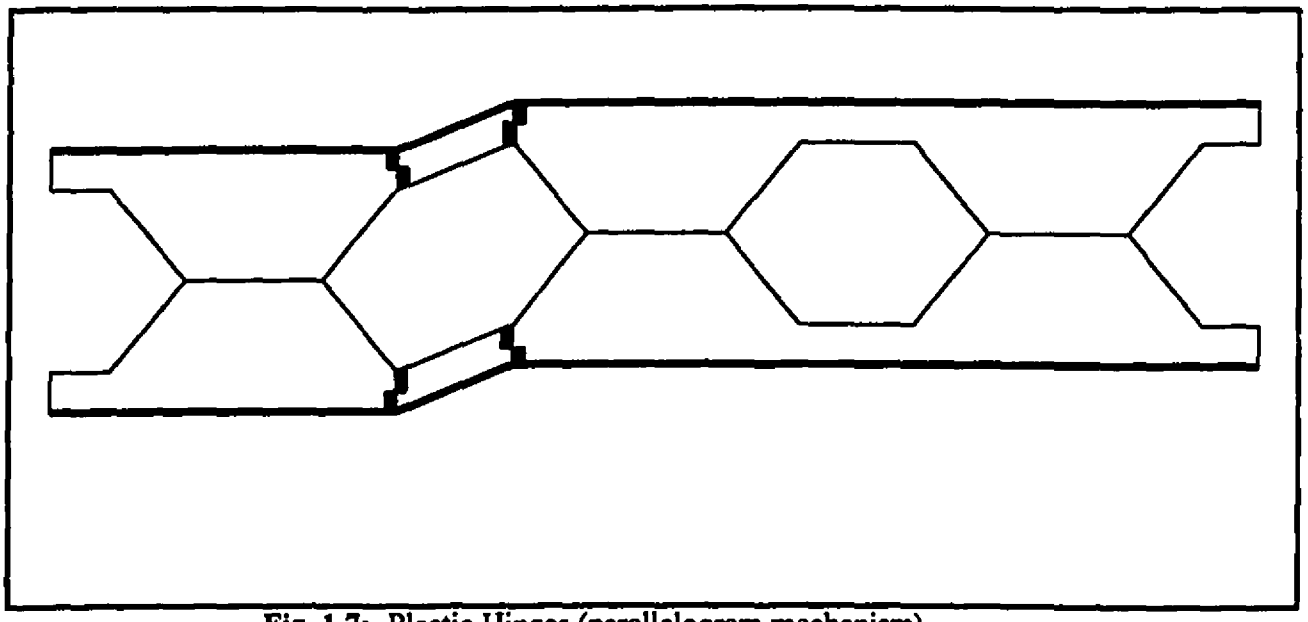

**Fig. 1.7:** Plastic Hinges (parallelogram mechanism)

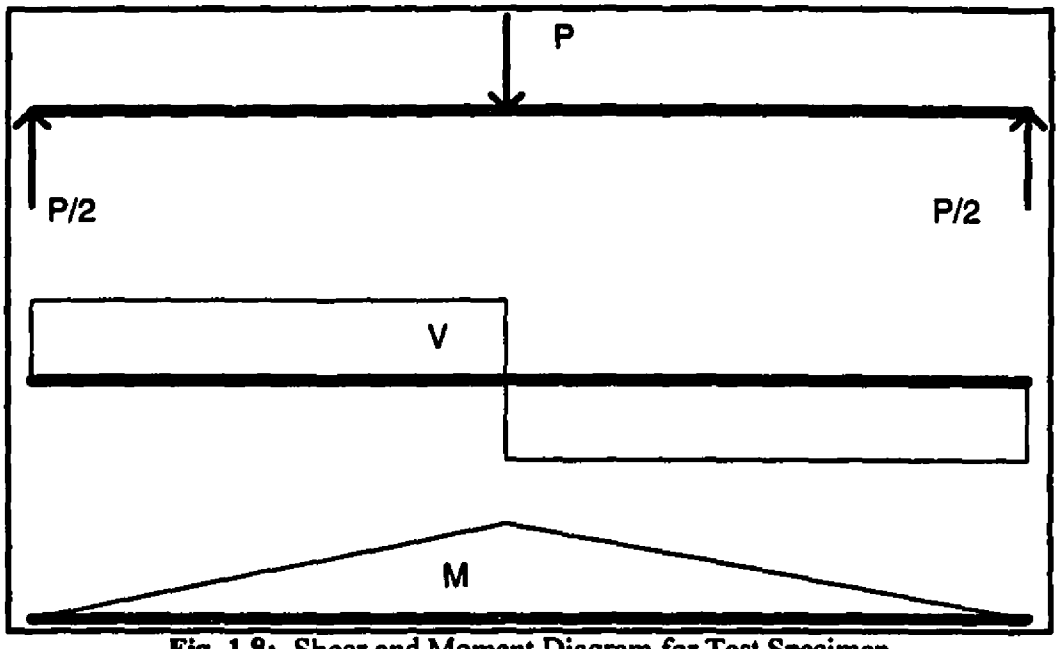


**Fig. 1.8:** Shear and Moment Diagram for Test Specimen

# Chapter 2

## Analysis

In this chapter, methods of analysis of castellated beams are summarized. These methods describe elastic stress analysis, overall and local (parallelogram) yield mechanism analysis and analysis of web post yielding and buckling.

### 2.1 Elastic Stress Distribution

Elastic analysis of castellated beams has been carried out in a manner similar to the method of solution traditionally used for Vierendeel Trusses. At each hole, bending and shear are transmitted by the top and bottom tee section (Mandel *et al.* 1971). On the assumptions of Vierendeel action, the longitudinal stress at the junction of tee and post consists of two components: the component due to bending $\sigma_m$, and the component due to shear $\sigma_V$. The total longitudinal stress $\sigma = \sigma_m + \sigma_v$.

#### 2.1.1 Bending Moment

Referring to Fig. 2.1, for a portion of a beam under pure bending moment, flexural stresses are found using the following assumptions:

- At the upper and lower tee section of the web opening (throat), flexural stresses are considered uniform, (Fig. 2.1), section A-A.

- At the solid section, the bending moment stress is assumed to vary in a straight line from the centerline of the beam, (Fig. 2.1), section B-B.

Therefore;

$\sigma_m = Mc/I$ where I = moment of inertia of the solid section.

Due to the first assumption, the flexural stresses in the tee-section give resultant normal forces acting at the centroid of this section (Fig. 2.2), and the following relations are derived (Altfillisch 1957):

$$M = N(d - 2y_t)$$

$$\sigma_m = \left(\frac{M}{d - 2y_t}\right)\left(\frac{1}{A_t}\right) \quad \text{.....[2.1]}$$

where:

M = bending moment at the throat section under consideration

$y_t$ = distance from extreme fiber to centroid of tee-section

$A_t$ = area of tee-section

$\sigma_m$ = normal stress caused by bending

N = normal resultant force at tee-section

### 2.1.2 Shear

A shear, V, at a section through the tee-section, is assumed to be resisted equally by the regions above and below the hole, (Fig. 2.3). This shear induces a secondary moment at the open-web tee-section. Assuming a point of inflection at mid-length, the

force V/2 at a distance of e/2, produces a secondary moment of $V_e/4$ . The, maximum stress occurs at the section in which the open web begins to vary in depth.

The resulting equations are as follows:

$$\text{knowing} \quad \sigma = \frac{Mc}{I}$$

$$\Rightarrow \qquad M = \frac{e}{2} \times \frac{V}{2} \quad \text{and}$$

$$\sigma_v = \frac{eV}{4} \times \frac{y_t}{I_t} \text{ or } \sigma_v = \frac{eV}{4} \times \frac{y_b}{I_t} \qquad \text{.....[2.2]}$$

where:

e = tee-section section length

V = shear at section

$y_t$ = distance from flange to centroid at tee-section

$y_b$ = distance from inner edge (at the cut) to centroid of tee-section

$I_t$ = moment of inertia of one tee-section

In conclusion, if both shear and moment are present, the maximum bending stress is calculated by the algebraic sum of equations [2.1] and [2.2], and the resulting stresses are shown in Fig. 2.4. Therefore, the total flexural stress in the tee-section, is a combination of a direct stress due to the normal force, and a secondary flexural stress due to the vertical shear. A spreadsheet was developed to perform the necessary calculations and to determine the stresses at the critical section. Samples are included in Appendix B.

It should be noted that the secondary stress can be reduced by decreasing the moment-arm, e/2; however, e is also the length of the welded web post joint, (Fig. 2.3). Too narrow a joint might cause the beam to fail along the weld (Hosain and Speirs 1971).

## 2.2 Shear at Welded Joints

The horizontal shear load which will cause yielding and rupture of the welded web-post joints was calculated. A spreadsheet was developed to simplify the repetitive calculations for different geometries of the castellated beams. A sample of this spread-sheet is included in Appendix B.

A free-body diagram section is taken between the center-lines of two adjacent openings and the weld at the intersection of the two halves (Redwood 1968). Referring to Fig. 2.5, the shearing force acting along the welded joint, is represented by $V_h$, and the relevant equations, by using the equilibrium equations, are as follows (Hosain and Spiers 1971; Altfillisch 1967):

Since $d = (d_g - 2y_t)$ from Fig. 2.5

$V \times S = M_2 - M_1$ from equilibrium in Fig. 2.4

$$V_h = \frac{V \times S}{d} \quad \text{from Fig. 2.5} \qquad \text{...[2.3]}$$

$$\therefore \quad \tau_n = \frac{M_2 - M_1}{d \times e \times t_w} \quad \text{where} \quad \tau_n = \frac{V_h}{t_w \times e}$$

If $\tau_n$ is taken as equal to the yield in shear, $\frac{F_y}{\sqrt{3}}$, $V_h$ may then be calculated and related to the applied load.

## 2.3 Formation of Mechanism (plastic analysis)

This plastic design is based on a method discussed by Redwood (1978). This procedure was again developed in a spreadsheet to facilitate the computation of the load that can cause the formation of this mechanism for different geometries of castellated beams. The method involves the collapse of a beam by the formation of a parallelogram mechanism, (Fig. 1.7). For the beam to attain this plastic failure, the web and flanges should remain stable up to the formation of the plastic hinges at the corners of an opening in a region of high shear force. As the load increases, the four corners form plastic hinges due the combined primary and secondary stresses resulting from the moment and shear that are acting at the reduced section. The result of this analysis can be expressed in the form of an interaction diagram relating $M/M_p$ and $V/V_p$. This gives a failure surface which provides the set of ratios $V/V_p$ and $M/M_p$, at which failure occurs. The related equations are as follows;

$$\frac{M}{M_p} = \frac{1-\frac{A_w}{4A_f}\left(1-\frac{h_o}{d_g}\right)\frac{1}{\sqrt{1+\bar{\alpha}}}\left[2k_1\left(1+\frac{k_1}{2}\right)-1-\frac{h_o}{d_g}(1-k_1)^2\right]}{1+\frac{A_w}{4A_f}} \quad \text{.....[2.4]}$$

where: $\bar{\alpha} = \alpha k_1^2 (2-k_1)^2$ and $0.0 \le k_1 \le 1.0$

and $\alpha = \frac{3}{16}\left(\frac{d_s}{\frac{e}{2}}\right)^2\left(1-\frac{h_o}{d_g}\right)^2$

and

$$\frac{V}{V_p} = \left(1-\frac{h_o}{d_g}\right)\sqrt{\frac{\bar{\alpha}}{1+\bar{\alpha}}} \quad \text{.....[2.5]}$$

where:

$A_w$ = area of web

$A_f$ = area of one flange

$h_o$= total height of opening

$d_g$ = total depth

$M_p$ = plastic moment

$V_p$ = plastic shear

A straight line, which passes through the origin, with a slope of $\frac{M}{M_p}$ over $\frac{V}{V_p}$, which is equivalent to $\ell'\left(\frac{V_p}{M_p}\right)$, where $\ell'$ is the moment-to-shear ratio, is drawn on the same interaction diagram.

Knowing;

$$V = \frac{P}{2}$$

$$M = \frac{P}{2} \times \ell' \qquad \therefore \frac{M}{V} = \ell' \text{.....[2.5a]}$$

$$\therefore \frac{\frac{M}{M_p}}{\frac{V}{V_p}} = \frac{M}{V} \times \frac{V_p}{M_p} = \ell' \times \frac{V_p}{M_p} \text{.....[2.5b]}$$

The intersection of this line with the failure surface represents the values of $\frac{M}{M_p}$ and $\frac{V}{V_p}$ which will cause the failure mechanism at that opening. A sample of this analysis is included in Appendix B.

## 2.4 Buckling Analysis

Three approaches to the lateral-torsional buckling analysis of the web post were considered. One buckling analysis was performed with the finite element package NASTRAN. The details of this analysis will be discussed in a following chapter. The other two analysis were based on a study by Aglan and Redwood (1974), and by Blodgett (1963).

### 2.4.1 Aglan and Redwood (1974)

The web post is considered to be acted upon by two equal and opposite end moments and shearing forces, (Fig. 1.4). The post will undergo lateral buckling accompanied by simultaneous rotation at a critical moment $M_{o\,cr}$. This may be related to shearing force at the ends of the post, $V_{h\,cr}$, by the relation, $V_{h\,cr} = \frac{M_{o\,cr}}{\frac{h_o}{2}}$. The stress-strain curve of the material of the post is considered as tri-linear elasto-plastic strain hardening. The governing differential equation is obtained and is solved using a finite difference approximation. The equations obtained involve the mechanical properties of the sections at the nodal points. These were computed at each node, depending on the

load level and the corresponding elastic or inelastic stress distributions. The finite difference equations can be arranged in the following form:

$$(C - \lambda I)\, X = 0 \quad \text{.....[2.7]}$$

where

C non-symmetric matrix

$\lambda$ eigenvalue ($\lambda = 1 - M_{oi}$ where $M_{oi}$ is the critical end moment acting on the post)

I identity matrix

X eigenvector

Results were presented as a series of graphs which may be used as design aids. Fig. 2.6 is a sample of such graphs. To make use of these, the following parameters, which are presented in Figs. 2.7 and 1.2, are needed ;

- the ratio of hole height to min. width of web, $h_o/e$
- the ratio of min. web post width to web thickness, $e/t_w$
- the ratio of height of intermediate plate to total height of hole, $h_p/h_o$
- the angle of inclination to the horizontal of the corners of the castellations, $\phi$

From the graphs, the ratio of $\frac{M_{o\,cr}}{M_p}$ is obtained based on the above parameters. Knowing $M_p = 0.25 \times t_w \times F_y \times (S-e)^2$ the value of $M_{o\,cr}$ may be obtained. $V_h$ may be calculated as $V_h = \frac{M_{o\,cr}}{\frac{h_o}{2}}$. The vertical shear at the section is then given by

$V = \frac{\left( V_h \times 2 \times \frac{(d_g - 2y_t)}{2} \right)}{S}$. For the test set-up used in this study, the applied load at mid-span of the beam that will cause lateral torsional buckling of the web post is 2×V. A spread-sheet was developed to generate the values need to use the design aid graphs.

### 2.4.2 Blodgett

The Wedge Method, originally proposed by W. R. Osgood and later modified by H. C. Olander, was used to analyze the section, shown in Fig. 2.9. The non-parallel sides are extended out to where they intersect, at point 0. Taking this point as center, an arc is drawn through the wedge section. This will create section, a. The forces and moments applied to the section are then transferred to point 0, where the horizontal force , $V_h$, causes a moment at that point, Fig. 2.9a. These force and moments acting at point, 0, cause the bending stresses on the curved section, a, shown in Fig. 2.9b, (Blodgett, 1963). The above approach results in the greatest bending stress along "a".

$$\sigma_{r_{(max)}} = \frac{3V_h \tan(\theta)}{4t_w e(\theta)^2} \quad \text{.....[2.8]}$$

Using the 1978 AISC design code the allowable compressive bending stress along the sloping edge of the wedge section of the web is determined. This is done by considering the web post of height, $h_o$, (Fig. 2.8), to be a prismatic member, and then applying the column buckling stress formulae from AISC (1978), the following is then obtained:

when $\sqrt{\frac{102\times10^3\times C_b}{F_y}} \le \frac{\ell}{r_t} \le \sqrt{\frac{510\times10^3\times C_b}{F_y}}$

$$F_b = \left[\frac{2}{3} - \frac{F_y\left(\frac{\ell}{r_t}\right)^2}{1530\times10^3 C_b}\right] F_y \quad \text{.....[2.9a]}$$

when $\frac{\ell}{r_t} \ge \sqrt{\frac{510\times10^3\times C_b}{F_y}}$

$$F_b = \frac{170\times10^3\times C_b}{\left(\frac{\ell}{r_t}\right)^2} \quad \text{.....[2.9b]}$$

where:

$\ell = h_o$

$r_t$ = radius of gyration, $\frac{t_w}{\sqrt{12}}$

$A_f$ = area of compression flange

$$C_b = 1.75 + 1.05\left(\frac{M_1}{M_2}\right) + 0.3\left(\frac{M_1}{M_2}\right)^2 \quad \text{but} \quad \le 2.3$$

where, $M_1 = M_2 = M$, is shown in Fig. 2.8

Equating the maximum bending stress from [2.8] to the allowable $F_b$, from [2.9], the resulting equation is;

$$\tau \le \frac{4\times(90-\phi)^2}{3\times\tan(90-\phi)} \times F_b \quad \text{.....[2.10]}$$

and $V_h = \tau \times t_w \times e$ .....[2.11]

From $V_h$, the value of the transverse shear which will cause lateral torsional buckling of the web post can be determined.

$$V = \frac{V_h \times (d_g - 2y_t)}{S}$$

But the AISC is an allowable stress method, therefore the result must be multiplied by a factor of 1.67 to get the actual stress.

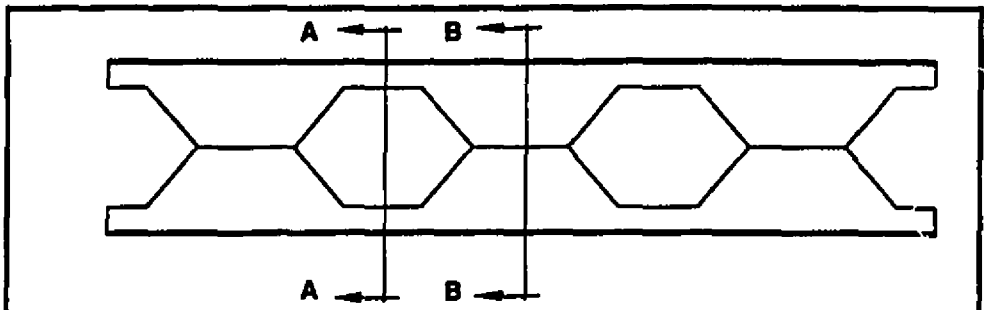


Fig. 2.1: Elevation View

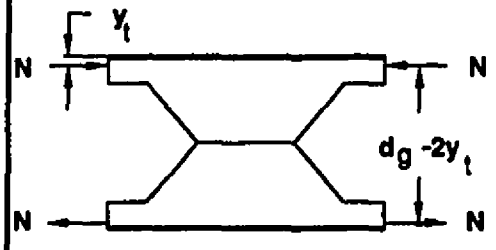


Fig. 2.2: Longitudinal Forces

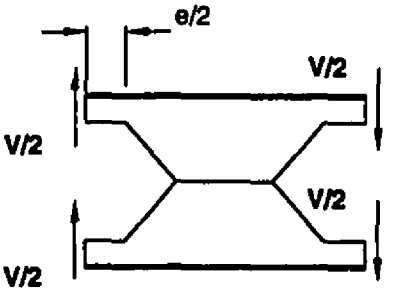


Fig. 2.3: Transverse Forces

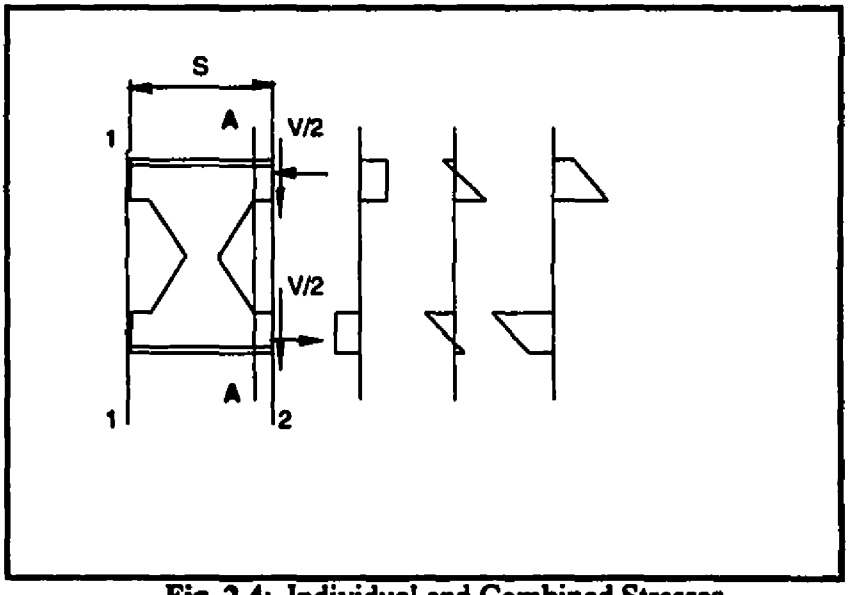


**Fig. 2.4: Individual and Combined Stresses**

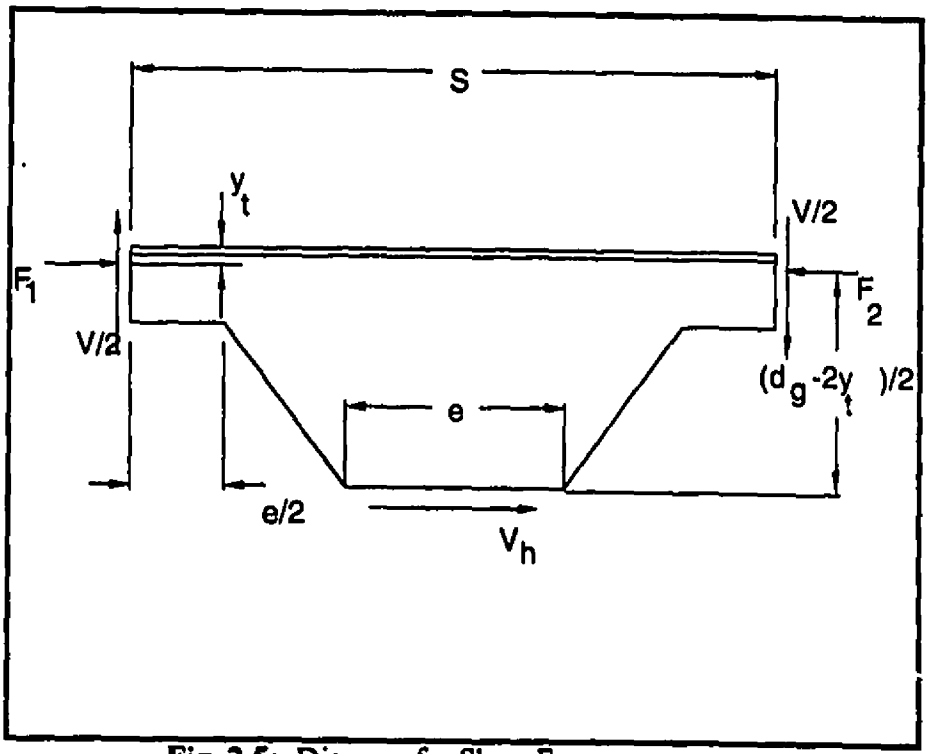


**Fig. 2.5:** Diagram for Shear Force

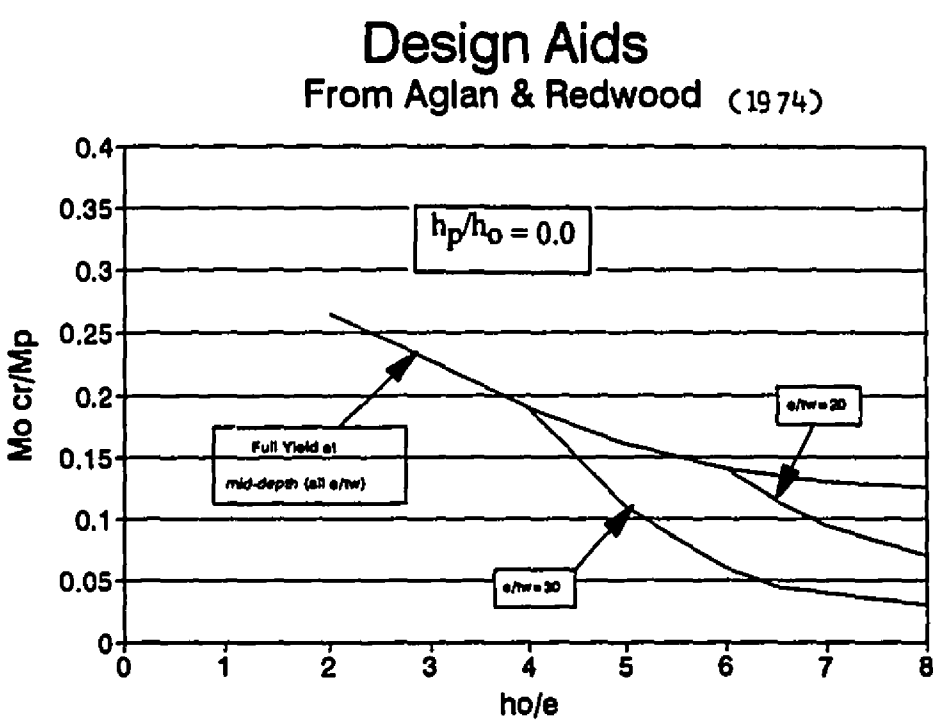


phi=45

**Fig. 2.6:** Design Aids

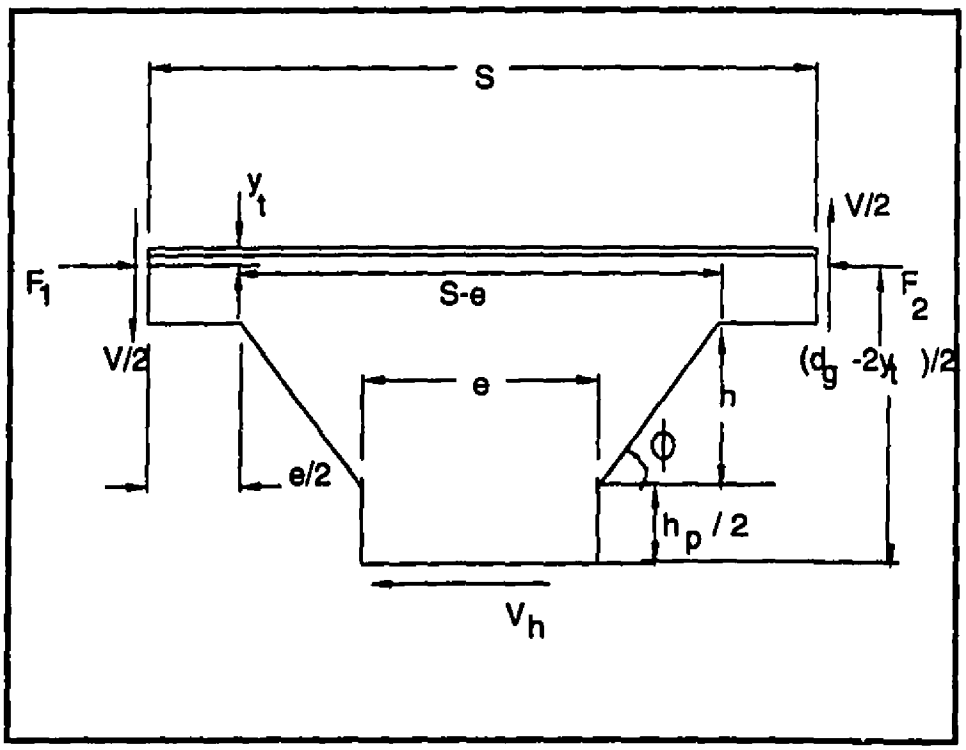


**Fig. 2.7:** Section With Intermediate Plate

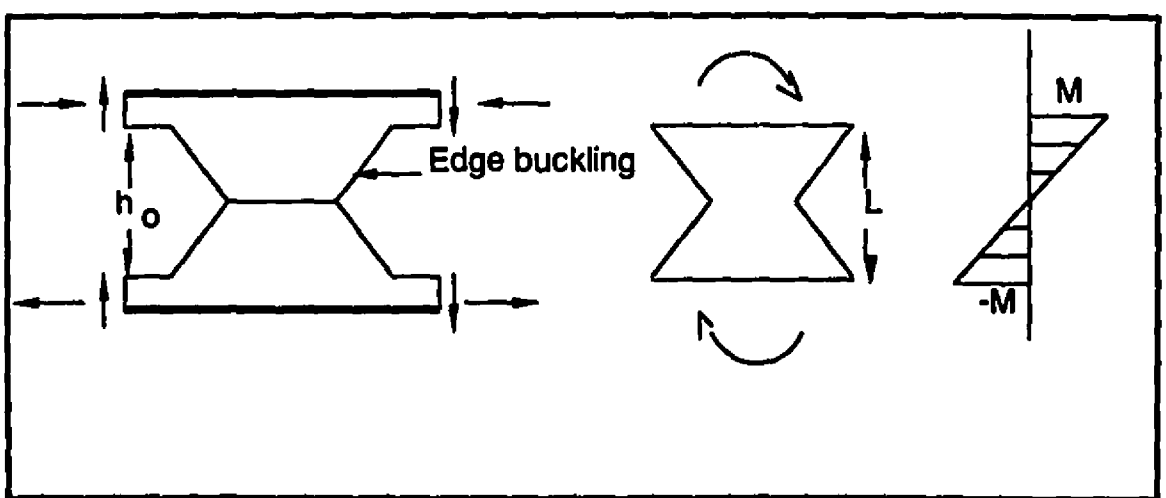


**Fig. 2.8:** Buckling (Blodgett 1963)

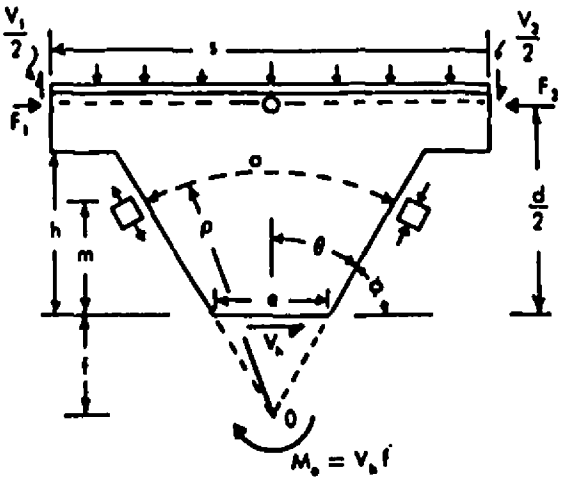


Fig. 2.9a

a: arc drawn through the wedge section

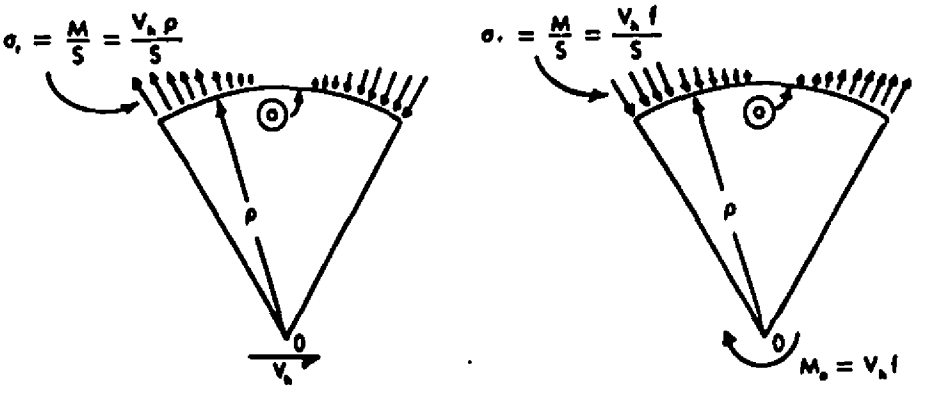


Fig. 2.9b

**Fig. 2.9:** Buckling Stresses (Blodgett 1963)

# Chapter 3

## Finite Element Analysis

### 3.1 Introduction

This chapter describes the use of the finite element method to analyze the web post buckling, taking into account the inelastic behavior of the material. The finite element program MSC/NASTRAN was used. An overview of the capabilities, theory and solution strategies available in this program, as related to the needs of this study, are presented. Specific options used and their corresponding parameters are referenced.

### 3.2 Analytical Options

#### (a) Linear Structural Analysis

In a linear analysis, MSC/NASTRAN imposes the following, (Macneal-Schwendler Corp. 1991a):

- Kinematic relationship is linear, and displacements are small.
- Element compatibility and constitutive relationships are linear, and the stiffness matrix does not change. No yielding, and small strains..

- The equilibrium is satisfied in the undeformed configuration.
- Loads are independent of deformation.
- Displacements are directly proportional to the loads.
- Results for different loads can be superimposed.
- User interface is the command:
    - SOL 105
    - EIGB

**(b) Nonlinear Structural Analysis**

The nonlinear analysis capabilities in MSC/NASTRAN are the following (Macneal-Schwendler Corp. 1985; 1992a):

Geometric nonlinear analysis.

- The kinematic relationship is nonlinear.
- Displacements and rotations are large (displacement transformation matrix is nonlinear).
- Equilibrium and compatibility are satisfied in a deformed configuration.
- User interface is the command:
    - PARAM, LGDISP

Material nonlinear analysis.

- Element stiffness matrix is not constant.
- Element constitutive relationship is nonlinear. Elements may yield.
- Element forces are no longer equal to stiffness times displacements.

- User interface is the command:
    - MATS1.

The solution strategy is described in a more detailed manner in Appendix A.

Buckling analysis.

- The force transformation matrix is not the transpose of displacement transformation matrix.
- The equilibrium is satisfied in the perturbed configuration.
- User interface is the following:
    - SOL 106
    - EIGB
    - NLPARM
    - PARAM, BUCKLE

In conclusion.

- Displacements are not directly proportional to the loads.
- Results for different loads cannot be superimposed.

Material and geometric nonlinearities can be combined together.

## 3.3 Modeling of Beams

The finite element analysis was used to determine the load deflection response and buckling behavior of castellated beams. The modeling used was based on the arrangement used in the test program where the critical webs are those on either side of the mid-span load point (maximum moment and shear) as shown in Fig. 1.8. The model used for the web post, is shown in Fig. 3.1. The reason for choosing part of the beam and not the whole is to have a more refined mesh with an acceptable processing time.

### 3.3.1 Load Application

The model was loaded with the corresponding proportions of shear and moment that are acting on the beam at the section. The moment on each side of the model is replaced by horizontal forces acting at the center of gravity of the upper and lower tee-sections, which is similar to the assumptions in the previously performed analyses. The shear is split into two equal forces acting on the center of gravity of the upper and lower tee-sections. The applied forces are shown in Fig. 3.2. The point loads caused some stress concentrations. The point loads were replaced by a linear distribution of loads and the value of the buckling load which resulted from the point loads was compared to that which resulted from the linear distribution of loads. The results were the same. The variation in load application did not affect the value of the buckling load.

**Shear Force**

$$V_{(tee-section)} = \frac{P}{4}$$

where:

$V_{(tee-section)}$ = shear at the center of gravity of the tee-section

$P$ = applied load

**Horizontal Force**

$$F_x = \frac{M_x}{d'}$$

where:

$Fx$ = horizontal force at the center of gravity of the tee-section

$M_x$ = moment at section under consideration

$d' = d_g - 2y_t$

### 3.3.2 Boundary Conditions

In Fig. 3.2, the boundary conditions which were assumed in the analysis are shown. The notations X, Y and Z indicate "zero" displacement along the specified direction. The top and bottom horizontal lines in Fig. 3.2 represent the flanges. They are located in the XZ plane and are generated with four sided shell elements, one on each side of the flange. The simplest boundary conditions were adopted, that is, displacements were prevented but no constraints were imposed on rotations. (Macneal-Schwendler Corp. 1993a)

### 3.3.3 Mesh and Element Type

The final model is made up of four-sided shell elements. The first mesh was a very coarse one, (Fig. 3.3), comprising three and four-sided shell elements with a total of only 86 elements. The mesh was then refined, (Figs. 3.4 to 3.7), using only four-sided shell elements, up to a point where it consisted of 236 or 268 elements depending on the existence of an intermediate plate or not. Fig. 3.7 shows a typical model used for the analysis which includes an intermediate plate. This number of elements was chosen because it satisfied the recommended number of nodes, five on a half sign wave of a deformed shape, (Macneal-Schwendler Corp. 1988). A finer mesh was developed at the critical sections (Macneal-Schwendler Corp. 1983). The most important region was the area around the mid-height of the model. A model and its buckled shape are illustrated in Appendix A. The procedure followed to attain an adequately refined mesh was by trial method. The first mesh was a very coarse one. The second was more refined. This refinement continued until the value of buckling had converged to a specific value. At that point, it was decided to stop the refinement. This was the indicator of the accuracy

of the mesh. Table 3.1 gives a summary of the converging critical loads as the mesh is refined.

### 3.3.4 Load Convergence

The variation of the relative deflection in the y-direction obtained from the finite element analysis between hole centerlines is shown in Fig. 3.8 as the load increases. These results were obtained without buckling being considered. Thus it incorporated only geometric and material nonlinearities. In addition, the applied load value predicted to cause the mechanism failure, (Redwood 1978), is also shown. A comparison is drawn between the two results to determine the correspondence between the two failure modes. Fig. 3.8 shows that the asymptote to the Load vs. Relative Flange Deflection graph corresponds to the mechanism failure load. Specimen 8-3 failed by the buckling of the tee-section, and therefore the close correspondence between these results could be anticipated. Fig. 3.9 shows that the convergence of the Load vs. Relative Flange Deflection curve towards the value of the load which causes the mechanism failure is very slow. This indicates early widespread yield, which is consistent with experimental observations of web post buckling.

## 3.4 Application of MSC/NASTRAN

### 3.4.1 Input File

Referring to Appendix A, the capabilities of MSC/NASTRAN that are related and of use in determining the buckling load are discussed in detail. A sample input data is also included in the Appendix A, Table A.1. The input was made up of two separate files, the cold start and the restart file. A sample buckled shape of the model is also given in Fig. A.11.

### 3.4.2 Cold Start

The cold start begins with SOL 106 which specifies a nonlinear static analysis. The run is subdivided into different subcases each having a specific load to be reached, (Macneal-Schwendler Corp. 1991a). The number of increments to be used to achieve that load, in each subcase, is specified in the NLPARM option. The method for controlling stiffness update and the convergence criteria are also specified in the NLPARM card. The parameter LGDISP is used to have large displacement effects. CQUAD4 elements are used because of their nonlinear capabilities. Material properties are defined in the MATS1 card. The material properties, including the yield stress, and the stress strain curve is specified in this card; therefore, we end up with a model which is undergoing a nonlinear static analysis (Macneal-Schwendler Corp. 1992b). It has geometric nonlinearities because of the large displacement, and the material is defined to be nonlinear. The solution strategy is discussed in a more detailed manner in Appendix A.

In the cold run, the load keeps increasing, with the specified increments, until instability. At that point, the analysis is transferred to the restart option.

### 3.4.3 Restart

A restart requests that data stored in a previous run be used in the current run. The restart is initiated a couple of load steps before the instability detected in the cold run. In this run, the parameter BUCKLE is used to impose a nonlinear buckling analysis and the option EIGB defines data needed to perform the buckling analysis (Macneal-Schwendler Corp. 1992b).

**Table 3.1:** Convergence of Critical Load With Mesh Refinement (Specimen 8-2)

| Typical Mesh No. | Buckling Load FEM * (kips) |
|---|---|
| 1 | 13.48 |
| 2 | 11.89 |
| 3 | 11.32 |
| 4 | 11.10 |
| 5 | 11.10 |

* Experimental Buckling Load = 11.20 kips

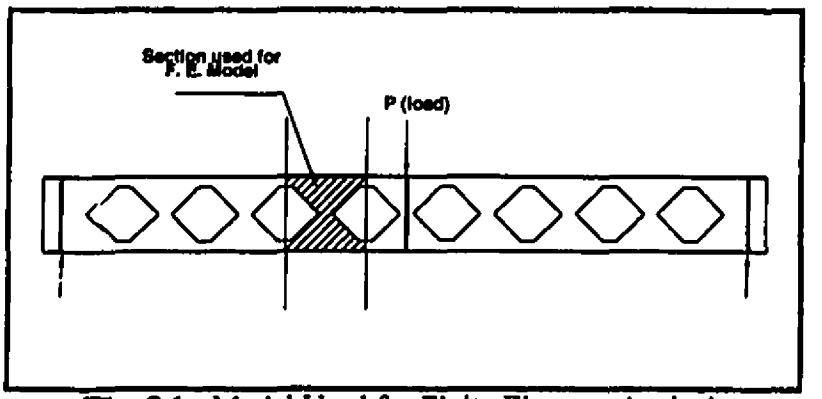


**Fig. 3.1:** Model Used for Finite Element Analysis

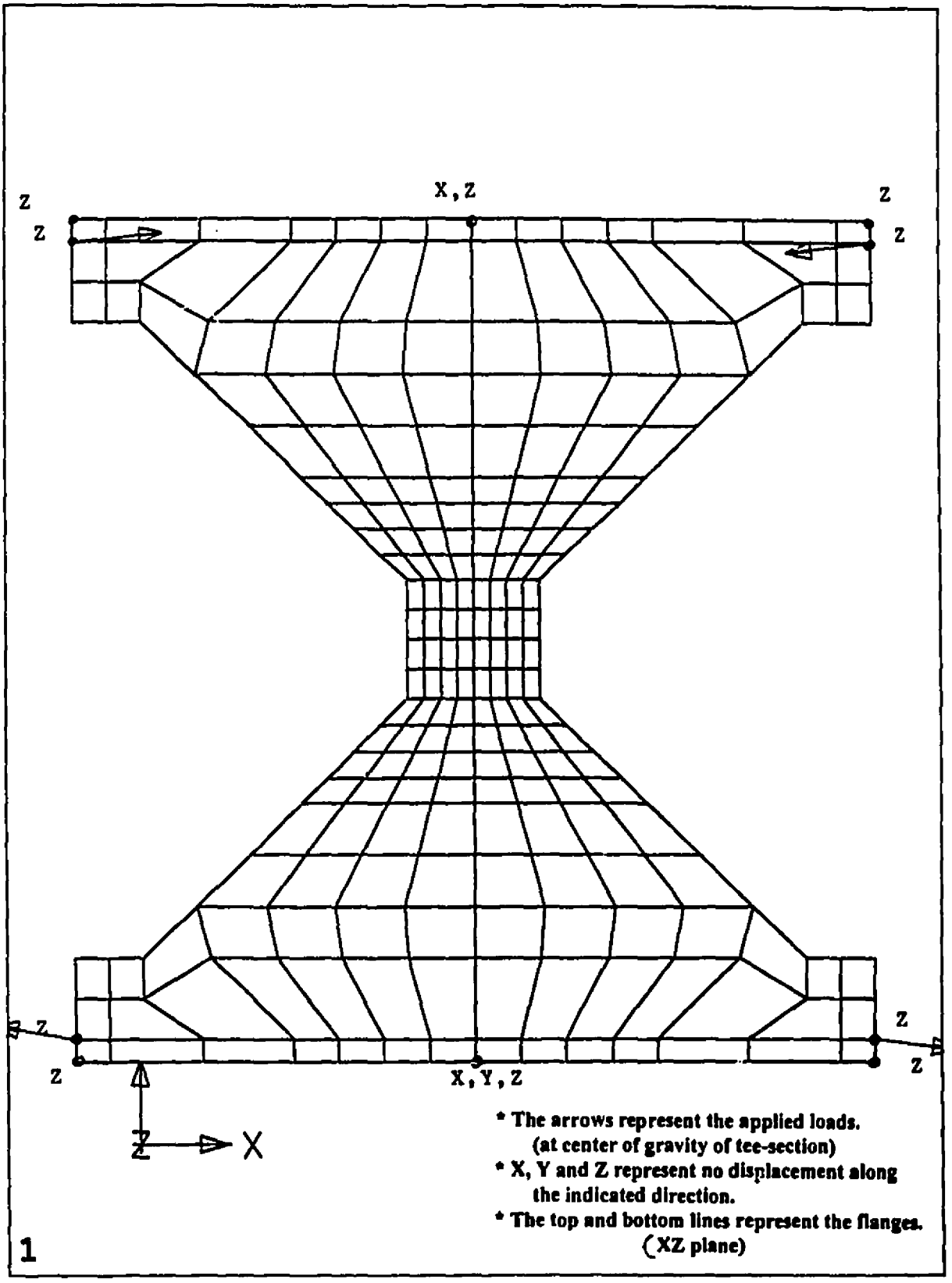


**Fig. 3.2:** Typical Mesh

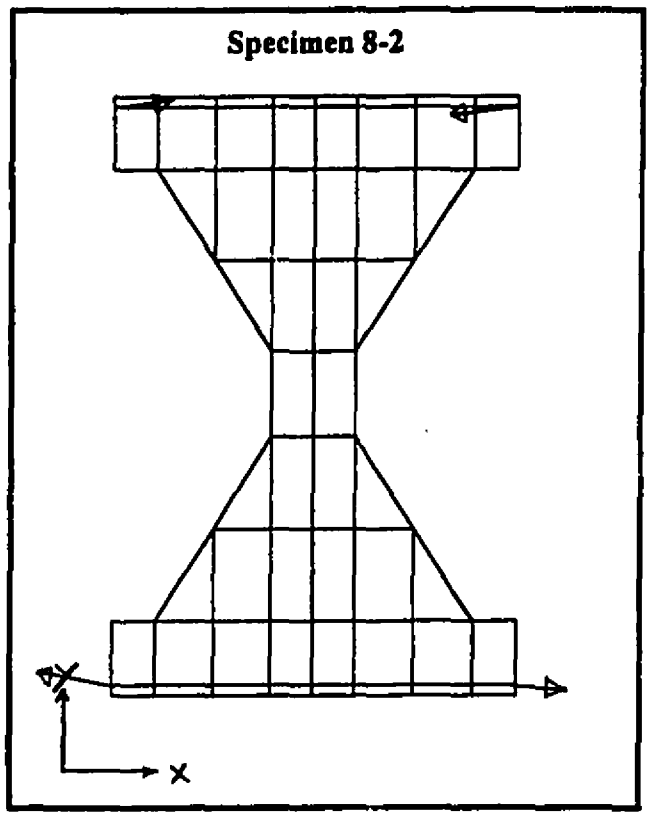


Fig. 3.3: Typical Mesh (1)

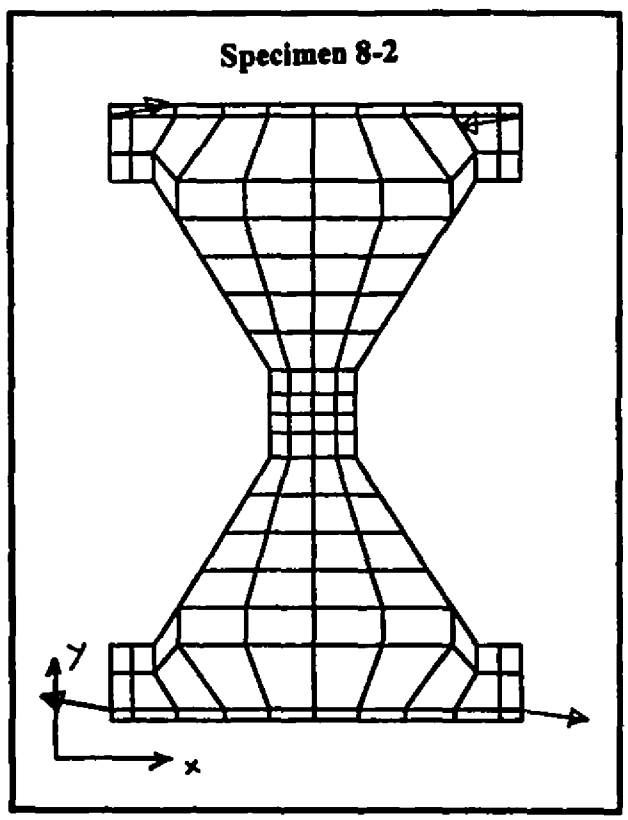


Fig. 3.4: Typical Mesh (2)

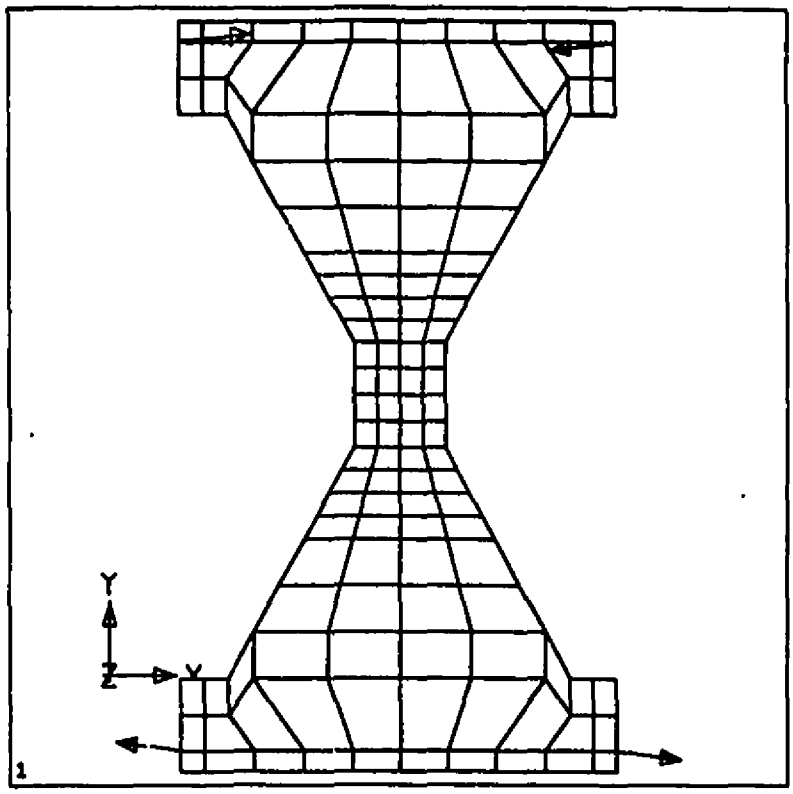


**Fig. 3.5:** Typical Mesh (3)

**Specimen 8-2**

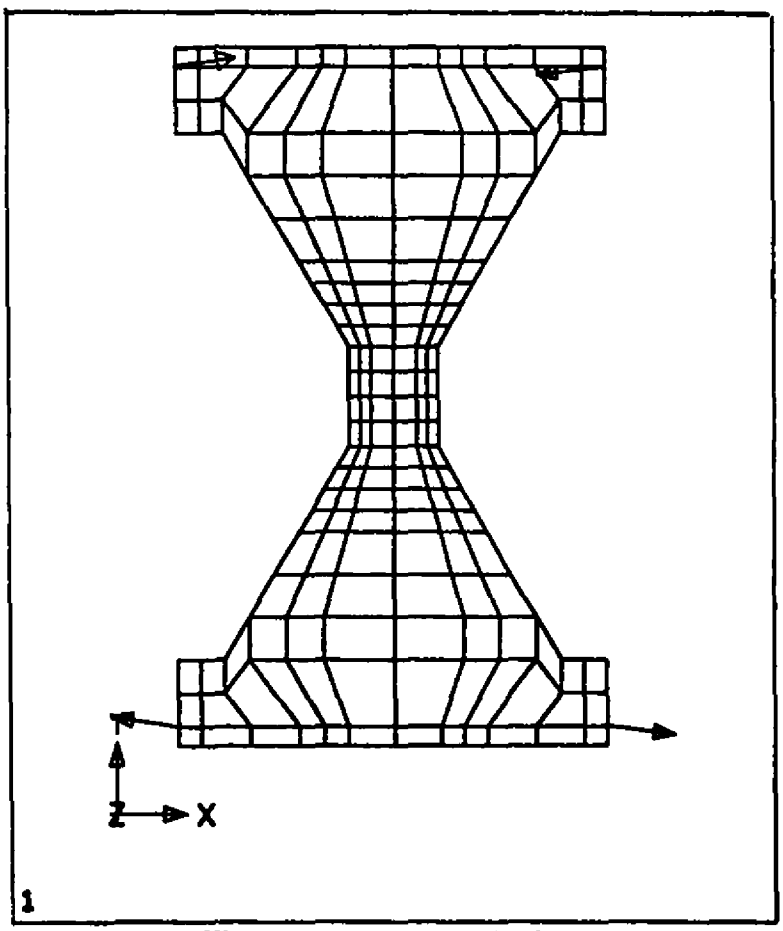


**Fig. 3.6:** Typical Mesh (4)

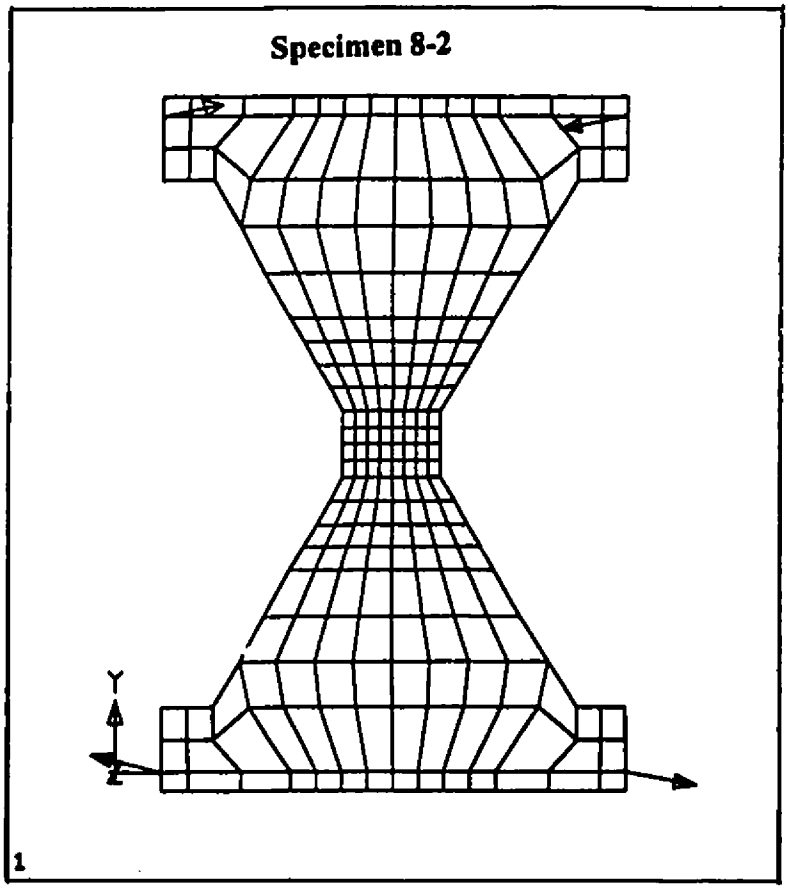


**Fig. 3.7:** Typical Mesh (5)

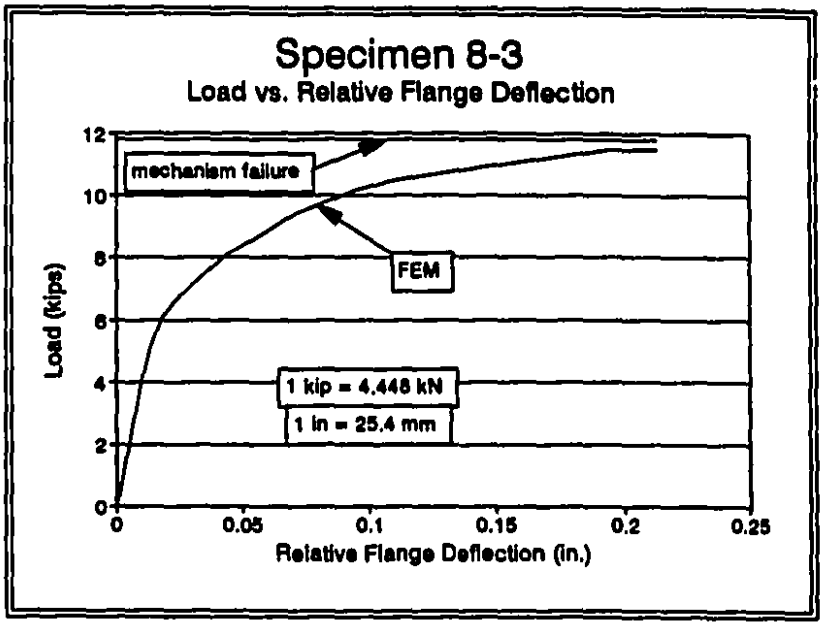


**Fig. 3.8:** Load vs. Relative Flange Deflection (8-3)

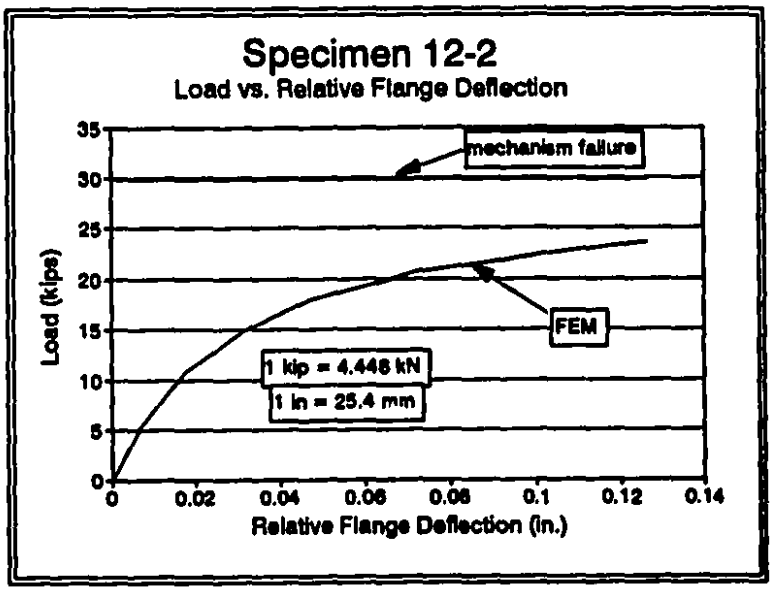


**Fig. 3.9:** Load vs. Relative Flange Deflection (12-2)

# CHAPTER 4

## Test Set-up and Test Specimen

### 4.1 Test Specimen and Section Properties

The testing of castellated steel beams was done in two stages. Pilot tests were first performed on four beams, 8-1a, 8-2a, 8-3a, and 8-4a. The objective was to develop an adequate test set-up with the proper supports and measuring instrumentation, to identify if web post buckling can, in fact, occur, and to make a preliminary evaluation of the applicability of the finite element model. Following these tests, 10 specimens, 8-3, 8-4, 10-1, 10-2, 10-3, 10-4, 12-1, 12-2, 12-3 and 12-4, were chosen for the final testing based on preliminary calculations indicating the probability of web post buckling. Specimens 8-3a and 8-4a were replicated as 8-3 and 8-4 in the final test program. The specimen dimensions are summarized in Appendix C, Table C.1. The specimens differ in their cutting pattern and the existence of intermediate plates. This variation results in a diversity of depths, number of openings and the cross sectional dimensions. A list of all the nominal dimensions is included in Appendix C. The specimens originated from Bantam beams of 8", 10" and 12".

For each specimen tested, a 1 ft. (305 mm) section of the original beam was provided for coupon testing. The mill report specified a yield value of 50.0 ksi (345 $N/mm^2$). A number of coupons were tested for the final test program to achieve a more

reliable and a better representation of the yield stress. Testing indicated an average dynamic yield strength of 49.6 ksi. (342 MPa) and a modulus of elasticity of 190000.0 MPa, based on 9 tests. This value was used for the analysis. Table 4.1 is a summary of the coupon testing. It indicates the number of tests, the cross sectional area, the location from where the coupons were taken (web or flange), the yield and ultimate loads as well as the yield stresses. From the start of loading of the coupons until strain hardening was well established, the rate of loading was 0.002 in/min. (0.051 mm/min.) for each inch of gauge length, which was 1.97 in. (50.0 mm). After strain hardening and up until failure, the rate of loading is increased to 0.02 in/min. (0.5 mm/min.) for each inch of gauge length.

## 4.2 Measurements

Initial measurements were taken for the beam dimensions. In addition to that, the beam camber, sweep, and the out-of-plane deflections in the web above and below the weld line were measured. These values are listed in Table 4.2.

## 4.3 Test Set-Up

### 4.3.1 Vertical End Supports

The supports used should provided minimum restraint to the beam. Based on this, the beams were supported at the ends by two rollers. The rollers were placed directly under the bearing stiffeners.

### 4.3.2 Load Application

The load was applied using a Baldwin 440 kips. (1960 kN) capacity test machine. The beams were loaded with a concentrated force at the mid-span. The resulting shear and bending moment diagrams are shown in Fig. 1.8 The load was applied at a small offset distance from the centre-line of the beam, to initiate failure on one side, through a steel plate of dimensions 3.9×5.9 in. (89×150 mm.) and a thickness of 0.8 in. (20 mm.), as shown in Fig. 4.1. The load offset was 1 " (25.4 mm). The plate was positioned with the long edge perpendicular to the beam axis , and was placed over the stiffener located at mid-span of the beam in order to avoid any local failures or indentations. This plate was loaded through a roller. A load cell was used. The beam was kept in place by the head of the Baldwin machine, Fig. 4.1.

### 4.3.3 Lateral Supports

Lateral supports were provided at the top and bottom flanges of the beam. They were provided by a frame supporting adjustable greased plates. The locations of the lateral supports are shown in Fig. 4.2. The frames were placed in position on the base, aligned properly and then welded in place. The adjustable plates were welded to threaded bars which fitted into the channels providing fine adjustment using nuts on each side of the channels to hold the plates in position. A very small clearance was allowed between the adjustable plates and the flanges during testing to avoid any external resistance Fig. 4.3.

In order to avoid lateral torsional buckling of the overall specimen calculations were based on CAN/CSA-S16.1-M89 (CSA 1989). Some modifications were incorporated in computing the torsional constant to take account of the holes. The area of

the holes was subtracted from the total area of the web to represent the decrease in stiffness. The steps that were followed are:

- Determine the section class
- Determine the value of $M_u$, which is:

$$M_u = \frac{\omega_2 \pi}{L}\sqrt{EI_yGJ + \left(\frac{\pi E}{L}\right)^2 I_y C_w} \quad \text{.....[2.6]}$$

where $C_w$ is calculated based on Galambos (1968)

- Compare $M_u$ to $M_p$ or $M_y$ depending on the section class
- Determine $M_r$

Due to the mode of application of the load, the location of the load point could be considered to be laterally supported. To be conservative, the $\omega_2$ values were assumed as 1.0 in the middle sections and 1.75 at the ends.

### 4.3.4 Bearing Stiffeners

Bearing stiffeners were provided 3 " (76.2 mm) from the ends , on both sides, and at the mid-span of the castellated beam specimens. The dimensions of the stiffeners were based on CAN/CSA-S16.1-M89, Clause 15.6, and they were designed as columns in accordance with Clause 13.3. The main column section was assumed to be made of the pair of stiffeners and a strip of the web equal to not more than 25 or 12 times its thickness for stiffeners located at the interior or at the ends of the web respectively. The effective length was taken as 3/4 of the length of the stiffeners.

## 4.4 Instrumentation

### 4.4.1 Strain Gauges

The load was offset to one side, therefore that side was provided with a more complete system of instrumentation. The other side had only minimum measuring devices, as a precaution in case failure unexpectedly occurred on that side. The strain gauge locations are indicated in Figs. 4.4. The beam was marked at the locations where the strain gauges should be positioned. These areas were ground, cleaned and smoothed. The gauges were then installed. The position of gauges in pairs such as 1-2 and 3-4, was to detect the buckling of the web post. The strain gauges were oriented parallel to the edge of the hole, and were located on opposite sides at a distance of 0.4 in. (10.2 mm.) from the edge. It is seen from the test results that as the load initially increases, the strain pairs move together. As the load gets closer to the buckling value, they diverge, which allows interpretation of the value of the buckling load. The location of gauge 5 was for observing one of the critical points where a combination of moment and shear (which causes a secondary moment) can cause a high stress concentration which may lead to the plastification of that section. Gauge 5 was located at the centre of the flange and oriented parallel to the axis of the beam.

### 4.4.2 Vertical Deflections

LVDTs were provided to measure vertical deflections. The values of deflection vs. load at mid-span were plotted. In addition, relative deflections between adjacent LVDT's were plotted. The objective was to determine the overall beam profile during deflection and to detect sudden changes in adjacent LVDT's. Their locations are specified in Fig. 4.4.

### 4.4.3 Jig for Web Deformations

A jig was made to measure the initial web profile and the deformed web profile at each load increment. The jig was supported on the top and bottom of the web by two pairs of adjustable screws attached to the jig and resting on the web, as close as possible to the flanges. The screws were adjusted on a flat surface to eliminate any rocking. The jig was held in position by a pair of springs which wrapped around the beam. The jig had moveable arms with LVDTs attached to them, Fig. 4.5. The arm could be moved across the web post, from top to bottom, and positioned at the required point along the web. The web post was marked at vertical intervals and web deflection measurements were taken at these locations. Initially, the jig was zeroed on a flat surface, thus providing a datum, then it was positioned on the web. The jig was used to measure the initial and final web profiles of the two webs closest to the load point, on both sides. During testing, the jig was positioned on the most critically loaded web post i.e. closest to the load point and on the side where the load was offset.

For the specimens which were part of the first pilot test, specimens 8-1a, 8-2a, 8-3a and 8-4a, the jig had only one moveable arm with one LVDT. That LVDT was zeroed at point 0, Fig. 5.1, and the web deformations, at each load increment, at the other points along the web were measured with respect to point 0. This yielded a very irregular profile, Fig. 5.10, and led to the use of the new jig described above.

## 4.5 Testing Procedure

The beam was positioned and lateral supports were adjusted in such a way that a sheet of paper could just be slipped between the flange and the adjustable plate. The web measuring jig was positioned on the critical web post. LVDTs were put in place and all

the instrumentation was connected. The gauges and LVDTs were then zeroed. The load was applied in increments of 400 lb. (1779 N), reducing to 200 lb (890.0 N) used near the predicted failure load of the specimens. Readings were taken after the load was stabilised at each increment. The load was increased until failure occurred.

**Table 4.1:** Summary of Coupon Testing

| Coupon From Specimen | Taken From (web/flange) | Area[1] ($\times 10^{-2}$ in$^2$) | % reduction in area | % elongation | $\sigma^2_{ult.}$ (ksi) | $\sigma_{yield}$ (ksi) |
|---|---|---|---|---|---|---|
| 8-3 | w | 7.12 | 43.4 % | 19.4 % | 70.9 | 54.5 |
| 8-4 | w | 7.11 | 41.2 % | 19.8 % | 70.6 | 54.1 |
| 8-4 | f | 9.71 | 57.8 % | 20.3 % | 66.7 | 49.4 |
| 10-2 | w | 7.20 | 41.3 % | 18.9 % | 72.6 | 51.4 |
| 10-4 | w | 7.17 | 45.3 % | 19.4 % | 72.8 | 52.2 |
| 10-4 | f | 8.46 | 41.3 % | 20.1 % | 73.3 | 49.6 |
| 12-1 | w | 9.10 | 52.3 % | 20.1 % | 66.3 | 44.8 |
| 12-4 | w | 9.10 | 48.6 % | 20.3 % | 67.3 | 45.6 |
| 12-1 | f | 10.31 | 53.9 % | 20.7 % | 66.9 | 44.6 |
| | | | | | Average yield | 49.6 |

w = from 1/4 the height of the web

f = from middle strip of the flange

[1] 1 in$^2$ = (645.16)$^2$mm$^2$
[2] 1 ksi = 6.9 N/mm$^2$

**Table 4.2:** Sweep, Camber and Web Offset **(1 in = 25.4 mm)**

| Specimen | Measured Sweep+ (in.) | Measured Camber+ (in.) | Measured Web Flatness (in.) (Max. out-of-plane deflection) | d/150 * (in.) |
|---|---|---|---|---|
| 8-1a | ——— | ——— | 0.08 | 0.08 |
| 8-2a | ——— | ——— | 0.08 | 0.09 |
| 8-3a | ——— | ——— | 0.17 | 0.08 |
| 8-4a | ——— | ——— | 0.16 | 0.09 |
| 8-3 | 0.28 | 0.16 | 0.07 | 0.08 |
| 8-4 | 0.59 | 0.20 | 0.25 | 0.09 |
| 10-1 | 0.2 | 0.08 | 0.13 | 0.10 |
| 10-2 | 0.12 | 0.04 | 0.42 | 0.11 |
| 10-3 | 0.16 | 0.16 | 0.07 | 0.10 |
| 10-4 | 0.16 | 0.08 | 0.31 | 0.11 |
| 12-1 | 0.20 | 0.08 | 0.20 | 0.13 |
| 12-2 | 0.08 | 0.12 | 0.22 | 0.14 |
| 12-3 | 0.24 | 0.04 | 0.25 | 0.12 |
| 12-4 | 0.08 | 0.28 | 0.07 | 0.13 |

+ Acceptable tolerance from CAN/CSA-G40.20-M87 is 0.24 in.
  Acceptable tolerance from AISC (1978) is 0.25 in.
* Acceptable tolerance in web flatness from CAN/CSA-G40.20-M87
  Acceptable tolerance from AISC (1978) is 0.188 in.

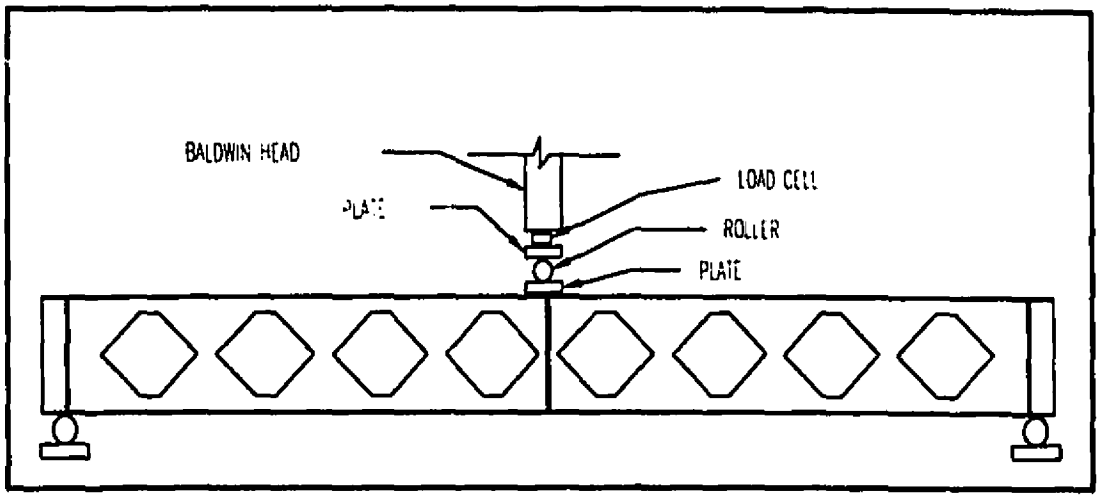


**Fig. 4.1:** Load and Support Point Details

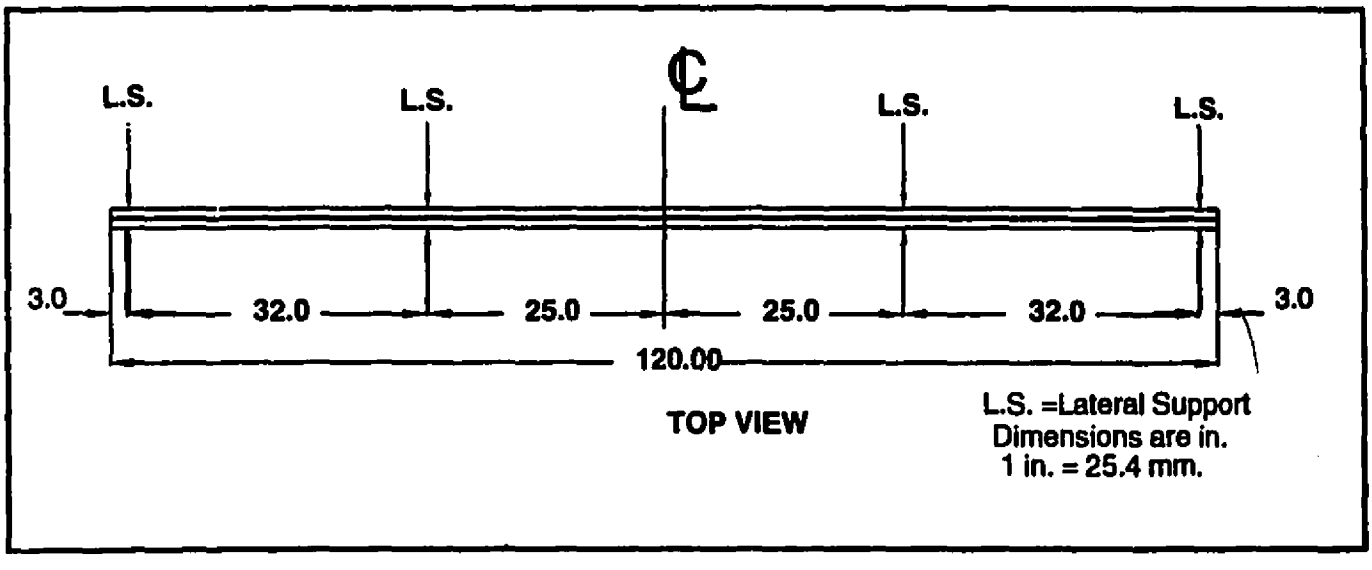


**Fig. 4.2:** Location of Lateral Supports

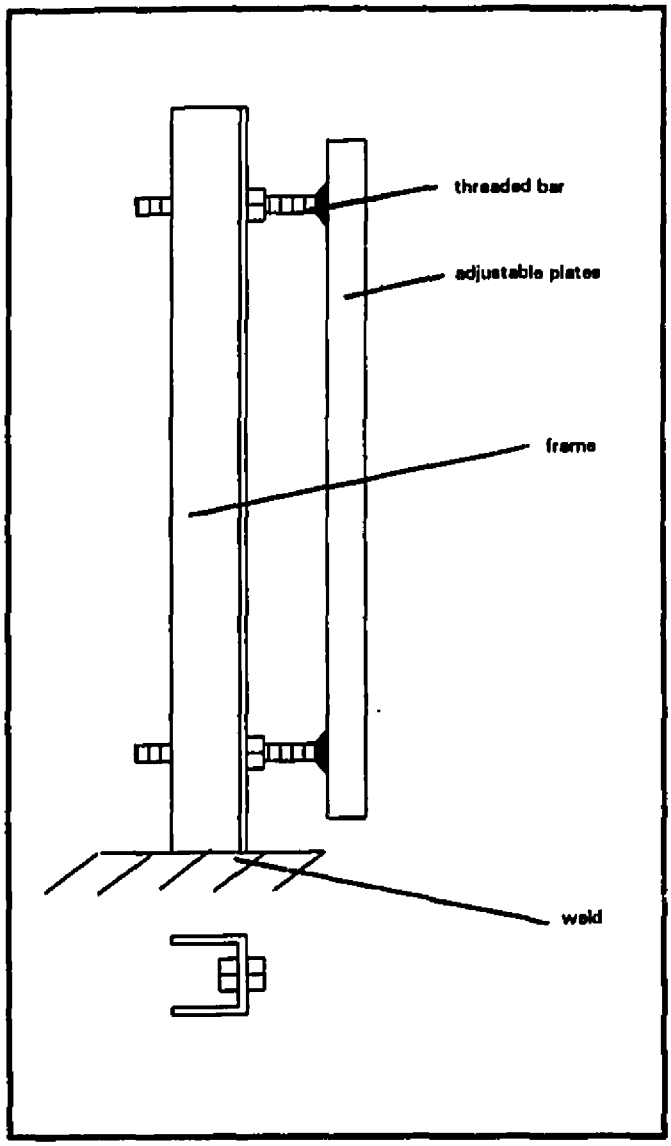


**Fig. 4.3: Lateral Support**

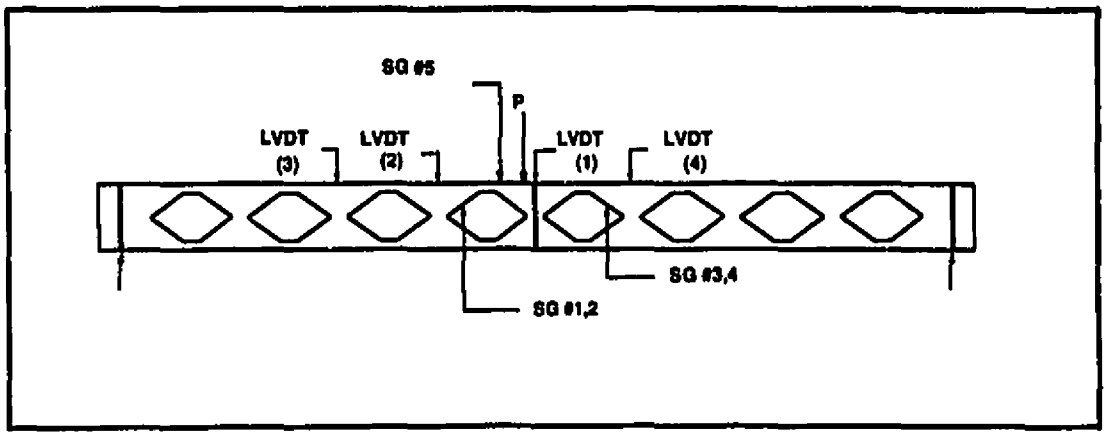


Fig. 4.4: Location of LVDT and Strain Gauges

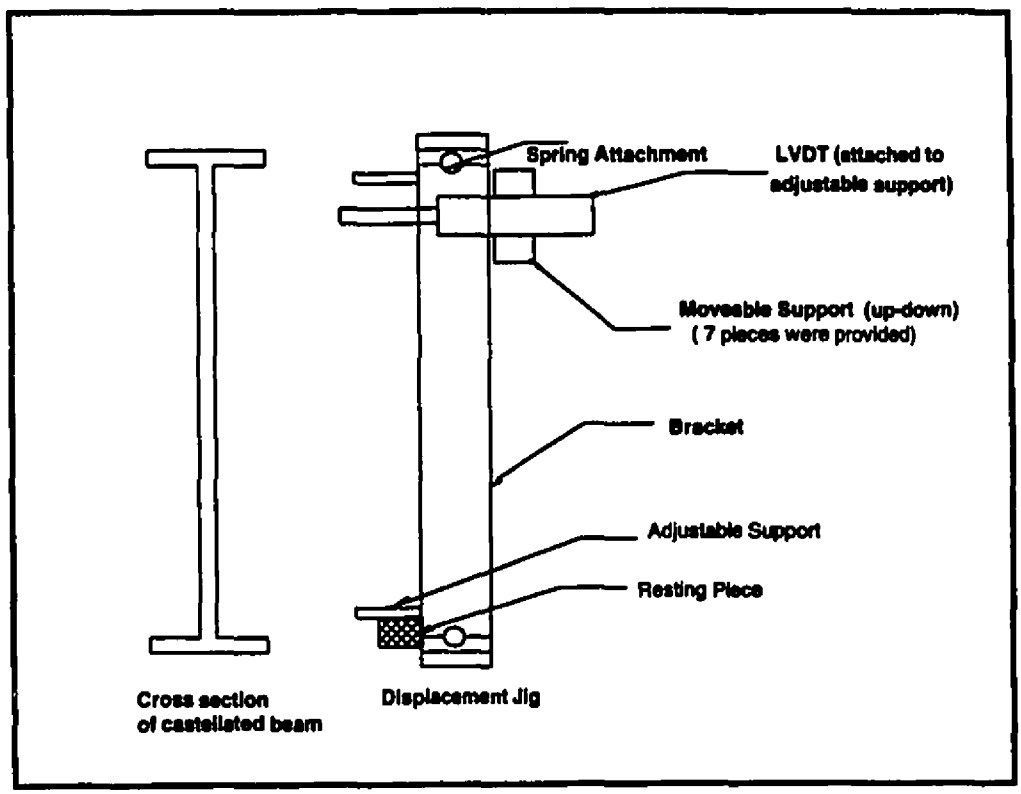


Fig. 4.5: Displacement Measuring Jig

# Chapter 5

## Test Results and Observations

### 5.1 General

Initial measurements were taken for each specimen to determine the beam camber, sweep, and the out-of-plane deflections in the web posts. These values are given in Table 5.1 along with the acceptable tolerances.

For each specimen in the final test program, a combination of 12 graphs, based on data acquired during the test, provide a clear image of the behavior of the beam. Since specimens 8-1a and 8-2a were not re-tested, the complete 12 graphs could not be reproduced for these; however, the essential data is available from the limited graphs that were produced. Graphs for specimens 8-3a and 8-4a, which were replicated as 8-3 and 8-4 in the final test program, are also reproduced.

The Load vs. Web Strain graphs are used as an indication of the failure load and in the case of failure by web-post buckling they are an indication of the buckling load. Three values are retrieved from those graphs. One indication of the failure load is the asymptote to the web strains, the other is the load value at which the slope of the strain vs. load relationship changes sign. In both cases two values are available, one each from the two strain gauge pairs. In general the asymptote was only clearly defined by one of these, and the greater of the loads at slope reversal is given. These values are listed in rows 2 & 3 of Table 5.2 and the locations of the strain gauges are shown in Fig. 4.4. The

Load vs. Strain Difference is a plot of the applied load vs. the absolute difference between the pair of strain gauges on a web post. From these graphs, a third indicator of the failure load is the asymptote to the curve of the relative strains given in row 8 of Table 5.2.

The asymptote to the flange strain in the Load vs. Flange Strain graph is another indication of the value of the failure load. This value is in row 4 of Table 5.2.

The asymptote to the horizontal web deflection in the Load vs. Horizontal Web Deflection graph could also be a pointer to the value of the failure load. This is given in row 5 of Table 5.2 and the location of the LVDTs on the web posts are shown in Fig. 5.1.

Similarly, the asymptote to the vertical deflection at mid-span in the Load vs. Vertical Deflection graph could also be an indicator of the value of the failure load. This is given in row 7 of Table 5.2 and the positions of the LVDTs are indicated in Fig. 4.4.

As the applied load increases, the vertical deflection at mid-span and at the adjacent web posts increase, with the larger deflection being at mid-span; in addition to that, the deflection at mid-span takes place at a larger rate. This is reflected in the graphs of Load vs. Relative Deflection by the positive slope at the beginning of loading, indicating an increase in the relative deflection; then in a sudden manner, at a well defined value of load, the difference between adjacent LVDTs decreases. For this to happen, there should be a sudden decrease in the relative vertical deflection, of the top flange, of the adjacent LVDTs. This is an indication that a failure has occurred in the adjacent web post. The value of this load is in row 6 of Table 5.2 and is shown in Fig. 5.80.

The maximum test load, ultimate load, reached for each specimen is also given in row 8 of Table 5.2 and should be considered as the failure load.

The above 8 indicators of failure load were obtained for each specimen, and are summarized in Table 5.2.

For the graphs representing the initial web profile and the web profile at failure, the upper and lower thick lines represent the flanges. The web profiles are distinguished by "NORTH SIDE" and "SOUTH SIDE", representing the side of the beam where the load is offset and the other side respectively.

In reviewing the following, it should be recognized that 8-1a, 8-2a, 8-3a and 8-4a formed the pilot test program, and hence have less complete instrumentation.

### 5.2 Tee-Section Buckling

The failure of specimens 8-1a and 8-3 was due to the torsional buckling of the tee-section, on the north side, adjacent to the loaded plate. The failure of the tee-section was followed by some lateral buckling between the lateral supports, on the same side. Close to the failure load, there were no visible signs of web-post buckling however, the deformations in the upper tee-section were very obvious. Referring to the Load vs. Flange Strain graphs it can be seen that close to the failure load there are high strains that were developed at point 5, close to the failure section. For specimen 8-3, the web profile at failure shows that there is some web movement but it does not correspond to the anticipated double curvature web-post buckling. When buckling occurs, it results in a larger displacement and a different shape (double curvature).

### 5.3 Overall Lateral Torsional Buckling

Specimen 8-3a, which was part of the pilot test program, failed by overall lateral torsioanl buckling, due to inadequate lateral supports. Specimen 8-3, which has the same geometry as specimen 8-3a, was tested as part of the final test program. The failure of specimen 8-3 was due to web-post buckling and will be discussed in the following section.

## 5.4 Web-Post Buckling

Failure of all the specimens, except 8-1a, 8-3a and 8-3 which were discussed in the previous sections, was associated with web-post buckling Figs. A.12 and A.13 are illustrations of test specimens which failed by the buckling of the web-post. The initial web profiles on the north and the south sides, as well as the final web profiles, are produced for each specimen. For those which were part of the pilot testing, the graphs of the Web Profiles were not a good representation of the web profiles, a sample is the graph for specimen 8-2a. This was one of the reasons why the jig was modified in the final tests. The final web profiles clearly define the shapes of the buckled web posts with double curvatures. The Load vs. Horizontal Web Deflection graphs are specified at a definite point on the web-post which is shown in Fig. 5.1. The exact location of that point is indicated in the corresponding graphs of Web Profiles.

For specimens 8-2a, 10-2 and 12-1, although the load was offset to one side, in order to initiate failure on that side, it occurred on the other side that did not have the complete system of instrumentation. However, the mode of failure was evident and so was the corresponding load. The failure mode was sudden, typical of buckling, and the buckling of the web posts were visible. Also, for these specimens, the Load vs. Horizontal Web Deflection graphs show very limited deflections because the jig was always placed on the north side, whereas buckling occurred on the south side.

It should be noted that although specimens 8-4 and 8-4a have the same section geometries, they are 8-4a failed at a lower buckling load than 8-4. This may be attributed to the inadequate lateral supports in the pilot testing set up. The end of the beam which was 25.5 in. (648 mm.) away from a lateral support showed some twisting.

**Table 5.1:** Mode of Failure, Maximum Test Load and Vertical Deflection

| Specimen | Maximum Test Load (kips) (1 kip = 4.448 kN) | Mode of Failure | Maximum Vertical Deflection * (in) ( 1 in = 25.4 mm) |
|---|---|---|---|
| 8-1a | 12.8 | Tee-Section Buckling | 1.40 |
| 8-2a | 11.2 | Web Post Buckling | 1.85 |
| 8-3a | 10.2 | Overall LTB[1] | 0.67 |
| 8-4a | 8.1 | Web Post Buckling | 1.78 |
| 8-3 | 13.0 | Tee-Section Buckling | 1.12 |
| 8-4 | 8.9 | Web Post Buckling | 1.43 |
| 10-1 | 17.8 | Web Post Buckling | 1.05 |
| 10-2 | 13.2 | Web Post Buckling | 0.87 |
| 10-3 | 16.6 | Web Post Buckling | 0.77 |
| 10-4 | 11.3 | Web Post Buckling | 0.99 |
| 12-1 | 25.8 | Web Post Buckling | 0.90 |
| 12-2 | 22.1 | Web Post Buckling | 0.73 |
| 12-3 | 26.2 | Web Post Buckling | 0.88 |
| 12-4 | 21.0 | Web Post Buckling | 0.68 |

* At load point

[1]Overall lateral torsional buckling due to inadequate lateral supports

**Table 5.2:** Estimation of Experimental Failure Loads (kips*** )

| Specimen | 8-1a | 8-2a | 8-3a | 8-4a | 8-3 | 8-4 | 10-1 | 10-2 | 10-3 | 10-4 | 12-1 | 12-2 | 12-3 | 12-4 |
|---|---|---|---|---|---|---|---|---|---|---|---|---|---|---|
| **Web strain asymptote** | 12.8 | 11.2 | 10.1 | 8.1 | 12.9 | 8.9 | 17.7 | 13.2 | 16.6 | 10.3 | 25.8 | 22.1 | 26.2 | 20.1 |
| **Slope reversal of web strains** | 9.0 | 5.7 | 6.0 | 8.0 | 10.5 | 5.3 | 12.2 | 11.7 | 12.2 | 7.0 | 22.0 | 8.0 | 15.0 | 17.0 |
| **Flange strain asymptote** | 12.8 | 11.2 | 10.1 | 8.1 | 12.9 | 8.9 | 17.7 | 13.2 | 16.6 | 11.3 | 25.8 | 22.1 | 26.2 | 21.0 |
| **Horizontal deflection asymptote** | --- | --- | --- | --- | 12.9 | 8.9 | 17.7 | 13.2 | 16.6 | 11.3 | 25.8 | 22.1 | 26.2 | 21.0 |
| **Point of decrease of relative deflection** | --- | --- | --- | 8.1 | 12.9 | 8.9 | 17.0 | 13.2 | 16.4 | 11.3 | 25.8 | 22.1 | 26.2 | 21.0 |
| **Vertical deflection asymptote** | 12.8 | 11.2 | 10.1 | 8.1 | 13.0 | 8.9 | 17.7 | 13.2 | 16.4 | 11.3 | 25.8 | 22.1 | 26.2 | 21.0 |
| **Strain difference asymptote** | 12.8 | 11.2 | 10.2 | 8.1 | 12.9 | 8.9 | 17.8 | 12.7 | 16.4 | 10.5 | 25.8 | 22.1 | 26.2 | 20.1 |
| **Maximum test load** | 12.8 | 11.2 | 10.2 | 8.1 | 13.0 | 8.9 | 17.8 | 13.2 | 16.6 | 11.3 | 25.8 | 22.1 | 26.2 | 21.0 |

*** 1 kip = 4.448 kN

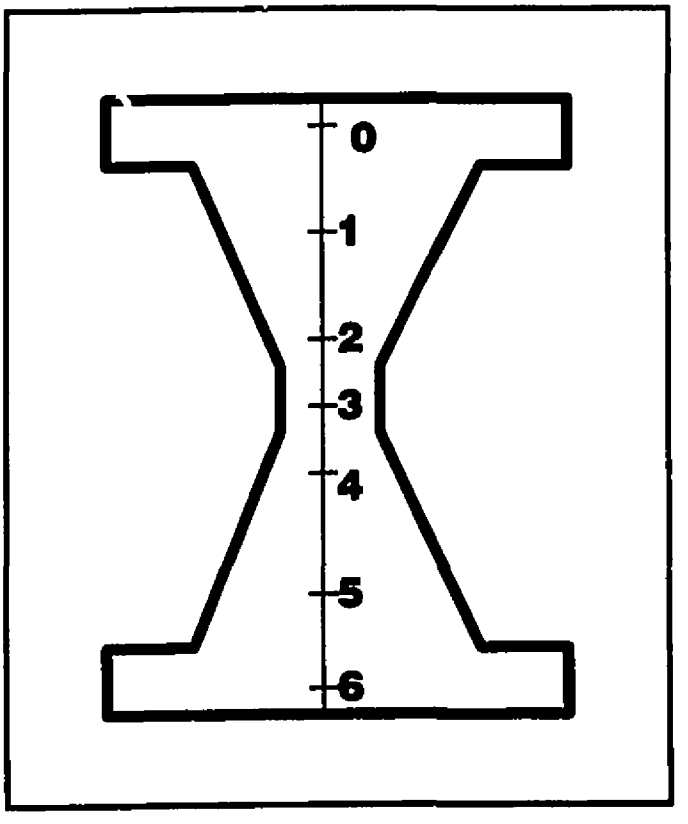


**Fig. 5.1:** Location of LVDTs on The Web Post

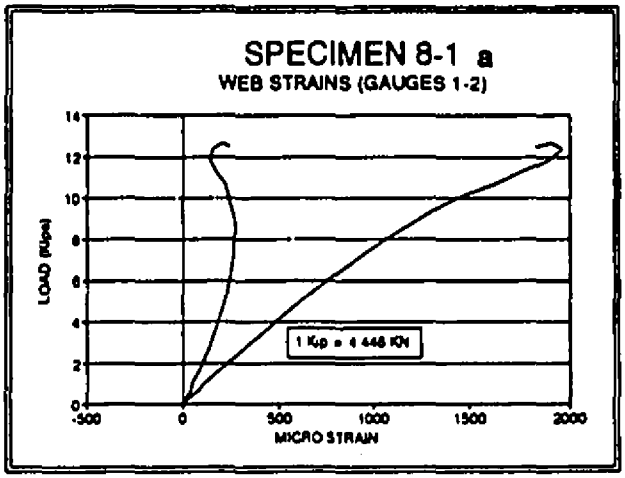


Fig. 5. 2 : LOAD vs. WEB STRAINS

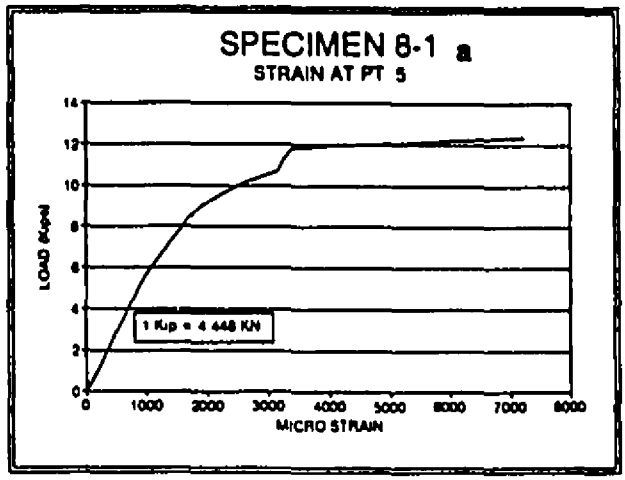


Fig. 5. 3 : LOAD vs. FLANGE STRAIN

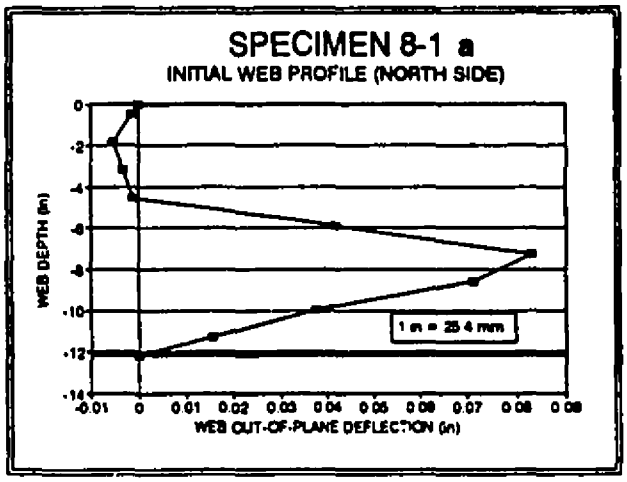


Fig. 5. 4 : INITIAL WEB PROFILE

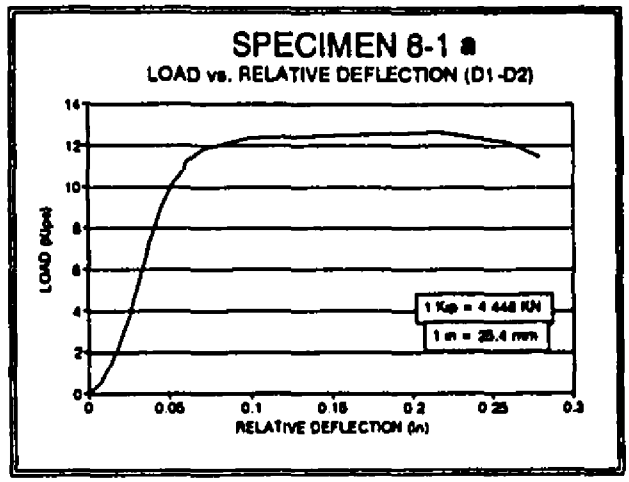


Fig. 5. 5 : LOAD vs RELATIVE DEFLECTION

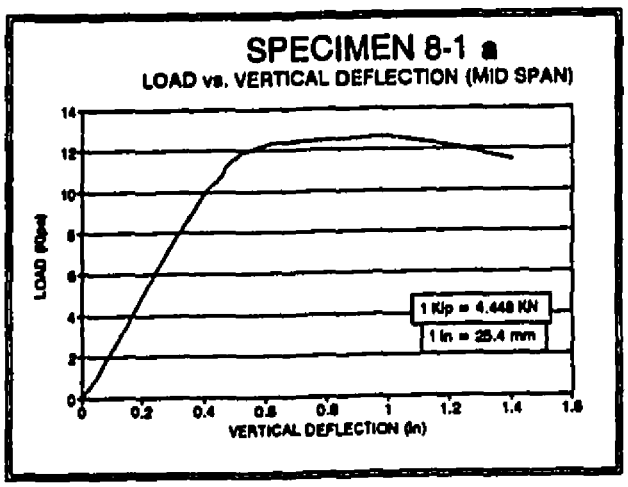


**Fig. 5. 6** : LOAD vs VERTICAL DEFLECTION

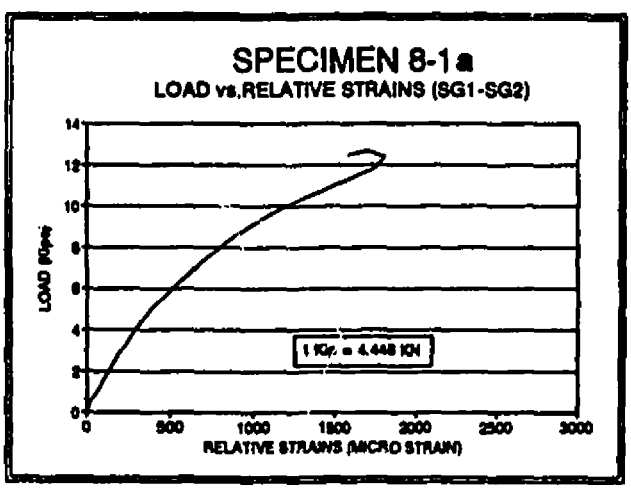


**Fig. 5.7:** LOAD vs. STRAIN DIFFERENCES

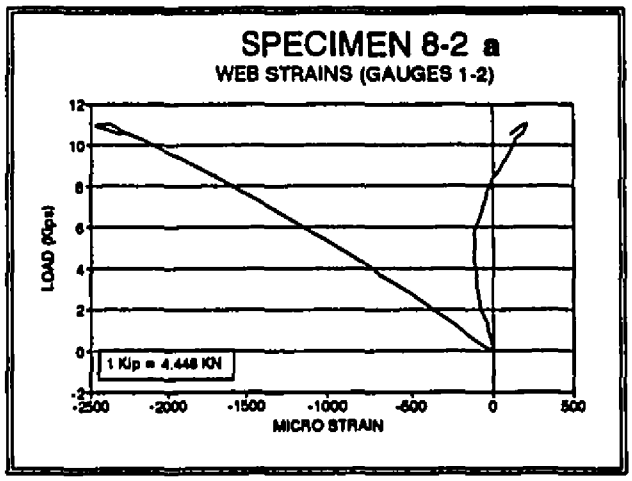


Fig. 5. 8 : LOAD vs. WEB STRAINS

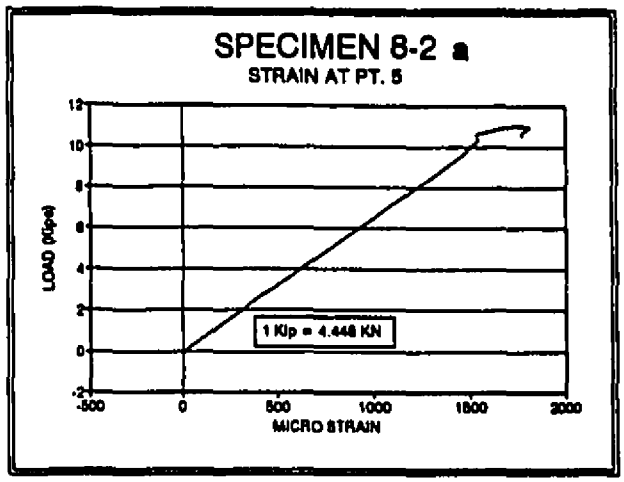


Fig. 5. 9 : LOAD vs FLANGE STRAIN

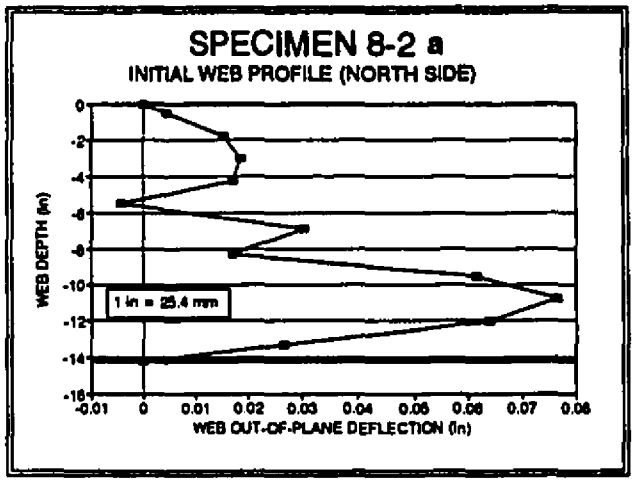


Fig. 5. 10 : INITIAL WEB PROFILE

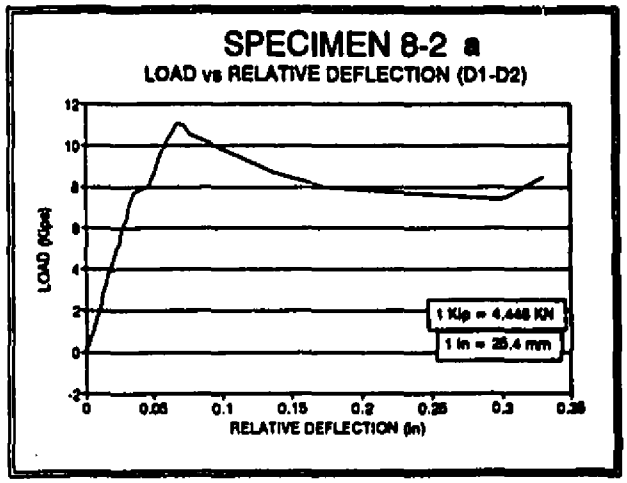


Fig. 5. 11 : LOAD vs RELATIVE DEFLECTION

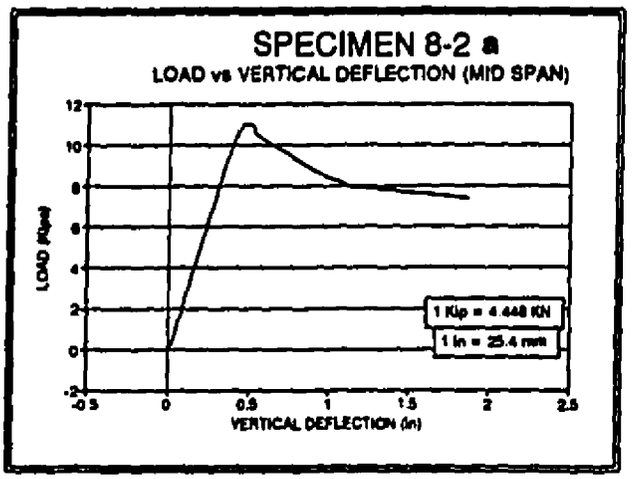


**Fig. 5. 12** : LOAD vs VERTICAL DEFLECTION

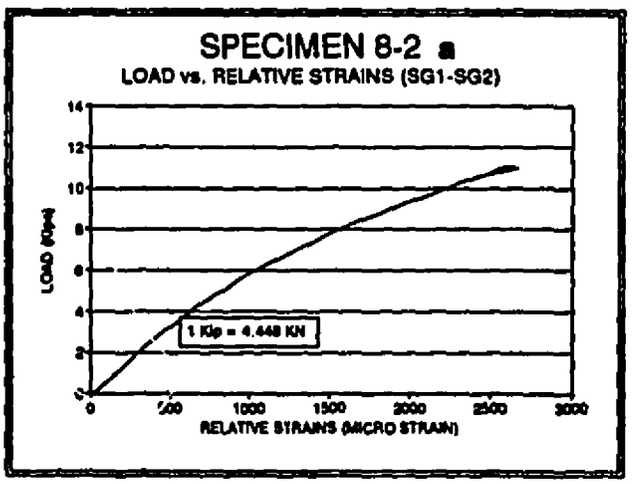


**Fig. 5. 13** : LOAD vs. RELATIVE STRAIN (8-2)

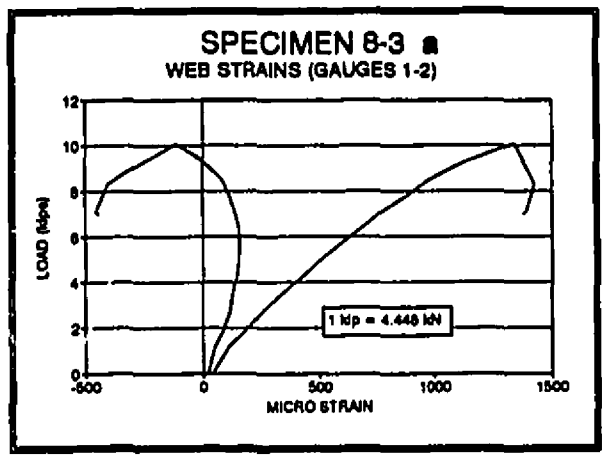


Fig. 5.14: LOAD vs. WEB STRAIN

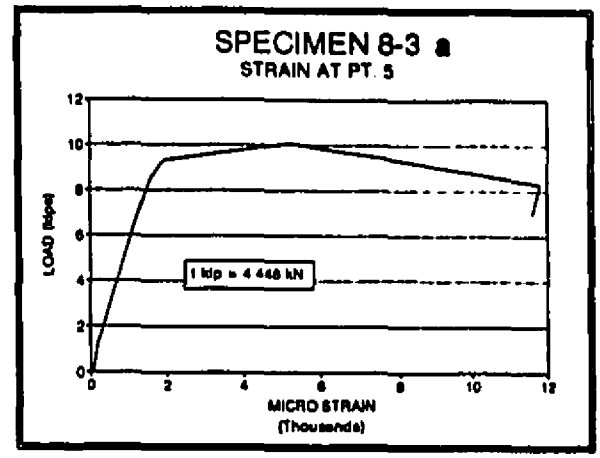


Fig. 5.15: LOAD vs. FLANGE STRAIN

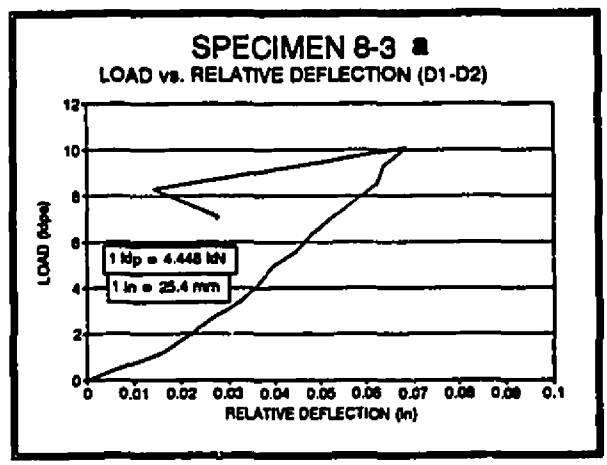


Fig. 5.16: LOAD vs. RELATIVE DEFLECTION

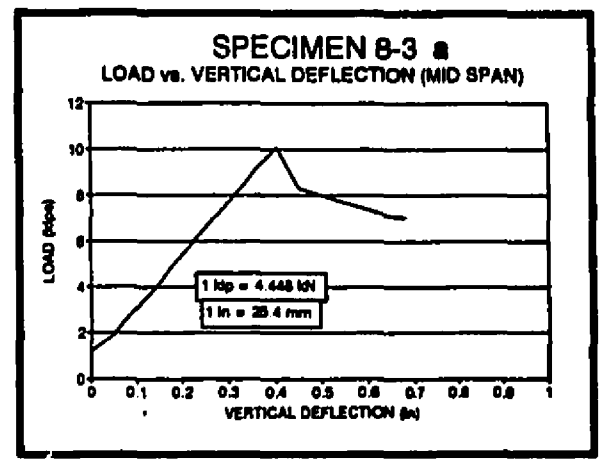


Fig. 5.17: LOAD vs. VERTICAL DEFLECTIOI

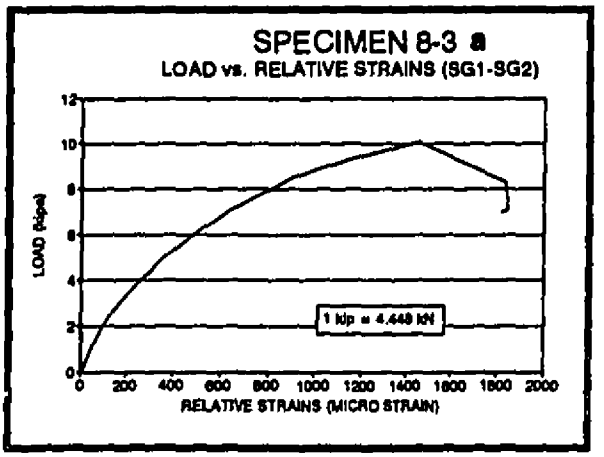


**Fig. 5.18:** LOAD vs. STRAIN DIFFERENCES

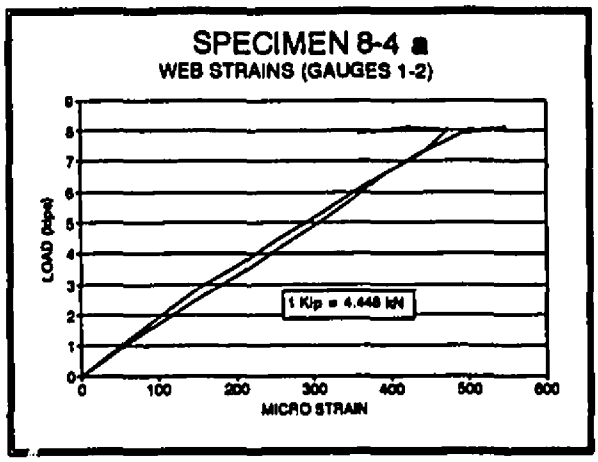


Fig. 5.19: LOAD vs. WEB STRAIN

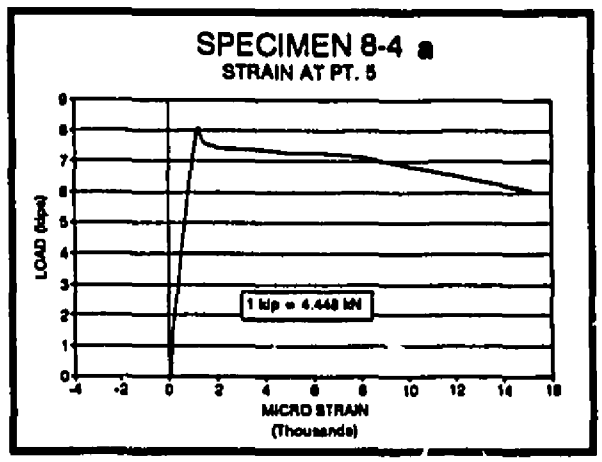


Fig. 5.20: LOAD vs. FLANGE STRAIN

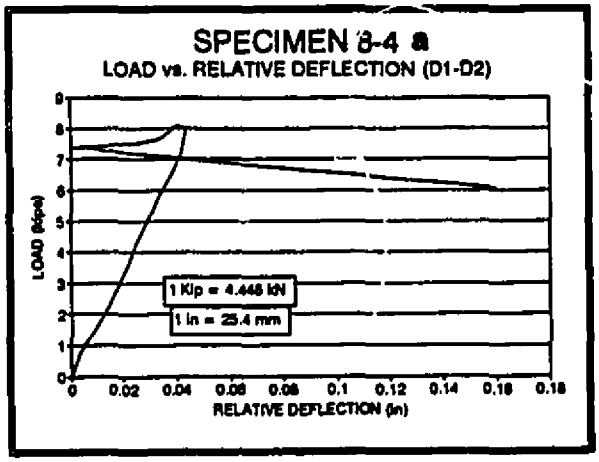


Fig. 5.21: LOAD vs. RELATIVE DEFLECTION

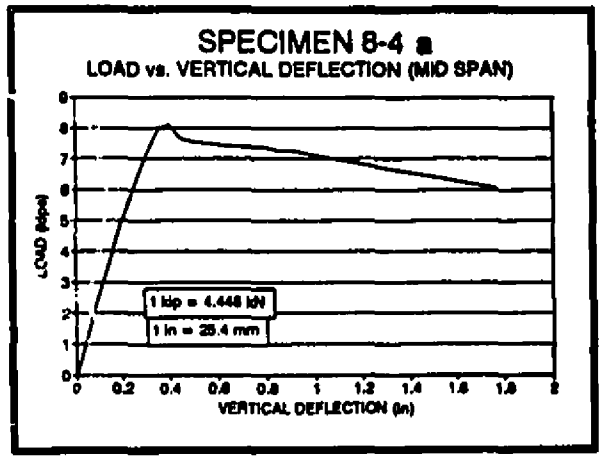


Fig. 5.22: LOAD vs. VERTICAL DEFLECTIC

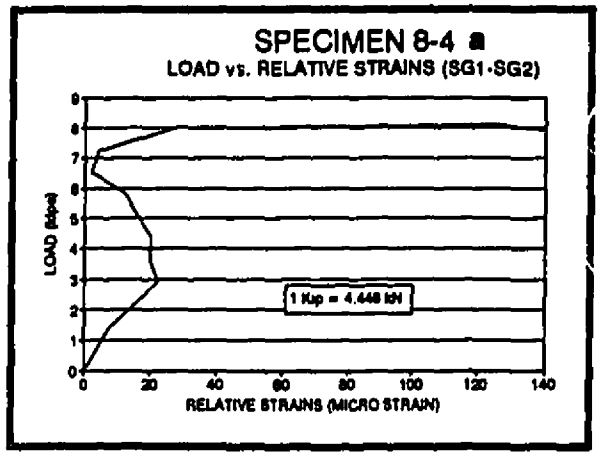


**Fig. 5.23:** LOAD vs. STRAIN DIFFERENCES

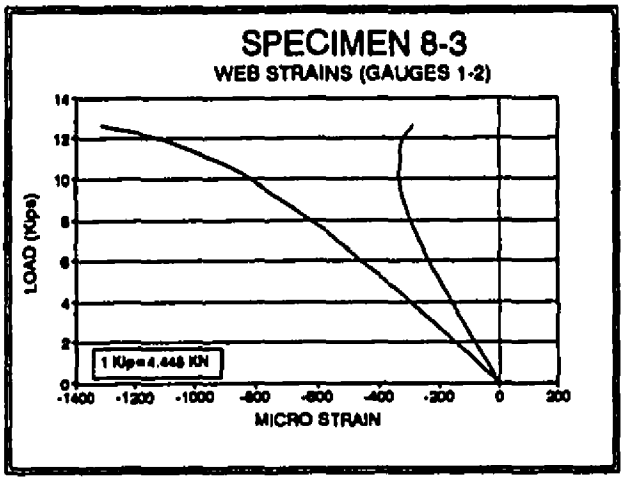


Fig. 5. 24 : LOAD vs. WEB STRAINS

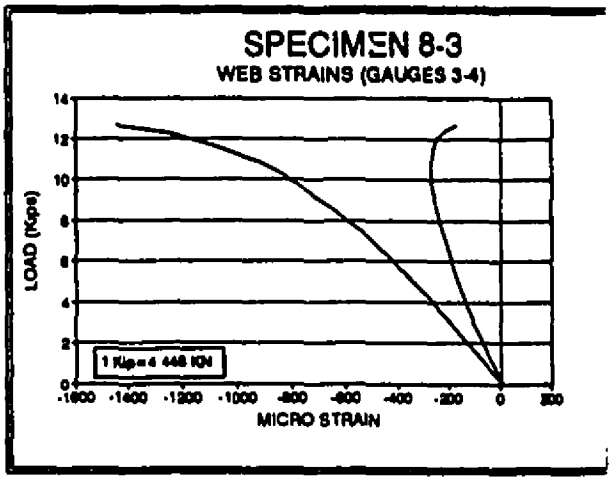


Fig. 5. 25 : LOAD vs. WEB STRAINS

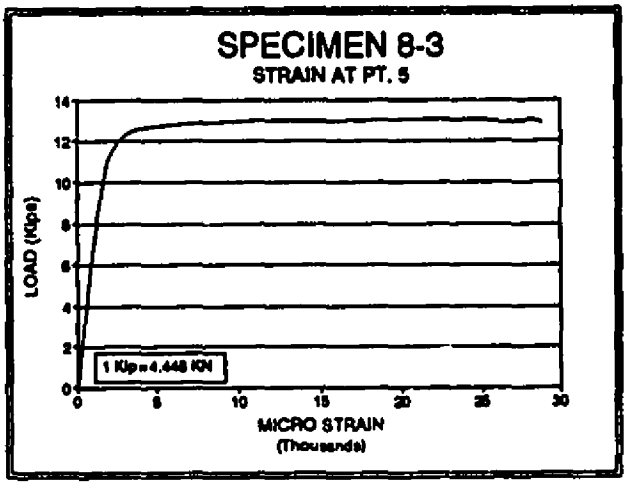


Fig. 5. 26 : LOAD vs. FLANGE STRAIN

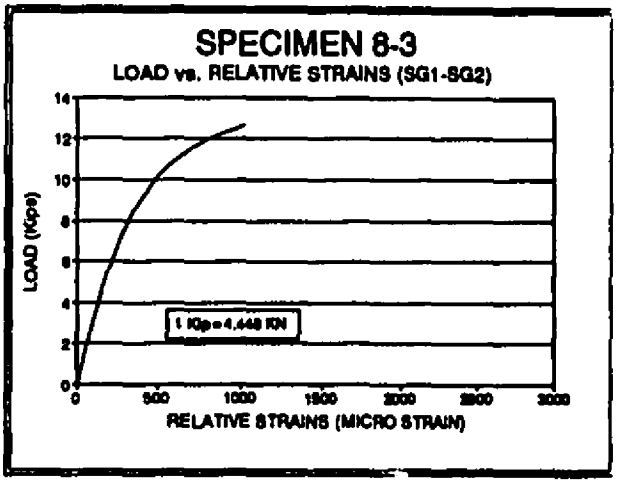


Fig. 5.27: LOAD vs. STRAIN DIFFERENCES

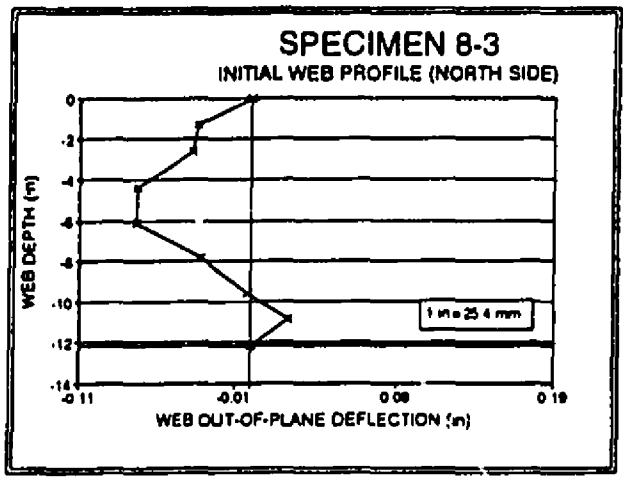


**Fig. 5.28:** INITIAL WEB PROFILE (NORTH SIDE)

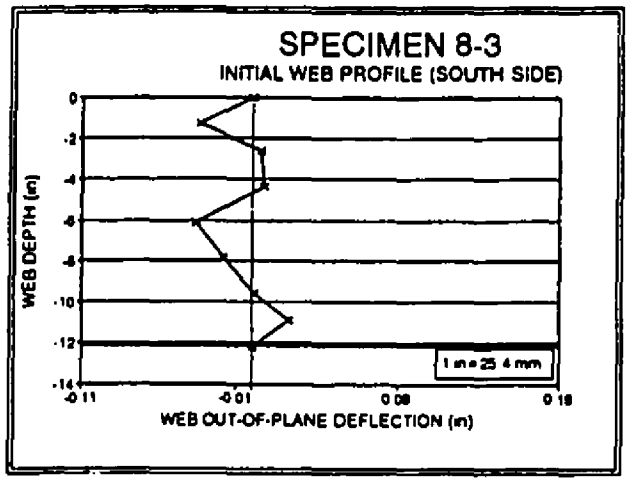


**Fig. 5.29:** INITIAL WEB PROFILE (SOUTH SIDE)

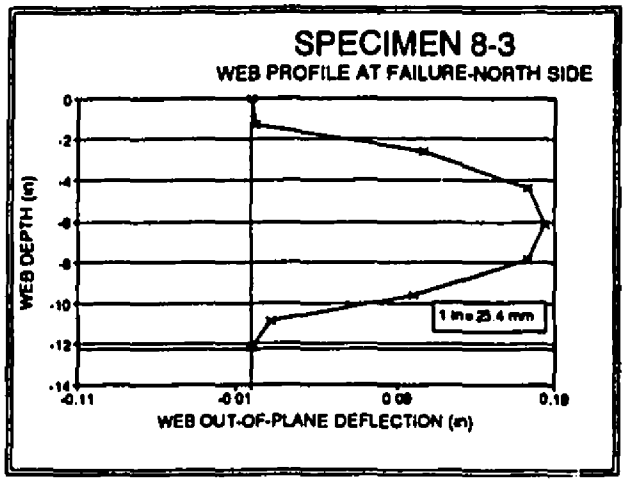


**Fig. 5.30:** FINAL WEB PROFILE (NORTH SIDE)

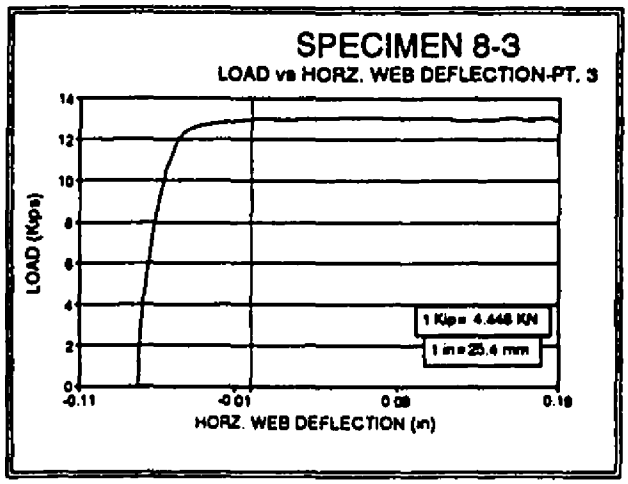


**Fig. 5.31:** LOAD vs. HORZ. WEB DEFLECTION

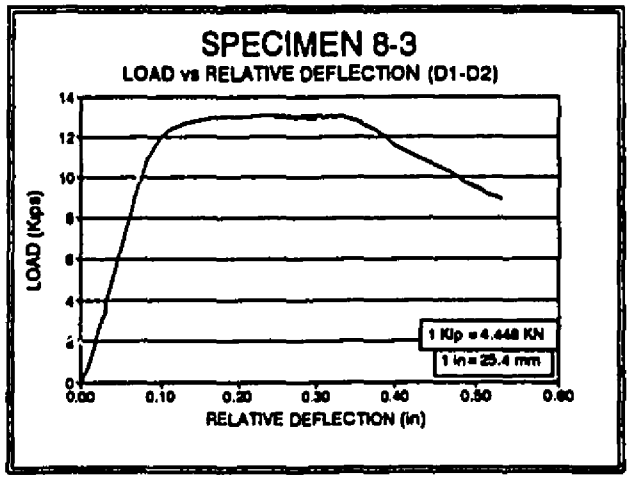


Fig. 5.32: LOAD vs. RELATIVE DEFLECTION

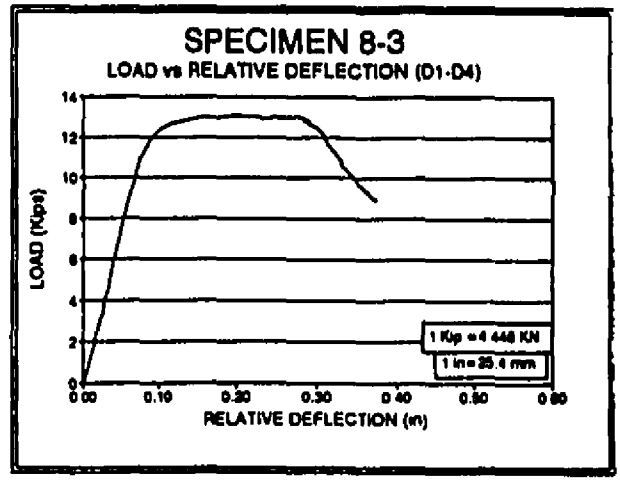


Fig. 5.33: LOAD vs. RELATIVE DEFLECTION

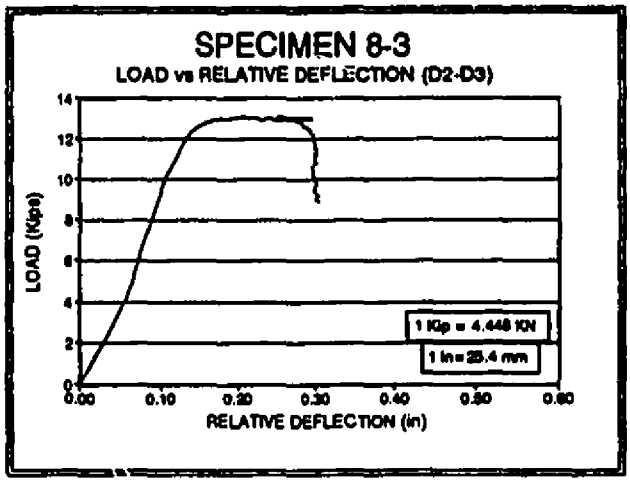


Fig. 5.34: LOAD vs. RELATIVE DEFLECTION

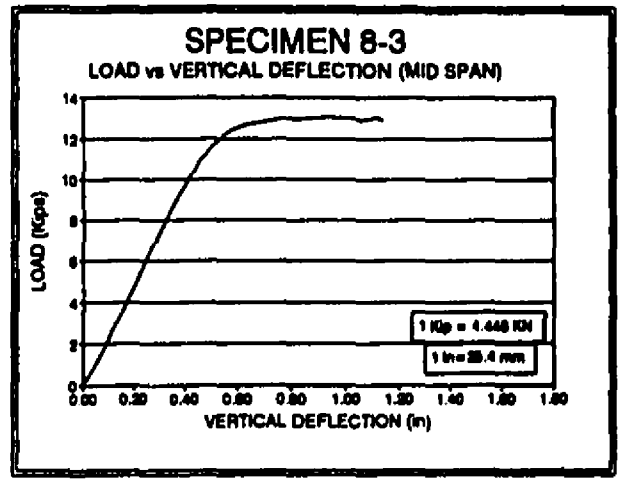


Fig. 5.35: LOAD vs. VERTICAL DEFLECTION

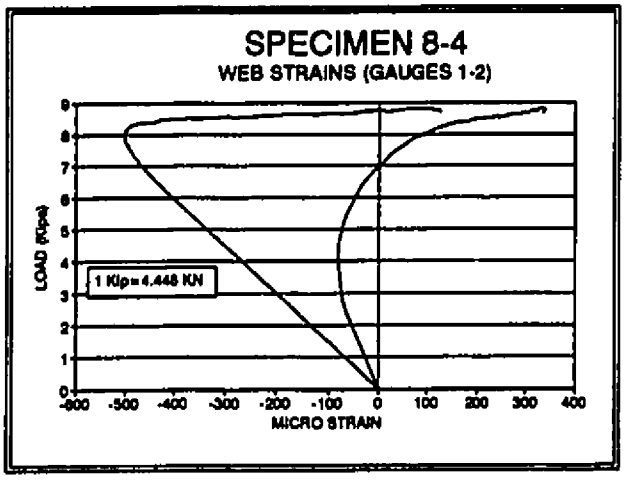


**Fig. 5.36:** LOAD vs. WEB STRAIN

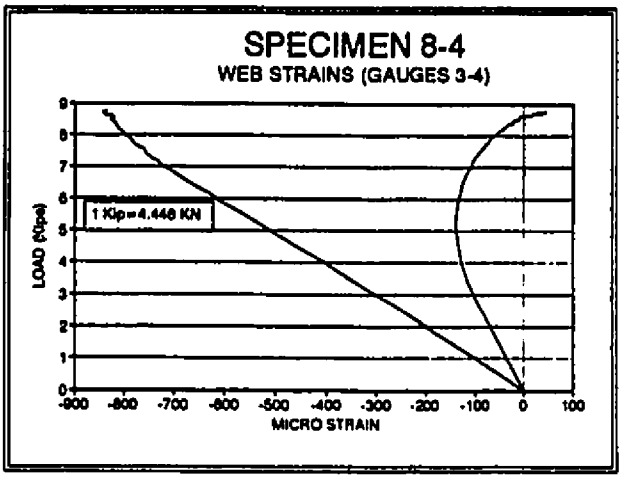


**Fig. 5.37:** LOAD vs. WEB STRAIN

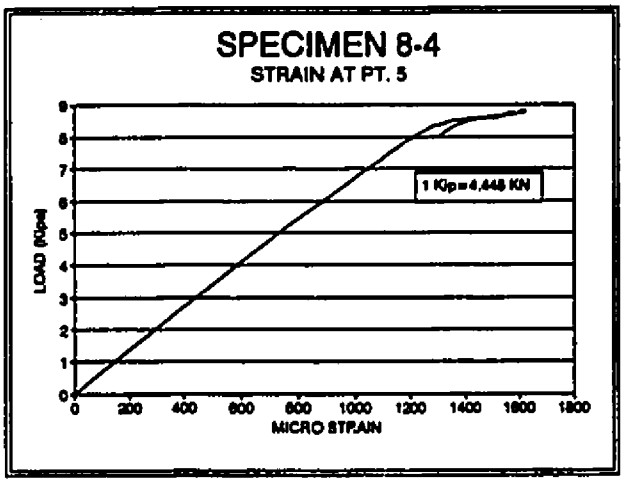


**Fig. 5.38:** LOAD vs. FLANGE STRAIN

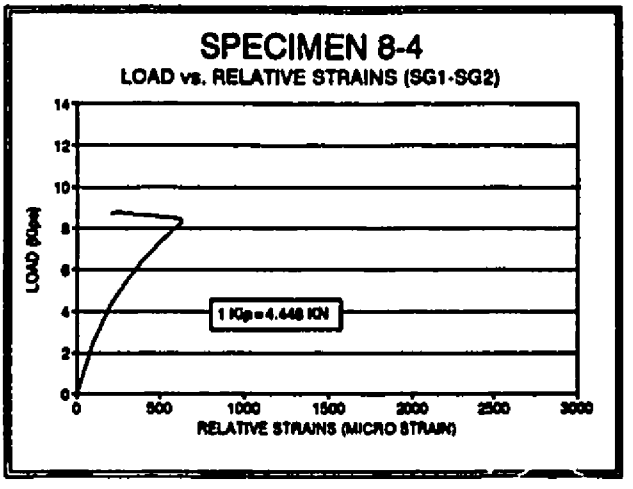


**Fig. 5.39:** LOAD vs. STRAIN DIFFERENCES

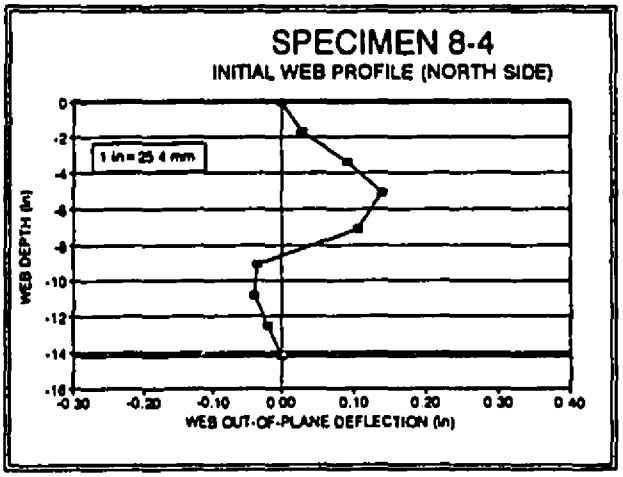


**Fig. 5.40:** INITIAL WEB PROFILE (NORTH SIDE)

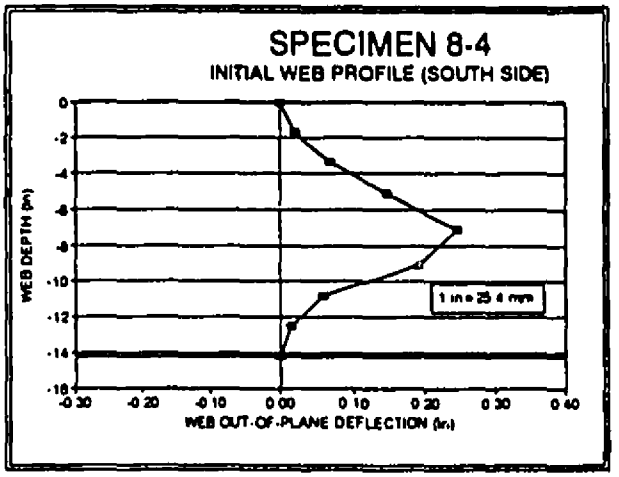


**Fig. 5.41:** INITIAL WEB PROFILE (SOUTH SIDE)

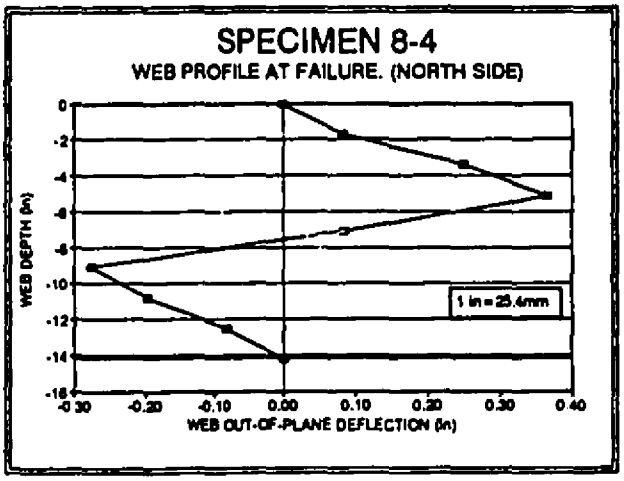


**Fig. 5.42:** FINAL WEB PROFILE (NORTH SIDE)

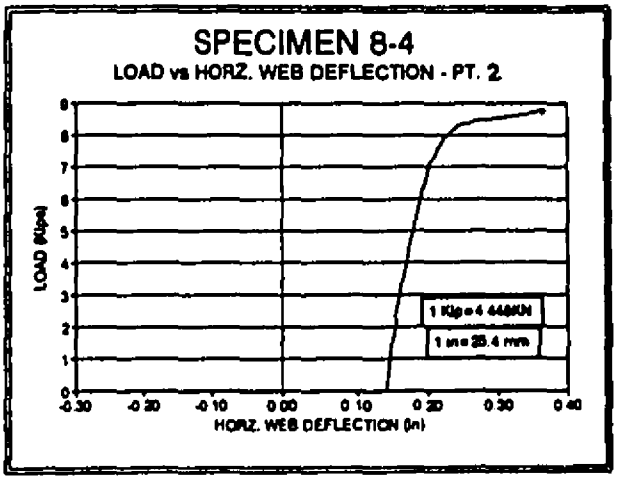


**Fig. 5.43:** LOAD vs. HORZ. WEB DEFLECTION

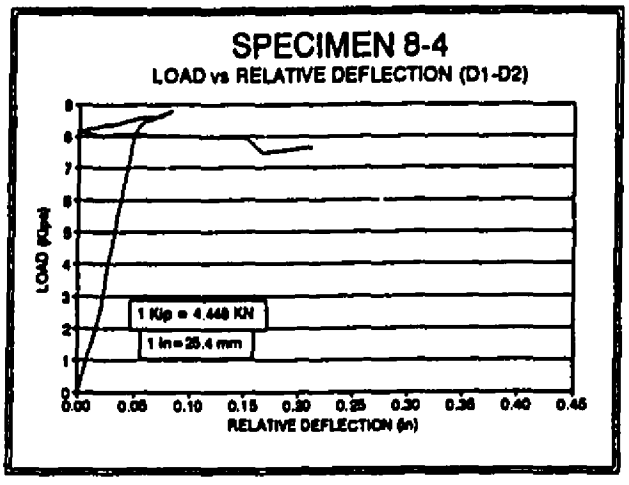


Fig. 5.44: LOAD vs. RELATIVE DEFLECTION

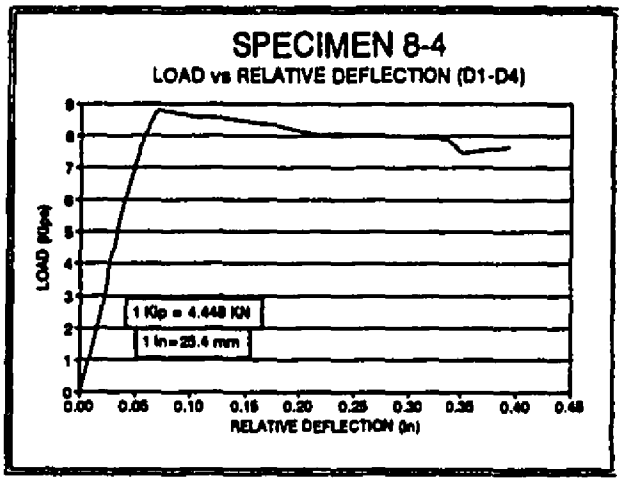


Fig. 5.45: LOAD vs. RELATIVE DEFLECTION

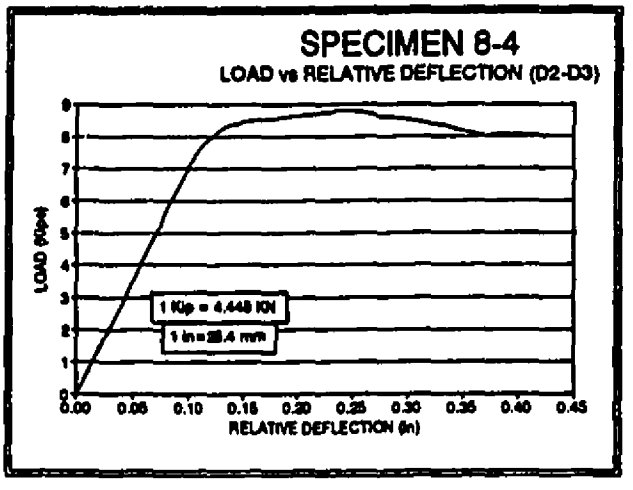


Fig. 5.46: LOAD vs. RELATIVE DEFLECTION

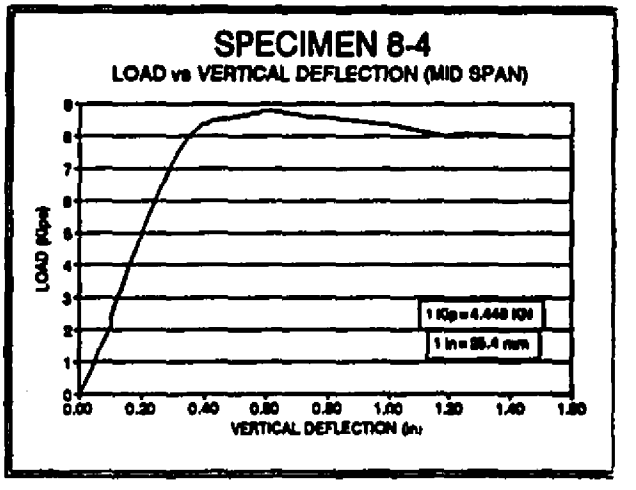


Fig. 5.47: LOAD vs. VERTICAL DEFLECTION

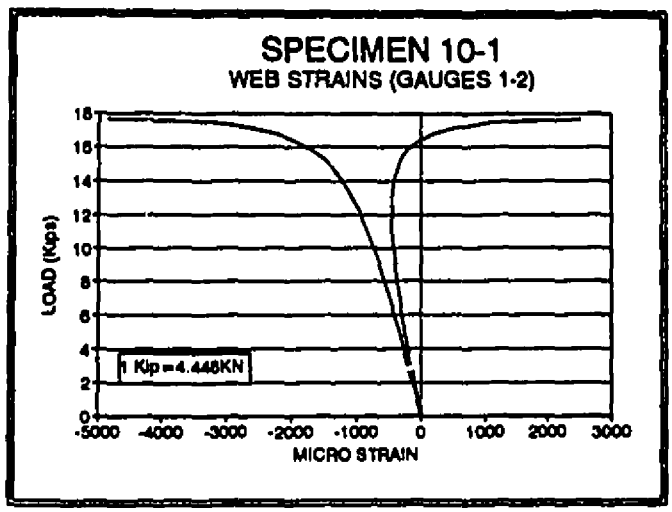


Fig. 5.48: LOAD vs. WEB STRAIN

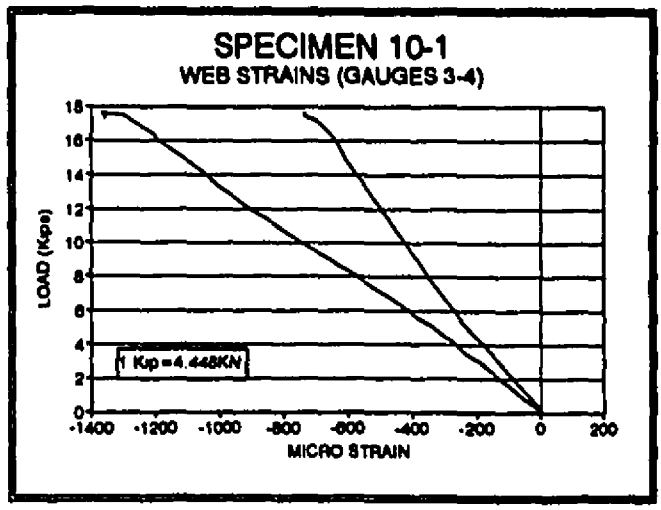


Fig. 5.49: LOAD vs. WEB STRAIN

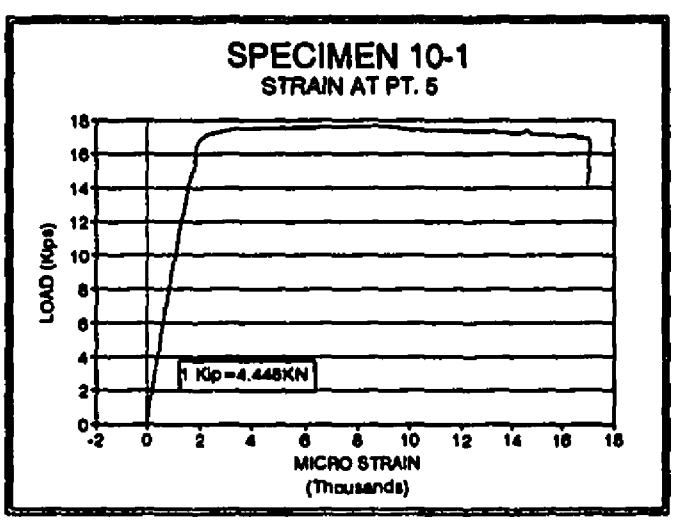


Fig. 5.50: LOAD vs. FLANGE STRAIN

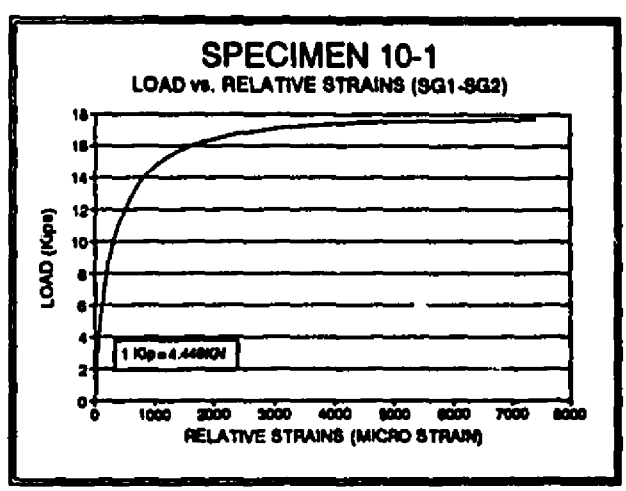


Fig. 5.51: LOAD vs. STRAIN DIFFERENCES

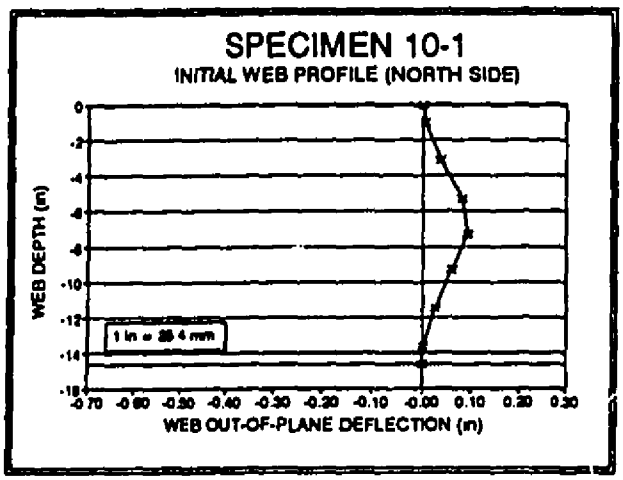


Fig. 5.52: INITIAL WEB PROFILE (NORTH SIDE)

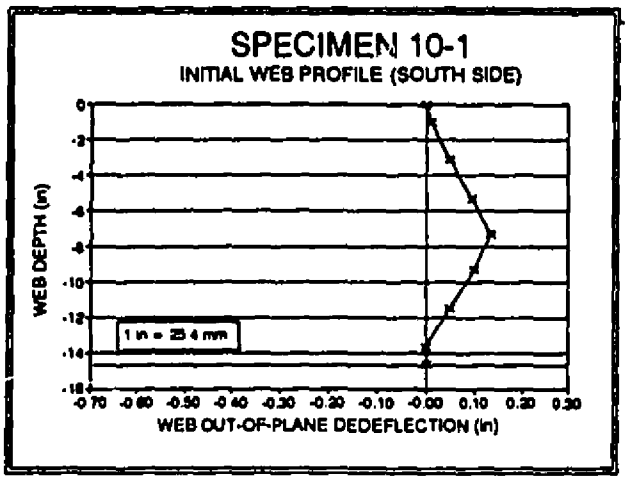


Fig. 5.53: INITIAL WEB PROFILE (SOUTH SIDE)

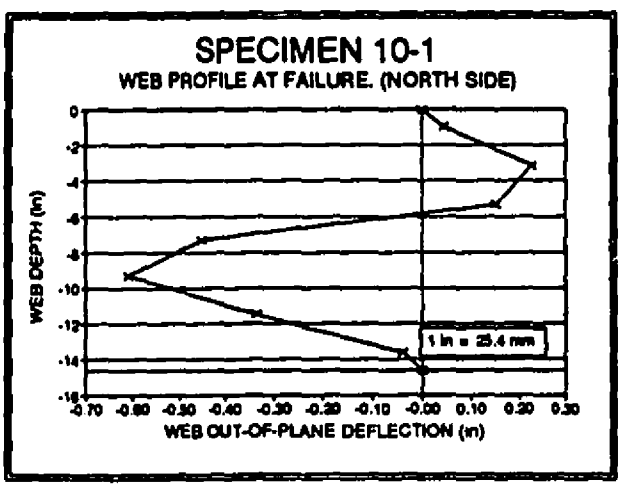


Fig. 5.54: FINAL WEB PROFILE (NORTH SIDE)

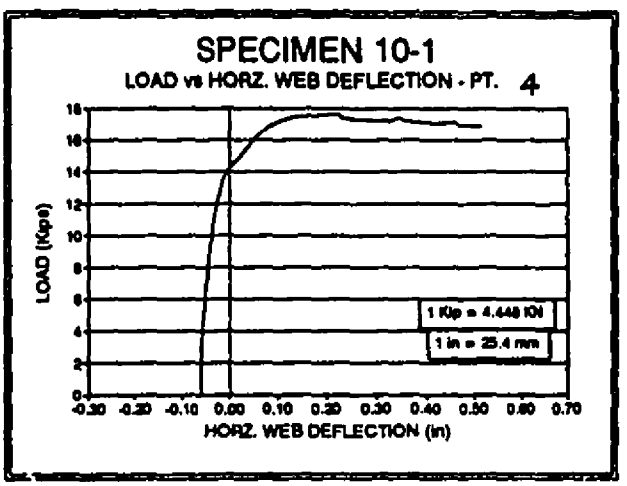


Fig. 5.55: LOAD vs. HORZ. WEB DEFLECTION

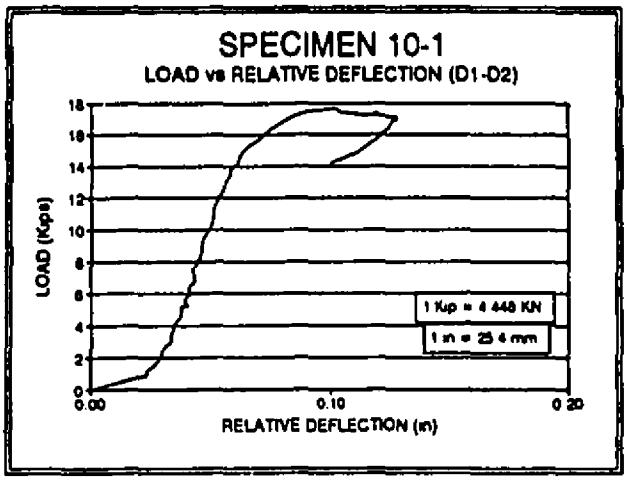


**Fig. 5.56:** LOAD vs. RELATIVE DEFLECTION

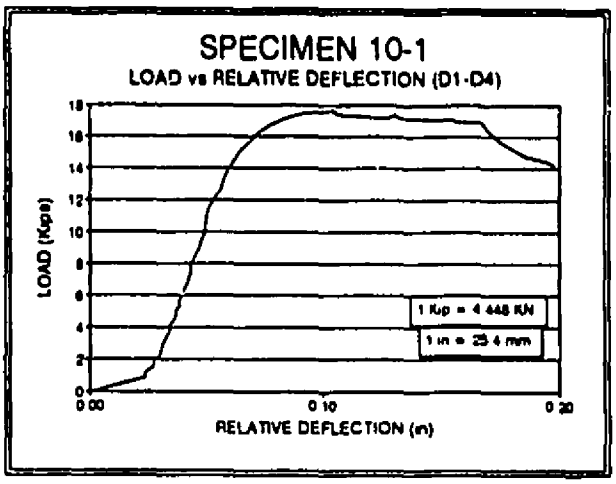


**Fig. 5.57:** LOAD vs. RELATIVE DEFLECTION

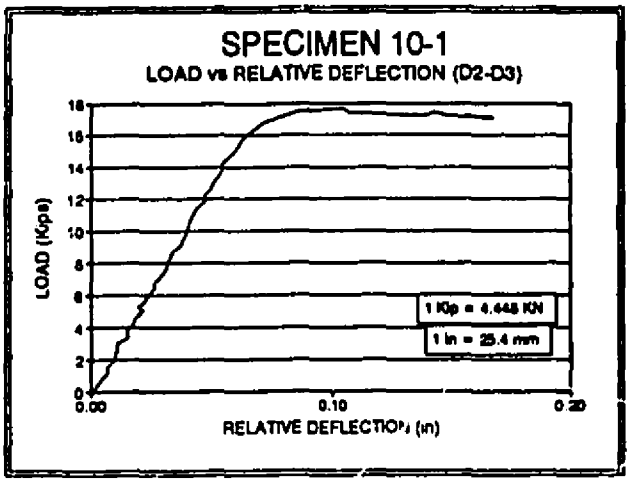


**Fig. 5.58:** LOAD vs. RELATIVE DEFLECTION

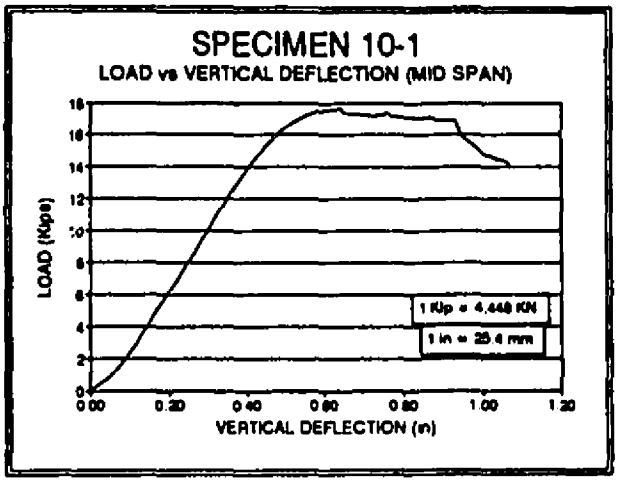


**Fig. 5.59:** LOAD vs. VERTICAL DEFLECTION

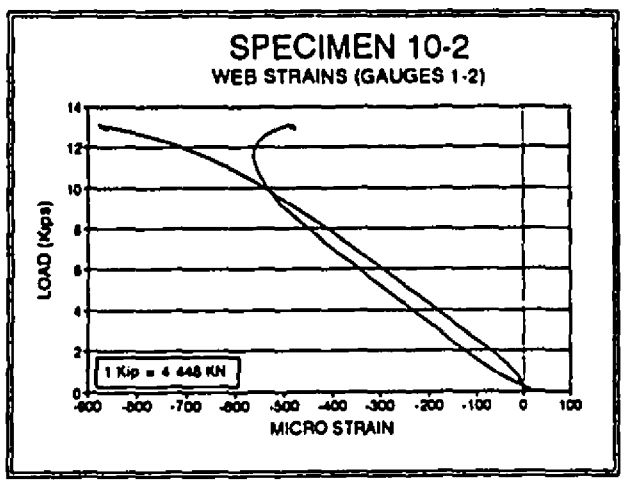


**Fig. 5.60:** LOAD vs. WEB STRAIN

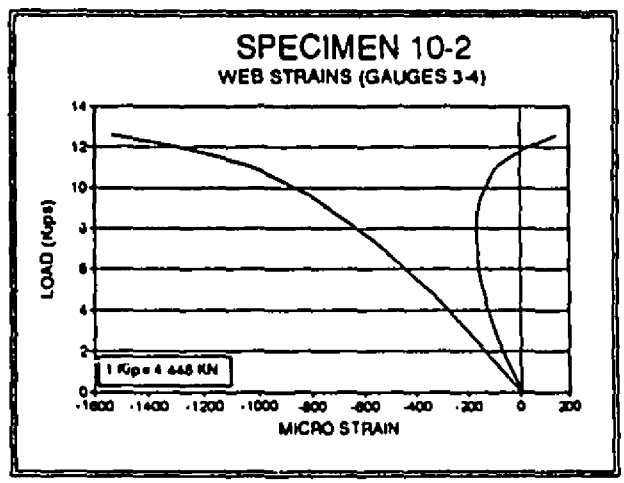


**Fig. 5.61:** LOAD vs. WEB STRAIN

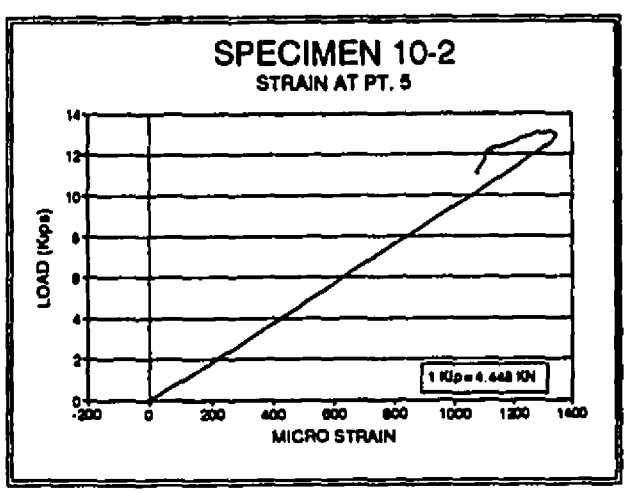


**Fig. 5.62:** LOAD vs. FLANGE STRAIN

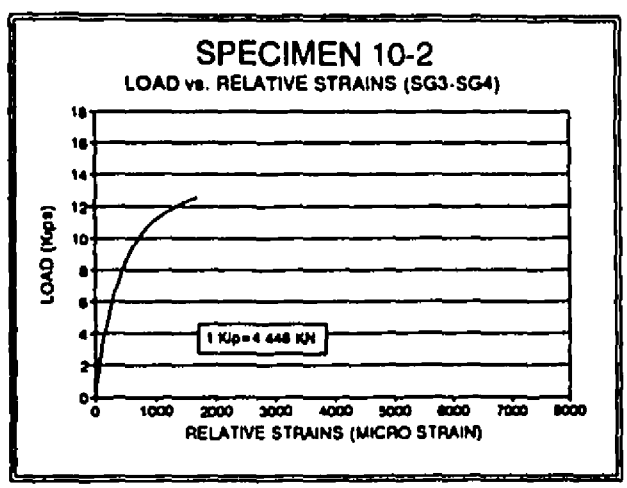


**Fig. 5.63:** LOAD vs. STRAIN DIFFERENCES

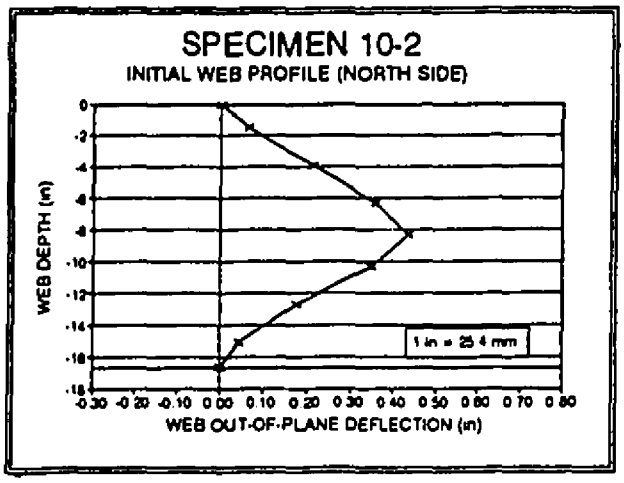


Fig. 5.64: INITIAL WEB PROFILE (NORTH SIDE)

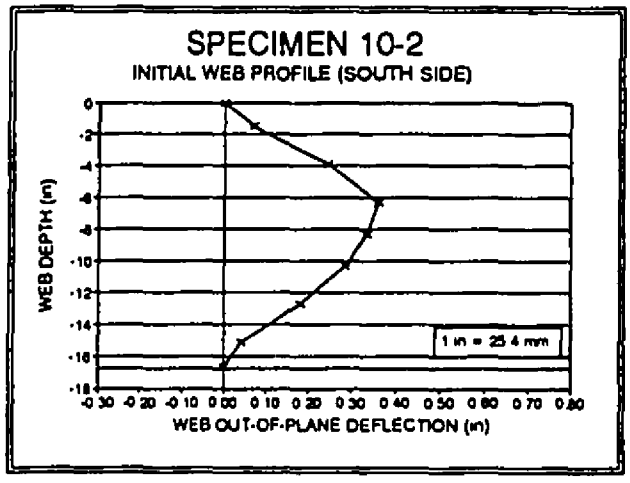


Fig. 5.65: INITIAL WEB PROFILE (SOUTH SIDE)

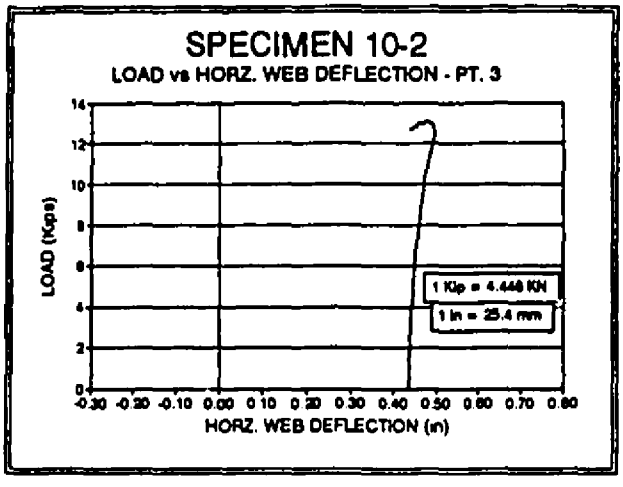


Fig. 5.66: LOAD vs. HORZ. WEB DEFLECTION

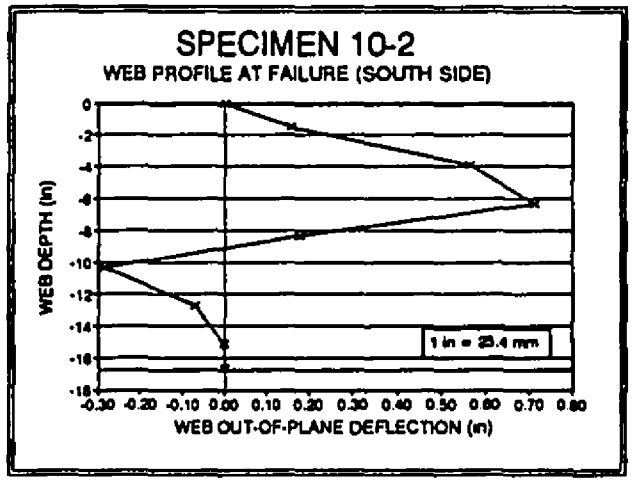


Fig. 5.67: FINAL WEB PROFILE (SOUTH SIDE)

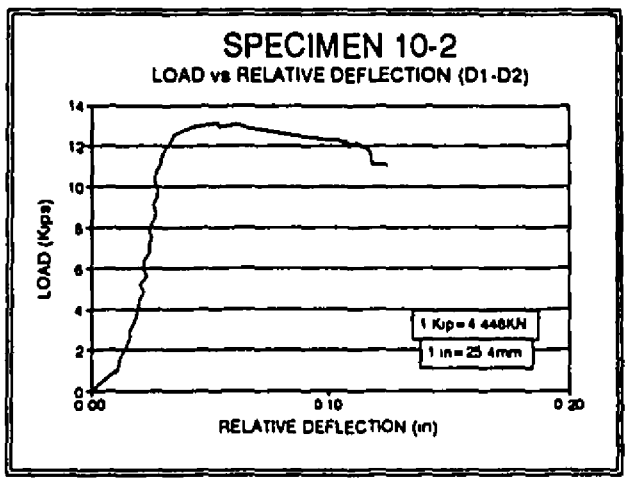


Fig. 5.68: LOAD vs. RELATIVE DEFLECTION

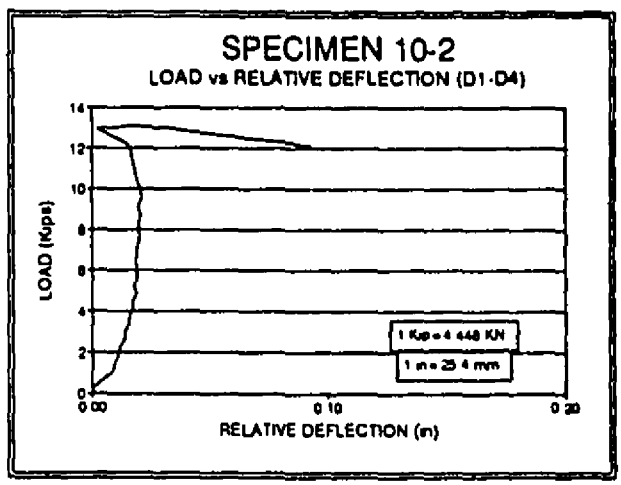


Fig. 5.69: LOAD vs. RELATIVE DEFLECTION

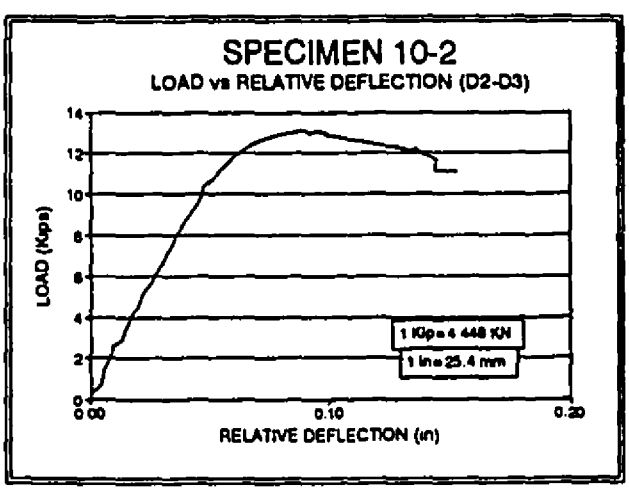


Fig. 5.70: LOAD vs. RELATIVE DEFLECTION

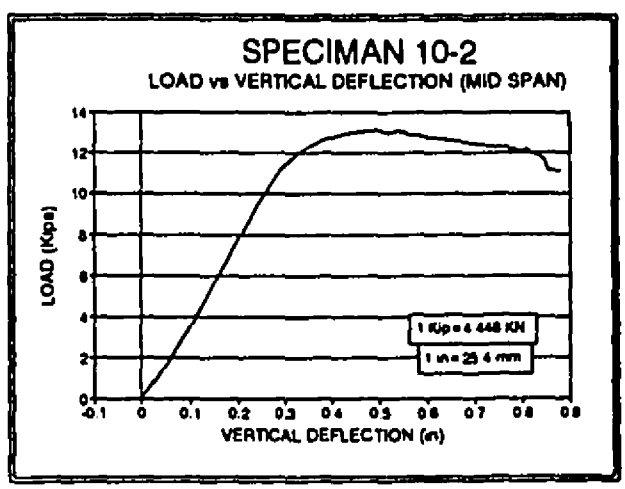


Fig. 5.71: LOAD vs. VERTICAL DEFLECTION

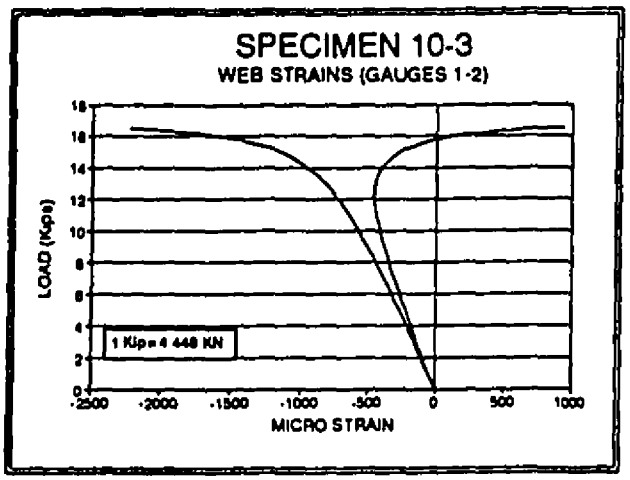


**Fig. 5.72:** LOAD vs. WEB STRAIN

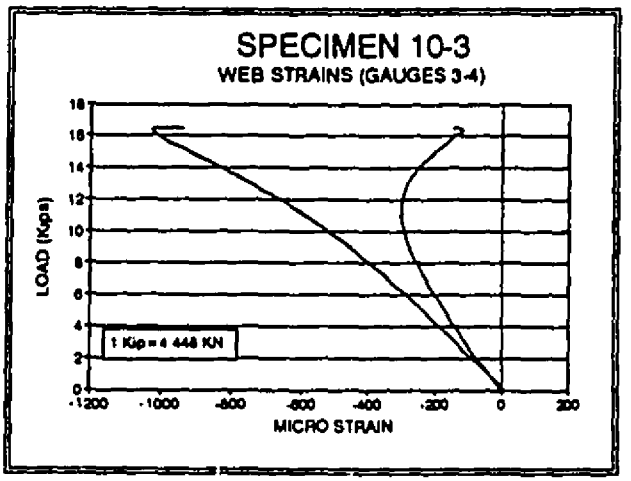


**Fig. 5.73:** LOAD vs. WEB STRAIN

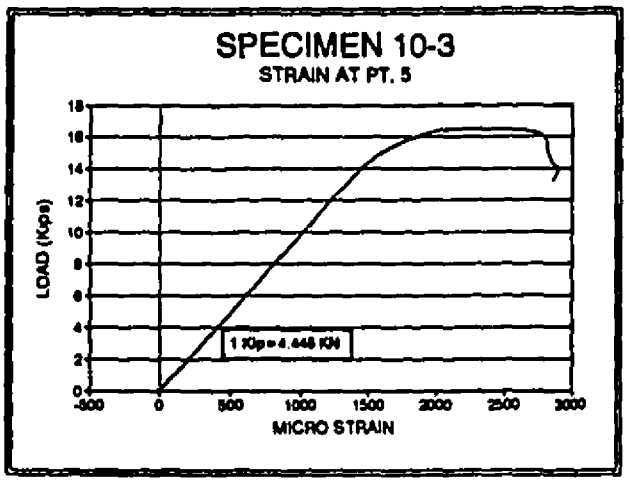


**Fig. 5.74:** LOAD vs. FLANGE STRAIN

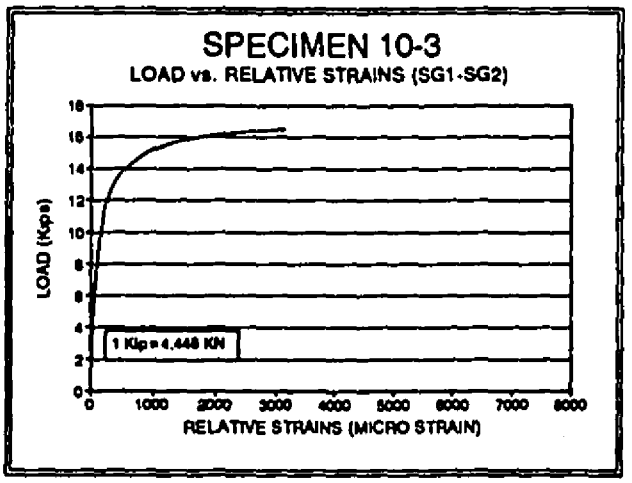


**Fig. 5.75:** LOAD vs. STRAIN DIFFERENCES

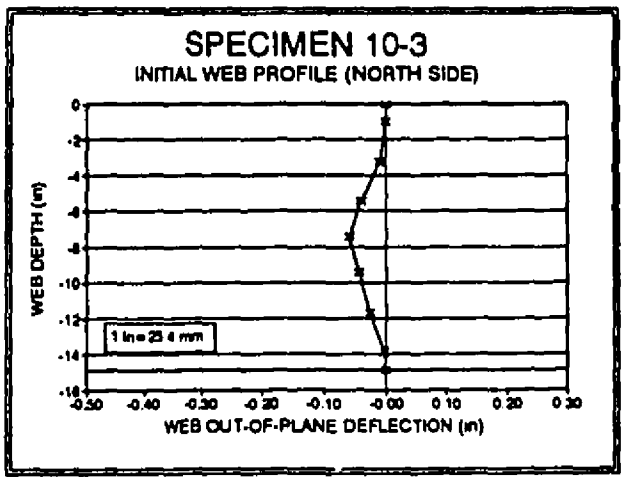


**Fig. 5.76:** INITIAL WEB PROFILE (NORTH SIDE)

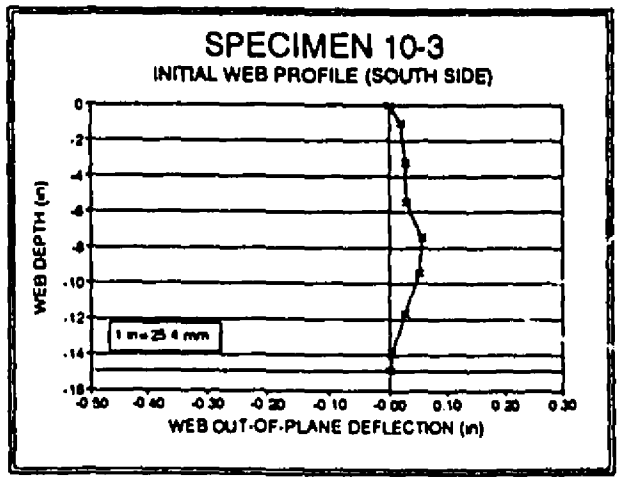


**Fig. 5.77:** INITIAL WEB PROFILE (SOUTH SIDE)

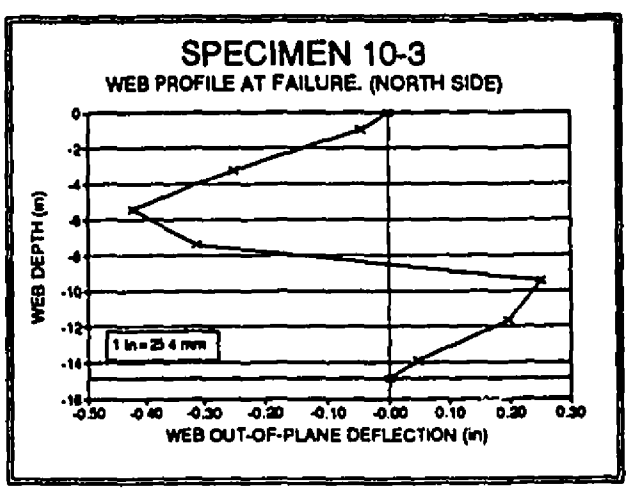


**Fig. 5.78:** FINAL WEB PROFILE (NORTH SIDE)

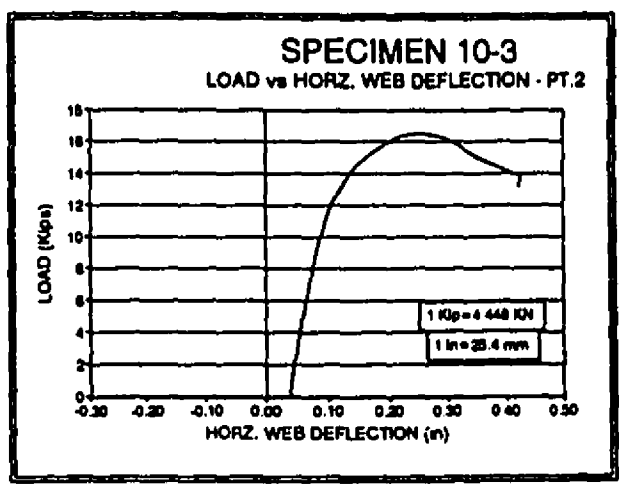


**Fig. 5.79:** LOAD vs. HORZ. WEB DEFLECTION

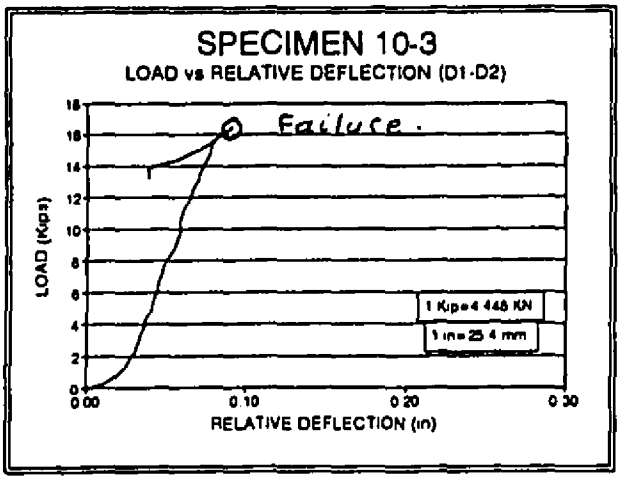


**Fig. 5.80:** LOAD vs. RELATIVE DEFLECTION

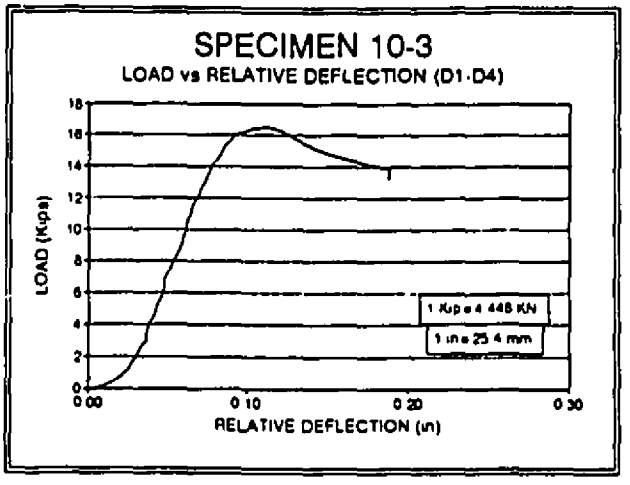


**Fig. 5.81:** LOAD vs. RELATIVE DEFLECTION

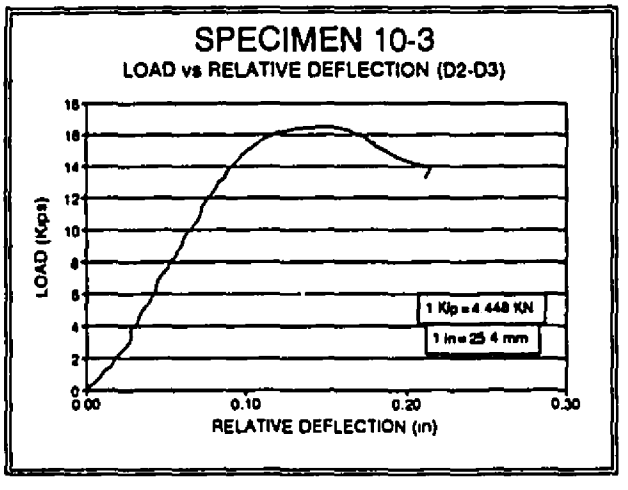


**Fig. 5.82:** LOAD vs. RELATIVE DEFLECTION

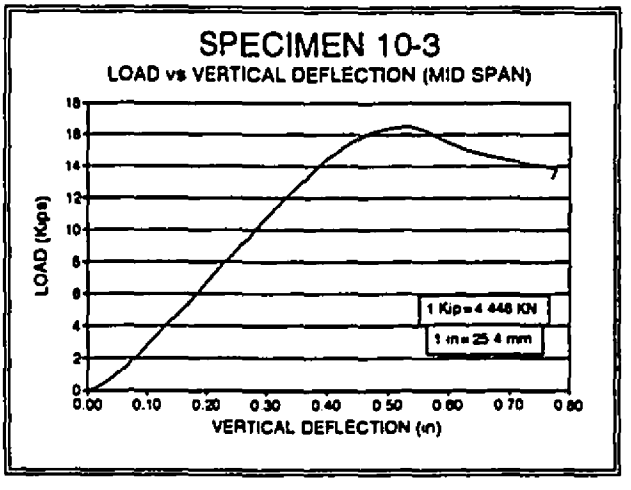


**Fig. 5.83:** LOAD vs. VERTICAL DEFLECTION

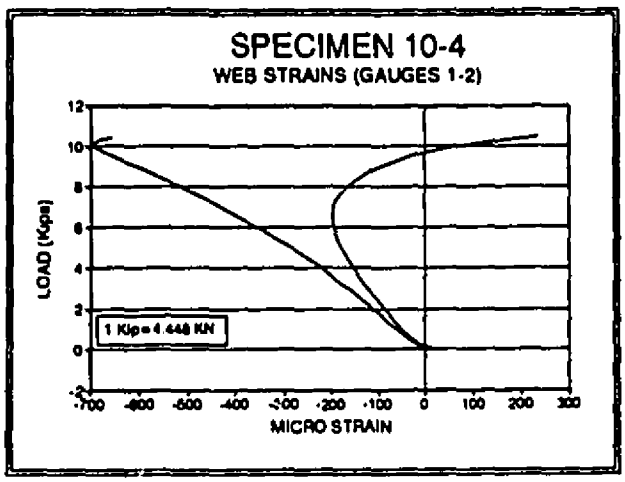


Fig. 5.84: LOAD vs. WEB STRAIN

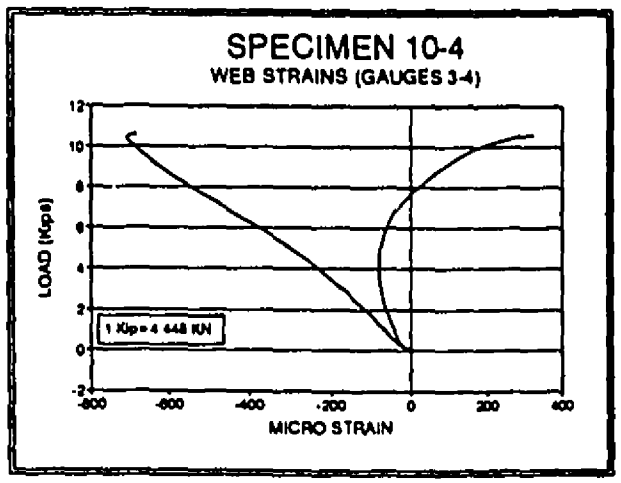


Fig. 5.85: LOAD vs. WEB STRAIN

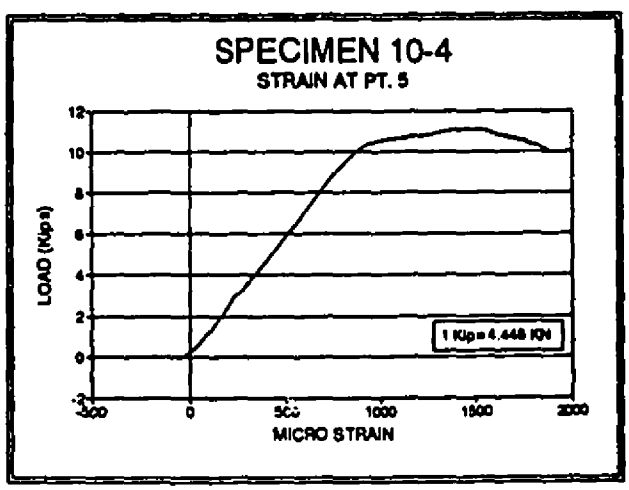


Fig. 5.86: LOAD vs. FLANGE STRAIN

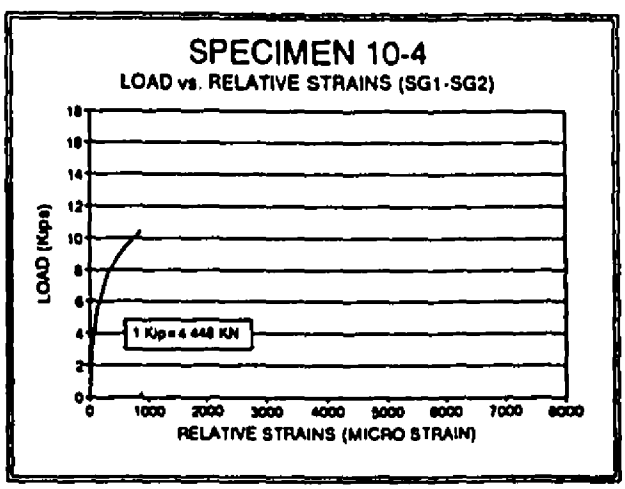


Fig. 5.87: LOAD vs. STRAIN DIFFERENCES

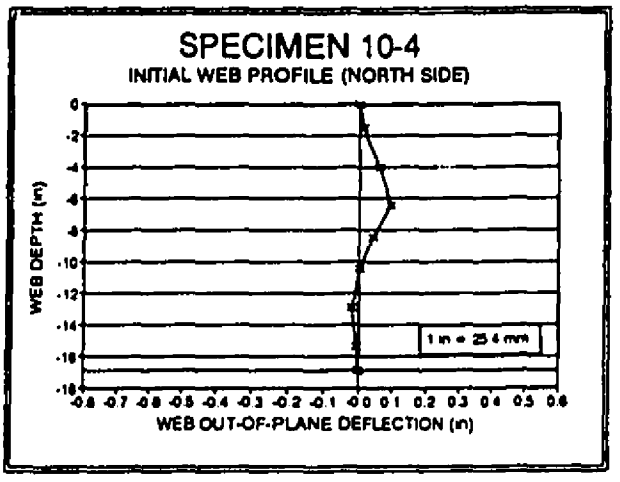


Fig. 5.88: INITIAL WEB PROFILE (NORTH SIDE)

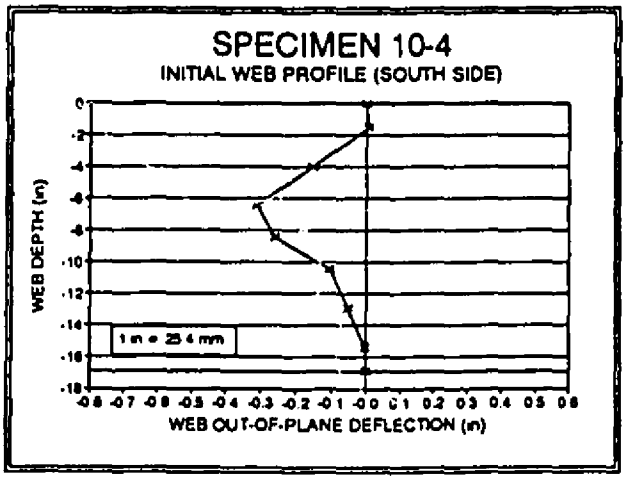


Fig. 5.89: INITIAL WEB PROFILE (SOUTH SIDE)

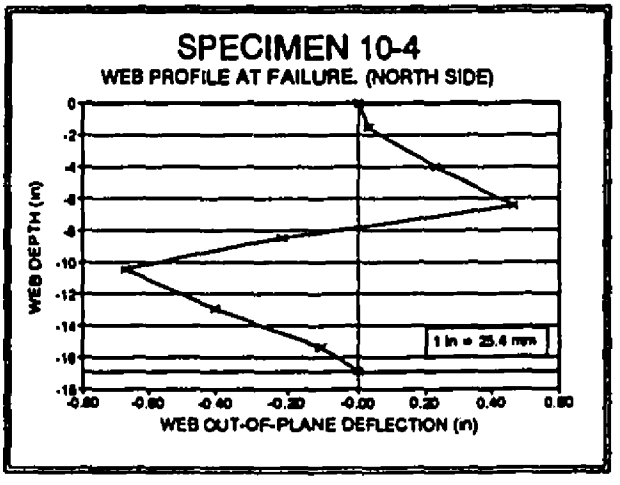


Fig. 5.90: FINAL WEB PROFILE (NORTH SIDE)

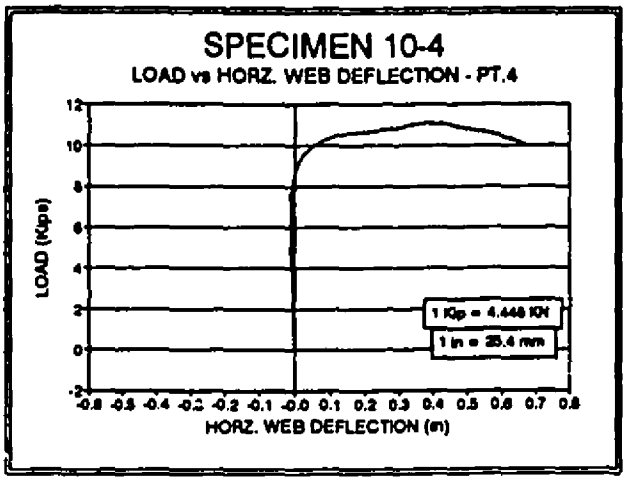


Fig. 5.91: LOAD vs. HORZ. WEB DEFLECTION

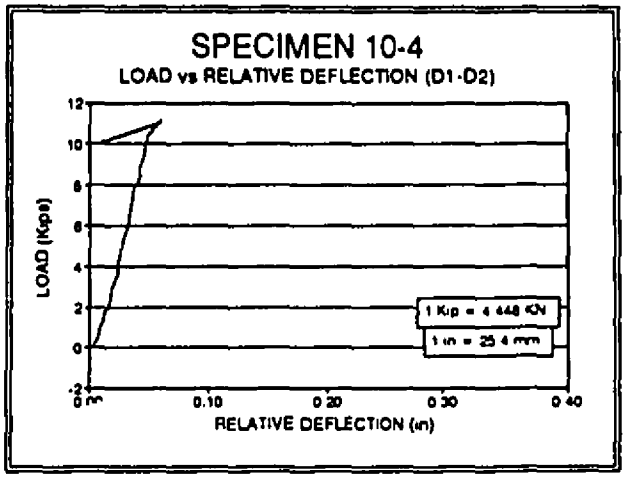


**Fig. 5.92:** LOAD vs. RELATIVE DEFLECTION

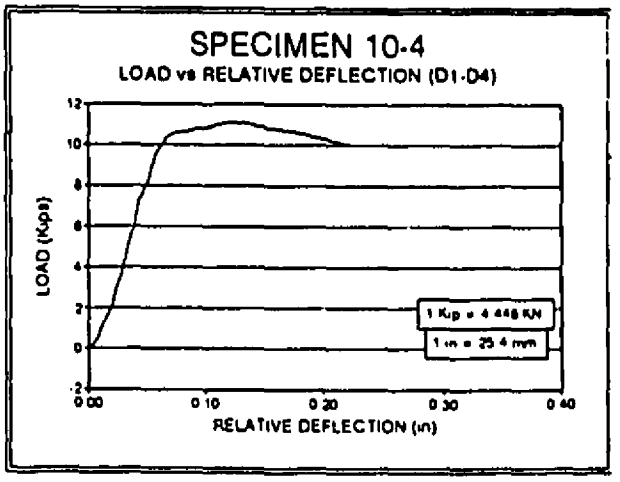


**Fig. 5.93:** LOAD vs. RELATIVE DEFLECTION

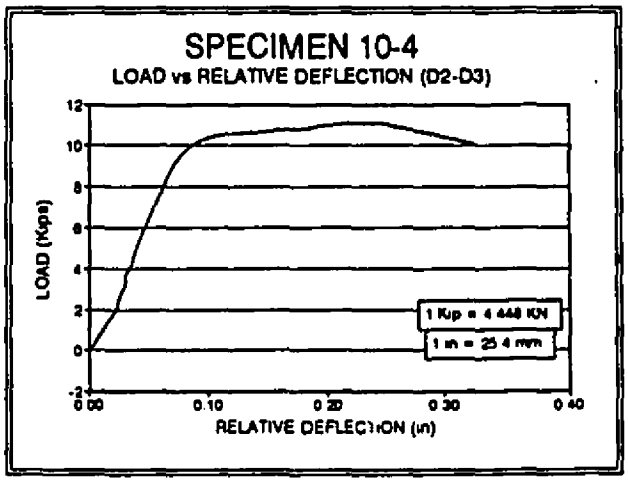


**Fig. 5.94:** LOAD vs. RELATIVE DEFLECTION

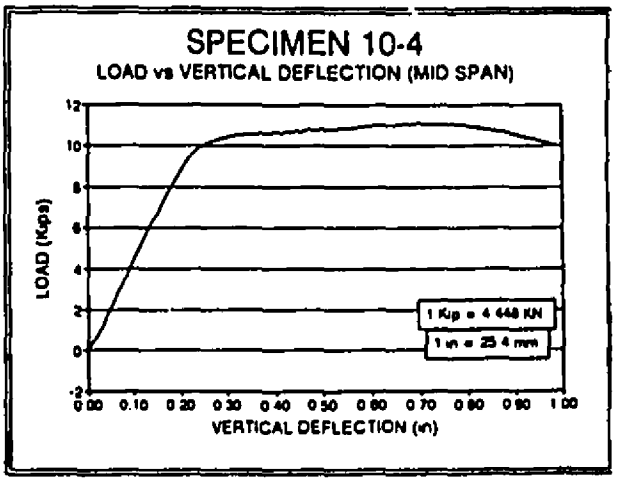


**Fig. 5.95:** LOAD vs. VERTICAL DEFLECTION

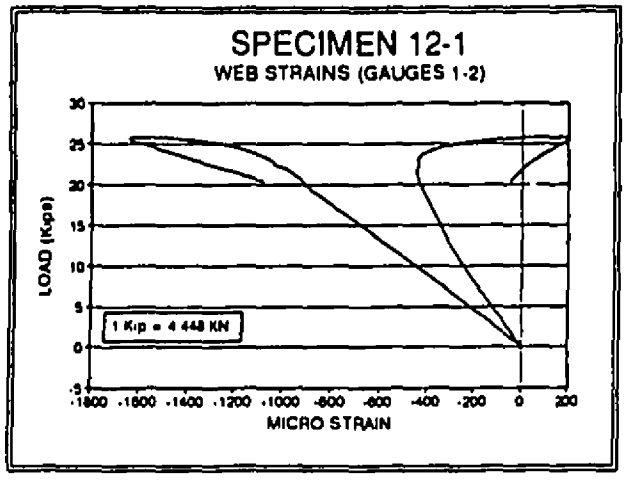


**Fig. 5.96:** LOAD vs. WEB STRAIN

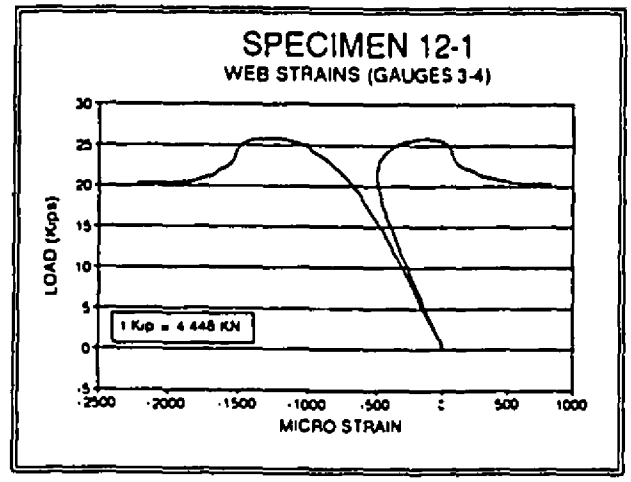


**Fig. 5.97:** LOAD vs. WEB STRAIN

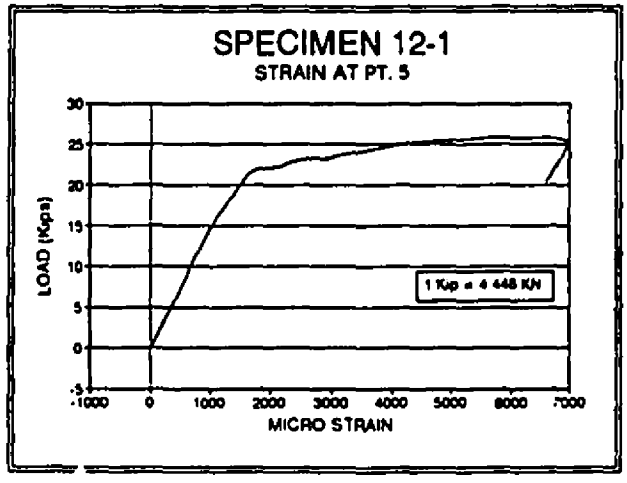


**Fig. 5.98:** LOAD vs. FLANGE STRAIN

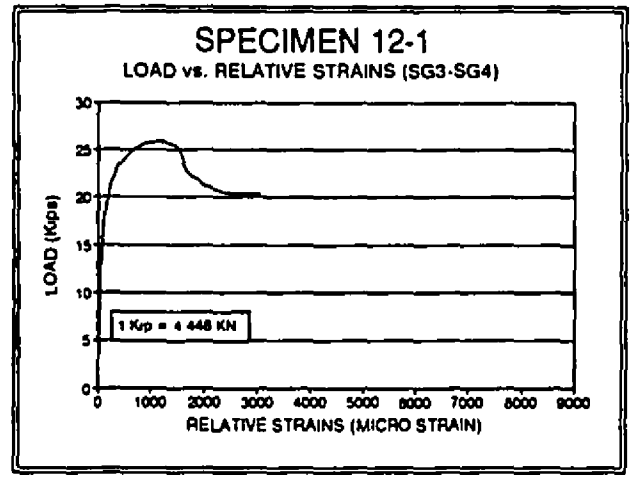


**Fig. 5.99:** LOAD vs. STRAIN DIFFERENCES

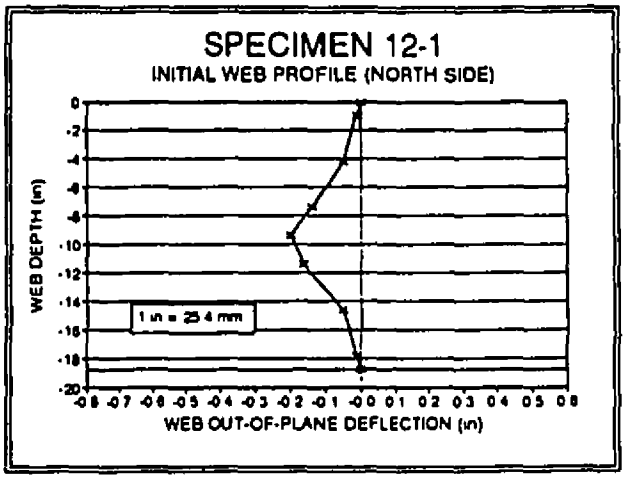


**Fig. 5.100:** INITIAL WEB PROFILE (NORTH SIDE)

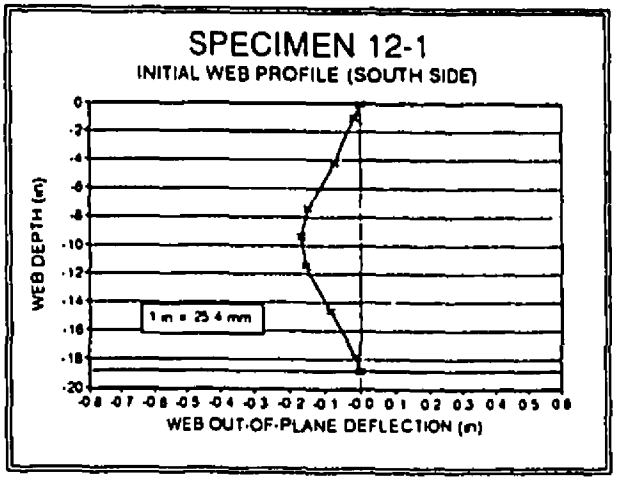


**Fig. 5.101:** INITIAL WEB PROFILE (SOUTH SIDE)

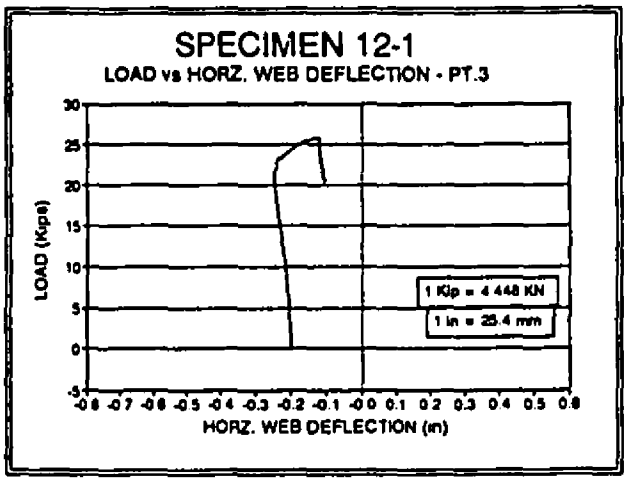


**Fig. 5.102:** LOAD vs. HORIZONTAL WEB DEFLECTION

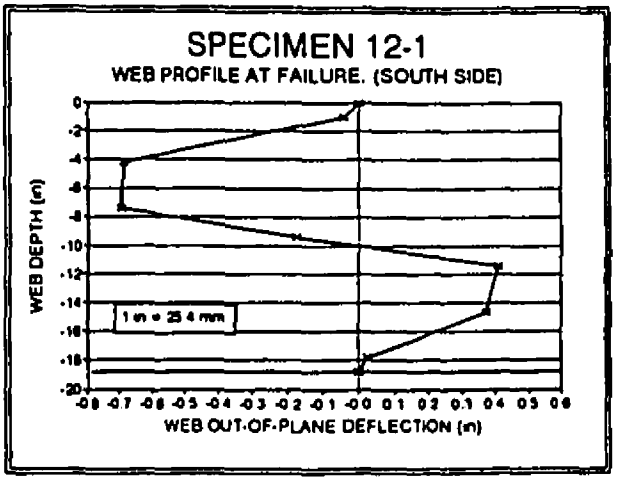


**Fig. 5.103** FINAL WEB PROFILE (SOUTH SIDE)

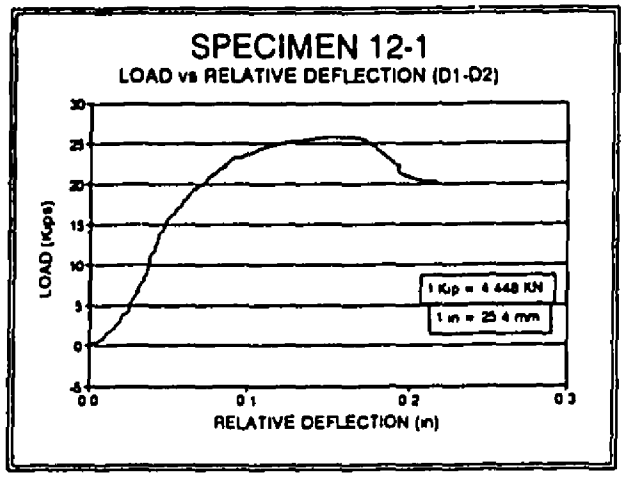


**Fig. 5.104:** LOAD vs. RELATIVE DEFLECTION

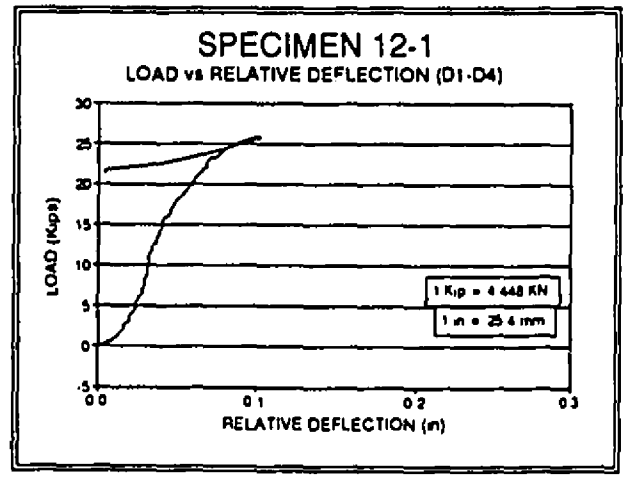


**Fig. 5.105:** LOAD vs. RELATIVE DEFLECTION

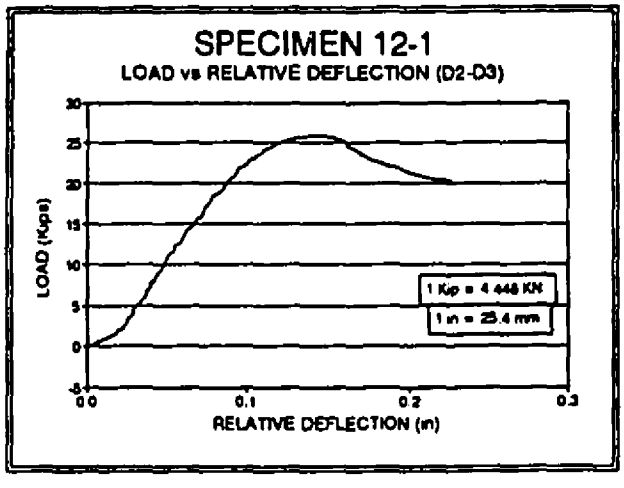


**Fig. 5.106:** LOAD vs. RELATIVE DEFLECTION

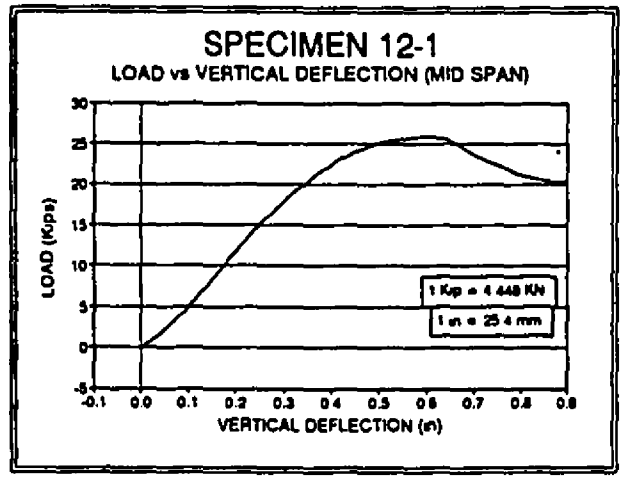


**Fig. 5.107:** LOAD vs. VERTICAL DEFLECTION

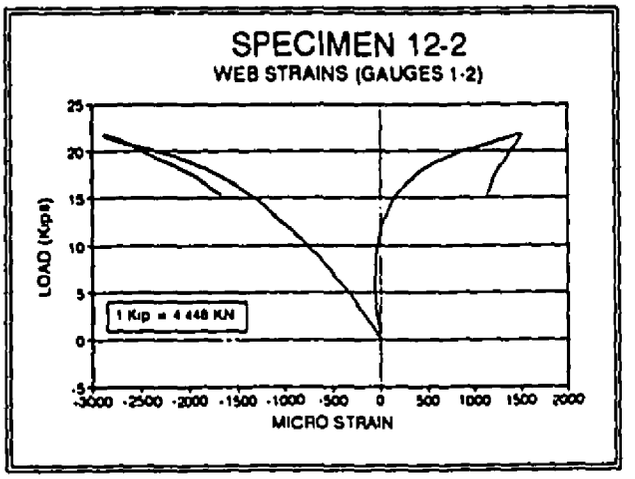


Fig. 5.108: LOAD vs. WEB STRAIN

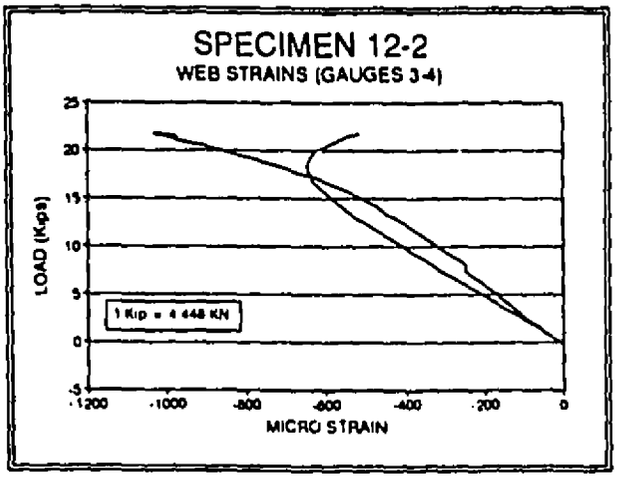


Fig. 5.109: LOAD vs. WEB STRAIN

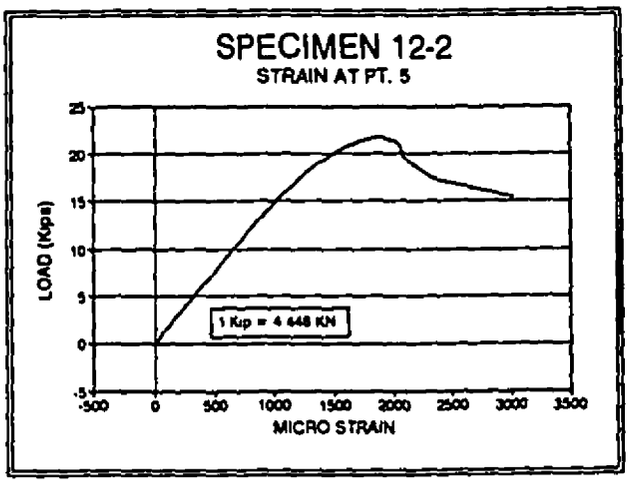


Fig. 5.110: LOAD vs. FLANGE STRAIN

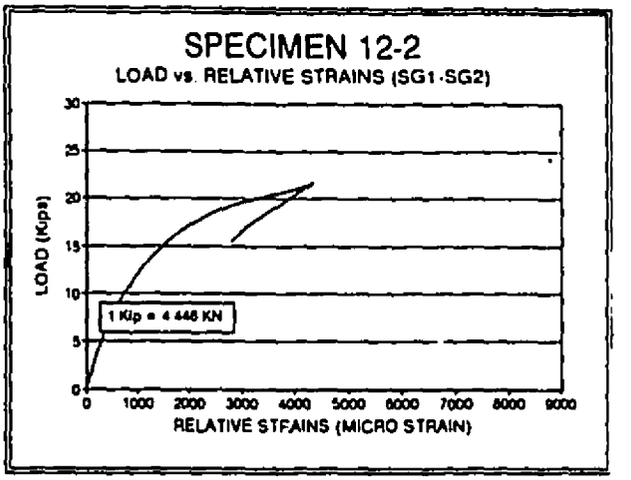


Fig. 5.111: LOAD vs. STRAIN DIFFERENCES

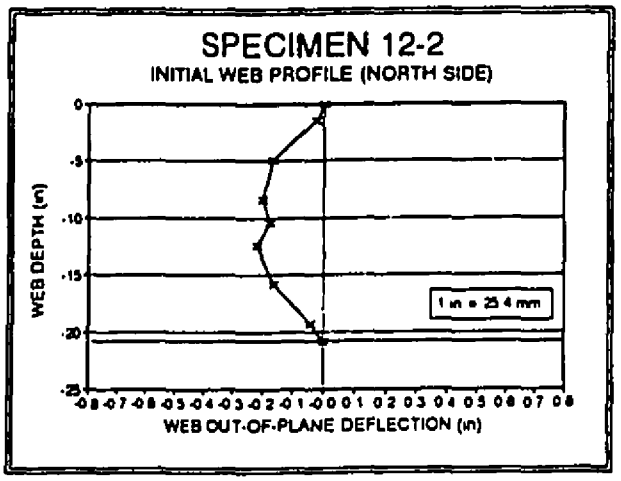


**Fig. 5.112:** INITIAL WEB PROFILE (NORTH SIDE)

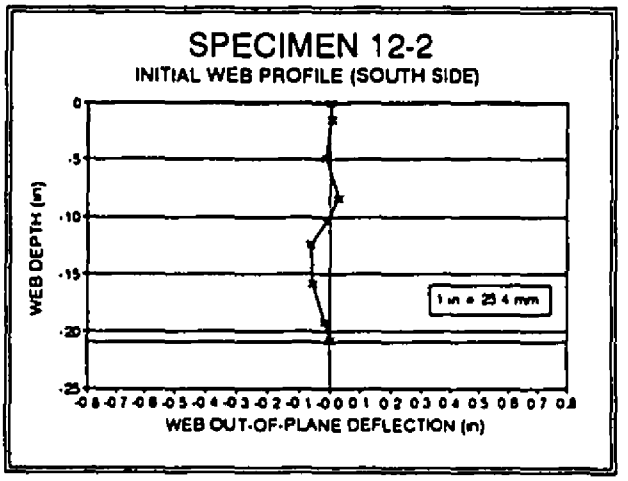


**Fig. 5.113:** INITIAL WEB PROFILE (SOUTH SIDE)

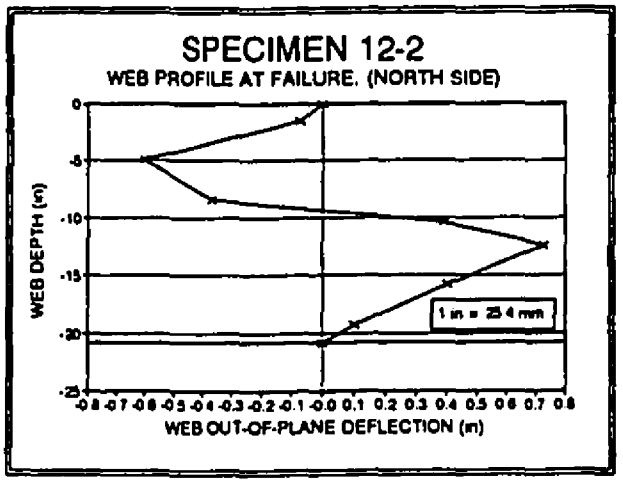


**Fig. 5.114:** FINAL WEB PROFILE (NORTH SIDE)

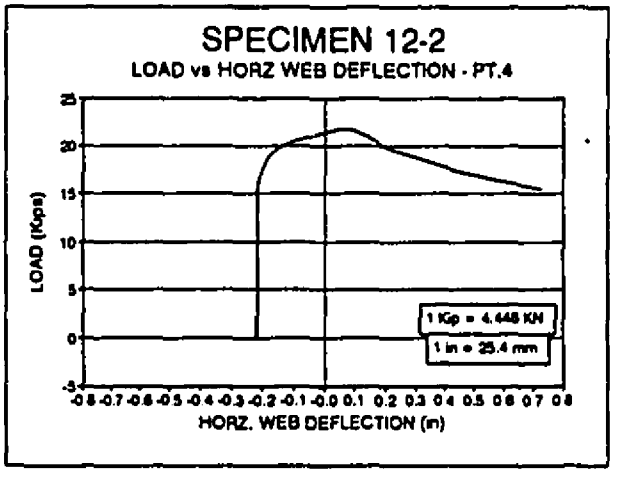


**Fig. 5.115:** LOAD vs. HORIZONTAL WEB DEFLECTION

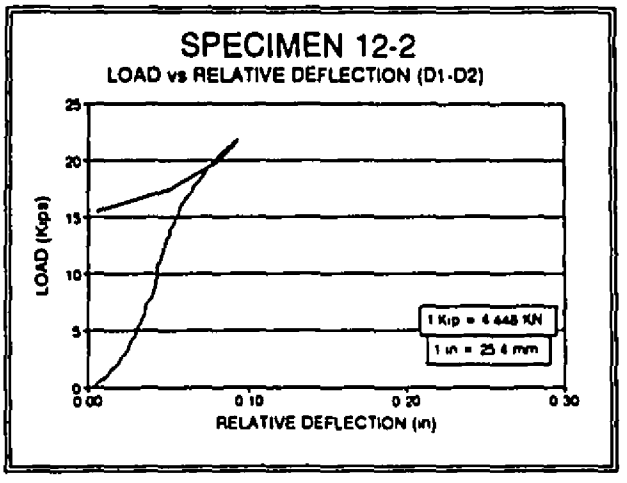


**Fig. 5.116:** LOAD vs. RELATIVE DEFLECTION

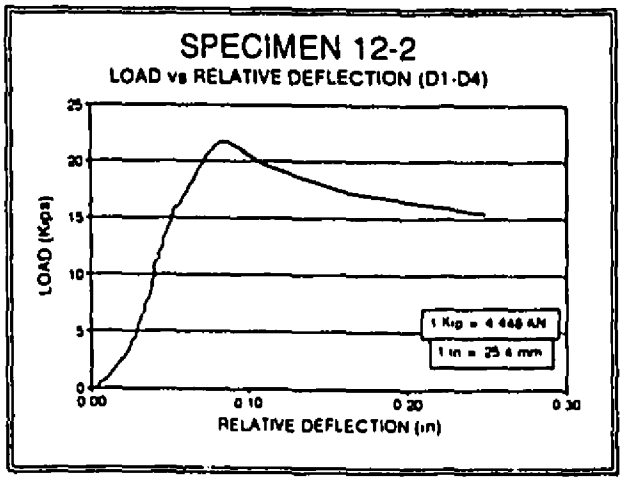


**Fig. 5.117:** LOAD vs. RELATIVE DEFLECTION

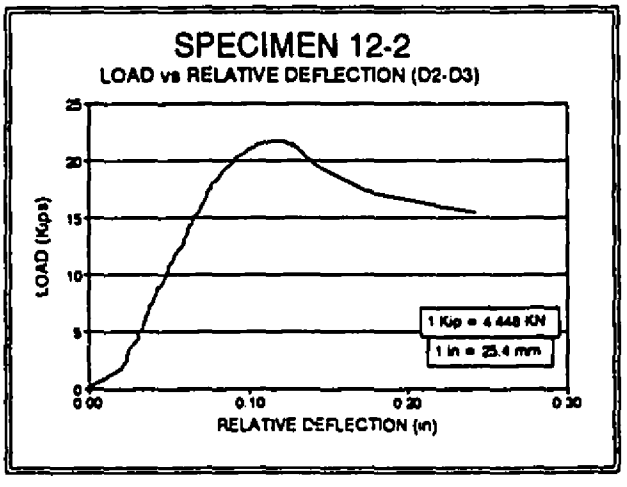


**Fig. 5.118:** LOAD vs. RELATIVE DEFLECTION

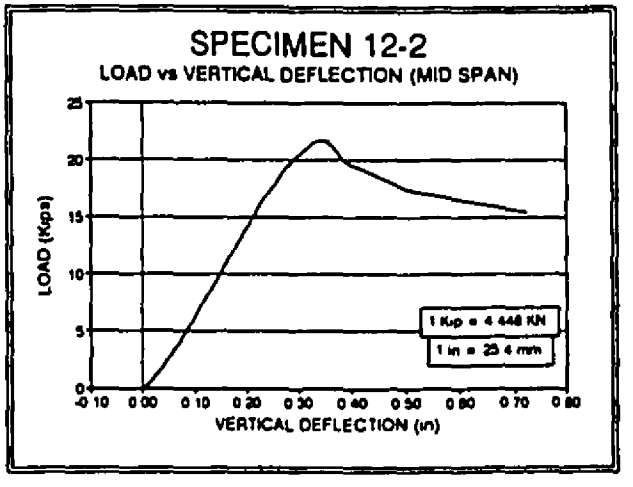


**Fig. 5.119:** LOAD vs. VERTICAL DEFLECTION

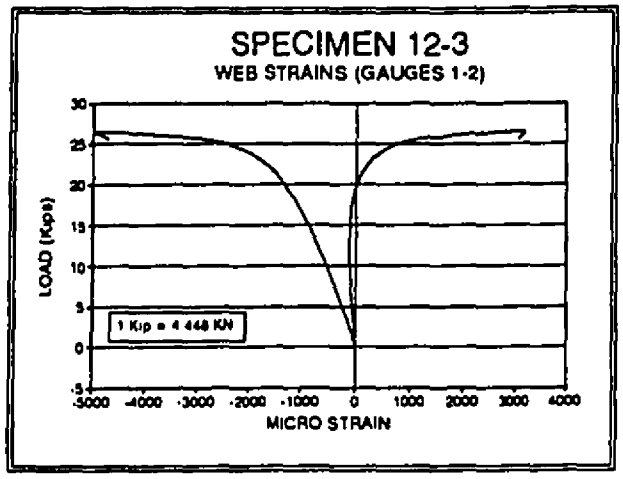


**Fig. 5.120:** LOAD vs. WEB STRAIN

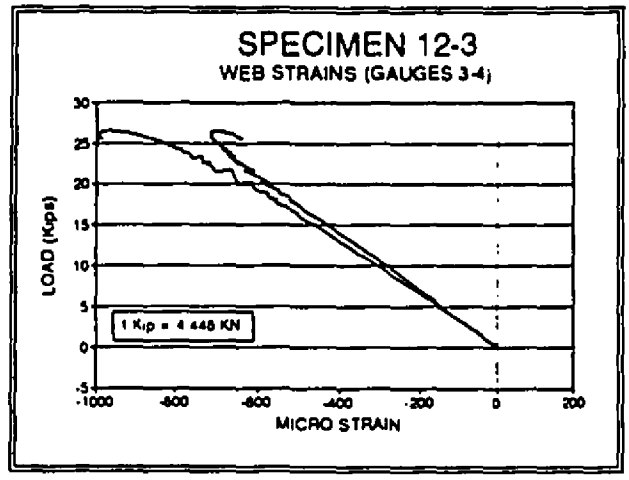


**Fig. 5.121:** LOAD vs. WEB STRAIN

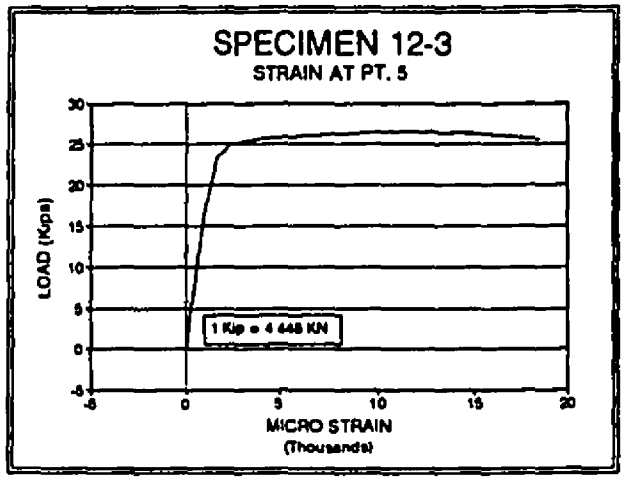


**Fig. 5.122:** LOAD vs. FLANGE STRAIN

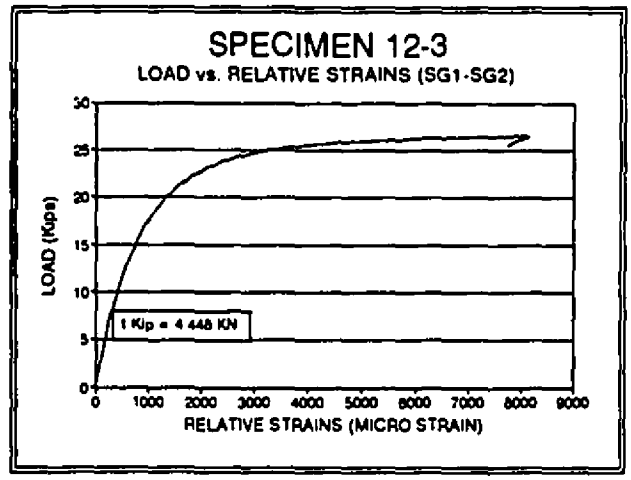


**Fig. 5.123:** LOAD vs. STRAIN DIFFERENCES

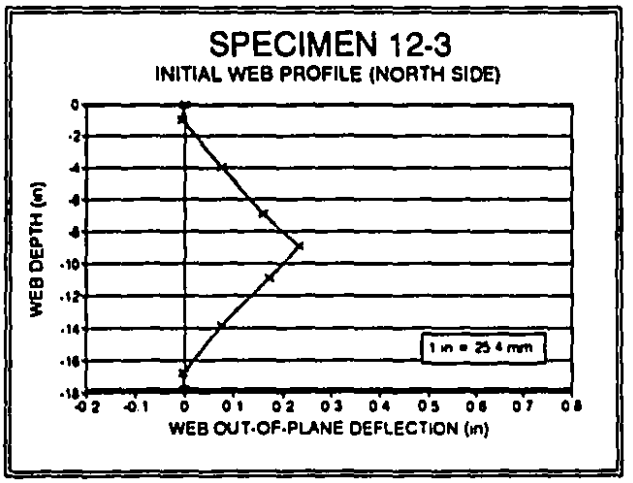


**Fig. 5.124:** INITIAL WEB PROFILE (NORTH SIDE)

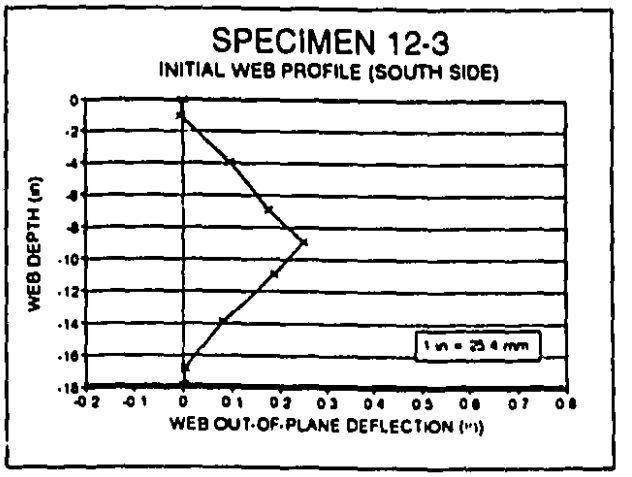


**Fig. 5.125:** INITIAL WEB PROFILE (SOUTH SIDE)

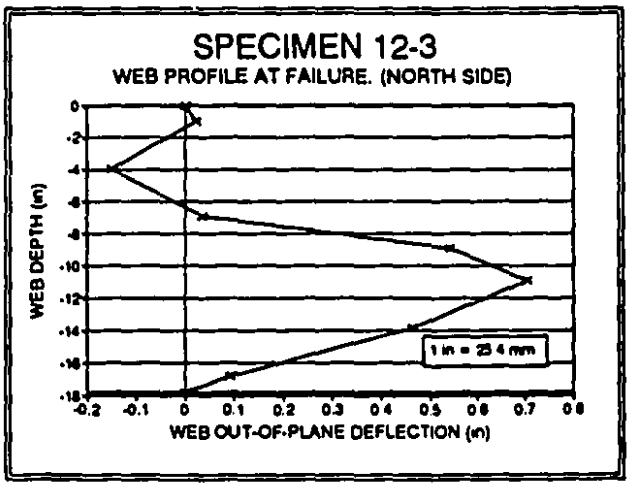


**Fig. 5.126:** FINAL WEB PROFILE (NORTH SIDE)

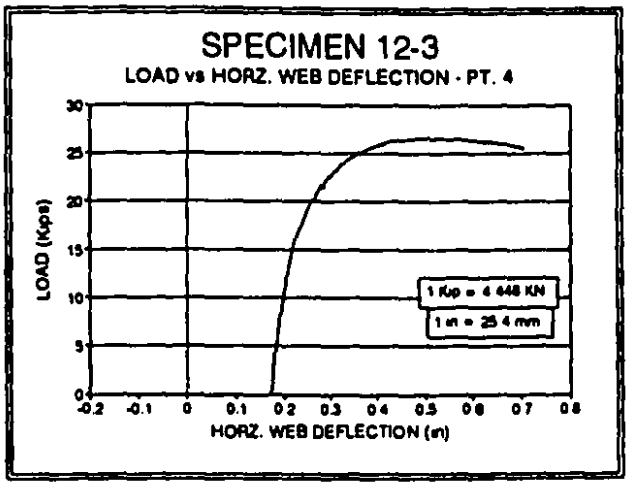


**Fig. 5.127:** LOAD vs. HORIZONTAL WEB DEFLECTION

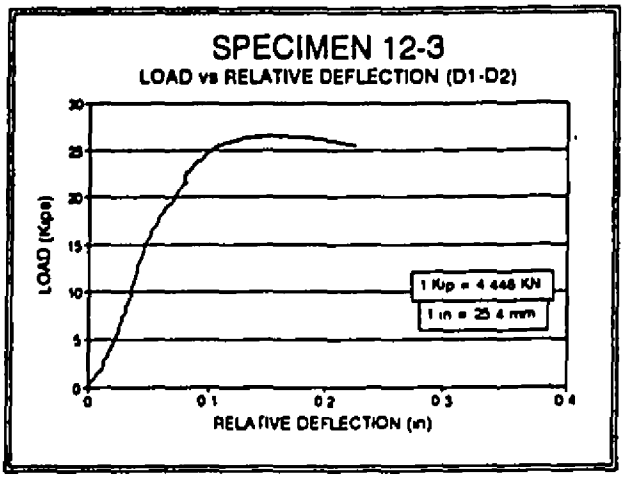


Fig. 5.128: LOAD vs. RELATIVE DEFLECTION

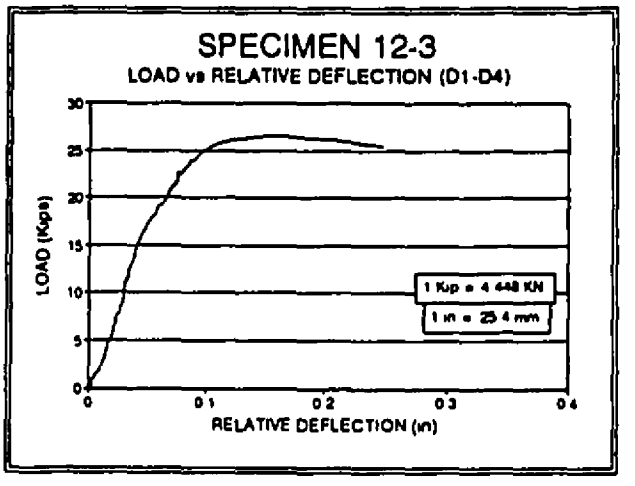


Fig. 5.129: LOAD vs. RELATIVE DEFLECTION

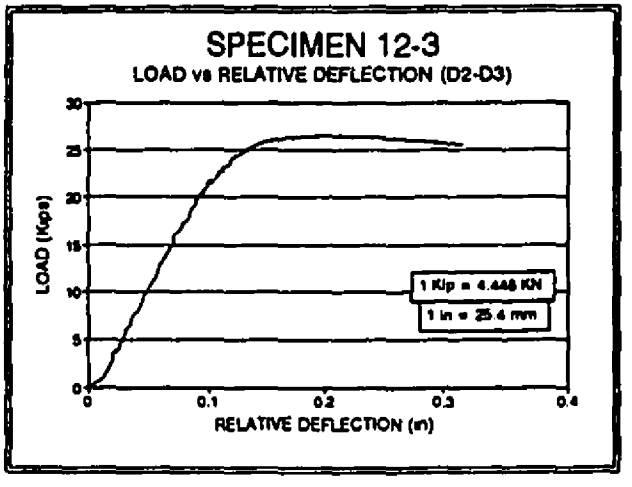


Fig. 5.130: LOAD vs. RELATIVE DEFLECTION

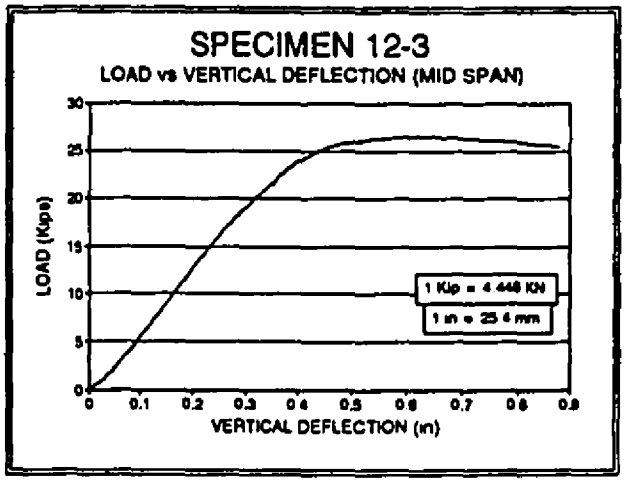


Fig. 5.131: LOAD vs. VERTICAL DEFLECTION

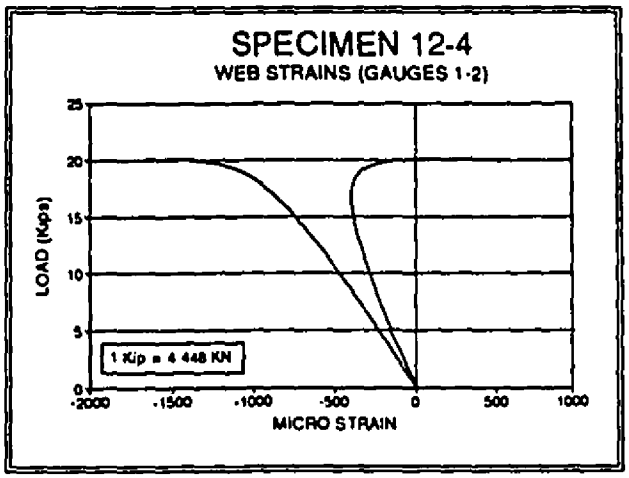


**Fig. 5.132:** LOAD vs. WEB STRAIN

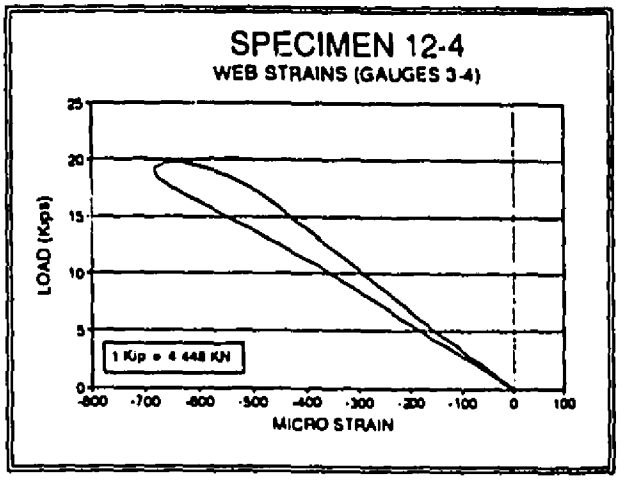


**Fig. 5.133:** LOAD vs. WEB STRAIN

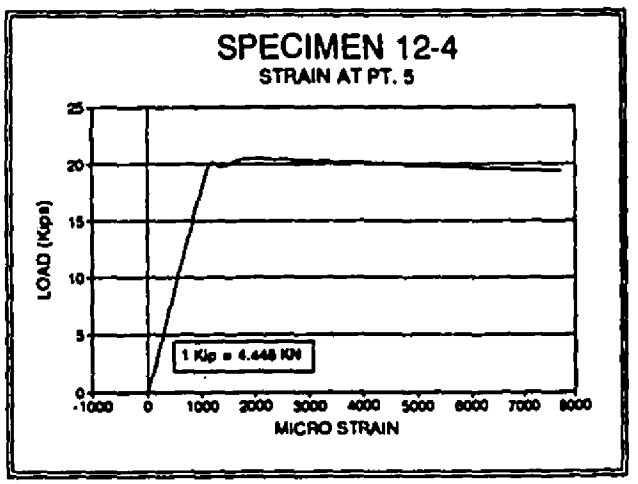


**Fig. 5.134:** LOAD vs. FLANGE STRAIN

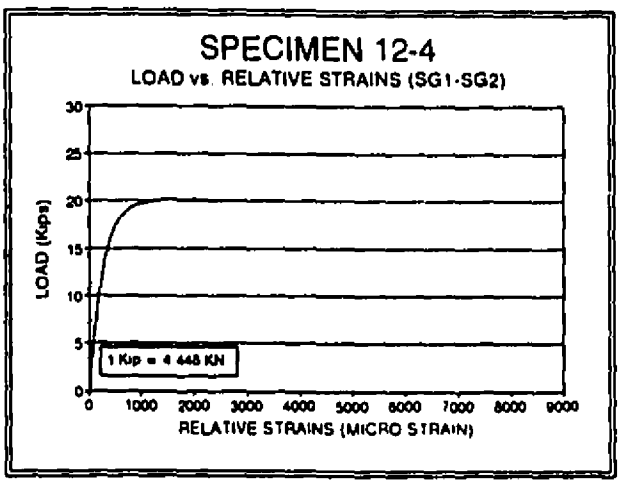


**Fig. 5.135:** LOAD vs. STRAIN DIFFERENCES

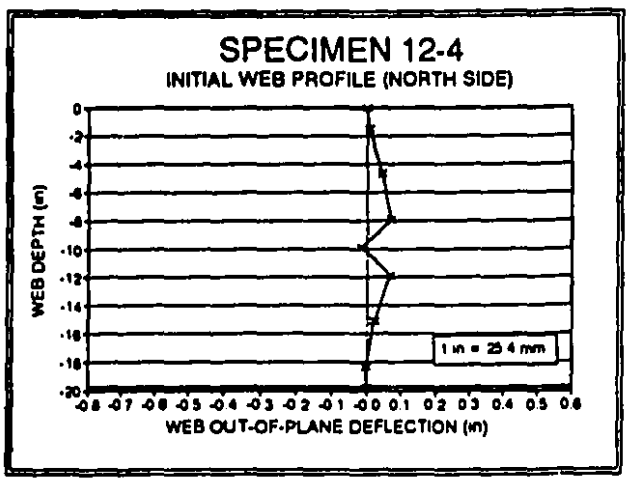


Fig. 5.136: INITIAL WEB PROFILE (NORTH SIDE)

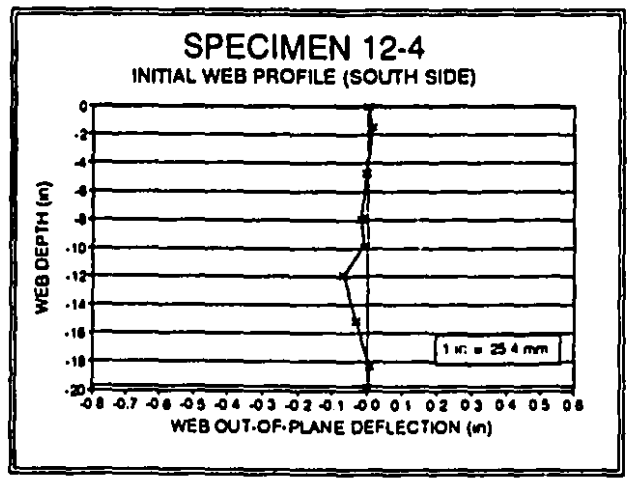


Fig. 5.137: INITIAL WEB PROFILE (SOUTH SIDE)

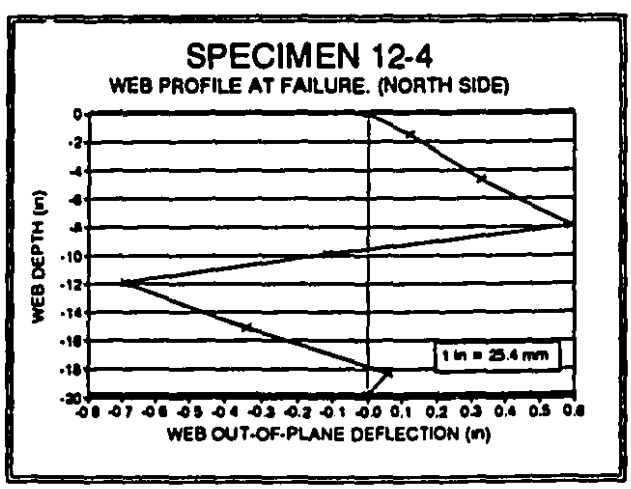


Fig. 5.138: FINAL WEB PROFILE (NORTH SIDE)

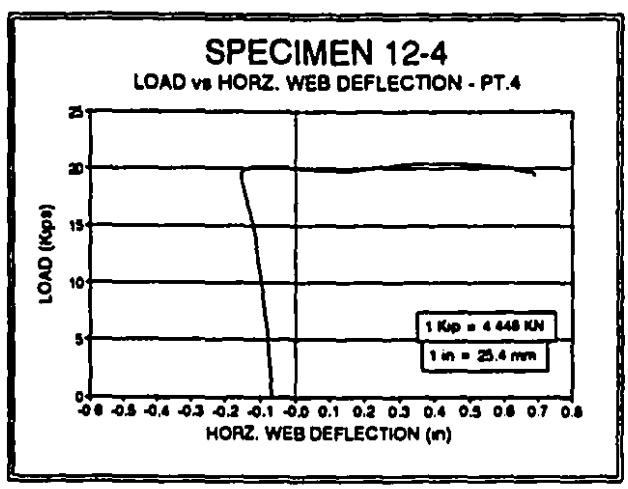


Fig. 5.139: LOAD vs. HORIZONTAL WEB DEFLECTION

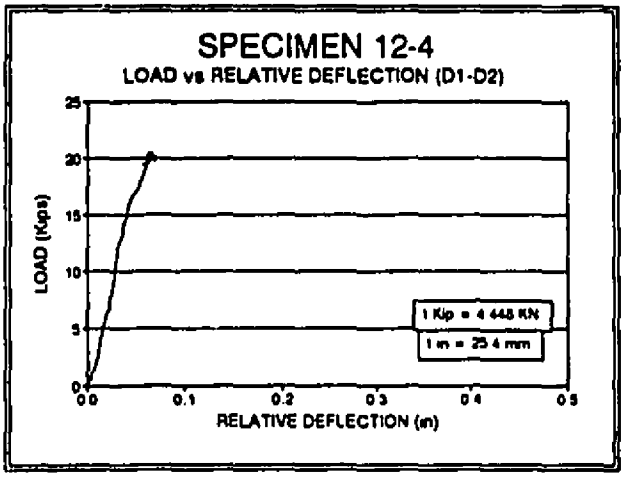


**Fig. 5.140:** LOAD vs. RELATIVE DEFLECTION

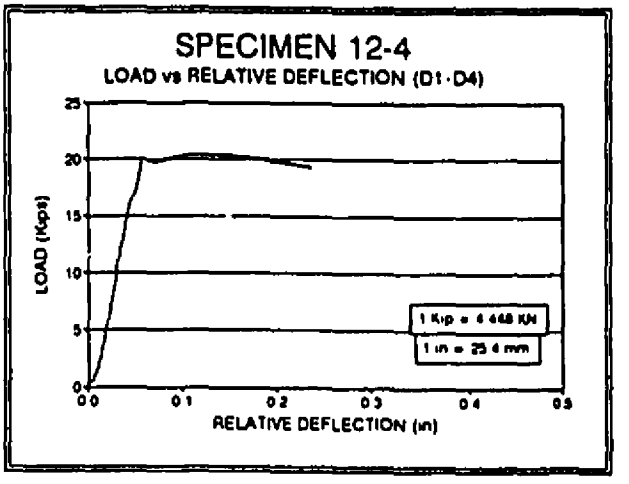


**Fig. 5.141:** LOAD vs. RELATIVE DEFLECTION

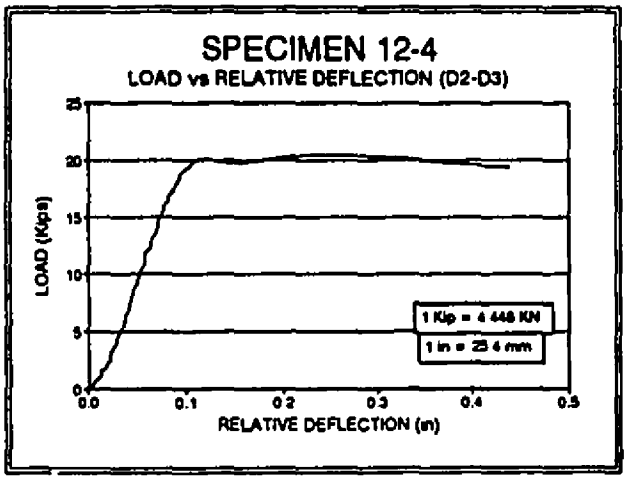


**Fig. 5.142:** LOAD vs. RELATIVE DEFLECTION

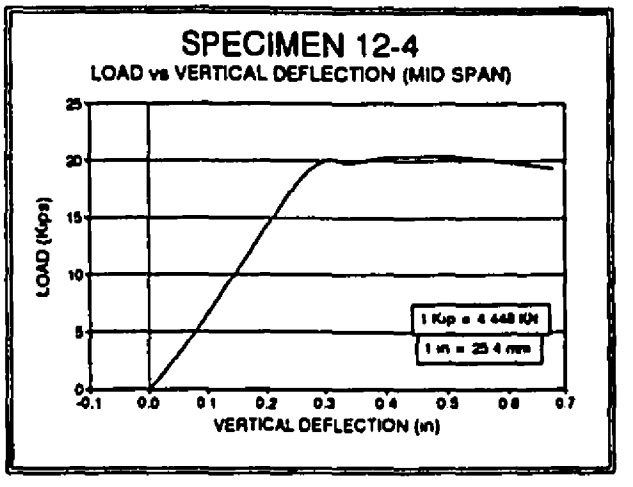


**Fig. 5.143:** LOAD vs. VERTICAL DEFLECTION

# Chapter 6

## Results and Discussion

### 6.1 Prediction of The Mode of Failure

Due to the very thin webs of the beams, which result in slender web-posts, the predicted mode of failure for most of the available specimens was web-post buckling. As a preliminary guide for the prediction of the modes of failure, a number of analyses based on previous studies were carried out and a nonlinear finite element analysis was also performed.

Referring to the moment and shear force diagram (Fig. 1.8), resulting from the test set up, the loads which will cause the formation of the mechanism (Redwood 1974), horizontal shear (Blodgett 1963), and the buckling load (predicted by the finite element analysis) were calculated. The yield failure is given in Table 6.1 as $P_y$, which is the smaller of the load predicted to cause the formation of the mechanism and the load required to cause horizontal yielding of the web-post at mid-depth.

A comparison between the load values predicted for a buckling failure of the web-post, using NASTRAN, and the load causing the yield failure is presented in Table 6.2 for the test specimens. Specimens 8-3a and 8-4a are excluded from this discussion because their modes of failure were dominated by lateral-torsional buckling of the beam. Column 4 of this table shows the percentage difference. A large percentage, the buckling load being lower than the yield load, could be interpreted as an indication of sensitivity to web-post buckling.

In column 4 of Table 6.2, specimen 8-3 has a difference of only 2.5 % between the predicted yield failure load and the load predicted by NASTRAN to cause a web-post buckling failure. Thus either mode may be expected. In all other specimens, buckling was predicted to be the governing mode of failure. Referring to column 5, giving the experimental mode of failure, specimen 8-3 failed by local buckling and torsion of the tee-section. This may have occurred before the full yield load was reached or at the full yield load, (probably the latter). Thus was therefore not unexpected based on the predicted loads.

For all other specimens, except 8-1a, the predicted mode of failure, which was web-post buckling, was also the observed experimental mode of failure. For specimen 8-1a, the experimental mode of failure was the buckling of the tee-section while the prediction was buckling of the web-post. Fig. 6.1 is a bar chart which shows a comparison between the buckling loads predicted by the finite element analysis (NASTRAN) and the load needed to cause a yield failure.

## 6.2 Failure by the Formation of the Mechanism

The calculations for the mechanism failure is based on a study by Redwood (1978). Table 6.3 and Fig. 6.2 show a comparison between the experimental failure loads and the calculated mechanism failure loads for specimens 8-1a and 8-3. They were the only specimens to fail in a mode other than the buckling of the web-post. The method suggested by Redwood (1978), shows a close and consistent agreement with the experimental results. It should be noted that the mechanism theory is a lower bound value; strain-hardening is ignored. In the past, experimental results used to justify this theory by taking the "yield failure load" not as the maximum load in a test, but as an intercept to the two tangents as shown in Fig. 6.4.

## 6.3 Comparison of Buckling Loads

The prediction of the buckling loads was estimated using the three methods discussed earlier, (Blodgett (1963), Aglan and Redwood (1974) and the nonlinear finite element analysis). The comparisons are summarised in a tabular form as well as in a bar chart form. Specimens 8-1a and 8-3, which did not fail by web-post buckling, are omitted in this comparison.

### 6.3.1 Blodgett

Table 6.4 gives a comparison between the buckling load predicted by Blodgett's (1963) method, $P_B$ and the maximum test buckling load, $P_{test}$. $P_B$ is very conservative, and it seems this method is not valid for such small thicknesses. The predicted buckling values are, consistently, conservative, by amounts varying from 53.1 % to 70.7 %.

### 6.3.2 Aglan and Redwood

Table 6.5 is a comparison between the buckling load predicted by Aglan and Redwood (1974), $P_{AR}$ , and the maximum test buckling loads, $P_{test}$. $P_{AR}$ is conservative except for specimens 10-3 and 12-3, (indicated by a negative value). These results are also presented in the bar chart in Figs. 6.3b and 6.3c. These two values are, however, close to the experimental buckling loads, (6.6 % and 4.2 %). It should be noted that for specimens 10-1 and 12-1, the method proposed by Aglan and Redwood (1974) predicted a buckling load higher than the yield failure given in Table 6.1, and therefore, a yield mechanism is the predicted failure mode.

### 6.3.3 Finite Element Analysis (NASTRAN)

Table 6.6 gives a comparison between the maximum test buckling loads and the predicted web-post buckling based on the finite element analyses, using NASTRAN. The predictions by NASTRAN, are within 15 % of the test results, except for specimen 10-4, which is 26.5% higher. The finite element analysis predicted a buckling failure at 14.3 kips (63.6 kN) while experimentally it failed at 11.3 kips (50.3 kN). The mean of the test to predicted results for all 10 specimens is 0.993 with a standard deviation of 0.12.

## 6.4 Overall Comparison

An overall comparison is summarised in Table 6.7. This gives $P_y$, which is the yield failure, i.e. the smaller of the load which causes the formation of the mechanism and the load required to cause horizontal yielding at mid-depth of the web-post. $P_y$ may be compared with $P_{cr}$ which is taken to be the load predicted by the finite element model. The smallest of $P_{cr}$ and $P_y$ is compared to the maximum test load $P_{test}$. Table 6.8 summarises the analytical and experimental results.

## 6.5 Influence of Parameters on Section Behaviour

One of the important results of this study is the data acquired from the tested specimen. A meaningful comparison can be drawn between the pairs of castellated beam geometries that are similar in all aspects except the presence of an intermediate plate or its absence, Figs. 2.5 and 2.7. Figs. 6.5 to 6.16 show the Load vs. Web Strains of the tested specimen. Each group of four beams, which originated from the same shape, are plotted on the same scale.

**Sections with or without Intermediate Plates**

The pairs (8-1a 8-2a), (8-3 8-4), (10-1 10-2), (10-3 10-4), (12-1 12-2) and (12-3 12-4) have the same geometries except for the presence of an intermediate plate or its absence. The second of each pair has an intermediate plate. There is a significant drop in the carrying capacity of beams with intermediate plates compared to those without such plates.

In buckling analysis, the mid-height of a specimen is a critical section in determining the buckling load. In the cases where an intermediate plate exists, the small plate section at mid-height compared to the upper and lower sections of the web with inclined sides, acts as a weak section (Fig. 6.17).

A study of the graphs of Load vs. Web Strains (Figs. 6.5 to 6.16), suggest that the sections with no intermediate plates have a more clearly defined response in the post buckling range. The sections with intermediate plates seem to show a sudden failure mode with no load resistance after buckling. On the other hand, the sections with no intermediate plates show additional load resistance after buckling.

**Sections with no Intermediate Plates**

Comparing the pairs of sections with no intermediate plates but with different angles of cut and geometries, and in particular the two pairs (10-1 10-3) and (12-1 12-3), it can be deduced that the angle of cut $\phi$, is not the only parameter which affects the behaviour of the beams that originate from the same shape. The other influential parameters are e, b, $d_t$ and h. Fig 1.2 is a typical section which identifies these parameters. A comparison between specimen 10-1 and 10-3 shows that 10-1 has a more favourable response in the post buckling range and a higher buckling load (taking the asymptote of the strain curves); on the other hand, a comparison between 12-1 and 12-3 shows that 12-3 has a more favourable response in the post-buckling range and the buckling loads are very close to each other.

**Sections With Intermediate Plates**

Referring to the pairs of sections with intermediate plates that originated from the same shapes, in particular (10-2 10-4) and (12-2 12-4), it can be seen that for the available geometries, the sections with a phi value of around 45°, has a lower buckling load than the sections with a phi value of around 60°; however, the latter shows a less favourable response in the post buckling range. From this, it may be deduced that the other parameters e, b, h and $d_t$, which had an important influence on the beams with no intermediate plate, have less influence when an intermediate plate is introduced. It seems that the phi angle is the most influential factor in the post-buckling behaviour where we have a section with an intermediate plate.

## 6.6 Influence of Initial Imperfections

The web out-of-plane flatness causes a decrease in the carrying capacity of the web-posts. If the imperfections are large, the web-post will undergo large deformations at loads smaller than the theoretical value of the buckling load (Chajes 1974). A good representation is Fig. 6.14 which shows the Load vs. Web Strains for specimen 12-2. The web-post has an initial out-of-plane deflection of 0.22" (5.6 mm). From the start of loading, the strains immediately move away from each other. The instability seems to be characterised by a large increase in lateral deflection as the load increases, rather than a sudden loss of stability. In the case where a web-post undergoes inelastic buckling the initial out-of-plane deflections become more critical, since the web-post is more sensitive to initial imperfections in the case of inelastic buckling. This is a typical behaviour of slender columns with large imperfections.

For some specimens, even though the load was offset (1 in, 25.4 mm) to initiate failure on one side, buckling occurred on the south side, i.e. the side opposite to where the load was offset. This failure may be attributed to the initial large imperfections in the web-

posts. Table 5.1 is a summary of the initial web-out-of-plane deflections, camber and sweep.

### 6.7 Lateral Supports

To avoid any overall lateral torsional buckling, the calculations were based on the CAN/CSA-S16.1-M89. The area of the holes was subtracted from the total area of the web to represent the decrease in strength, in particular the torsional constant. This proved to be a good approach since overall buckling did not occur in the final test program.

### 6.8 Analysis of Beam Sections Tested by Bazile and Texier (1968)

An experimental study on seven castellated steel beams was performed in France, (Bazile and Texier 1968). Five of the seven beams which were tested failed by web-post buckling. These beams are referred to as specimens A, B, C, D, and E. Their nominal dimensions are given in Table C.1d. The length of the beams was chosen as a function of a multiple of sixteen times the pitch. The load was distributed to eight application points. This choice of loading fitted with the span of 16 times the pitch opening, and resulted in a bending moment and a shear force diagram close to that for a uniformly distributed load. The load points were located at one pitch from the end supports, from both ends, and at intervals of two times the pitch length along the span of the beam, Fig. 6.18. The beam supports were hinged at each end with the possibility of longitudinal displacement. Vertical lateral supports were provided along the beam to prevent any overall lateral buckling.

The beams tested at McGill University had a ratio of $(d_g-2t_f)/t_w$ varying from 88.9 to 118.8, while the beams tested by Bazile and Texier (1968) had a ratio varying from 46.9 to 72.6.

Specimens A, B, C, D, and E were analysed to determine the load required to cause the first yield (Blodgett 1963), the load required to cause the formation of a mechanism failure (Redwood 1978) and the load required to cause the horizontal yield at mid-depth of the web-post (Blodgett 1968). The smaller of the loads causing the formation of a mechanism or the horizontal yield is denoted as yield failure and is given in Table 6.9. The yield stress was taken as 43.5 ksi (303 $N/mm^2$) which is the average of the results obtained from the coupon tests done for the five specimens.

The load required to cause the buckling of the web-post based on Blodgett (1968), Aglan and Redwood (1974) and a finite element analysis using NASTRAN were calculated and are given in Table 6.10. The finite element model and the mesh used were the same as was discussed in Chapter 3. The web-post which is adjacent to the end support of the beam was analysed. This represents the section with maximum shear. Referring to Table 6.10, the load required to cause a yield failure is always larger than the load needed to cause failure of the beams by web-post buckling, predicted by any of the three methods. Therefore, all three methods suggest a failure by web-post buckling. This corresponds to the experimental mode of failure of all five specimens.

Table 6.11 gives a comparison between the experimental failure loads and the buckling loads predicted by the three different methods. Blodgett's method does not consistently overestimate or underestimate the experimental buckling load. It fluctuates from 1.5 % to -30.1 %. The method suggested by Aglan and Redwood (1974) gives a buckling load which is always lower than the experimental buckling load. It varies from 10.1 % to 33.3 % lower than the test results. The load predicted by the finite element analysis varies from -12.4 % to +10.6 % of the experimental results, which is a good prediction. For these five specimens the mean of test to predicted values is 0.980 with standard deviation 0.095. For these and the ten specimens failing by web-post buckling described earlier, the mean of test to predicted values is 0.989 with standard deviation 0.109.

**Table 6.1:** Predicted Yield Failure Loads

| Test Specimen | $P_m$[1] (mechanism) (kips*) | $P_{hy}$[2] (horizontal yield) (kips) | $P_y$[3] (kips) | Failure Mode |
|---|---|---|---|---|
| | | | | |
| 8-1a | 11.72 | 18.64 | 11.72 | mechanism |
| 8-2a | 13.08 | 21.90 | 13.08 | mechanism |
| 8-3 | 11.80 | 14.50 | 11.80 | mechanism |
| 8-4 | 13.48 | 17.04 | 13.48 | mechanism |
| 10-1 | 17.04 | 24.06 | 17.04 | mechanism |
| 10-2 | 19.42 | 27.64 | 19.42 | mechanism |
| 10-3 | 18.48 | 17.00 | 17.00 | horizontal yield |
| 10-4 | 19.71 | 19.46 | 19.46 | horizontal yield |
| 12-1 | 29.35 | 38.32 | 29.35 | mechanism |
| 12-2 | 29.94 | 42.66 | 29.94 | mechanism |
| 12-3 | 31.70 | 26.38 | 26.38 | horizontal yield |
| 12-4 | 33.48 | 29.60 | 29.60 | horizontal yield |

**Table 6.2:** Prediction of the Failure Mode

| Test Specimen | $P_y$ (kips) | $P^4_{FEM}$ (buckling, FEM) (kips) | $\frac{(P_y - P_{FEM})}{P_y}$ | Experimental Mode of Failure |
|---|---|---|---|---|
| | | | | |
| 8-1a | 11.72 | 10.0 | 14.7 % | tee-section buckling |
| 8-2a | 13.08 | 11.1 | 15.1 % | web post buckling |
| 8-3 | 11.80 | 11.5 | 2.5 % | tee-section buckling |
| 8-4 | 13.48 | 9.9 | 26.6 % | web post buckling |
| 10-1 | 17.04 | 15.2 | 10.8 % | web post buckling |
| 10-2 | 19.42 | 13.9 | 28.4 % | web post buckling |
| 10-3 | 17.00 | 14.7 | 13.5 % | web post buckling |
| 10-4 | 19.46 | 14.3 | 26.5 % | web post buckling |
| 12-1 | 29.35 | 23.8 | 18.9 % | web post buckling |
| 12-2 | 29.94 | 21.3 | 28.8 % | web post buckling |
| 12-3 | 26.38 | 24.7 | 6.4 % | web post buckling |
| 12-4 | 29.60 | 24.1 | 18.6 % | web post buckling |

[1]Redwood 1978
* 1 kip=4.448 kN
[2]Blodgett 1963
[3]Smaller of $P_m$ and $P_{hy}$
[4]Buckling load predicted by finite element method (NASTRAN)

**Table 6.3:** Failure by the Formation of a Mechanism

| Test Specimen | Pm (mechanism) (kips) | $P^{5}_{test}$ (kips) | $\frac{P_{test} - P_m}{P_{test}}$ | Experimental Mode of Failure |
|---|---|---|---|---|
| | | | | |
| 8-1a | 11.72 | 12.8 | 8.4 % | tee-section buckling |
| 8-3 | 11.80 | 13.0 | 9.2 % | tee-section buckling |

**Table 6.4:** Comparison of $P^{6}_{B}$ vs. $P_{test}$

| Test Specimen | $P_B$ (web buckling) (kips) | $P_{test}$ (experimental buckling) (kips) | $\frac{P_{test}-P_B}{P_{test}}$ | Predicted Mode of Failure[7] |
|---|---|---|---|---|
| 8-1a | 5.27 | ***** | ***** | tee-section buckling |
| 8-2a | 4.10 | 11.2 | 63.4 % | tee-section buckling |
| 8-3 | 5.37 | ***** | ***** | tee-section buckling |
| 8-4 | 4.17 | 8.9 | 53.1 % | tee-section buckling |
| 10-1 | 6.03 | 17.8 | 66.1 % | tee-section buckling |
| 10-2 | 4.77 | 13.2 | 63.9 % | tee-section buckling |
| 10-3 | 5.03 | 16.6 | 69.7 % | tee-section buckling |
| 10-4 | 4.00 | 11.3 | 64.6 % | tee-section buckling |
| 12-1 | 7.63 | 25.8 | 70.4 % | tee-section buckling |
| 12-2 | 6.47 | 22.1 | 70.7 % | tee-section buckling |
| 12-3 | 9.3 | 26.2 | 64.5 % | tee-section buckling |
| 12-4 | 7.63 | 21.0 | 63.7 % | tee-section buckling |

[5]Maximum test load (Table 5.3)
[6]Blodgett 1963
[7]Predictions based on Blodgett (1963)

**Table 6.5:** Comparison of $P^{8}_{AR}$ vs $P_{test}$

| Test Specimen | $P_{AR}$ (web buckling) (kips) | $P_{test}$ (experimental buckling) (kips) | $\frac{P_{AR}-P_{test}}{P_{test}}$ | Predicted Mode of Failure[9] |
|---|---|---|---|---|
| 8-1a | 17.70 | ***** | ***** | yield failure |
| 8-2a | 11.83 | 11.20 | 5.6 % | web post buckling |
| 8-3 | 14.63 | ***** | ***** | yield failure |
| 8-4 | 12.90 | 8.90 | 44.9 % | web post buckling |
| 10-1 | 21.90 | 17.80 | + | yield failure |
| 10-2 | 15.20 | 13.20 | 15.2 % | web post buckling |
| 10-3 | 15.50 | 16.60 | -6.6 % | web post buckling |
| 10-4 | 14.10 | 11.30 | 24.8 % | web post buckling |
| 12-1 | 36.80 | 25.80 | + | yield failure |
| 12-2 | 26.40 | 22.10 | 19.4 % | web post buckling |
| 12-3 | 25.10 | 26.20 | -4.2 % | web post buckling |
| 12-4 | 24.10 | 21.00 | 14.7 % | web post buckling |

**Table 6.6:** Comparison of $P^{10}_{FEM}$ vs $P_{test}$

| Test Specimen | $P_{FEM}$ (web buckling) (kips) | $P_{test}$ (experimental buckling) (kips) | $\frac{P_{FEM}-P_{test}}{P_{test}}$ | Predicted Mode of Failure[11] |
|---|---|---|---|---|
| 8-1a | 10.0 | ***** | ***** | web post buckling |
| 8-2a | 11.1 | 11.20 | -1.0 % | web post buckling |
| 8-3 | 11.5 | ***** | ***** | yield failure |
| 8-4 | 9.9 | 8.90 | 11.2 % | web post buckling |
| 10-1 | 15.2 | 17.80 | -14.6 % | web post buckling |
| 10-2 | 13.9 | 13.20 | 5.3 % | web post buckling |
| 10-3 | 14.7 | 16.60 | -11.4 % | web post buckling |
| 10-4 | 14.3 | 11.30 | 26.5 % | web post buckling |
| 12-1 | 23.8 | 25.80 | - 7.7 % | web post buckling |
| 12-2 | 21.3 | 22.10 | 3.6 % | web post buckling |
| 12-3 | 24.7 | 26.20 | -5.7 % | web post buckling |
| 12-4 | 24.1 | 21.00 | 14.7 % | web post buckling |

[8]Aglan and Redwood 1974
[9]Predictions based on Aglan and Redwood (1974)
+ Invalid comparison since $P_{AR}$ exceeds the yield failure
[10]Buckling load predicted by finite element method (NASTRAN)
[11]Based on predictions by finite element method (NASTRAN)

**Table 6.7:** Table of Analytical Results

| Test Specimen | $P_y$ | $P_{cr}$ | | | $P^{12}$ | $P^{13}_{test}$ |
|---|---|---|---|---|---|---|
| | | Blodgett | Aglan & Redwood | FEM | | |
| | | | | | | |
| 8-1a | 11.72 | 5.27 | 17.70 | 10.0 | 10.0 | 12.8 |
| 8-2a | 13.08 | 4.10 | 11.83 | 11.1 | 11.1 | 11.2 |
| 8-3 | 11.80 | 5.37 | 14.63 | 11.5 | 11.5 | 13.0 |
| 8-4 | 13.48 | 4.17 | 12.90 | 9.9 | 9.9 | 8.9 |
| 10-1 | 17.04 | 6.03 | 21.90 | 15.2 | 15.2 | 17.8 |
| 10-2 | 19.42 | 4.77 | 15.20 | 13.9 | 13.9 | 13.2 |
| 10-3 | 17.00 | 5.03 | 15.50 | 14.7 | 14.7 | 16.6 |
| 10-4 | 19.46 | 4.00 | 14.10 | 14.3 | 14.3 | 11.3 |
| 12-1 | 29.35 | 7.63 | 36.80 | 23.8 | 23.8 | 25.8 |
| 12-2 | 29.94 | 6.47 | 26.40 | 21.3 | 21.3 | 22.1 |
| 12-3 | 26.38 | 9.3 | 25.10 | 24.7 | 24.7 | 26.2 |
| 12-4 | 29.60 | 7.63 | 24.10 | 24.1 | 24.1 | 21.0 |

[12] P is the predicted failure load based on the minimum of $P_y$ and $P_{cr}$ based on the FEM. The latter always controls.

[13] $P_{test}$ is the ultimate test load from Table 5.3

**Table 6.8:** Summary of Results

| Test Specimen | $P^{15}$ ($1^{st}$ yield) (kips) | Pm (mech) (kips) | $P_{hy}$ (horiz. yield) (kips) | $P_B$ (web buckling) (kips) | $P_{AR}$ (web buckling) (kips) | $P_{FEM}$ (web buckling) (kips) | $\frac{(P_y - P_{FEM})}{P_y}$ | $P_{test}$ (kips) | Experimental Mode of Failure |
|---|---|---|---|---|---|---|---|---|---|
| | | | | | | | | | |
| 8-1a | 9.76 | 11.72 | 18.64 | 5.27 | 17.70 | 10.0 | 14.7 % | 12.8 | tee-section buckling |
| 8-2a | 10.40 | 13.08 | 21.90 | 4.10 | 11.83 | 11.1 | 15.1 % | 11.2 | web post buckling |
| 8-3 | 9.20 | 11.80 | 14.50 | 5.37 | 14.63 | 11.5 | 2.5 % | 13.0 | tee-section buckling |
| 8-4 | 9.74 | 13.48 | 17.04 | 4.17 | 12.90 | 9.9 | 26.6 % | 8.9 | web post buckling |
| 10-1 | 16.50 | 17.04 | 24.06 | 6.03 | 21.90 | 15.2 | 10.8 % | 17.8 | web post buckling |
| 10-2 | 17.36 | 19.42 | 27.64 | 4.77 | 15.20 | 13.9 | 28.4 % | 13.2 | web post buckling |
| 10-3 | 15.98 | 18.48 | 17.00 | 5.03 | 15.50 | 14.7 | 13.5 % | 16.6 | web post buckling |
| 10-4 | 16.80 | 19.71 | 19.46 | 4.00 | 14.10 | 14.3 | 26.4 % | 11.3 | web post buckling |
| 12-1 | 21.08 | 29.35 | 38.32 | 7.63 | 36.80 | 23.8 | 18.9 % | 25.8 | web post buckling |
| 12-2 | 21.84 | 29.94 | 42.66 | 6.47 | 26.40 | 21.3 | 28.8 % | 22.1 | web post buckling |
| 12-3 | 27.84 | 31.70 | 26.38 | 9.3 | 25.10 | 24.7 | 6.4 % | 26.2 | web post buckling |
| 12-4 | 28.94 | 33.48 | 29.60 | 7.63 | 24.10 | 24.1 | 18.6 % | 21.0 | web post buckling |

[15] Blodgett 1963

Table 6.9: Predicted Yield Failure (Bazile and Texier 1968)

| Test Specimen | $P_1^{st}$ yield (kips) | $P_m$ (mechanism) (kips) | $P_{hy}$ (horiz. yield) (kips) | $P_y$ (kips) |
|---|---|---|---|---|
| A | 161.40 | 210.01 | 243.52 | 210.01 |
| B | 210.71 | 259.72 | 293.23 | 259.72 |
| C | 164.62 | 217.61 | 347.42 | 217.61 |
| D | 212.84 | 259.04 | 345.16 | 259.04 |
| E | 93.44 | 133.13 | 159.34 | 133.13 |

Table 6.10: Summary of Results (Bazile and Texier 1968)

| Test Specimen | $P_y$ (kips) | $P_B$ (web buckling) (kips) | $P_{AR}$ (web buckling) (kips) | $P_{FEM}$ (web buckling) (kips) | $P_{test}$ (experimental) (kips) | Experimental Mode of Failure |
|---|---|---|---|---|---|---|
| A | 210.01 | 183.71 | 120.62 | 158.51 | 180.98 | web post buckling |
| B | 259.72 | 166.32 | 138.41 | 157.85 | 154.00 | web post buckling |
| C | 217.61 | 94.24 | 107.22 | 149.23 | 134.89 | web post buckling |
| D | 259.04 | 121.31 | 117.56 | 145.01 | 139.38 | web post buckling |
| E | 133.13 | 55.05 | 55.91 | 68.36 | 62.95 | web post buckling |

Table 6.11: Comparison of Results (Bazile and Texier 1968)

| Test Specimen | $\frac{P_B - P_{test}}{P_{test}}$ | $\frac{P_{AR} - P_{test}}{P_{test}}$ | $\frac{P_{FEM} - P_{test}}{P_{test}}$ |
|---|---|---|---|
| A | 1.5 % | -33.3 % | -12.4 % |
| B | 8.0 % | -10.1 % | 2.5 % |
| C | -30.1 % | -20.5 % | 10.6 % |
| D | -12.9 % | -15.6 % | 4.0 % |
| E | -12.5 % | -11.2 % | 8.6 % |

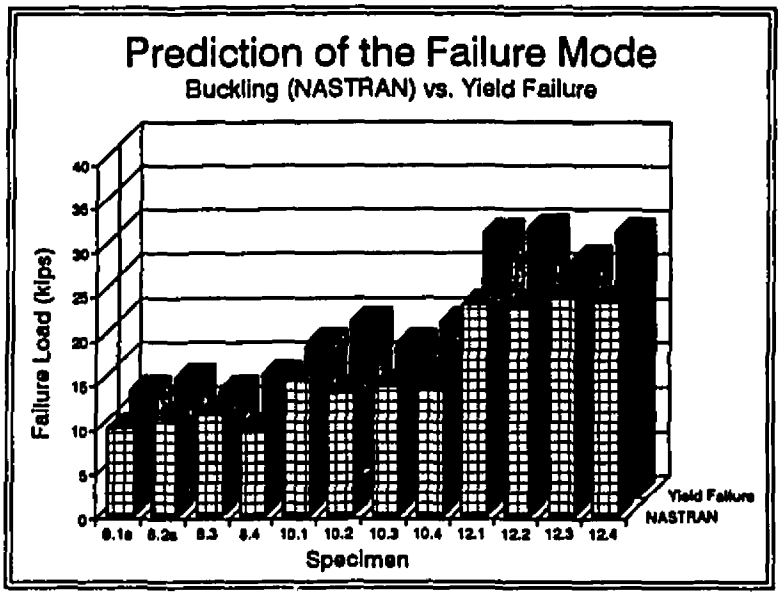


Fig. 6.1: Prediction of the Failure Mode

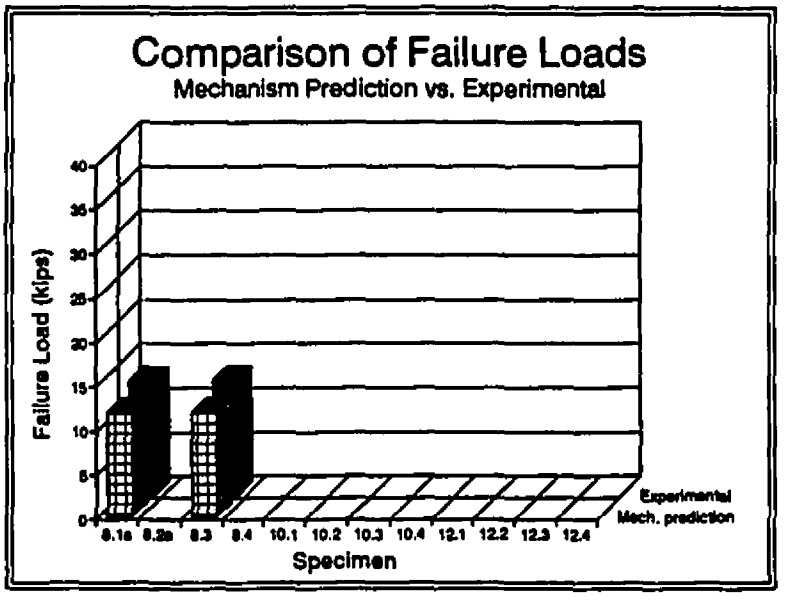


Fig. 6.2: Comparison of the Mechanism Failure Load

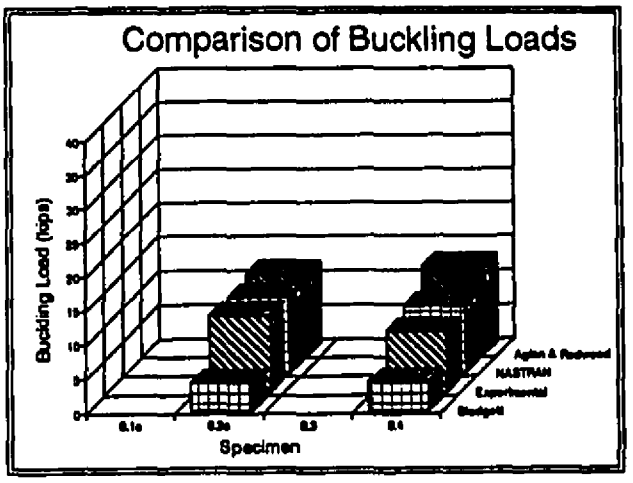


Fig. 6.3a: Comparison of Buckling Loads (Specimen 8- )

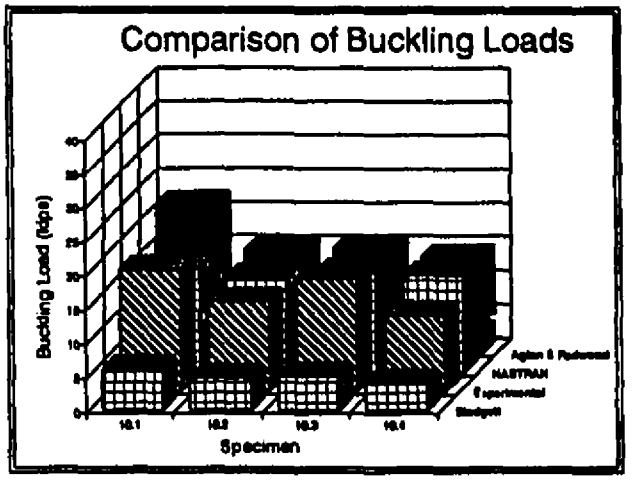


Fig. 6.3b: Comparison of Buckling Loads (Specimen 10-

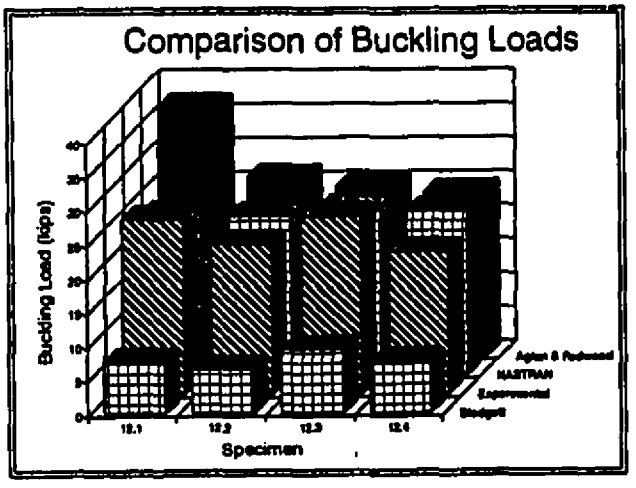


Fig. 6.3c: Comparison of Buckling Loads (Specimen 12- )

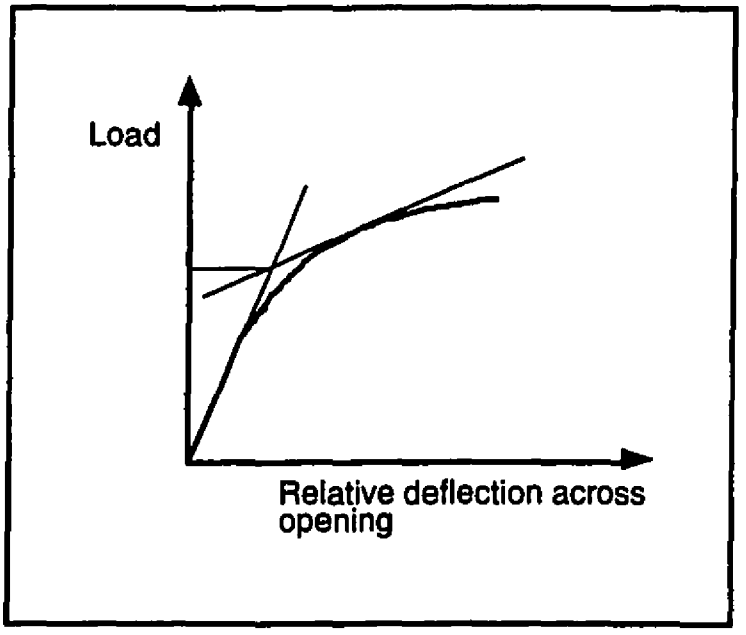


**Fig. 6.4:** Earlier Interpretation of Experimental Results

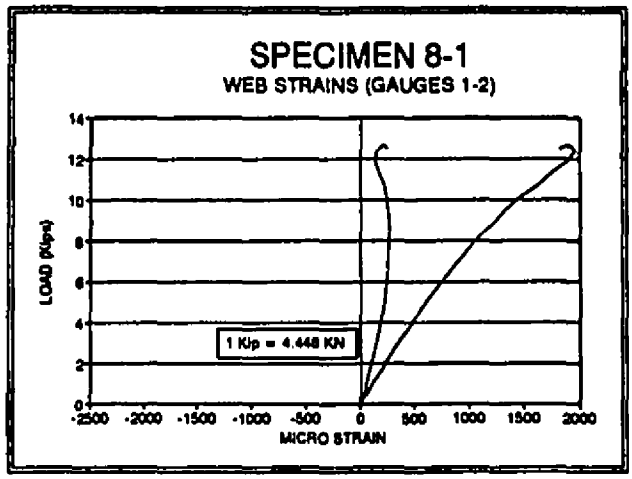


Fig. 6.5: Load vs. Web Strains (8-1a)

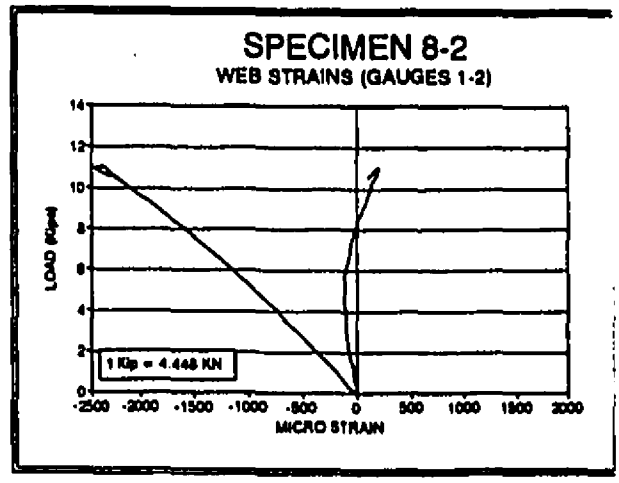


Fig. 6.6: Load vs. Web Strains (8-2a)

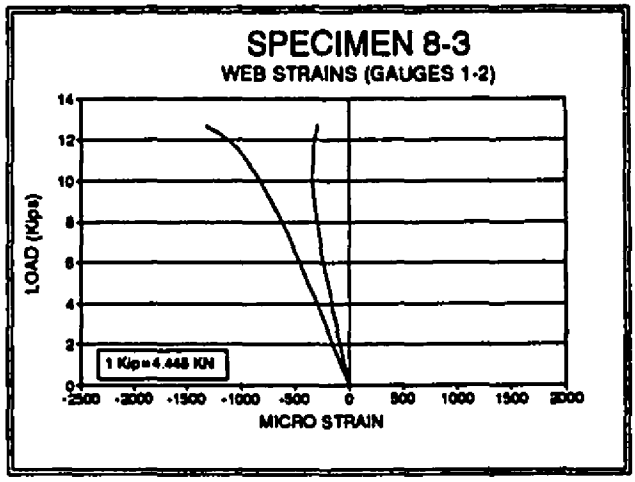


Fig. 6.7: Load vs. Web Strains (8-3)

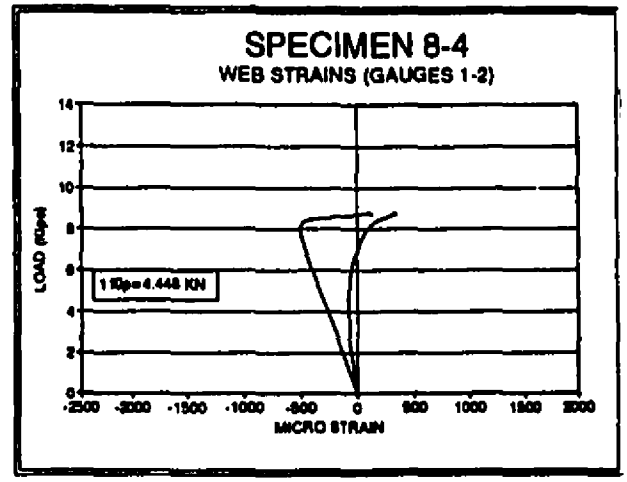


Fig. 6.8: Load vs. Web Strains (8-4)

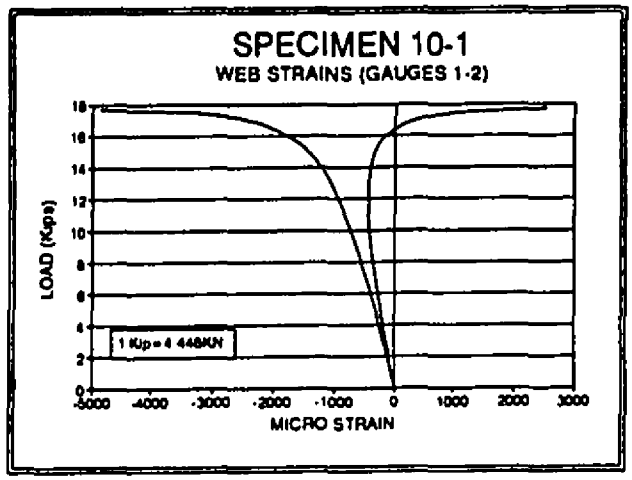


**Fig. 6.9:** Load vs. Web Strains (10-1)

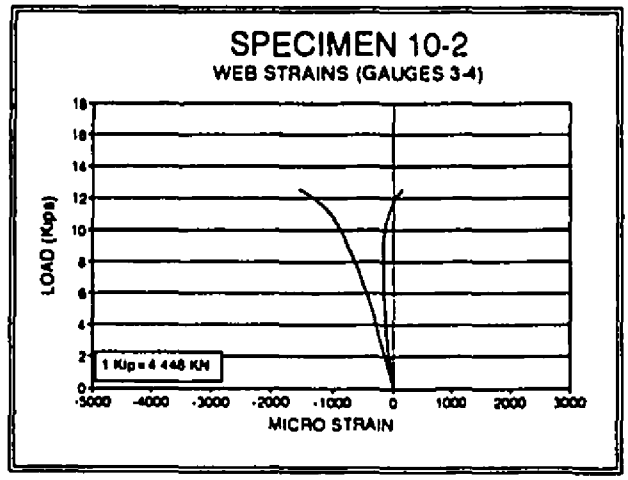


**Fig. 6.10:** Load vs. Web Strains (10-2)

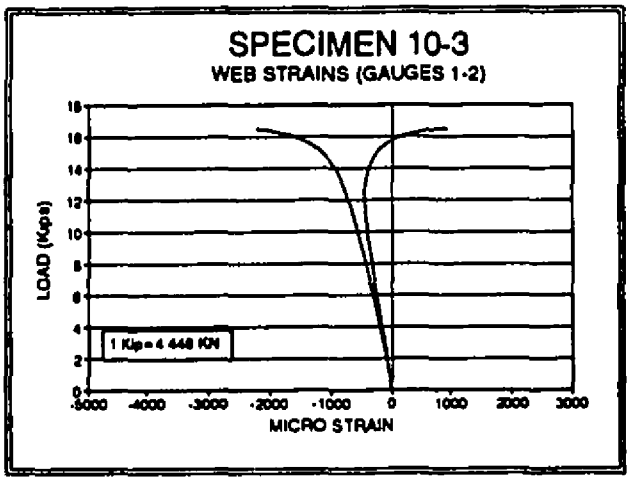


**Fig. 6.11:** Load vs. Web Strains (10-3)

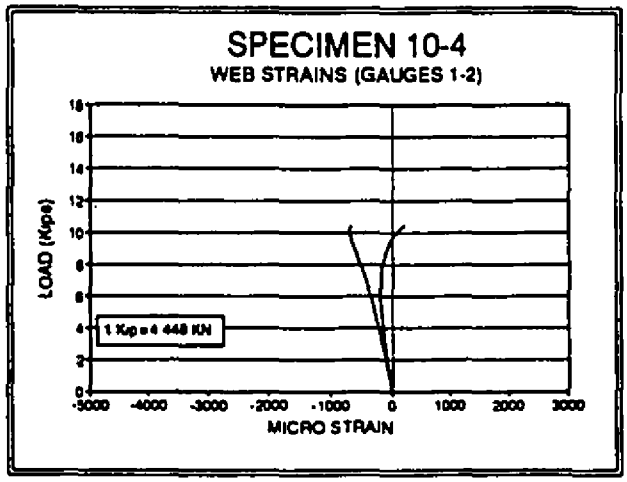


**Fig. 6.12:** Load vs. Web Strains (10-4)

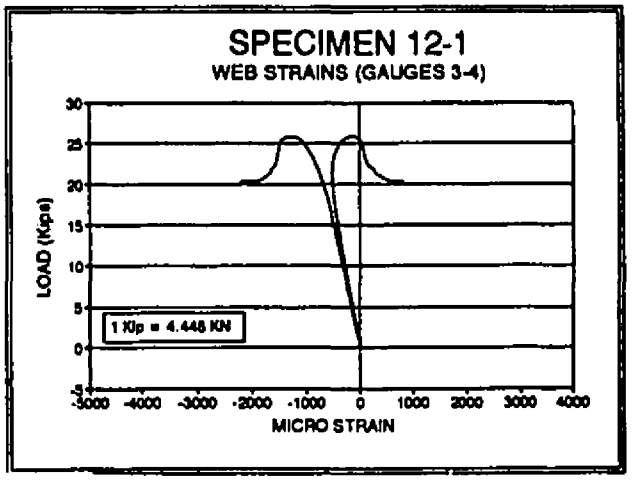


Fig. 6.13: Load vs. Web Strains (12-1)

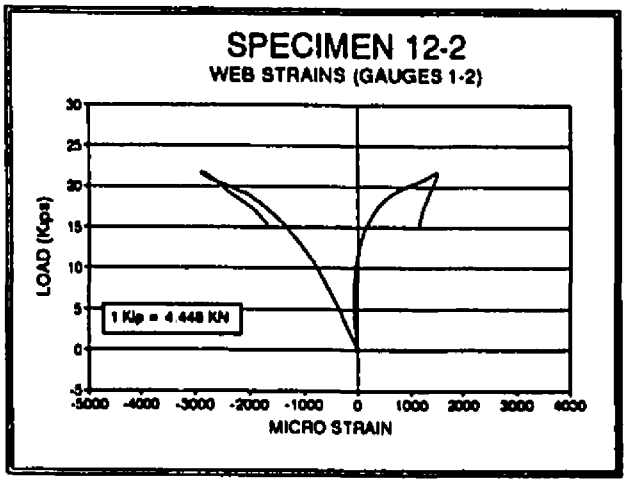


Fig. 6.14: Load vs. Web Strains (12-2)

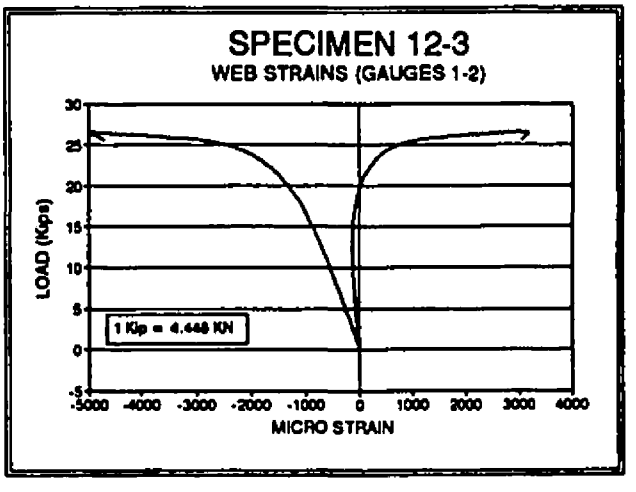


Fig. 6.15: Load vs. Web Strains (12-3)

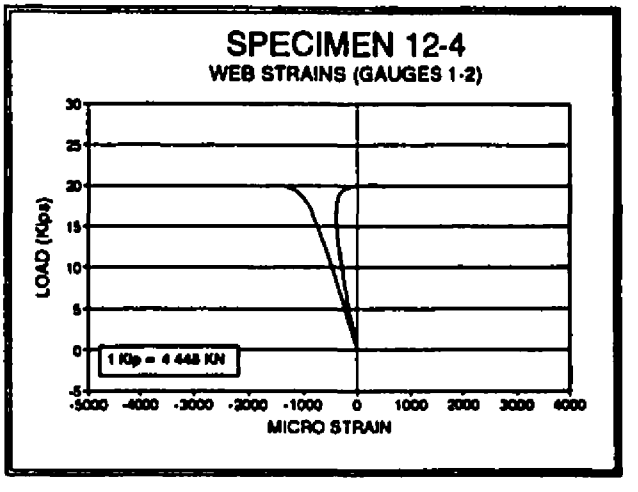


Fig. 6.16: Load vs. Web Strains (12-4)

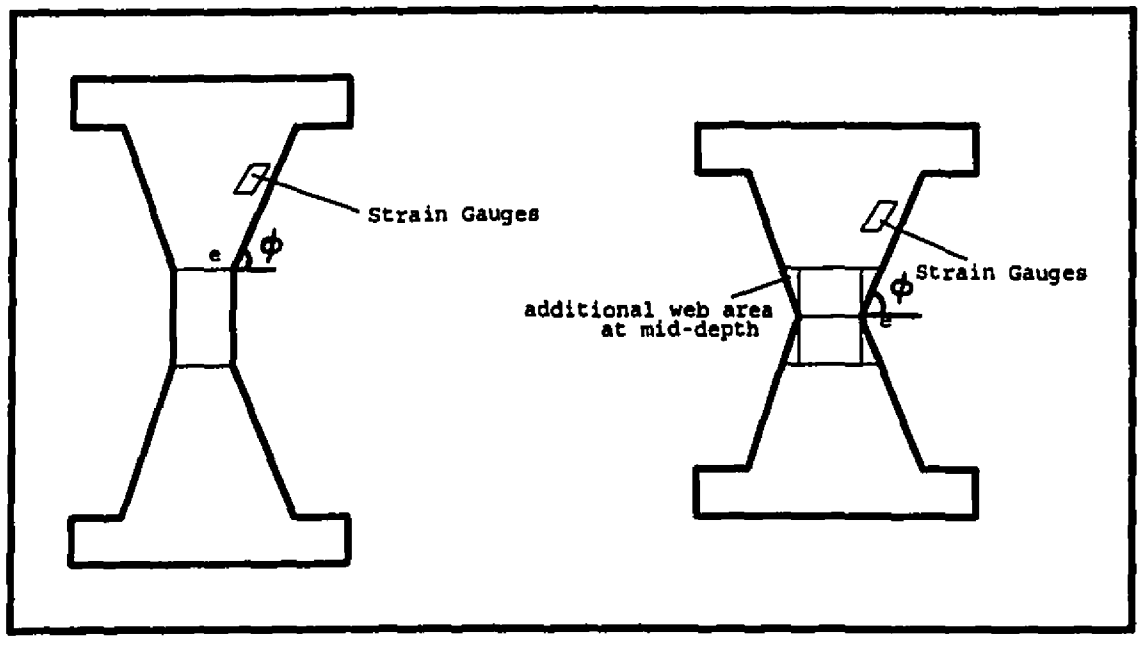


Fig. 6.17: Typical Web Post Section (With and Without an Intermediate Plate)

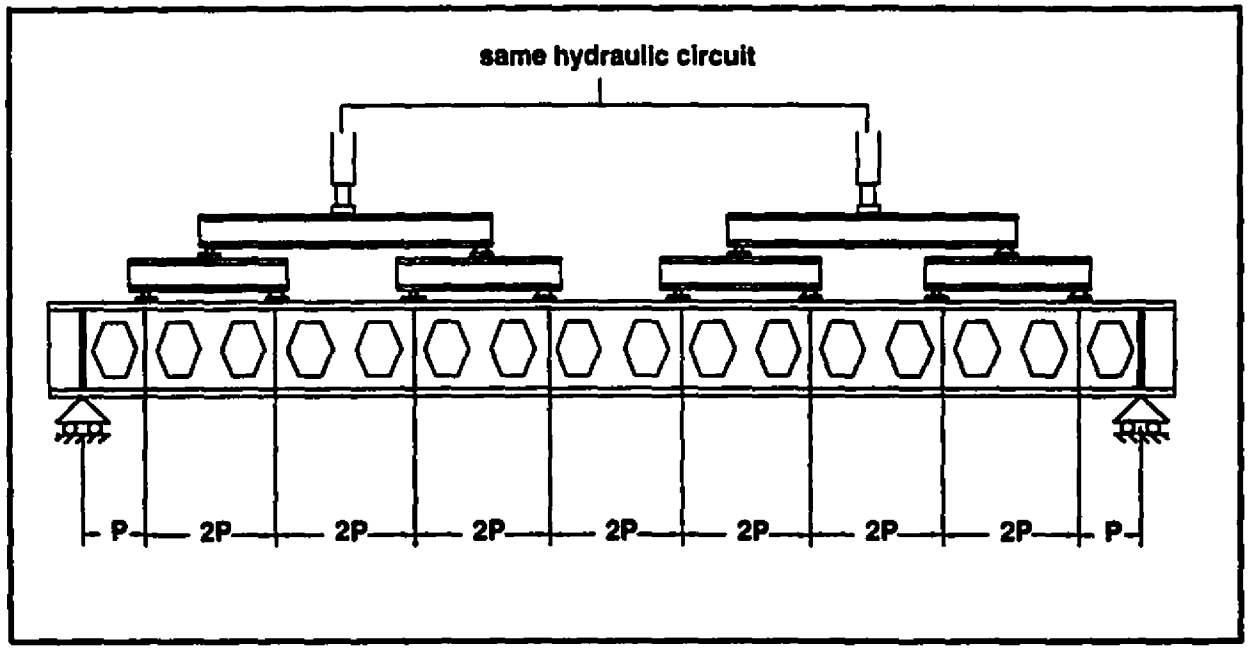


Fig. 6.18: Loading at 8 Points (Bazile and Texier 1968)

# Chapter 7

## Summary and Conclusion

### 7.1 Summary

The main objective of this investigation was to detect, analyse and test castellated beams for which the geometry was predicted to be susceptible to web post buckling. The modes of failure and their corresponding loads were predicted based on a number of previous studies.

In order to provide a new assessment tool, a nonlinear finite element analysis was carried out. NASTRAN was used because of its nonlinear buckling analysis capabilities. The results from NASTRAN were used as a prediction for the mode of failure and its corresponding load. To determine the accuracy of the model and the analysis, the results were compared to the experimental failure loads, which were obtained from a series of laboratory tests.

The beams were provided by Chaparral Steel. They were fabricated by CANAM. The notable feature of these beams is their thin webs.

The applied load which causes the formation of the mechanism failure (Redwood 1978) was calculated. This value was compared to the load which causes a horizontal shear failure, which was based on an analysis of Blodgett (1963). The smaller of these two loads, $P_y$, was compared to the buckling load determined from NASTRAN. A large difference, with the yield failure being the larger value, was an indication of a web post failure before any other mode of failure.

The load at first yield was also calculated, based on an analysis of Blodgett (1963).

In addition to the buckling predictions produced from NASTRAN, a method suggested by Aglan and Redwood (1974) and another by Blodgett (1963) were used to predict the load at which buckling of the web posts occurs. An experimental study by Bazile and Texier (1968) is discussed briefly. The beams in this test program which failed by web post buckling were analysed.

The results of this work are discussed and compared in Chapters 5 and 6.

## 7.2 Conclusion

From this study, conclusions can be drawn based on the experimental results, and on the methods used to predict the modes of failure and their corresponding loads.

i. For the available shapes, Bantam Beam Shapes, web post buckling can be the critical mode of failure. Due to the very thin web posts, the beams which were tested failed due to the buckling of their web posts, except for specimens 8-1a and 8-3 which failed due to the buckling of the tee-section.

ii. Beams with intermediate plates have a lower failure load than beams with no intermediate plates. In many cases there is a significant drop in the load carrying capacity for these beams. The ratios of like pairs vary from 1.16 to 1.46.

iii. Beams with no intermediate plate have a more favourable behaviour after buckling. They show additional load resistance after buckling deformations were observed. Specimens 10-1 and 12-3 are an example of this kind of behaviour, as illustrated in Figs. 6.9 and 6.15.

iv. For beams with no intermediate plates, the parameters e, $d_t$, h, b and phi all have an influence on the carrying capacity and the behaviour of the web post after buckling.

v. For beams with intermediate plates, the phi angle seems to have the greatest effect on the behaviour after buckling. The phi angle of $45^o$ shows a more favourable post-buckling behaviour.

vi. Castellated beams undergo a number of cutting and welding procedures during the fabrication process. Sweep, camber and out-of-plane deflections, are above the allowable limits in some of the specimens. These values are given in Table 5.1.

vii. The method suggested by Redwood (1978) for the prediction of the mechanism mode of failure is reasonably conservative and accurate. The theory is a lower bound value, strain-hardening is ignored.

viii. The buckling predictions suggested by Blodgett (1963), for the specimens which were tested at McGill University, yielded conservative results, by amounts varying from 53.1 % to 70.7 %. On the other hand, for the specimens which were tested by Bazile and Texier (1968), Blodgett's method showed an improved estimation of the buckling load. For these the predictions varied from +1.5 % to -30.1 %. It seems that this method is not valid for specimens with very thin webs as is the case for the beams tested at McGill University with a ratio of $(d_g-2t_f)/t_w$ varying from 88.9 to 118.8. This ratio varies between 46.9 and 72.6 for the beams tested by Bazile and Texier (1968).

ix. The buckling prediction suggested by Aglan and Redwood (1974) is a very simple method to use by making use of the design aids, and yielded conservative results for

the specimens which were tested at McGill University and for the specimens tested by Bazile and Texier (1968). The test to predicted ratios are given in Tables 6.5 and 6.11.

x. The buckling results produced from the finite element analysis required a considerable amount of work but the results were close to the experimental loads. The prediction, from NASTRAN, for the specimens tested at McGill University are within 15 % of the test results, except for specimen 10-4, which is 26.5 % higher. The buckling predictions for the specimens tested by Bazile and Texier (1968) varied by amounts from +2.5 % to -12.4 %. The buckling predictions from the finite element analysis are in the same range for the two sets of beams. The analysis does not seem to be affected by the change in the web or flange thicknesses nor in any change in the other variables. The test to predicted ratios are given in Tables 6.6 and 6.11. The finite element analysis is a dependable method of analysis.

xi. The mean of test to predicted results, based on the finite element analysis, for all 10 specimens tested at McGill University is 0.993 with standard deviation 0.120. For the five specimens tested by Bazile and Texier (1968), which failed by web-post buckling, the mean of test to predicted values is 0.980 with standard deviation 0.095. For these and the ten tested specimens, at McGill University, which failed by web-post buckling, the mean of test to predicted values is 0.989 with standard deviation 0.109.

# References

Aglan, A. A., and Redwood, R. G., (1974). "Web Buckling in Castallated Beams". Proc. ICE., Part 2, No. S7, 307-320.

AISC, (1978). "Manual of Steel Construction". American Institute of Steel Construction, Chicago, Il.

Altfillisch, M.D., Cooke, B.R., and Toprac, A.A., (1957). "An Investigation of Welded Open-Web Expanded Beams". Journal of American Welding Society. Welding Research Supplement, 77s-88s.

Bazile, A. and Texier, J., (1968). "Essais de Poutres Ajourées". Construction Métallique, No. 3, 12-25.

Blodgett, O. W., (1963). "Design of Welded Structures". The James F. Lincoln Arc Welding Foundation, Cleveland, Ohio.

Canadian Standards Association, (1987). "General Requirements for Rolled or Welded Structural Quality Steel", CAN/CSA-G40.20-M87, Rexdale, Ontario.

Canadian Standards Association (CSA), (1989). Limit States Design of Steel Structures, CAN/CSA-S16.1-M89, Rexdale, Ontario.

Chajes, A., (1974). "Principles of Structural Stability Theory". Prentice Hall, N.J.

Halleux, P., (1967). "Limit Analysis of Castellated Steel Beams". Acier-Stahl-Steel, Vol. 32, No. 3, 133-144.

Hatch Associates Consultants, Inc., (1993). "Castellated and Light Beam Development Program". Interim Report No. 2.

Hope, B. B., and Sheikh, M. A., (1969). "The Design of Castellated Beams". The Engineering Journal, TRANSACTIONS of the Enginnering Institute of Canada, Vol. 12, No. A-8.

Hosain, M.U., and Speirs, W.G., (1971). "Failure of Castelated Beams due to Rupture of Welded Joints". Acier-Stahl-Steel, Vol. 36, No. 1, 34-40.

Knowles, P. R. (1985). "Design of Castellated Beams". The Steel Construction Institute.

Macneal Schwendler Corporation / NASTRAN, (1983). "Msgmesh Analyst's Guide". Los Angeles, California.

Macneal Schwendler Corporation / NASTRAN, (1985). "Demonstration Problem Manual". Los Angeles, California.

Macneal Schwendler Corporation / NASTRAN, (1988). "Verification Problem Manual". Los Angeles, California.

Macneal Schwendler Corporation / NASTRAN, (1991a). "User's Manual,". Vol. 1. Los Angeles, California.

Macneal Schwendler Corporation / NASTRAN, (1991b). "User's Manual,". Vol. 2. Los Angeles, California.

Macneal Schwendler Corporation / NASTRAN, (1992a). "Handbook for Nonlinear Analysis". Los Angeles, California.

Macneal Schwendler Corporation / NASTRAN, (1992b). "Quick Reference Guide". Los Angeles, California.

Macneal Schwendler Corporation / XL, (1993a). "Command Syntax". Los Angeles, California.

Macneal Schwendler Corporation / NASTRAN, (1993b). "Common Questions and Answers". Los Angeles, California.

Mandel, J.A., Brennan, P.J., Wasil, B.A., and Antoni, C.M., (1971). "Stress Distribution in Castellated Beams". Journal of the Structural Division, Proceedings of the American Society of Civil Engineers, Vol 97, No. ST7, 1947-1967.

Pattanayak, U. C. and Chesson, E., (1974). "Lateral Instability of Castellated Beams". AISC Engineering Journal, Vol. 11, No. 3, 73-79.

Redwood, R. G., (1968). "Ultimate Strength Design of Beams With Multiple Openings". Paper presented at the ASCE Structural Engineering Conference, Pittsburg.

Redwood, R. G., (1978). "Analyse et Dimensionnement des Poutres Ayant des Ouvertures dans les Ames". Construction Métalique, No.3, 15-27.

Toprac, A. A., and Cooke, B. R., (1959). "An Experimental Investigation of Open-Web Beams". welding Researche Council, Bulletin New York Series, No. 47.

Ward, J. K., (1990). "Design of Composite and Non-Composite Cellular Beams". The Steel Construction Institute.

# Appendix A

## Finite Element Analysis

### A.1 Nonlinear Static Analysis Strategies

A nonlinear solution strategy is required to solve nonlinear problems (Macneal-Schwendler Corp. 1992a). There are five basic tasks in a nonlinear solution scheme.

- Determine an increment to advance forward.
- Stiffness update.
- Displacement prediction.
- Element state update.
- Unbalanced force and convergence check.

There are a number of different advancing schemes, stiffness updates and convergence criterium.

An algorithm is presented to clarify the solution strategy:

1. Determine an increment to move forward on the equilibrium path.
2. Determine an estimate of a tangent stiffness matrix.
3. Determine the displacement increment to move forward, generally by solving equilibrium equations.
4. Calculate the element resisting forces.

5. Calculate the unbalanced load and check for convergence. If converged, go to step 1.

If not converged, continue, as follows, with the correcting phase (iteration phase).

6. Determine an estimate of tangent stiffness matrix.
7. Determine the displacement increment due to the unbalanced load.
8. Calculate the element resisting forces.
9. Calculate the unbalanced load and check for convergence. If converged, go to Step 1. If not, go to step 6.

Please refer to Fig. A.1.

The different tasks in a nonlinear solution strategy will be discussed individually in the sections that follow.

### A.1.1 Advancing Schemes

- Constant load increments

  The number of load increments are specified for a particular subcase. This is done in the user interface NLPARM. The more load increments you have, the better are the chances of obtaining an accurate result.

- Displacement increment

  Constant displacements are specified for selected individual or sets of degrees of freedom. The displacement is processed incrementally in the subcase. This option may be used in combination with load increment. The user interface is SPCD or SPC.

- Arc length increments

  1. Crisfiel Method:

     Specify increments in terms of an arc in load-displacement space Fig. A.2. It is useful for following the equilibrium path in the unstable region as the load increment can be negative, Fig. A.3.

$$\Delta l^2 = \Delta\mu^2 + \Delta u^T \Delta u \quad \text{.....[A.1]}$$

$$P_i = \mu_i P$$
$$\Delta\mu = \mu_i - \mu_{i-1}$$

Where $\Delta\mu = incremental\ load\ factor$
$\Delta l = arc\ length$

2. Riks:

Riks method avoids the solution of the quadratic equation, which needs to be done in the arc length method, by enforcing a normal plane constraint, Fig. A.4.

3. Modified Riks:

Modified Riks method continues to change the normal plane constraint with every iteration Fig. A.5.

User Interface:

- NLPCI: For Arc Length Increment
- NLPARM: For Load Increment
- SPCD or SPC: For Displacement Increment

Note: NLPCI is used in combination with NLPARM. The initial arc length is based on the load increment specified in the NLPARM.

### A.1.2 Stiffness Update

- Newton-Raphson (NR) Method

Concept.

1- Advance forward by constant and positive load increments.

2- Tangent stiffness is formed at every iteration from the current element state.

3- Displacement is predicted and corrected by solving equilibrium equations.

Weaknesses.

- Cannot trace the unstable or post-buckling behavior.
- No convergence if total applied load is greater than the structure strength.
- Path-dependent state determination.(Use of non converged reference state may cause the inelastic material response to differ from the true response. Please refer to Fig. A.6.

- Modified Newton Raphson Method

  Stiffness update at every k-th iteration, which has to be specified. This may be done by the user interface NLPARM with the KSTEP option.

- Based On The Rate of Convergence

  The stiffness update is based on the rate of convergence. The logic is hardware dependent. For the same problem, the solution path may be different depending on the hardware.

- Quasi-Newton Stiffness Update
  - Modified stiffness matrix should be a secant stiffness matrix for the displacements calculated in the previous iterations.
  - Modified stiffness should preserve symmetry and be positive definite.

- The inverse of the modified stiffness is inexpensive to calculate. Invert by Sherman-Morrison identity to get $K_m^{-1}$. No need for matrix generation and decomposition.
- Displacement increment using modified stiffness should be inexpensive to calculate.

By, using the available defaults, the stiffness update schemes are automated and the user does not have to select the method to use.

### A.1.3 Displacement Prediction

- Solution of Equilibrium Equations
- Line Search Method

Concept

- Improves displacement increment calculated from the equilibrium equation, because those displacement increments are not necessarily the best estimates of the equilibrium state.
- Seeks a multiple of displacement increment ($\alpha$) that minimizes a measure of work done by unbalanced forces. This is applicable for each iteration.

### A.1.4 Element State Update

Update element state to calculate element forces.

where:

$$F = \int B^T \sigma \, dV$$

### A.1.5 Convergence Criteria

There are three convergence criteria. The user has the option of using one or a combination of the three which is tested at every iteration after the line search.

- Error tolerance for displacement criterion
- Error tolerance for load criterion
- Error tolerance for work criterion

Note:

- It is important to consider the convergence criteria depending on the available system, if it is a stiffening or softening system. In a stiffening system, for example, an error in the load will cause a small error in the displacement while in a softening system, an error in the load will result in a large error in the displacement.
- Tightening up the convergence tolerances will cause a waste of computing resources while loose tolerances will cause inaccuracy and difficulties in the subsequent steps.

## A.2 Restarts

A restart run requests that data stored in a previous run be used in the current run. In the case of buckling analysis, one may make use of this option. Nonlinear analysis is performed until there is no convergence. The following message is conveyed; "max. number of bisections or min. load step has been reached" or "the following degrees of freedom have negative terms on the factor diagonal of matrix decomposition", (Macneal-Schwendler Corp. 1991b). At a few increments below that point, a restart run is initiated to carry on with the buckling analysis.

## A.3 Buckling

### A.3.1 Instability

There are two types of instability phenomenon. One is snap-through and the other is bifurcation buckling (Macneal-Schwendler Corp. 1992).

- Snap-Through:

  For loads beyond a stationary point in the load-deflection curve, loss of stability occurs. The structure assumes a completely different displaced configuration, Fig. A.7.

- Bifurcation:

  A bifurcation point is a point where two or more equilibrium paths intersect in the load-deflection curve. For loads beyond that point, loss of stability occurs and the structure buckles, Fig. A.8.

### A.3.2 Linear vs. Nonlinear Buckling

The following is a comparison between the linear and nonlinear buckling options.

| *Linear* | *Nonlinear* |
|---|---|
| Kinematic relationship is linear | Kinematic relationship is nonlinear |
| Constitutive relationship is linear | Constitutive relationship may be nonlinear |
| Equilibrium is satisfied in perturbed configuration | Equilibrium is satisfied in deformed configuration |
| Geometric stiffness is assumed proportional to the load | Geometric stiffness is assumed proportional to displacement increment. |
| User interface SOL 105 | User interface SOL 106 |

### A.3.3 Concept and User Interface

Concept

The buckling load is reached by using the command "PARAM, Buckle" in a restart run (Macneal-Schwendler Corp. 1993b). The theory is as follows:

- Eigenvalue problem:

$$[K_n + \lambda \Delta K][\phi] = \{0\} \quad \text{.....[A.2]}$$

with $\Delta K = K_n - K_{n-1}$

$\Delta K$ = *Incremental Stiffness*

- $K_n$ and $K_{n-1}$ are evaluated at the known solution points in the vicinity of instability.

$$F_{cr} \cong F_{(u_n)} + \int_{u_n}^{u_{cr}} K(u)du = F_n + \int_0^{\lambda} K(\lambda)\Delta u d\lambda \quad \text{.....[A.3]}$$

- Critical displacement

$$\{u_{cr}\} = \{u_n\} + \lambda\{\Delta u\}$$
$$\textit{where} \quad \{\Delta u\} = \{u_n\} - \{u_{n-1}\} \quad \text{.....[A.4]}$$

- Critical buckling load by matching virtual work

$$\Delta u^T F_{cr} = \Delta u^T P_{cr}$$
$$\{P_{cr}\} = \{P_n\} + \alpha\{\Delta P\} \quad \text{.....[A.5]}$$

*where* $\{\Delta P\} = \{P_n\} - \{P_{n-1}\}$

$$\alpha = \frac{\lambda\{\Delta u\}^T\left[K_n + \frac{1}{2}\lambda\Delta K\right]\{\Delta u\}}{\{\Delta u\}^T\{\Delta P\}}$$

- The tangent stiffness is assumed to change linearly with displacement

- Internal loads are quadratic functions of displacement increments, Fig. A.9.

User Interface

Run SOL 106 until a negative determinant of [K] is encountered

Make a restart run for buckling analysis by including the following (Macneal-Schwendler Corp. 1992b):

Use

- PARAM, BUCKLE,1
- PARAM, LGDISP, 1
- NLPARM
- EIGB
- Provide two small loading steps below the buckling point

## A.4 Nonlinear Elements

### A.4.1 Types of Nonlinear Elements

QUAD4 elements were used in the analysis because they are nonlinear elements and thus have large strain capabilities among other properties. These are discussed in the section that follows.

### A.4.2 Nonlinear Shell and Plate Elements

The QUAD4 element has the following properties:

- Isoparametric elements
- Membrane and plate bending applicable to nonlinear material
- Transverse shear (Mindlin) remains linear
- Simulate thick or thin curved shell
- Each connecting node has 6 DOFs
- Pass constant stress patch test
- No shear locking
- Force components:

*Membrane forces*: $F_x, F_y, F_{xy}$
*Bending moments*: $M_x, M_y, M_{xy}$
*Transverse shear forces*: $Q_x, Q_y$

- Stress components:

$\sigma_x, \sigma_y, \tau_{xy}$ (*at center*)

- Displacement components:

  $u_i$

  $\theta_x, \theta_y$

- Nonlinear capabilities:

  Geometric nonlinear

  Material nonlinear

TABLE A.1: LISTING OF COLD START.



```
ID prop12b,NLB
SOL 106
TIME 900
CEND
TITLE=INELASTIC BUCKLING OF SPEC3
SET 1=16,30,216,230
ECHO = UNSORT
  DISP = 1
  MAXLINES= 300000
SUBCASE 1
  LOAD = 9
  NLPARM = 9
SUBCASE 2
  LOAD = 19
  NLPARM = 19
SUBCASE 3
  LOAD = 29
  NLPARM = 29
OUTPUT(POST)
BEGIN BULK
PARAM,POST,0
PARAM,DBCCONV,XL
PARAM,LGDISP,1
PARAM,DBDRNL,-1
PARAM,K6ROT,10000.0
NLPARM,9,10, ,AUTO, , ,UPW,YES
NLPARM,19,10, ,AUTO, , ,UPW,YES
NLPARM,29,10, ,AUTO, , ,UPW,YES
GRID,1, ,0.0,528.8,0.0, ,3
=,*(1), ,19.8,=,=, ,0
=,*(1), ,*(39.7),=,=, ,0
=,*(1), ,*(39.7),=,=, ,0
=,*(1), ,*(19.8),=,=, ,0
=,*(1), ,*(19.8),=,=, ,0
=,*(1), ,*(19.8),=,=, ,0
=,*(1), ,*(19.8),=,=, ,13
=,*(1), ,*(19.8),=,=, ,0
=,*(1), ,*(19.8),=,=, ,0
=,*(1), ,*(19.8),=,=, ,0
=,*(1), ,*(19.8),=,=, ,0
=,*(1), ,*(39.7),=,=, ,0
=,*(1), ,*(39.7),=,=, ,0
=,*(1), ,*(19.8),=,=, ,3
GRID,201, ,0.0,0.0,0.0, ,3
=,*(1), ,19.8,=,=, ,0
=,*(1), ,*(39.7),=,=, ,0
=,*(1), ,*(39.7),=,=, ,0
=,*(1), ,*(19.8),=,=, ,0
=,*(1), ,*(19.8),=,=, ,0
=,*(1), ,*(19.8),=,=, ,0
=,*(1), ,*(19.8),=,=, ,123
=,*(1), ,*(19.8),=,=, ,0
=,*(1), ,*(19.8),=,=, ,0
=,*(1), ,*(19.8),=,=, ,0
=,*(1), ,*(19.8),=,=, ,0
=,*(1), ,*(39.7),=,=, ,0
=,*(1), ,*(39.7),=,=, ,0
=,*(1), ,*(19.8),=,=, ,3
GRID,16, ,0.0,514.3,0.0, ,3
=,*(1), ,19.8,=,=, ,0
=,*(1), ,*(39.7),=,=, ,0
=,*(1), ,*(39.7),=,=, ,0
=,*(1), ,*(19.8),=,=, ,0
=,*(1), ,*(19.8),=,=, ,0
=,*(1), ,*(19.8),=,=, ,0
=,*(1), ,*(19.8),=,=, ,0
=,*(1), ,*(19.8),=,=, ,0
=,*(1), ,*(19.8),=,=, ,0
=,*(1), ,*(39.7),=,=, ,0
=,*(1), ,*(39.7),=,=, ,0
=,*(1), ,*(19.8),=,=, ,3
GRID,216, ,0.0,14.5,0.0, ,3
=,*(1), ,19.8,=,=, ,0
=,*(1), ,*(39.7),=,=, ,0
=,*(1), ,*(39.7),=,=, ,0
=,*(1), ,*(19.8),=,=, ,0
=,*(1), ,*(19.8),=,=, ,0
=,*(1), ,*(19.8),=,=, ,0
=,*(1), ,*(19.8),=,=, ,0
=,*(1), ,*(19.8),=,=, ,0
=,*(1), ,*(19.8),=,=, ,0
=,*(1), ,*(19.8),=,=, ,0
=,*(1), ,*(19.8),=,=, ,0
=,*(1), ,*(39.7),=,=, ,0
=,*(1), ,*(39.7),=,=, ,0
=,*(1), ,*(19.8),=,=, ,3
GRID,31, ,0.0,489.8,0.0, ,0
=,*(1), ,19.05,=,=, ,0
=,*(1), ,*(19.05),=,=, ,0
=,*(10), ,*(280.6),=,=, ,0
=,*(1), ,*(19.05),=,=, ,0
=,*(1), ,*(19.05),=,=, ,0
GRID,231, ,0.0,39.0,0.0, ,0
=,*(1), ,19.05,=,=, ,0
=,*(1), ,*(19.05),=,=, ,0
=,*(10), ,*(280.6),=,=, ,0
=,*(1), ,*(19.05),=,=, ,0
=,*(1), ,*(19.05),=,=, ,0
GRID,34, ,66.04,465.3,0.0, ,0
=,*(1), ,*(27.94),=,=, ,0
=(7)
GRID,234, ,66.04,63.5,0.0, ,0
=,*(1), ,*(27.94),=,=, ,0
=(7)
GRID,46, ,0.0,465.3,0.0, ,0
=,*(1), ,19.05,=,=, ,0
=,*(1), ,*(19.05),=,=, ,0
GRID,246, ,0.0,63.5,0.0, ,0
=,*(1), ,19.05,=,=, ,0
=,*(1), ,*(19.05),=,=, ,0
GRID,58, ,318.4,465.3,0.0, ,0
=,*(1), ,*(19.05),=,=, ,0
=,*(1), ,*(19.05),=,=, ,0
GRID,258, ,318.4,63.5,0.0, ,0
=,*(1), ,*(19.05),=,=, ,0
=,*(1), ,*(19.05),=,=, ,0
GRID,49, ,58.3,429.7,0.0, ,0
=,*(1), ,*(29.8),=,=, ,0
=(7)
```

```
GRID,249, ,58.3,98.1,0.0, ,0
=,*(1), ,*(29.8),=,=, ,0
=(7)
GRID,61, ,78.2,394.0,0.0, ,0
=,*(1), ,*(24.7),=,=, ,0
=(7)
GRID,261, ,78.2,132.7,0.0, ,0
=,*(1), ,*(24.7),=,=, ,0
=(7)
GRID,70, ,98.2,359.4,0.0, ,0
=,*(1), ,*(19.7),=,=, ,0
=(7)
GRID,270, ,98.2,168.4,0.0, ,0
=,*(1), ,*(19.7),=,=, ,0
=(7)
GRID,79, ,108.7,341.6,0.0, ,0
=,*(1), ,*(17.14),=,=, ,0
=(7)
GRID,279, ,108.7,186.2,0.0, ,0
=,*(1), ,*(17.14),=,=, ,0
=(7)
GRID,88, ,119.2,323.7,0.0, ,0
=,*(1), ,*(14.6),=,=, ,0
=(7)
GRID,288, ,119.2,203.0,0.0, ,0
=,*(1), ,*(14.6),=,=, ,0
=(7)
GRID,97, ,129.6,307.0,0.0, ,0
=,*(1), ,*(12.1),=,=, ,0
=(7)
GRID,297, ,129.6,221.0,0.0, ,0
=,*(1), ,*(12.1),=,=, ,0
=(7)
GRID,106, ,139.1,289.1,0.0, ,0
=,*(1), ,*(9.5),=,=, ,0
=(7)
GRID,306, ,139.1,239.0,0.0, ,0
=,*(1), ,*(9.5),=,=, ,0
=(7)
GRID,115, ,139.1,276.4,0.0, ,0
=,*(1), ,*(9.5),=,=, ,0
=(7)
GRID,315, ,139.1,251.7,0.0, ,0
=,*(1), ,*(9.5),=,=, ,0
=(7)
GRID,124, ,139.1,264.4,0.0, ,0
=,*(1), ,*(9.5),=,=, ,0
=(7)
GRID,401, ,0.0,528.8,-38.9, ,0
=,*(1), ,19.8,=,=, ,0
=,*(1), ,*(39.7),=,=, ,0
=,*(1), ,*(39.7),=,=, ,0
=,*(1), ,*(19.8),=,=, ,0
=,*(1), ,*(19.8),=,=, ,0
=,*(1), ,*(19.8),=,=, ,0
=,*(1), ,*(19.8),=,=, ,0
=,*(1), ,*(19.8),=,=, ,0
=,*(1), ,*(19.8),=,=, ,0
=,*(1), ,*(39.7),=,=, ,0
=,*(1), ,*(39.7),=,=, ,0
=,*(1), ,*(19.8),=,=, ,0
GRID,501, ,0.0,528.8,38.9, ,0
=,*(1), ,19.8,=,=, ,0
=,*(1), ,*(39.7),=,=, ,0
=,*(1), ,*(39.7),=,=, ,0
=,*(1), ,*(19.8),=,=, ,0
=,*(1), ,*(19.8),=,=, ,0
=,*(1), ,*(19.8),=,=, ,0
=,*(1), ,*(19.8),=,=, ,0
=,*(1), ,*(19.8),=,=, ,0
=,*(1), ,*(19.8),=,=, ,0
=,*(1), ,*(19.8),=,=, ,0
=,*(1), ,*(39.7),=,=, ,0
=,*(1), ,*(39.7),=,=, ,0
=,*(1), ,*(19.8),=,=, ,0
GRID,701, ,0.0,0.0,38.9, ,0
=,*(1), ,19.8,=,=, ,0
=,*(1), ,*(39.7),=,=, ,0
=,*(1), ,*(39.7),=,=, ,0
=,*(1), ,*(19.8),=,=, ,0
=,*(1), ,*(19.8),=,=, ,0
=,*(1), ,*(19.8),=,=, ,0
=,*(1), ,*(19.8),=,=, ,0
=,*(1), ,*(19.8),=,=, ,0
=,*(1), ,*(19.8),=,=, ,0
=,*(1), ,*(19.8),=,=, ,0
=,*(1), ,*(39.7),=,=, ,0
=,*(1), ,*(39.7),=,=, ,0
=,*(1), ,*(19.8),=,=, ,0
CQUAD4,1,99,16,17,2,1, ,0.0
=,*(1),99,*(1),*(1),*(1),*(1), ,0.0
=(12)
CQUAD4,201,99,201,2??,217,216, ,0.0
=,*(1),99,*(1),*(1),*(1),*(1), ,0.0
=(12)
CQUAD4,15,99,31,32,17,16, ,0.0
=,*(1),99,*(1),*(1),*(1),*(1), ,0.0
=(12)
CQUAD4,215,99,216,217,232,231, ,0.0
=,*(1),99,*(1),*(1),*(1),*(1), ,0.0
=(12)
CQUAD4,29,99,46,47,32,31, ,0.0
=,*(1),99 ,*(1),*(1),*(1),*(1), ,0.0
```

```
*(12)
CQUAD4,229,99,231,232,247,246, ,0.0
*,*(1),99,*(1),*(1),*(1),*(1), ,0.0
*(12)
CQUAD4,43,99,61,62,50,49, ,0.0
*,*(1),*,*(1),*(1),*(1),*(1), ,0.0
*(6)
CQUAD4,243,99,249,250,262,261, ,0.0
*,*(1),*,*(1),*(1),*(1),*(1), ,0.0
*(6)
CQUAD4,51,99,70,71,62,61, ,0.0
*,*(1),*,*(1),*(1),*(1),*(1), ,0.0
*(6)
CQUAD4,251,99,261,262,271,270, ,0.0
*,*(1),*,*(1),*(1),*(1),*(1), ,0.0
*(6)
CQUAD4,59,99,79,80,71,70, ,0.0
*,*(1),*,*(1),*(1),*(1),*(1), ,0.0
*(6)
CQUAD4,259,99,270,271,280,279, ,0.0
*,*(1),*,*(1),*(1),*(1),*(1), ,0.0
*(6)
CQUAD4,67,99,88,89,80,79, ,0.0
*,*(1),*,*(1),*(1),*(1),*(1), ,0.0
*(6)
CQUAD4,267,99,279,280,289,288, ,0.0
*,*(1),*,*(1),*(1),*(1),*(1), ,0.0
*(6)
CQUAD4,75,99,97,98,89,88, ,0.0
*,*(1),*,*(1),*(1),*(1),*(1), ,0.0
*(6)
CQUAD4,275,99,288,289,298,297, ,0.0
*,*(1),*,*(1),*(1),*(1),*(1), ,0.0
*(6)
CQUAD4,83,99,106,107,98,97, ,0.0
*,*(1),*,*(1),*(1),*(1),*(1), ,0.0
*(6)
CQUAD4,283,99,297,298,307,306, ,0.0
*,*(1),*,*(1),*(1),*(1),*(1), ,0.0
*(6)
CQUAD4,91,11,115,116,107,106, ,0.0
*,*(1),*,*(1),*(1),*(1),*(1), ,0.0
*(6)
CQUAD4,291,11,306,307,316,315, ,0.0
*,*(1),*,*(1),*(1),*(1),*(1), ,0.0
*(6)
CQUAD4,99,11,124,125,116,115, ,0.0
*,*(1),*,*(1),*(1),*(1),*(1), ,0.0
*(6)
CQUAD4,299,11,315,316,125,124, ,0.0
*,*(1),*,*(1),*(1),*(1),*(1), ,0.0
*(6)
CQUAD4,401,100,1,2,402,401, ,0.0
*,*(1),*,*(1),*(1),*(1),*(1), ,0.0
*(12)
CQUAD4,501,100,501,502,2,1, ,0.0
*,*(1),*,*(1),*(1),*(1),*(1), ,0.0
*(12)
CQUAD4,601,100,201,202,602,601, ,0.0
*,*(1),*,*(1),*(1),*(1),*(1), ,0.0
*(12)
CQUAD4,701,100,701,702,202,201, ,0.0
*,*(1),*,*(1),*(1),*(1),*(1), ,0.0
*(12)
MAT1,1,190000.0, ,0.3
MATS1,1, ,PLASTIC,0.0,1,2,342.0
PSHELL,99,1,4.5,1
PSHELL,11,1,4.5,1
PSHELL,100,1,5.72,1
FORCE,9,16, ,15000.0,0.0,1.0,0.0
*,*,30, ,15000.0,0.0,-1.0,0.0
*,*,216, ,15000.0,0.0,1.0,0.0
*,*,230, ,15000.0,0.0,-1.0,0.0
*,*,16, ,59460.0,1.0,0.0,0.0
*,*,30, ,80760.0,-1.0,0.0,0.0
*,*,216, ,59460.0,-1.0,0.0,0.0
*,*,230, ,80760.0,1.0,0.0,0.0
FORCE,19,16, ,20000.0,0.0,1.0,0.0
*,*,30, ,20000.0,0.0,-1.0,0.0
*,*,216, ,20000.0,0.0,1.0,0.0
*,*,230, ,20000.0,0.0,-1.0,0.0
*,*,16, ,79280.0,1.0,0.0,0.0
*,*,30, ,107680.0,-1.0,0.0,0.0
*,*,216, ,79280.0,-1.0,0.0,0.0
*,*,230, ,107680.0,1.0,0.0,0.0
FORCE,29,16, ,35000.0,0.0,1.0,0.0
*,*,30, ,35000.0,0.0,-1.0,0.0
*,*,216, ,35000.0,0.0,1.0,0.0
=,*,230, ,35000.0,0.0,-1.0,0.0
*,*,16, ,138740.0,1.0,0.0,0.0
*,*,30, ,188440.0,-1.0,0.0,0.0
*,*,216, ,138740.0,-1.0,0.0,0.0
*,*,230, ,188440.0,1.0,0.0,0.0
ENDDATA
```

```
RESTART VERSION=1 KEEP
ASSIGN MASTER = 'prop12b.MASTER'
ID SPECJR,NLB
SOL 106
TIME 900
CEND
TITLE=RESTART FOR BUCKLING
SET 2 = 38,53,65,74
ECHO = UNSORT
  DISP = 2
  METHOD=90
PARAM,BUCKLE,1
PARAM,SUBID,4
PARAM,LOOPID,10
SUBCASE 1
  LOAD = 9
  NLPARM = 9
SUBCASE 2
  LOAD = 19
  NLPARM = 19
SUBCASE 3
  LOAD = 29
  NLPARM = 29
SUBCASE 4
 LOAD = 29
 NLPARM = 69
BEGIN BULK
EIGB,90,SINV,-5.0,5.0,20,3,3, ,+EIGB
+EIGB,MAX
NLPARM,69,2, .AUTO,1, , ,YES
ENDDATA
```

## Concept

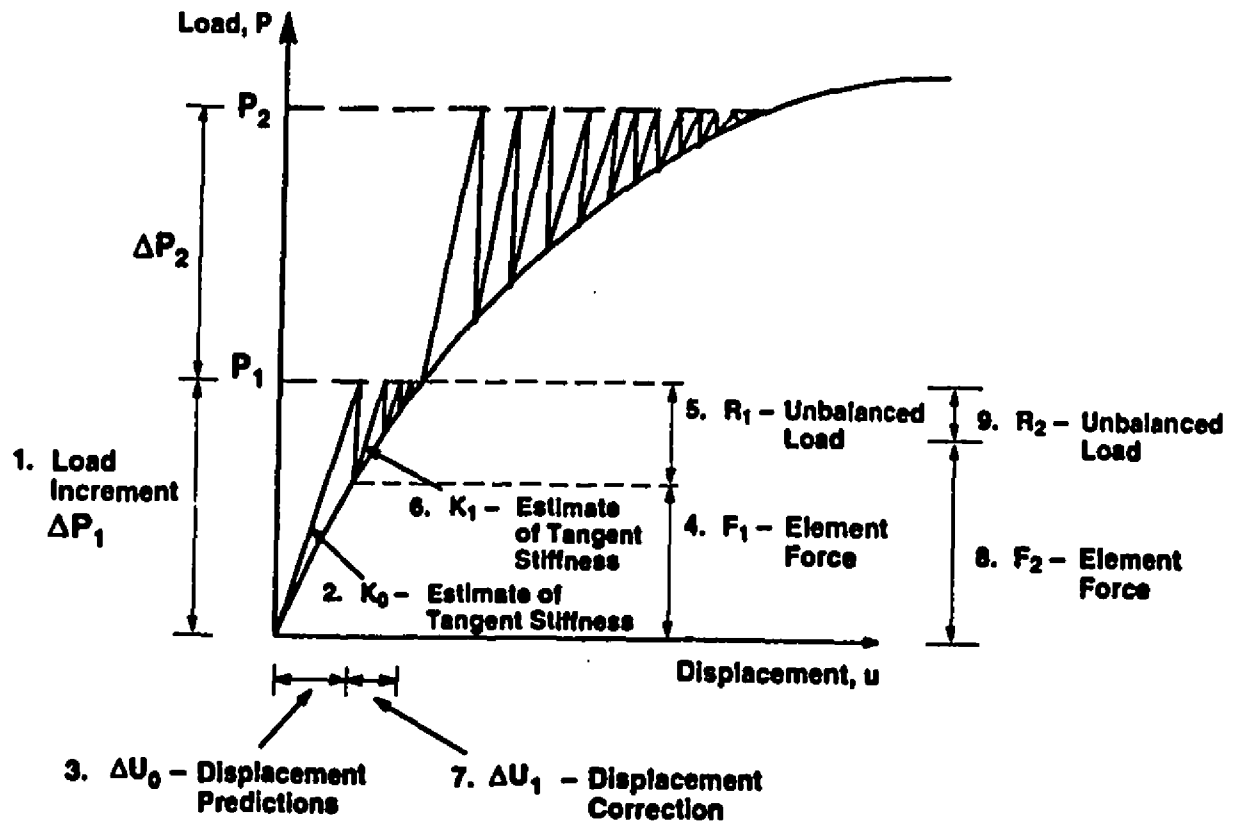


**where Steps 1 through 5 = advancing (predicting) phase.**

**Steps 6 through 9 = correcting (iterating) phase.**

- $\Delta P_1$ need not equal $\Delta P_2$.
- $K_0$ need not equal $K_1$.

Fig. A.1: Nonlinear Analysis Concept (MSC*)

* Taken from Lee (1992)

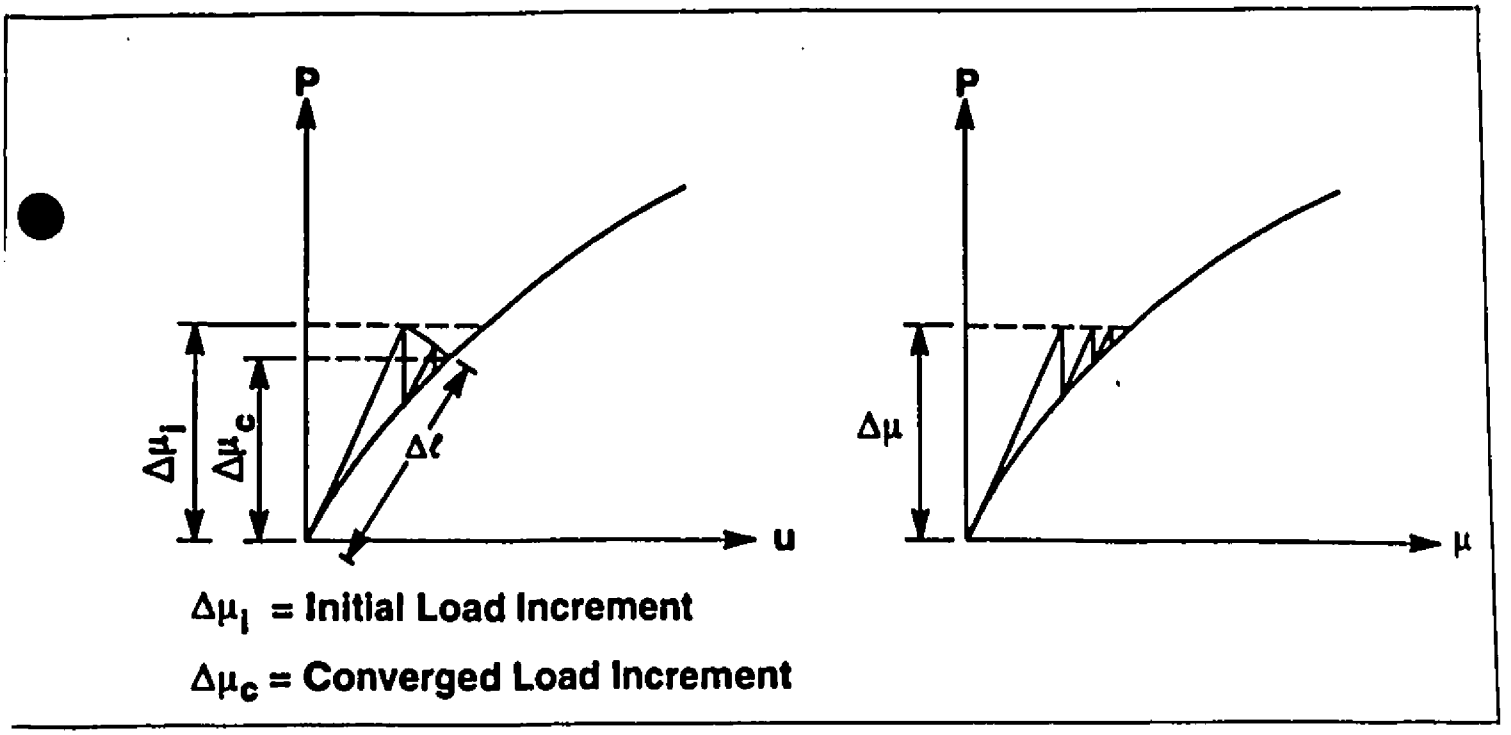


**Fig. A.2:** Crisfield vs. Load Increment Method (MSC*)

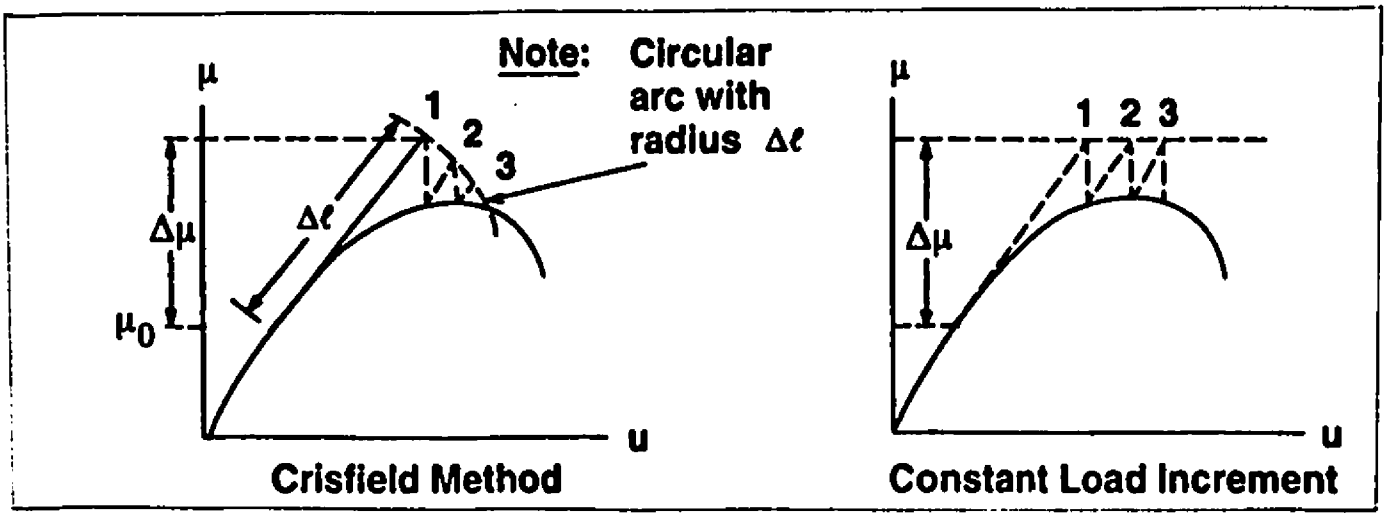


**Fig. A.3:** Crisfield Method in Unstable Region (MSC*)

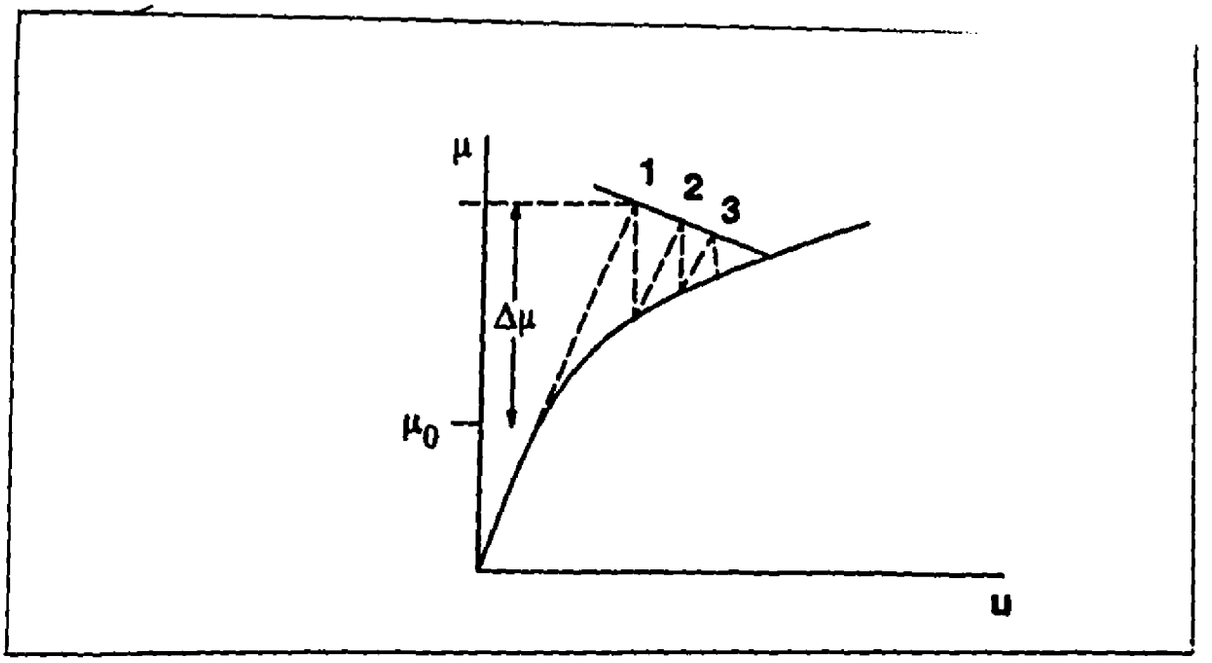


Fig. A.4: Riks Method (MSC*)

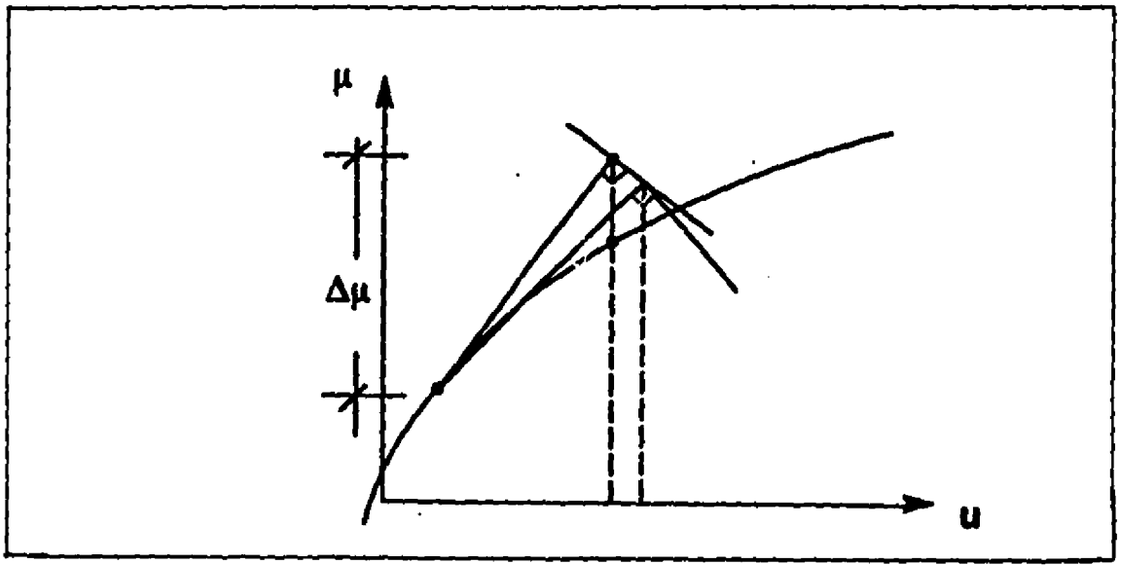


Fig. A.5: Modified Riks Method (MSC*)

## Concept

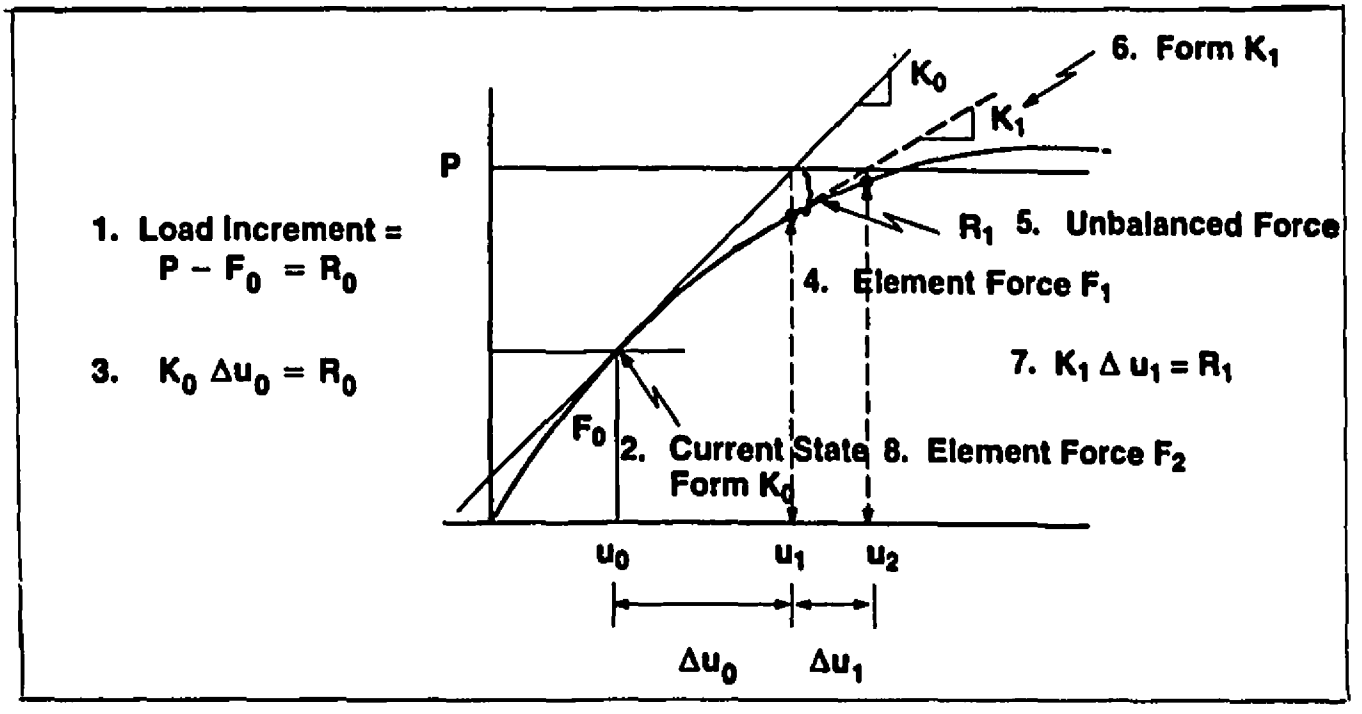


where Steps 1 through 5 = advancing phase.

Steps 6 through 9 = correcting phase.

- Advance forward by constant and positive load increments.
- Tangent stiffness is formed at every iteration.
- Displacement is predicted and corrected by solving equilibriu equations.

Fig. A.6: Newton Raphson Method (MSC®)

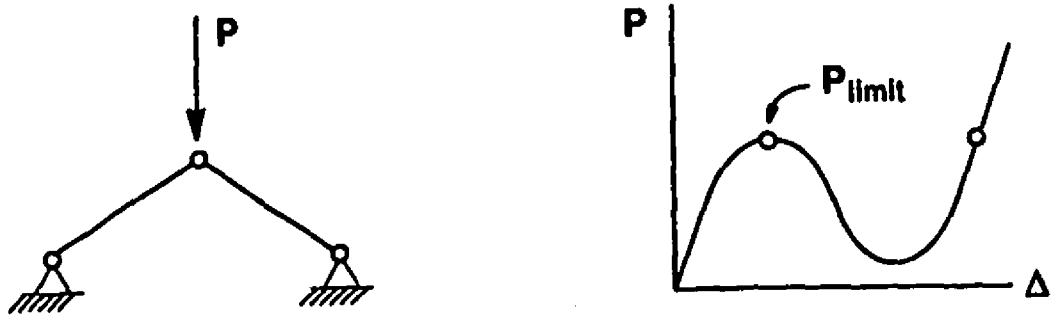


Fig. A.7: Snap Through (MSC*)

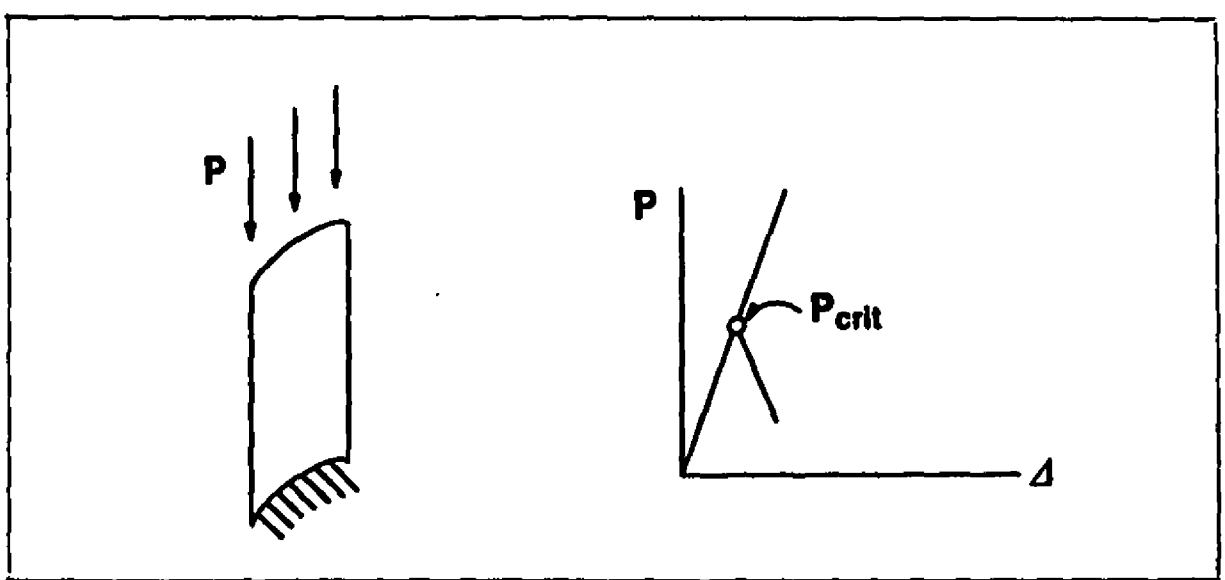


Fig. A.8: Bifurcation Buckling (MSC*)

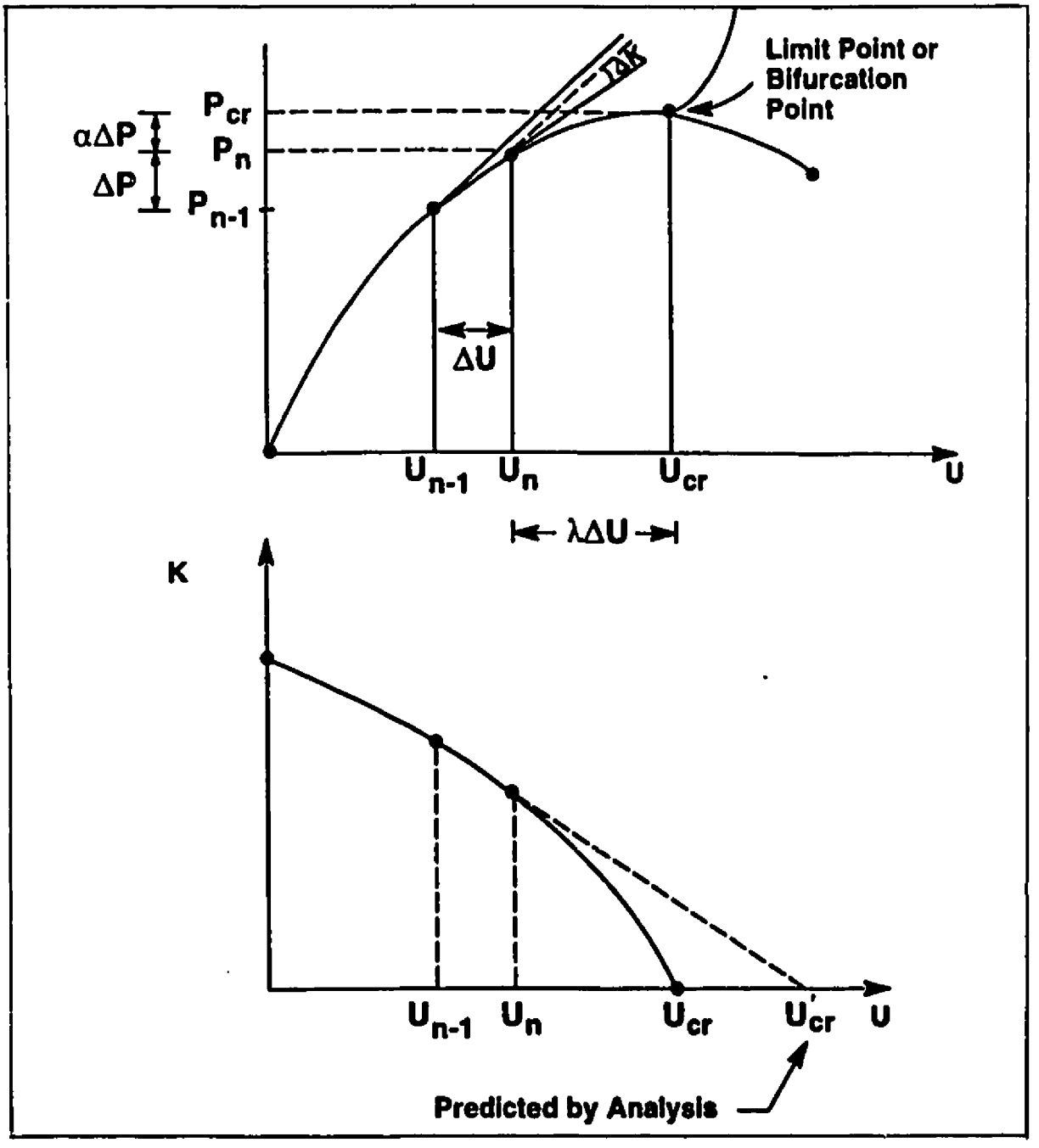


**Note:** **The error in $U_{cr}$ may be large, but the corresponding error in $P_{cr}$ is small.**

Fig. A.9: Buckling Concept (MSC*)

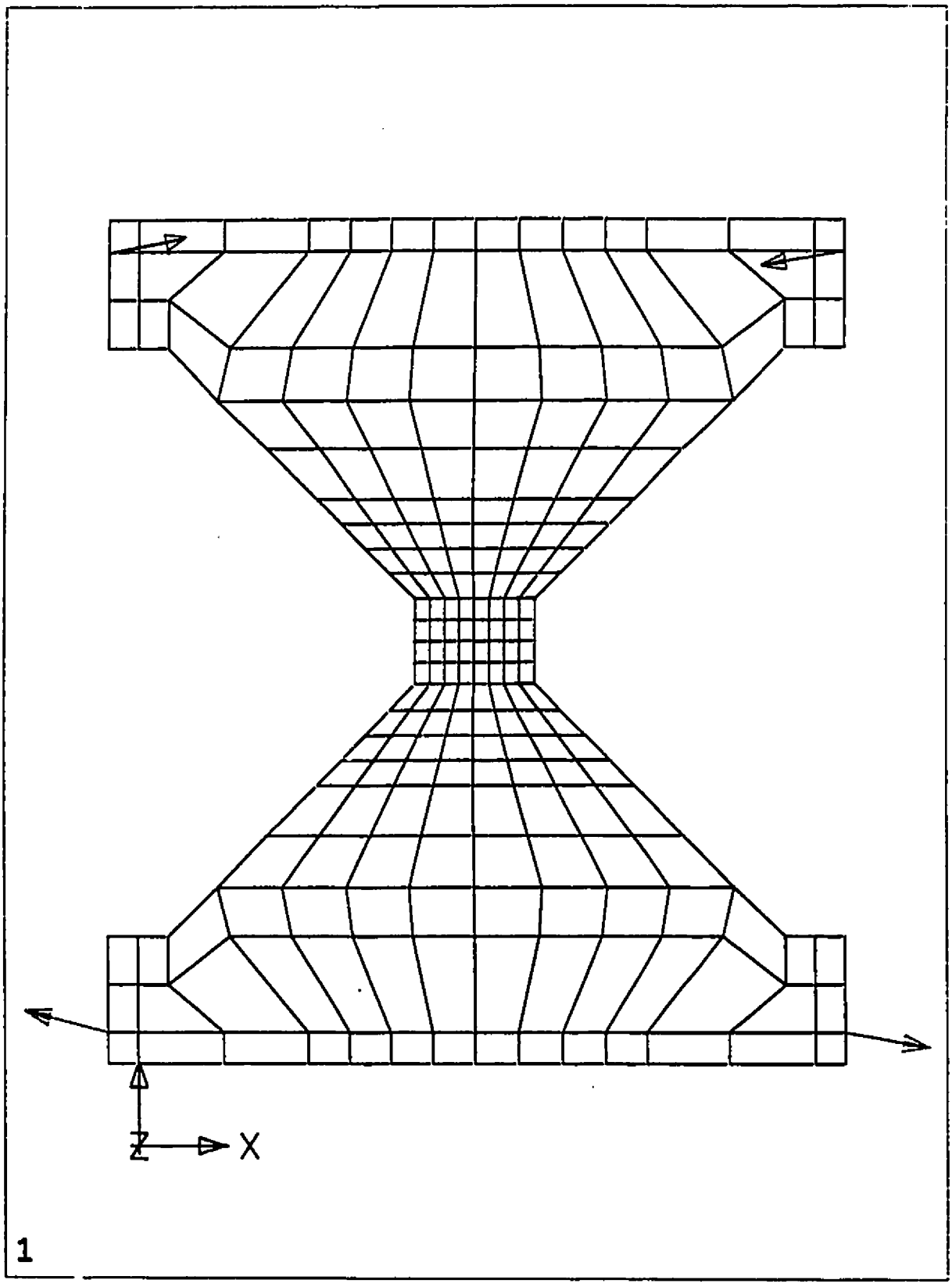


FIG A.10: FINITE ELEMENT MODEL

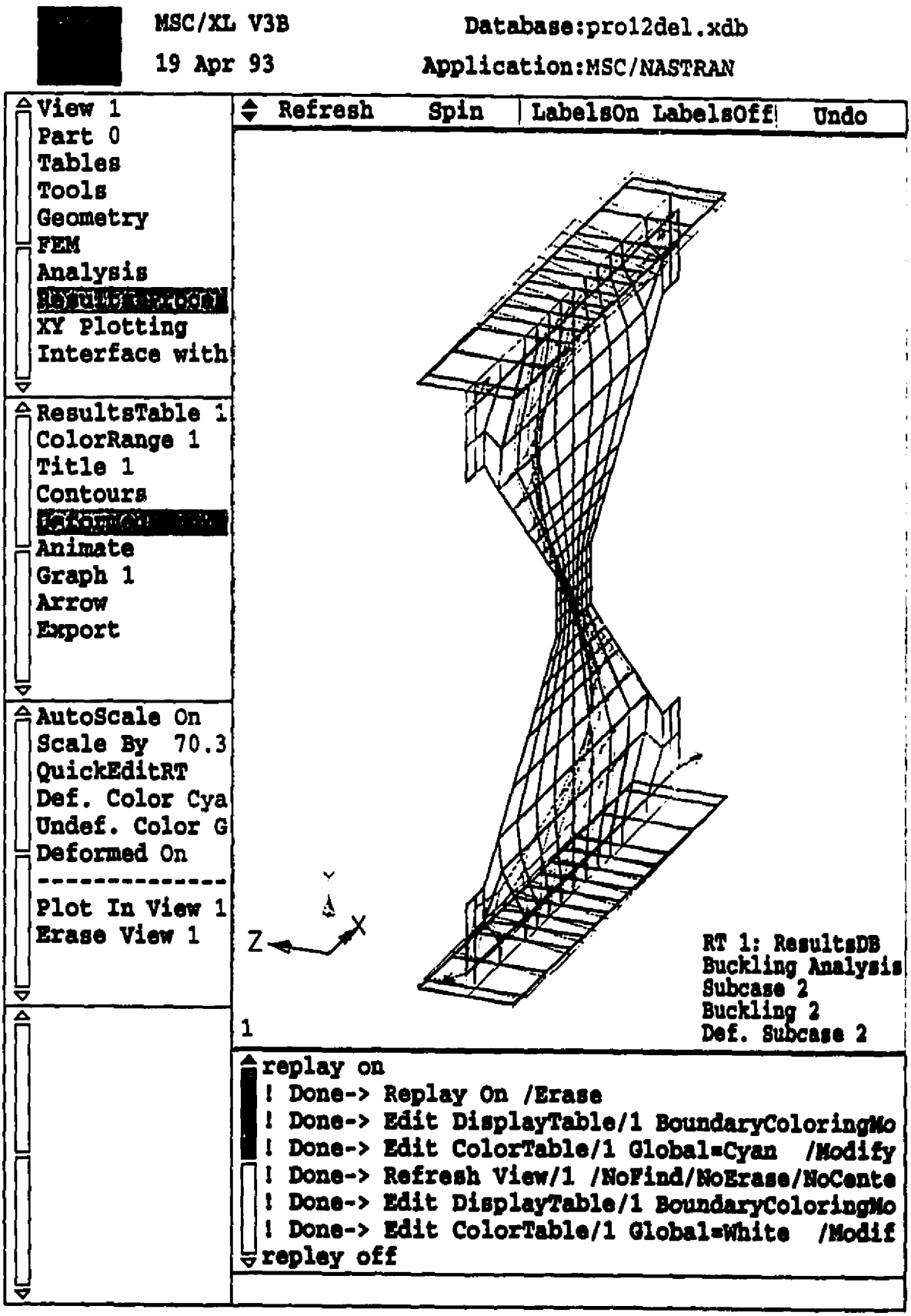


**Fig. A.11:** Finite Element Model (Buckled Shape)

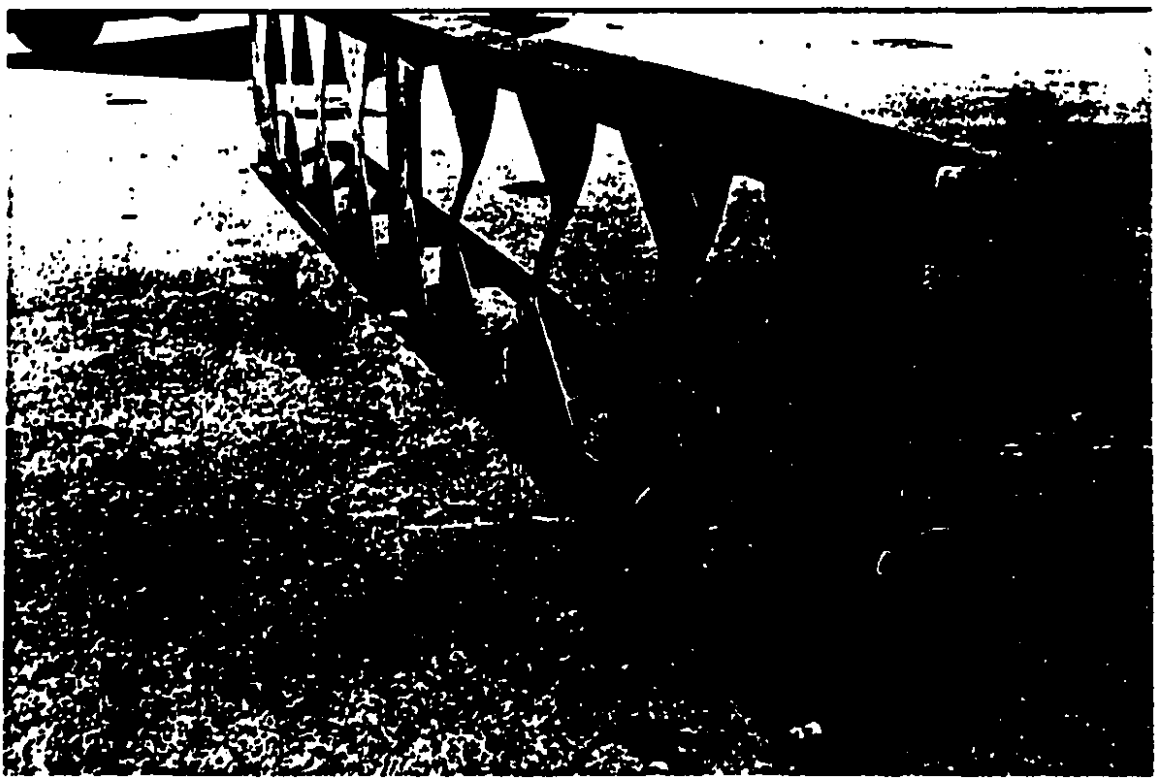

Fig. A.12: Failed Test Specimen (12-2)

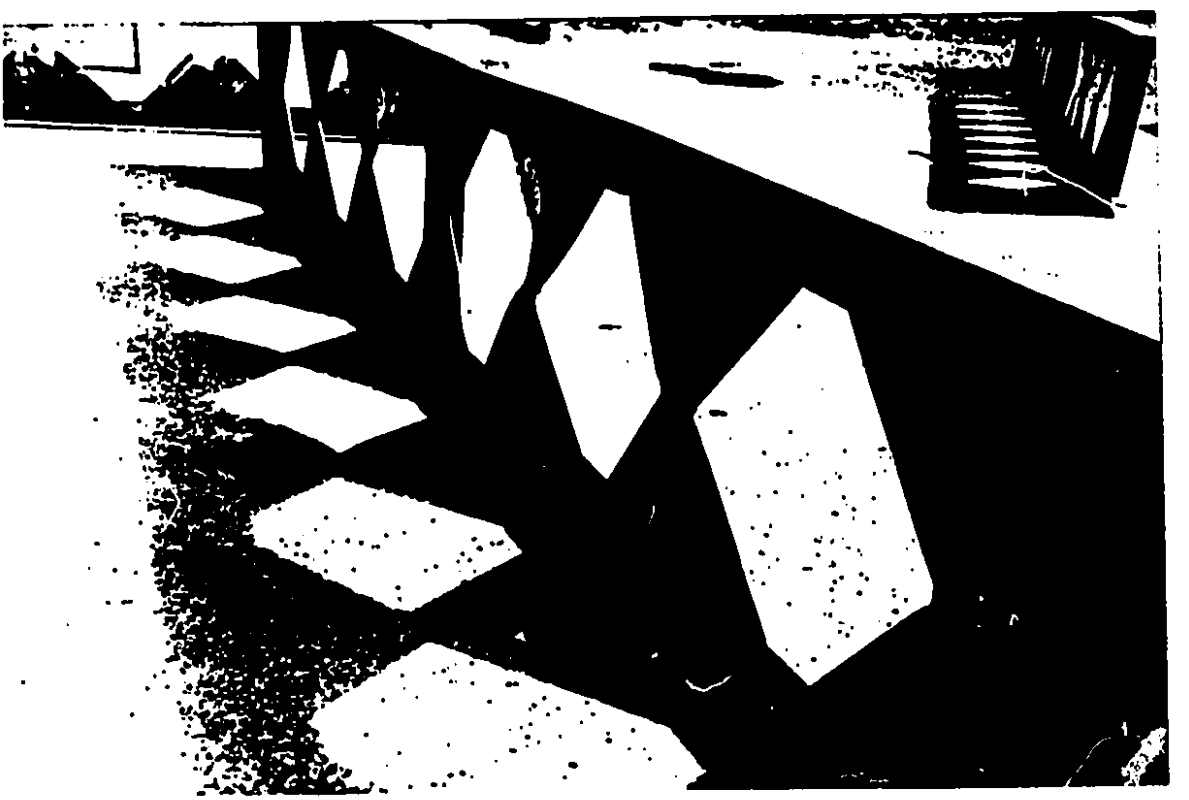

Fig. A.13: Failed Test Specimen (12-3)

# Appendix B

## Spreadsheet Samples

TABLE B.1: **SAMPLE INPUT & OUTPUT NEEDED FOR FURTHER CALCULATIONS**

| INPUT | | | | | |
|---|---|---|---|---|---|
| bf | = | Width of flange | = | 3.065 | in. |
| tf | = | Thickness of flange | = | 0.225 | in. |
| tw | = | Thickness of web | = | 0.177 | in. |
| dt | = | Depth of tee | = | 3.000 | in. |
| S | = | Cl to Cl of hole | = | 17.250 | in. |
| L | = | length of beam | = | 120.000 | in. |
| Fy | = | yield stress | = | 50.000 | ksi |
| do | = | original depth | = | 11.91 | in. |
| e | = | width at top of hole (e) | = | 2.745 | in. |
| phi | = | angle of inclination | = | 45.170 | deg. |

| OUTPUT | | | | | |
|---|---|---|---|---|---|
| d | = | total depth of castell. (do not put) | = | 19.820 | in. |
| 2H | = | total height in opening (do not put) | = | 13.820 | in. |
| dw | = | Depth of web of tee section (do not put) | = | 2.775 | in. |
| CG | = | dt-yt | = | 0.74 | in. |
| theta | = | 90-phi | = | 0.78 | rad. |
| do | = | original depth | = | 11.91 | in. |
| h | = | d-2*tf | = | 19.37 | in. |
| Aw | = | (d-2*tf)*tw | = | 3.43 | in^2 |
| Af | = | bf*tf | = | 0.69 | in^2 |
| Alpha | = | (3/16)*(d/(e/2))^2*(1-(2h/d))^2 | = | 3.58 | |
| Mp | = | (bf*tf*(d-tf)+0.25*tw*h^2)*Fy | = | 1505.78 | kips-in |
| Vp | = | tw*(d-2*tf)*Fy/@sqrt(3) | = | 98.97 | kips |
| L' | = | L/2-S/2 | = | 51.375 | in. |
| L'' | = | L/2-S/2-S | = | 34.13 | in. |
| yt | = | ((bf*tf)*(dt-tf/2)+(tw*dw^2/2))/((bf*tf)+(tw*dw) | = | 2.26 | in. |
| phi | = | angle of inclination | = | 0.788 | rad. |
| hp | = | ht of plate | = | 2.000 | in. |
| b | = | horizontal length of slope (b) (do not put) | = | 5.880 | in. |
| h(slope) | = | height of slope alone | = | 5.91 | in. |

Table B.2: **CALCULATION OF FIRST YIELD**

| | | | | | |
|---|---|---|---|---|---|
| Ig | = | bf*d ^ 3/12-((bf-tw)*(d-2*tf) ^ 3/12+(tw*(2*(2H/2 | = | 200.67 | in ^ 4 |
| yt | = | ((bf*tf)*(dt-tf/2)+(tw*dw ^ 2/2))/((bf*tf)+(tw*dw)) | = | 2.26 | in |
| I(0) | = | bf*tf ^ 3/12+tw*dw ^ 3/12 | = | 0.32 | in ^ 4 |
| I(1) | = | bf*tf*(tf/2+dw-yt) ^ 2+tw*dw*(dw/2-yt) ^ 2 | = | 0.65 | in ^ 4 |
| I(T) | = | I(0) +I(1) | = | 0.96 | in ^ 4 |
| Sf | = | I(T)/(dt-yt) | = | 1.31 | in ^ 3 |
| Ss | = | I(T)/yt | = | 0.43 | in ^ 3 |
| Sg | = | 2*Ig/d | = | 20.25 | in ^ 3 |
| La | = | (L/2-(s/2)+(e/2)) | = | 52.75 | in |
| Lb | = | (L/2-(s/2)-(e/2)) | = | 50.00 | in |

**First Yield** (take smaller and multiply by 2 to get the load 'P')

| | | | | | |
|---|---|---|---|---|---|
| V (stem) | = | Fy/((+La*(2H/2)/Ig)+e/(4*Ss)) | = | 14.58 | kips |
| V (flange) | = | Fy/((+Lb/Sg)+(e/(4*Sf))) | = | 16.70 | kips |

TABLE B .3: **DATA FOR INTERACTION DIAGRAM (FAILURE BY FORMATION OF MECHANISM)**

| k1 | Alphabar | V/Vp | M/Mp | Vp/Mp | M/Mp(trial) |
|---|---|---|---|---|---|
| 0 | 0.00 | 0.000 | 0.731 | 0.066 | 0.000 |
| 0.1 | 0.13 | 0.102 | 0.660 | 0.066 | 0.346 |
| 0.2 | 0.46 | 0.170 | 0.585 | 0.066 | 0.576 |
| 0.3 | 0.93 | 0.210 | 0.525 | 0.066 | 0.710 |
| 0.4 | 1.47 | 0.233 | 0.477 | 0.066 | 0.788 |
| 0.5 | 2.02 | 0.247 | 0.439 | 0.066 | 0.836 |
| 0.6 | 2.53 | 0.256 | 0.406 | 0.066 | 0.865 |
| 0.7 | 2.97 | 0.262 | 0.376 | 0.066 | 0.884 |
| 0.8 | 3.30 | 0.265 | 0.348 | 0.066 | 0.896 |
| 0.9 | 3.51 | 0.267 | 0.319 | 0.066 | 0.902 |
| 1 | 3.58 | 0.268 | 0.289 | 0.066 | 0.904 |
| | | 0.268 | 0.000 | 0.066 | 0.904 |

## TABLE B.4: BUCKLING ANALYSIS BASED ON BLODGETT AND AISC

| | | | | | |
|---|---|---|---|---|---|
| l/rt | = | (2H/(.29*tw)) | = | 269.24 | |
| Fb | = | (170000*2.3)/((l/rt) ^ 2) | = | 5.39 | ksi |
| thaw-bar | = | ((4*theta ^ 2)*Fb)/(3*tan(theta)) | = | 4.43 | ksi |
| V h | = | thaw-bar*e*tw | = | 2.15 | kips |
| V-(buckling) | = | V h*(d-2*CG)/(s) | = | 2.29 | kips |
| P | = | Buckling load | = | 4.58 | kips |

## TABLE B.5: FAILURE DUE TO HORIZONTAL SHEAR (RUPTURE OF WELD)

| | | | | | |
|---|---|---|---|---|---|
| V (at welded joint) | = | (Fy*tw*e*(d-2*CG))/(S*@SQRT(3)) | = | 14.92 | kips |
| P | = | Buckling load | = | 29.84 | kips |

Table B.6: **Buckling Analysis Based on Aglan and Redwood**

| Input | | | | | | |
|---|---|---|---|---|---|---|
| tw | = | thickness of web | = | 0.177 | in. | |
| s | = | center line to center line | = | 14.000 | in. | |
| e | = | width of welded section | = | 3.000 | in. | |
| Fy | = | yield stress | = | 50.000 | ksi. | |
| hp | = | height of plate | = | 0.000 | in. | |
| h | = | height of slope alone | = | 6.910 | in. | |
| phi | = | angle of inclination | = | 1.046 | rad. | 59.935 deg. |
| dg | = | depth of castell. section | = | 16.820 | in. | |
| CG | = | centroid of tee (fr. top) | = | 0.570 | in. | |

| output | | | | | |
|---|---|---|---|---|---|
| s' | = | s-e | = | 11.00 | in. |
| Mp | = | 0.25*tw*(s')^2*Fy | = | 267.71 | kips-in |

| data needed to choose graph | | | | | |
|---|---|---|---|---|---|
| h'/h | = | (hp/2)/(h+hp/2) | = | 0.00 | |
| s/w | = | e/tw | = | 16.95 | |
| 2*h/s | = | (2*(h+hp/2))/(e) | = | 4.61 | |
| phi | = | angle of inclination | = | 59.935 | deg. |

| (from specific graph) | | | | |
|---|---|---|---|---|
| alpha | = | Mocr/Mp | = | 0.38 |

| | | | | | |
|---|---|---|---|---|---|
| Mocr | = | alpha*Mp | = | 101.73 | kips-in |
| Vh | = | Mocr/(h+hp/2) | = | 14.72 | kips |
| V | = | (Vh*2*((dg-2*CG)/2))/(s) | = | 18.59 | kips |
| P | = | Buckling load | = | 37.184 | kips |

Table B.7: **CALCULATIONS FOR LOCATION OF LATERAL SUPPORT SYSTEM**

| INPUT | | | | mm | in |
|---|---|---|---|---|---|
| bf | = | width of flange | = | 77.851 | 3.065 |
| tf | = | thick of flange | = | 5.715 | 0.225 |
| tw | = | thick of web | = | 4.496 | 0.177 |
| d | = | total depth of section | = | 503.499 | 19.823 |
| Fy | = | yield stress | = | 345.000 | MPa |
| w_2 | = | conservative | = | 1.000 | |
| Lu | = | unsupported length | = | 600.000 | |
| E | = | mod. of elasticity | = | 200000.000 | MPa |
| G | = | shear mod. | = | 77000 | MPa |
| SH | = | hd of opening | = | 351.089 | 13.820 |

| CLASS | | | | | | | | | |
|---|---|---|---|---|---|---|---|---|---|
| flange | = | bf/(2*tf) | = | 6.81 | 1 | class1_f | = | 145/(@SQRT(Fy)) | = 7.81 |
| | | | | | 2 | class2_f | = | 170/(@SQRT(Fy)) | = 9.15 |
| | | | | | 3 | class3_f | = | 200/(@SQRT(Fy)) | = 10.77 |
| | | | | | 4 | class4_f | | | |
| | | | | | | class_f | = | @IF(flange<=class1_f,1 | = 1 |
| web | = | (d-2*tf)/tw | = | 109.44 | 1 | class1_w | = | 1100/(@SQRT(Fy)) | = 59.22 |
| | | | | | 2 | class2_w | = | 1700/(@SQRT(Fy)) | = 91.58 |
| | | | | | 3 | class3_w | = | 1900/(@SQRT(Fy)) | = 102.30 |
| | | | | | 4 | class4_w | | | |
| | | | | | | class_w | = | @IF(web<=class1_w,1, | = 4 |

| class of section | = | @IF(class_f<=class_w,cl | = 3 |
|---|---|---|---|

| SECTION PROPERTIES | | | | |
|---|---|---|---|---|
| Ixx | = | (2*(((bf*tf^3)/12)+(bf*tf* | = 9.97E+07 | mm^4 |
| Iyy | = | ((tf*bf^3/12)*2)+((d-2*tf) | = 4.99E+06 | mm^4 |
| Sx | = | 2*Ixx/d | = 396199.92 | mm^3 |
| Z | = | 1/4*((bf*d^2)-((bf-tw)*(d-2* | = 463807.22 | mm^3 |
| *reduced J | = | (1/3)*((2*bf*tf^3)+(d-2*tf | = 14130.81 | mm^4 |
| Cw | = | (Iyy*(d-tf)^2)/4 | = 2.83E+10 | mm^6 |

| CLASS 1 and 2 | | | | | | CLASS 3 and 4 | | | | | |
|---|---|---|---|---|---|---|---|---|---|---|---|
| A | = | 2*Iyy*G*J | = | 9.83E+19 | MPa^2mm^6 | | | | | | |
| B | = | ((4/3)*E/Lu)^2*(Iyy*Cw) | = | 1.19E+22 | MPa^2mm^6 | | | | | | |
| Mu | = | (w_2*(pi/Lu)*(@sqrt(A+B | = | 3.37E+08 | N-mm | Mu | = | = | 3.37E+08 | N-mm | |
| My | = | Z*Fy | = | 1.70E+08 | N-mm | My | = | Sx*Fy | = 1.37E+08 | N-mm | |
| ***** | check_p | = 0.67*My | = | 1.14E+08 | N-mm | check_p | = | 0.67*My | = 9.18E+07 | N-mm | 0.9*My 1.23E+08 |
| | Mr_c | = (1.15*0.9*My)*(1-(0.28*My | = | 1.60E+08 | <= | Mr_c | = | (1.15*0.9*M | = 1.31E+08 | <= | |
| | Mr_b | = 0.9*Mu | = | 4.75E+08 | | Mr_b | = | 0.9*Mu | = 4.75E+08 | | |

| Mr_p | = | @IF(Mu>0.67*My,0.67*My,Mu) | = | 1.60E+08 | N-mm | Mr_p | = | @IF(Mu>My,My, | = 1.31E+08 | N-mm |
|---|---|---|---|---|---|---|---|---|---|---|

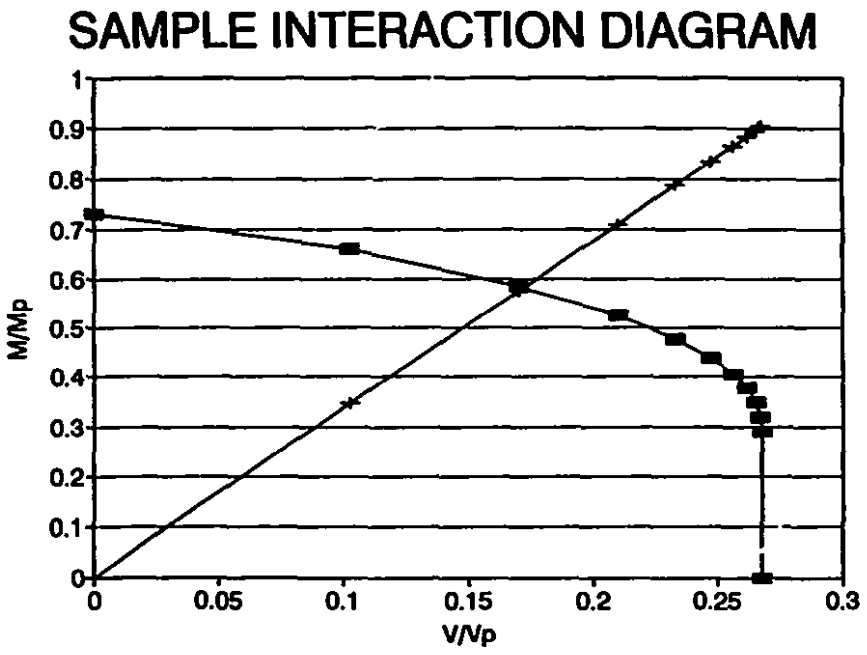


**Fig. B.1:** Sample Interaction Diagram (Specimen 12-4)

# Appendix C

## Shape Properties

**Table C.1a:** Nominal Dimensions of Test Specimens (in.)

| Beam Type | B8×6.5 | B8×6.5 | B8×6.5 | B8×6.5 |
|---|---|---|---|---|
| Specimen # | 8-1 | 8-2 | 8-3 | 8-4 |
| L* | 120.00 | 120.00 | 120.00 | 120.00 |
| S | 8.75 | 8.75 | 13.50 | 13.50 |
| phi (degree) | 60.13 | 60.13 | 44.04 | 44.04 |
| $h_p$[1] | 0.00 | 2.00 | 0.00 | 2.00 |
| $d_g$ | 12.20 | 12.20 | 12.20 | 14.20 |
| $d_f$ | 1.75 | 1.75 | 1.75 | 1.75 |
| e | 1.88 | 1.88 | 2.25 | 2.25 |
| $h_o$ | 8.70 | 10.70 | 8.70 | 10.70 |
| b | 2.50 | 2.50 | 4.50 | 4.50 |
| h | 4.35 | 4.35 | 4.35 | 4.35 |
| stiffener[2] | 1 " ×1/4 " | 1 " ×1/4 " | 1 " ×1/4 " | 1 " ×1/4 " |

**Table C.1b:** Nominal Dimensions of Test Specimens (in.)

| Beam Type | B10×8.0 | B10×8.0 | B10×8.0 | B10×8.0 |
|---|---|---|---|---|
| Specimen # | 10-1 | 10-2 | 10-3 | 10-4 |
| L | 120.00 | 120.00 | 120.00 | 120.00 |
| S | 10.00 | 10.00 | 14.50 | 14.50 |
| phi (degree) | 60.26 | 60.26 | 45.36 | 45.36 |
| $h_p$ | 0.00 | 2.00 | 0.00 | 2.00 |
| $d_g$ | 14.63 | 16.63 | 14.88 | 16.88 |
| $d_f$ | 2.50 | 2.50 | 2.37 | 2.37 |
| e | 2.25 | 2.25 | 2.25 | 2.25 |
| $h_o$ | 9.63 | 11.63 | 10.13 | 12.13 |
| b | 2.75 | 2.75 | 5.00 | 5.00 |
| h | 4.81 | 4.81 | 5.06 | 5.06 |
| stiffener | 1 " ×1/4 " | 1 " ×1/4 " | 1 " ×1/4 " | 1 " ×1/4 " |

**Table C.1c:** Nominal Dimensions of Test Specimens (in.)

| Beam Type | B12×11.8 | B12×11.8 | B12×11.8 | B12×11.8 |
|---|---|---|---|---|
| Specimen # | 12-1 | 12-2 | 12-3 | 12-4 |
| L | 120.00 | 120.00 | 120.00 | 120.00 |
| S | 14.00 | 14.00 | 17.25 | 17.25 |
| phi (degree) | 59.94 | 59.94 | 45.17 | 45.17 |
| $h_p$ | 0.00 | 2.00 | 0.00 | 2.00 |
| $d_g$ | 18.82 | 20.82 | 17.82 | 19.82 |
| $d_f$ | 2.50 | 2.50 | 3.00 | 3.00 |
| e | 3.00 | 3.00 | 2.75 | 2.75 |
| $h_o$ | 13.82 | 15.82 | 11.82 | 13.82 |
| b | 4.00 | 4.00 | 5.88 | 5.88 |
| h | 6.91 | 6.91 | 5.91 | 5.91 |
| stiffener | 1 " ×1/4 " | 1 " ×1/4 " | 1 " ×1/4 " | 1 " ×1/4 " |

* 1 in. = 25.4 mm

[1] Thickness of plate is equal to thickness of web

[2] Location: 3" from the edges and at mid span (both sides)

**Table C.1d:** Nominal Dimensions (Bazile and Texier 1968) (in.)

| Specimen | A | B | C | D | E |
|---|---|---|---|---|---|
| L | 16×S | 16×S | 16×S | 16×S | 16×S |
| S | 19.84 | 19.84 | 19.84 | 19.84 | 16.3 |
| $h_D$ | 0.00 | 5.12 | 7.87 | 9.06 | 5.51 |
| $d_g$ | 19.68 | 23.62 | 27.56 | 27.56 | 19.68 |
| $d_t$ | 3.94 | 4.53 | 3.94 | 4.53 | 3.54 |
| e | 6.61 | 6.61 | 6.61 | 6.61 | 5.43 |
| $t_w$ | 0.39 | 0.39 | 0.39 | 0.39 | 0.26 |
| $t_f$ | 0.69 | 0.69 | 0.69 | 0.69 | 0.40 |
| $b_f$ | 11.81 | 11.81 | 11.81 | 11.81 | 5.31 |
| b | 3.31 | 3.31 | 3.31 | 3.31 | 2.72 |
| h | 5.9 | 4.72 | 5.91 | 4.72 | 3.545 |

**Table C.2a:** Nominal and Measured Dimensions of Test Specimens (in.)

| Specimen # | 8-1a | | 8-2a | | 8-3a | | 8-4a | |
|---|---|---|---|---|---|---|---|---|
| | Nominal | Measured | Nominal | Measured | Nominal | Measured | Nominal | Measured |
| L | 120.00 | 120.88 | 120.00 | 120.93 | 120.00 | 120.15 | 120.00 | 120.10 |
| $d_g$ | 12.20 | 12.10 | 14.20 | 14.16 | 12.20 | 12.10 | 14.20 | 14.18 |
| e | 1.88 | 1.91 | 1.88 | 1.90 | 2.25 | 2.29 | 2.25 | 2.30 |
| $h_o$ | 8.70 | 8.75 | 10.70 | 10.66 | 8.70 | 8.72 | 10.70 | 10.63 |
| $t_w$ | 0.133 | 0.135 | 0.133 | 0.137 | 0.133 | 0.137 | 0.133 | 0.136 |
| $t_f$ | 0.186 | 0.185 | 0.186 | 0.186 | 0.186 | 0.180 | 0.186 | 0.184 |
| $b_f$ | 2.28 | 2.34 | 2.28 | 2.30 | 2.28 | 2.31 | 2.28 | 2.26 |

**Table C.2b:** Nominal and Measured Dimensions of Test Specimens (in.)

| Specimen # | 8-3 | | 8-4 | |
|---|---|---|---|---|
| | Nominal | Measured | Nominal | Measured |
| L | 120.00 | 119.90 | 120.00 | 120.13 |
| $d_g$ | 12.20 | 12.10 | 14.20 | 14.13 |
| e | 2.25 | 2.26 | 2.25 | 2.31 |
| $h_o$ | 8.70 | 8.75 | 10.70 | 10.63 |
| $t_w$ | 0.133 | 0.138 | 0.133 | 0.137 |
| $t_f$ | 0.186 | 0.180 | 0.186 | 0.186 |
| $b_f$ | 2.28 | 2.35 | 2.28 | 2.30 |

**Table C.2c:** Nominal and Measured Dimensions of Test Specimens (in.)

| Specimen # | 10-1 | | 10-2 | | 10-3 | | 10-4 | |
|---|---|---|---|---|---|---|---|---|
| | Nominal | Measured | Nominal | Measured | Nominal | Measured | Nominal | Measured |
| L | 120.00 | 119.80 | 120.00 | 120.00 | 120.00 | 119.90 | 120.00 | 119.85 |
| $d_g$ | 14.63 | 14.59 | 16.63 | 16.45 | 14.88 | 14.82 | 16.88 | 16.75 |
| e | 2.25 | 2.29 | 2.25 | 2.27 | 2.25 | 2.28 | 2.25 | 2.32 |
| $h_o$ | 9.63 | 9.68 | 11.63 | 11.62 | 10.13 | 10.25 | 12.13 | 12.13 |
| $t_w$ | 0.139 | 0.141 | 0.139 | 0.142 | 0.139 | 0.142 | 0.139 | 0.145 |
| $t_f$ | 0.183 | 0.173 | 0.183 | 0.157 | 0.183 | 0.175 | 0.183 | 0.168 |
| $b_f$ | 2.69 | 2.72 | 2.69 | 2.75 | 2.69 | 2.78 | 2.69 | 2.78 |

**Table C.2d:** Nominal and Measured Dimensions of Test Specimens (in.)

| Specimen # | 12-1 | | 12-2 | | 12-3 | | 12-4 | |
|---|---|---|---|---|---|---|---|---|
| | Nominal | Measured | Nominal | Measured | Nominal | Measured | Nominal | Measured |
| L | 120.00 | 120.00 | 120.00 | 120.00 | 120.00 | 120.1 | 120.00 | 120.2 |
| $d_g$ | 18.82 | 18.75 | 20.82 | 20.78 | 17.82 | 17.70 | 19.82 | 19.75 |
| e | 3.00 | 2.89 | 3.00 | 2.93 | 2.75 | 2.81 | 2.75 | 2.69 |
| $h_o$ | 13.82 | 13.89 | 15.82 | 15.90 | 11.82 | 11.91 | 13.82 | 13.77 |
| $t_w$ | 0.177 | 0.185 | 0.177 | 0.181 | 0.177 | 0.182 | 0.177 | 0.185 |
| $t_f$ | 0.225 | 0.210 | 0.225 | 0.211 | 0.225 | 0.211 | 0.225 | 0.210 |
| $b_f$ | 3.06 | 3.09 | 3.06 | 3.07 | 3.06 | 3.08 | 3.06 | 3.07 |

# BUILD A BETTER TOMORROW

CHAPARRAL STEEL

## Bantam Beams,

Shape Properties

and Load

Tables

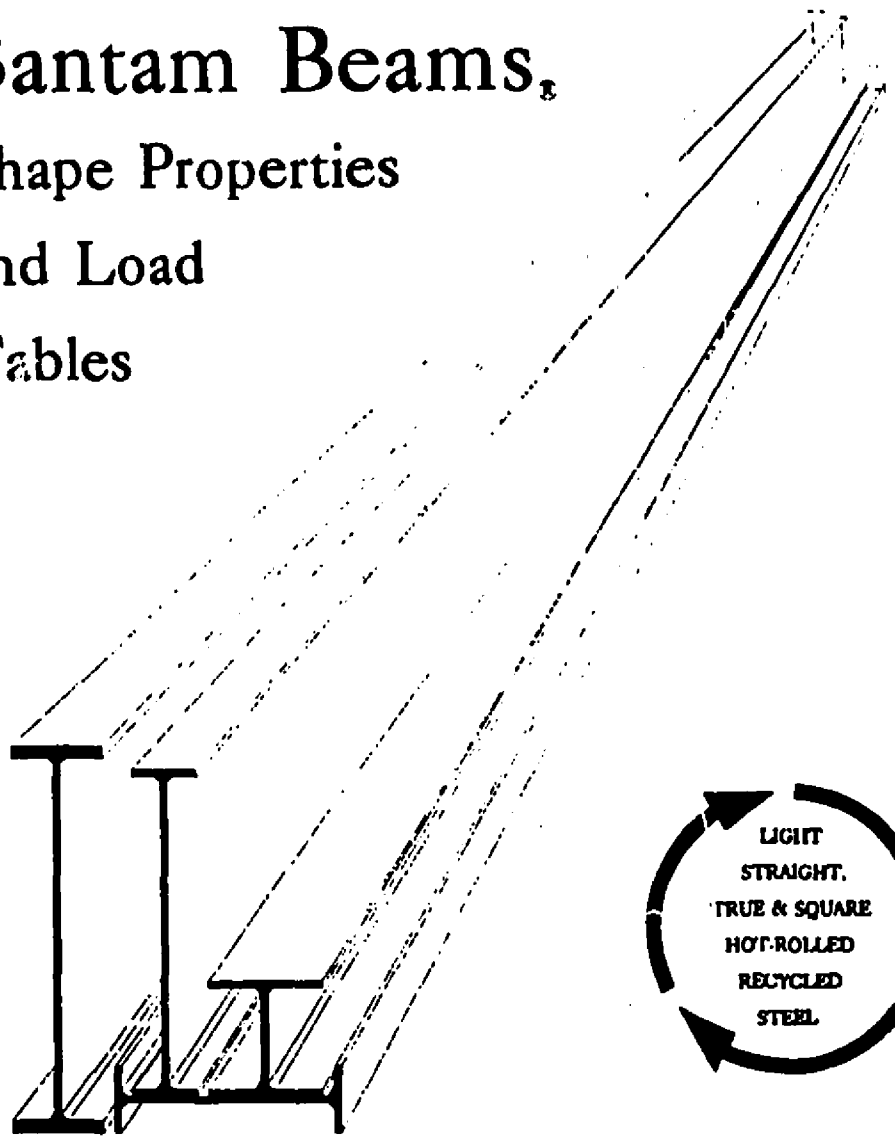

LIGHT
STRAIGHT,
TRUE & SQUARE
HOT-ROLLED
RECYCLED
STEEL

CHAPARRAL STEEL

300 Ward Road, Midlothian, Texas 76065.

Tel (800) 527-7979, (214) 775-8241

Fax (214) 775-6120

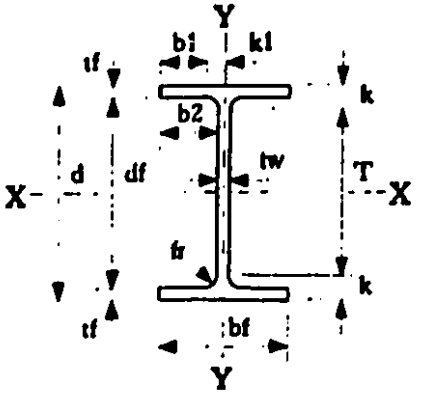


# BANTAM BEAMS

DIMENSIONS and PROPERTIES

| Physical Properties | | | | B4x6.0 | | B8x6.5 | | B10x8.0 | | B10x9.0 | | B12x10.8 | | B12x11.8 | |
|---|---|---|---|---|---|---|---|---|---|---|---|---|---|---|---|
| | | | Unit | Calc. | Nom. | Calc. | Nom. | Calc. | Nom. | Calc. | Nom. | Calc. | Nom. | Calc. | Nom. |
| Weight | W | per foot | (lbs/ft) | 5.975 | 6.000 | 6.534 | 6.500 | 8.082 | 8.000 | 9.082 | 9.000 | 10.877 | 10.800 | 11.858 | 11.800 |
| Area | A | X section | (in^2) | 1.756 | | 1.920 | | 2.375 | | 2.669 | | 3.197 | | 3.485 | |
| Dimensions | | | | Detail. | Nom. | Detail. | Nom. | Detail. | Nom. | Detail. | Nom. | Detail. | Nom. | Detail. | Nom. |
| Depth | d | overall | (in) | 3-13/16" | 3.790 | 7-7/8" | 7.852 | 9-13/16" | 9.814 | 9-7/8" | 9.860 | 11-7/8" | 11.872 | 11-15/16" | 11.910 |
| Web | tw | web thick. | (in) | 1/8" | 0.130 | 1/8" | 0.133 | 1/8" | 0.139 | 3/16" | 0.157 | 3/16" | 0.162 | 3/16" | 0.177 |
| | tw/2 | half web | (in) | 1/16" | | 1/16" | | 1/16" | | 1/16" | | 1/16" | | 1/16" | |
| Flange | bf | width | (in) | 3-15/16" | 3.910 | 2-1/4" | 2.280 | 2-11/16" | 2.690 | 2-11/16" | 2.690 | 3-1/16" | 3.065 | 3-1/16" | 3.065 |
| | tf | thickness | (in) | 3/16" | 0.160 | 3/16" | 0.186 | 3/16" | 0.183 | 3/16" | 0.206 | 3/16" | 0.206 | 1/4" | 0.225 |
| Distance | T | bet. fillets | (in) | 2-15/16" | | 6-7/8" | | 8-13/16" | | 8-7/8" | | 10-7/8" | | 10-15/16" | |
| | k | fillet edge | (in) | 7/16" | | 1/2" | | 1/2" | | 1/2" | | 1/2" | | 1/2" | |
| | k1 | fillet edge | (in) | 5/16" | | 3/8" | | 3/8" | | 3/8" | | 3/8" | | 3/8" | |
| Other | df | inside fl. | (in) | | 3.470 | | 7.480 | | 9.448 | | 9.448 | | 11.460 | | 11.460 |
| | fr | fillet radius | (in) | | 0.250 | | 0.300 | | 0.300 | | 0.300 | | 0.300 | | 0.300 |
| | b1 | flange ext. | (in) | | 1.640 | | 0.774 | | 0.976 | | 0.967 | | 1.152 | | 1.144 |
| | b2 | flange proj. | (in) | | 1.890 | | 1.074 | | 1.276 | | 1.267 | | 1.452 | | 1.444 |

| Geometric Properties | | | B4x6.0 | B8x6.5 | B10x8.0 | B10x9.0 | B12x10.8 | B12x11.8 |
|---|---|---|---|---|---|---|---|---|
| Elastic | Ixx | (in^4) | 4.728 | 18.145 | 34.278 | 38.537 | 65.765 | 71.764 |
| | Sxx | (in^3) | 2.495 | 4.622 | 6.986 | 7.817 | 11.079 | 12.051 |
| | rxx | (in) | 1.641 | 3.074 | 3.799 | 3.800 | 4.536 | 4.538 |
| | Iyy | (in^4) | 1.596 | 0.371 | 0.597 | 0.673 | 0.995 | 1.087 |
| | Syy | (in^3) | 0.816 | 0.325 | 0.444 | 0.501 | 0.649 | 0.709 |
| | ryy | (in) | 0.953 | 0.439 | 0.502 | 0.502 | 0.558 | 0.559 |
| Plastic | Zxx | (in^3) | 2.752 | 5.395 | 8.203 | 9.213 | 13.122 | 14.307 |
| | Zyy | (in^3) | 1.244 | 0.527 | 0.718 | 0.815 | 1.054 | 1.159 |
| Compact | bf/2tf | — | 12.219 | 6.129 | 7.350 | 6.529 | 7.439 | 6.811 |
| criteria | Fy | (Ksi) | 28.299 | — | — | — | — | — |
| (ASD) | d/tw | — | 29.154 | 59.038 | 70.604 | 62.803 | 73.284 | 67.288 |
| | F"y | (Ksi) | — | 18.950 | 13.250 | 16.746 | 12.298 | 14.588 |
| Compact | bf/2tf | — | 12.219 | 6.129 | 7.350 | 6.529 | 7.439 | 6.811 |
| criteria | hc/tw | — | 22.846 | 51.729 | 63.655 | 56.357 | 67.037 | 61.356 |
| (LRFD) | F"y | (Ksi) | — | 23.920 | 15.797 | 20.153 | 14.243 | 17.003 |
| | X1 | (Ksi) | 2,730 | 1,782 | 1,409 | 1,568 | 1,317 | 1,430 |
| | X2 x 10^6 | (1/Ksi)^2 | 2,406 | 21,554 | 55,770 | 36,765 | 77,107 | 55,947 |
| Misc. | IT (fl+1/6web) | (in^4) | 0.798 | 0.165 | 0.298 | 0.336 | 0.496 | 0.542 |
| | AT (fl+1/6web) | (in^2) | 0.728 | 0.629 | 0.750 | 0.840 | 0.979 | 1.066 |
| | rT (fl+1/6web) | (in) | 1.047 | 0.542 | 0.630 | 0.632 | 0.712 | 0.713 |
| | d/Al | — | 6.058 | 18.515 | 19.936 | 17.793 | 18.803 | 17.270 |
| Torsion | J | (in^4) | 0.016 | 0.022 | 0.025 | 0.035 | 0.042 | 0.053 |
| | Cw | (in^6) | 5.256 | 5.444 | 13.855 | 15.686 | 33.839 | 37.110 |
| | Sqrt(ECw/GJ) | /in) | 28.730 | 25.578 | 37.555 | 33.998 | 45.917 | 42.517 |
| | Wno | (in^2) | 3.548 | 4.370 | 6.477 | 6.492 | 8.939 | 8.954 |
| | Sw | (in^4) | 0.555 | 0.463 | 0.797 | 0.899 | 1.411 | 1.544 |
| | Qf | (in^3) | 0.571 | 0.836 | 1.214 | 1.349 | 1.853 | 2.008 |
| | Qw | (in^3) | 1.376 | 2.698 | 4.101 | 4.607 | 6.561 | 7.154 |
| Other | Surface Area | (sq ft/ft) | 1.875 | 2.004 | 2.466 | 2.471 | 2.930 | 2.934 |
| | S.A. less top fl. | (sq ft/ft) | 1.552 | 1.814 | 2.242 | 2.247 | 2.675 | 2.679 |

**BANTAM BEAMS** — **SAFE WORKING LOADS (ASD Design) IN KIPS PER FOOT**
(Based on pure bending. i.e. No axial loading)

| SHAPE | | B4x6.0 | | B8x6.5 | | B10x8.0 | | B10x9.0 | | B12x10.8 | | B12x11.8 | |
|---|---|---|---|---|---|---|---|---|---|---|---|---|---|
| SPAN (feet) | Limiting Factor | Fy(ksi) 36 | Fy(ksi) 50 | Fy(ksi) 36 | Fy(ksi) 50 | Fy(ksi) 36 | Fy(ksi) 50 | Fy(ksi) 36 | Fy(ksi) 50 | Fy(ksi) 36 | Fy(ksi) 50 | Fy(ksi) 36 | Fy(ksi) 50 |
| 6 | Stress | 0.998 | 1.386 | 2.034 | 2.825 | 3.074 | 4.269 | 3.439 | 4.777 | 4.875 | 6.771 | 5.302 | 7.365 |
| | *L/240* | *0.998* | *1.386* | *2.034* | *2.825* | *3.074* | *4.269* | *3.439* | *4.777* | *4.875* | *6.771* | *5.302* | *7.365* |
| 8 | Stress | 0.561 | 0.780 | 1.144 | 1.589 | 1.729 | 2.401 | 1.935 | 2.687 | 2.742 | 3.808 | 2.983 | 4.143 |
| | *L/240* | *0.561* | *0.595* | *1.144* | *1.589* | *1.729* | *2.401* | *1.935* | *2.687* | *2.742* | *3.808* | *2.983* | *4.143* |
| 10 | Stress | 0.359 | 0.499 | 0.732 | 1.017 | 1.107 | 1.537 | 1.238 | 1.720 | 1.755 | 2.437 | 1.909 | 2.651 |
| | *L/240* | *0.305* | *0.305* | *0.732* | *1.017* | *1.107* | *1.537* | *1.238* | *1.720* | *1.755* | *2.437* | *1.909* | *2.651* |
| 12 | Stress | 0.250 | 0.347 | 0.508 | 0.706 | 0.768 | 1.067 | 0.860 | 1.194 | 1.219 | 1.693 | 1.326 | 1.841 |
| | *L/240* | *0.176* | *0.176* | *0.508* | *0.677* | *0.768* | *1.067* | *0.860* | *1.194* | *1.219* | *1.693* | *1.326* | *1.841* |
| 14 | Stress | 0.183 | 0.255 | 0.374 | 0.519 | 0.565 | 0.784 | 0.632 | 0.877 | 0.895 | 1.244 | 0.974 | 1.353 |
| | *L/240* | *0.111* | *0.111* | *0.374* | *0.426* | *0.565* | *0.784* | *0.632* | *0.877* | *0.895* | *1.244* | *0.974* | *1.353* |
| 16 | Stress | 0.140 | 0.195 | 0.286 | 0.397 | 0.432 | 0.600 | 0.484 | 0.672 | 0.686 | 0.952 | 0.746 | 1.036 |
| | *L/240* | *0.074* | *0.074* | *0.285* | *0.285* | *0.432* | *0.539* | *0.484* | *0.606* | *0.686* | *0.952* | *0.746* | *1.036* |
| 18 | Stress | 0.111 | 0.154 | 0.226 | 0.314 | 0.342 | 0.474 | 0.382 | 0.531 | 0.542 | 0.752 | 0.589 | 0.818 |
| | *L/240* | *0.052* | *0.052* | *0.201* | *0.201* | *0.342* | *0.379* | *0.382* | *0.426* | *0.542* | *0.727* | *0.589* | *0.793* |
| 20 | Stress | — | — | 0.183 | 0.254 | 0.277 | 0.384 | 0.310 | 0.430 | 0.439 | 0.609 | 0.477 | 0.663 |
| | *L/240* | — | — | *0.146* | *0.146* | *0.276* | *0.276* | *0.310* | *0.310* | *0.439* | *0.530* | *0.477* | *0.578* |
| 22 | Stress | — | — | 0.151 | 0.210 | 0.229 | 0.318 | 0.256 | 0.355 | 0.363 | 0.504 | 0.394 | 0.548 |
| | *L/240* | — | — | *0.110* | *0.110* | *0.207* | *0.207* | *0.233* | *0.233* | *0.363* | *0.398* | *0.394* | *0.434* |
| 24 | Stress | — | — | 0.127 | 0.177 | 0.192 | 0.267 | 0.215 | 0.299 | 0.305 | 0.423 | 0.331 | 0.460 |
| | *L/240* | — | — | *0.085* | *0.085* | *0.160* | *0.160* | *0.160* | *0.160* | *0.305* | *0.307* | *0.331* | *0.335* |
| 26 | Stress | — | — | 0.108 | 0.150 | 0.164 | 0.227 | 0.183 | 0.254 | 0.260 | 0.361 | 0.282 | 0.392 |
| | *L/240* | — | — | *0.067* | *0.067* | *0.126* | *0.126* | *0.141* | *0.141* | *0.241* | *0.241* | *0.263* | *0.263* |
| 28 | Stress | — | — | 0.093 | 0.130 | 0.141 | 0.196 | 0.158 | 0.219 | 0.224 | 0.311 | 0.243 | 0.338 |
| | *L/240* | — | — | *0.053* | *0.053* | *0.101* | *0.101* | *0.113* | *0.113* | *0.193* | *0.193* | *0.211* | *0.211* |
| 30 | Stress | — | — | 0.081 | 0.113 | 0.123 | 0.171 | 0.138 | 0.191 | 0.195 | 0.271 | 0.212 | 0.295 |
| | *L/240* | — | — | *0.043* | *0.043* | *0.082* | *0.082* | *0.092* | *0.092* | *0.157* | *0.157* | *0.171* | *0.171* |
| 32 | Stress | — | — | — | — | 0.108 | 0.150 | 0.121 | 0.168 | 0.171 | 0.238 | 0.186 | 0.259 |
| | *L/240* | — | — | — | — | *0.067* | *0.067* | *0.076* | *0.076* | *0.129* | *0.129* | *0.141* | *0.141* |
| 34 | Stress | — | — | — | — | 0.096 | 0.133 | 0.107 | 0.149 | 0.152 | 0.211 | 0.165 | 0.229 |
| | *L/240* | — | — | — | — | *0.056* | *0.056* | *0.063* | *0.063* | *0.108* | *0.108* | *0.118* | *0.118* |
| 36 | Stress | — | — | — | — | 0.085 | 0.119 | 0.096 | 0.133 | 0.135 | 0.188 | 0.147 | 0.205 |
| | *L/240* | — | — | — | — | *0.047* | *0.047* | *0.053* | *0.053* | *0.091* | *0.091* | *0.099* | *0.099* |
| 38 | Stress | — | — | — | — | — | — | 0.086 | 0.119 | 0.122 | 0.169 | 0.132 | 0.184 |
| | *L/240* | — | — | — | — | — | — | *0.045* | *0.045* | *0.077* | *0.077* | *0.084* | *0.084* |
| 40 | Stress | — | — | — | — | — | — | — | — | 0.110 | 0.152 | 0.119 | 0.166 |
| | *L/240* | — | — | — | — | — | — | — | — | *0.066* | *0.066* | *0.072* | *0.072* |
| 42 | Stress | — | — | — | — | — | — | — | — | 0.099 | 0.138 | 0.108 | 0.150 |
| | *L/240* | — | — | — | — | — | — | — | — | *0.057* | *0.057* | *0.062* | *0.062* |
| 44 | Stress | — | — | — | — | — | — | — | — | 0.091 | 0.126 | 0.099 | 0.137 |
| | *L/240* | — | — | — | — | — | — | — | — | *0.050* | *0.050* | *0.054* | *0.054* |
| 46 | Stress | — | — | — | — | — | — | — | — | 0.083 | 0.115 | 0.090 | 0.125 |
| | *L/240* | — | — | — | — | — | — | — | — | *0.044* | *0.044* | *0.048* | *0.048* |
| 48 | Stress | — | — | — | — | — | — | — | — | — | — | 0.083 | 0.115 |
| | *L/240* | — | — | — | — | — | — | — | — | — | — | *0.042* | *0.042* |
| Compact | (web) | Yes | Yes | Yes | Yes | Yes | Yes | Yes | Yes | Yes | Yes | Yes | Yes |
| Compact | (flange) | No | No | Yes | Yes | Yes | Yes | Yes | Yes | Yes | Yes | Yes | Yes |
| Mmax | k-ft | 4.816 | 6.238 | 9.152 | 12.711 | 13.832 | 19.212 | 15.478 | 21.497 | 21.936 | 30.467 | 23.861 | 33.140 |
| Lc | ft | 4.127 | 3.502 | 2.407 | 1.800 | 2.322 | 1.672 | 2.602 | 1.873 | 2.462 | 1.773 | 2.681 | 1.930 |
| Lu | ft | 4.127 | 3.502 | 2.500 | 2.041 | 2.797 | 2.373 | 2.804 | 2.379 | 3.156 | 2.678 | 3.162 | 2.683 |
| Vmax | k | 7.095 | 9.854 | 15.038 | 20.886 | 19.644 | 27.283 | 22.291 | 30.960 | 27.695 | 38.465 | 30.356 | 42.161 |
| R1 | k | 3.166 | 4.397 | 3.839 | 5.333 | 3.988 | 5.539 | 4.719 | 6.554 | 4.869 | 6.763 | 5.520 | 7.666 |
| R2 | k/in | 3.089 | 4.290 | 3.160 | 4.389 | 3.303 | 4.587 | 3.730 | 5.181 | 3.849 | 5.346 | 4.206 | 5.841 |
| R3 | k | 3.825 | 4.508 | 4.267 | 5.029 | 4.522 | 5.330 | 5.760 | 6.788 | 6.037 | 7.115 | 7.206 | 8.492 |
| R4 | k/in | 2.217 | 2.613 | 0.986 | 1.162 | 0.915 | 1.079 | 1.166 | 1.374 | 1.064 | 1.254 | 1.266 | 1.492 |
| R | k | 11.585 | 13.653 | 7.718 | 9.093 | 7.726 | 9.105 | 9.841 | 11.598 | 9.761 | 11.503 | 11.638 | 13.716 |
| | Note: | R exceeds Vmax | | | | | | | | | | | |

PLEASE READ THESE TABLES IN CONJUNCTION WITH THE INFORMATION CONTAINED ON THE LAST PAGE OF THIS PUBLICATION.

All safe working loads are in Kips (1,000lbs) per foot and are the maximum permissable applied load including the self weight of the beam.

*All deflection figures (in italics) are total loads that will cause a deflection of 1/240th of the span.*

*For other values multiply figures by 240 and divide by new value - i.e for 1/360th of span factor load by 240/360.*

Mmax is max. moment beam will resist provided comp. flange is fully supported at intervals not greater than Lc for compact & Lu for non-compact shapes.

Lc is the maximum unsupported length of the compression flange at which the allowable bending stress may be taken at 66% of yield stress.

Lu is the maximum unsupported length of the compression flange for maximum bending stress calculations based on 60% of yield stress.